

**Characterization of the senescence-associated membrane protein
DMP1 and the DMP family in *Arabidopsis thaliana***

Dissertation

zur Erlangung des akademischen Grades des
Doktors der Naturwissenschaften (Dr. rer. nat.)

Eingereicht im
Fachbereich Biologie, Chemie, Pharmazie
der Freien Universität Berlin

vorgelegt von

Alexis Kasaras
aus Berlin

Januar 2012

1. Gutachter: Prof. Dr. Reinhard Kunze

2. Gutachter: Prof. Dr. Wolfgang Schuster

Tag der Disputation: 02.03.2012

Table of content

Summary	1
Zusammenfassung	4
General introduction	7
Aim of the thesis	20
References	20
Chapter 1	29
Expression, localization and phylogeny of a novel family of plant-specific membrane proteins	
Abstract	30
Introduction	31
Material and methods	32
Results	35
Discussion	46
Acknowledgements	48
References	49
Supporting Information	52
Chapter 2	57
<i>Arabidopsis</i> DMP1-eGFP induces membrane remodeling and proliferation at the ER and the tonoplast	
Abstract	58
Background	59
Results	60
Discussion	71
Conclusions	74
Methods	74
Authors' contribution	75
Acknowledgements	76
References	76
Additional files	79
Chapter 3	83
The amino-terminus is responsible for differential targeting of DMP1 protein isoforms to the tonoplast and the plasma membrane	
Abstract	84
Introduction	85
Results	86
Discussion	104
Outlook	109
Material and methods	109
References	112
Supporting Information	117

Chapter 4 **119**

DMPI is a senescence-associated WRKY-regulated gene presumably involved in cell death by protein-protein interaction with Bax Inhibitor-1 and Cytochrome b5

Abstract	120
Introduction	121
Results	122
Discussion	140
Conclusion and Outlook	148
Material and methods	149
Acknowledgements	155
References	155
Supporting Information	159
List of abbreviations, gene names and units	160
Acknowledgements	162

Summary

Leaf senescence is the final phase of leaf development through which nutrient remobilization from leaves to sink organs, especially developing seeds in *Arabidopsis*, is achieved. Leaf senescence is a genetically programmed process in which leaf cells undergo orderly changes in gene expression, metabolism and morphology before they eventually die. Although organelles and cellular membrane systems are strongly reorganized during senescence, hardly any transporters and membrane proteins with senescence-specific functions are known. In *Arabidopsis thaliana* approximately 2000 genes are significantly upregulated during natural senescence, among them many membrane proteins. In this thesis a novel senescence-associated membrane protein gene was identified and characterized. It belongs to a completely unknown plant-specific gene family which comprises ten members in *Arabidopsis thaliana* and was named *DMP1* (*DUF679 domain membrane protein 1*). All AtDMP proteins are predicted to have four transmembrane domains, with cytosolic amino- and carboxy-termini.

In chapter one, the investigation of *AtDMP* family is presented. The phylogenetic distribution of DMP proteins revealed that DMPs are ubiquitous in green plants and absent from other kingdoms suggesting an implication in plant-specific processes. Only one *DMP* copy was found in *Chlamydomonas reinhardtii* and *Physcomitrella patens* genomes whereas their number ranged from five to 13 in dicots and 11 to 16 in monocots. The expression patterns of *AtDMPs* were found to be markedly tissue- and development-specific, excluding functional redundancy for most DMP proteins. *DMPs* are expressed in tissues undergoing senescence (*DMP1*, -3, -4), dehiscence (*DMP1*) and abscission (*DMP1*, -2, -4, -7) suggesting an involvement of DMP proteins in different types of programmed cell death. When fused to eGFP, all DMP proteins localize to the tonoplast or the ER. Some fusion proteins localized in both membrane systems suggesting competitive targeting and retention signals.

In chapter two, the complex membrane reorganization events triggered by overexpression of DMP1-eGFP are described and discussed. In *Nicotiana benthamiana* DMP1-eGFP induces a range of membrane fusion, fission and remodeling events affecting the architecture of the ER and the vacuole. Induction of tonoplastic invaginations known as “bulbs”, changes in the architecture of the endoplasmic reticulum (ER) from tubular to cisternal elements, expansion of smooth ER, formation of crystalloid ER, emergence of vacuolar sheets and foamy structures inside the vacuole were observed. In a fraction of cells, this process culminates in cell death after breakdown of the entire ER network and the vacuole. In transgenic *Arabidopsis* DMP1-eGFP overexpression did not perturb ER and vacuole morphology, but expression from the endogenous promoter highlighted formation

of “boluses” at the ER and vesiculation of the entire ER network preceding fragmentation of the central vacuole during the latest steps of natural senescence and dark-induced senescence in siliques, rosette and cauline leaves. This suggests that DMP1 has direct or indirect membrane fission properties involved in breakdown of the ER and the vacuole during programmed cell death (PCD). In contrast, in roots tips *DMP1* is expressed in the cortex undergoing vacuole biogenesis, suggesting an involvement in membrane fusion. These inherent properties, exacerbated by transient overexpression, are proposed to be at least partially responsible for the dramatic membrane remodeling events which led to cell death in tobacco.

A discrepancy between the subcellular localization of the tonoplast-localized DMP1-eGFP and the plasma membrane-localized eGFP-DMP1, initiated the investigation described in chapter 3. A range of mutated fusion proteins were generated and their expression and subcellular localization was analyzed in tobacco and *Arabidopsis*. It turned out that, due to leaky ribosome scanning at the first translation initiation site, two protein isoforms are synthesized, DMP1.1 and DMP1.2 which lacks the 19 amino terminal residues. DMP1.1-eGFP is targeted to the tonoplast whereas DMP1.2-eGFP is located in the plasma membrane. By mutating amino acids 2 and 3 of DMP1.1 or truncating the four N-terminal amino acids, DMP1.1-eGFP is redirected to the plasma membrane. This suggests that the plasma membrane is the default pathway. The occurrence of DMP1.1 and DMP1.2 was verified in *Arabidopsis* WT plants using an antibody raised against DMP1. 5'-RACE-PCR and sequencing confirmed that the two protein isoforms are translated from a single transcript. Co-expression studies with DMP1.1-eGFP and DMP1.2-mRFP revealed interaction of the two isoforms. Dimerization of DMP1 was confirmed using the split-ubiquitin system and chemical cross-linking *in planta*. Thus, DMP1.2 is redirected to the tonoplast by interacting with DMP1.1. This finding is the first demonstration of dual targeting of a plant membrane protein to the tonoplast and plasma membrane displaying an “eclipsed” distribution.

In chapter four, *DMP1* function was investigated by using different reverse genetic approaches, performing genome-wide transcriptome analyses, screening for protein interactors and analyzing *DMP1* promoter. *DMP1* senescence-specific transcriptional activation was shown to be governed by WRKY transcription factors. Mutation of two W-boxes, the cognate binding site of WRKY proteins, in the *DMP1* promoter led to loss of *DMP1* expression during senescence. A *dmp1* T-DNA insertion mutant (*dmp1-ko*) and *DMP1* overexpressor plants both display precocious senescence without other phenotypical alterations, reinforcing a specific function of DMP1 during senescence. By RNA gel blot analysis, truncated transcripts were detected in *dmp1-ko* plants that potentially could give rise to truncated and possibly dysfunctional proteins. These might be responsible for the phenotype since suppression of *DMP1* expression using artificial microRNA did

not lead to a comparable phenotype. The effects of *DMP1* overexpression were investigated by transcriptomics. Strikingly, *CYP94B3* which is involved in catabolism of the active jasmonate form JA-Ile, showed the strongest downregulation. This might result in JA-Ile accumulation and lead to early senescence. Moreover, the level of OPDA, a precursor of jasmonic acid considered as intracellular marker for senescence, was quantified by GC-MS and found to be more than twice as high in the mutant than in the WT. To gain more insight in DMP1 function, a split-ubiquitin screen was carried out in yeast. DMP1 was found to interact with Bax Inhibitor-1 (BI-1) and the Cytochrome b5 isoforms E and D. These proteins interact with each other in the context of cell death, corroborating an involvement of DMP1 in programmed cell death during late senescence.

Zusammenfassung

Seneszenz ist die letzte Stufe der Blatentwicklung. Während dieses Vorgangs werden in den alternden Blättern gebundene Nährstoffe verfügbar gemacht und zu anderen Pflanzenteilen, wie z.B. jungen Samen, transportiert. Die Alterung ist ein genetisch streng gesteuerter Prozess, während dessen sich die Genexpression, der Metabolismus und die Morphologie der Blattzellen verändern, bis die Zellen schließlich absterben. Obwohl sich Organellen und Zellmembransysteme während der Seneszenz stark verändern, sind kaum seneszenzspezifische Membranproteine bzw. Transporter bekannt. In *Arabidopsis thaliana* werden während der natürlichen Seneszenz ca. 2000 Gene signifikant hochreguliert, darunter viele Membranproteine. Im Rahmen dieser Arbeit wurde ein neues seneszenzassoziiertes Membranprotein identifiziert und charakterisiert. Das Gen wurde *DMP1* (*DUF679 domain membrane protein*) genannt und gehört zu einer bislang unbekanntem pflanzenspezifischen Genfamilie, die in *Arabidopsis* mit 10 Mitgliedern vertreten ist. Für alle AtDMP Proteine werden vier Transmembranbereiche vorhergesagt, wobei sich sowohl der Amino- als auch der Carboxyterminus auf der cytosolischen Seite der Membran befinden.

Im ersten Kapitel dieser Arbeit wurde die *AtDMP* Genfamilie untersucht. Eine phylogenetische Untersuchung ergab, dass *DMPs* ausschließlich in Pflanzen vorkommen, was vermuten lässt, dass diese Proteine in pflanzenspezifische Prozesse involviert sind. In den Genomen von *Chlamydomonas reinhardtii* und *Physcomitrella patens* kommt jeweils nur ein *DMP* Gen vor, wohingegen Dicotylen zwischen 11 und 16 und Monocotylen zwischen 5 und 13 Gene besitzen. Es zeigte sich, dass die Expressionsmuster der *AtDMPs* deutlich gewebe- und entwicklungspezifisch sind, was eine funktionelle Redundanz der Proteine unwahrscheinlich macht. *DMPs* sind in verschiedenen Stadien der Blattalterung aktiv, im Einzelnen während der Seneszenz (*DMP1*, -3, -4), der Dehiszenz (*DMP1*) und dem Blattwurf (*DMP1*, -2, -4, -7). Dieses Expressionsverhalten lässt vermuten, dass *DMPs* in verschiedenen Typen des programmierten Zelltods involviert sind. Proteinfusionen mit eGFP zeigten, dass alle *DMPs* entweder im Tonoplasten oder in der ER-Membran lokalisiert sind. Manche Fusionsproteine konnten in beiden Membransystemen detektiert werden, was auf kompetitive Ziel- bzw. Rückhaltesignale hindeutet.

Die komplexen Vorgänge während der Membranzumstrukturierung, hervorgerufen durch die Überexpression von *DMP1-eGFP*, sind Thema des zweiten Kapitels. In *Nicotiana benthamiana* induziert transient exprimiertes *DMP1-eGFP* eine Reihe von Membranfusionen und -teilungen, sowie Veränderungen der ER- und Vakuolenarchitektur. Einstülpungen des Tonoplasten (sogenannte „bulbs“), Umwandlung von tubulären ER-Bereichen in ER-Zisternen, Vergrößerung des glatten ERs, Bildung von kristallartigem ER sowie Veränderungen des Tonoplasten, die zu

einer schaumartigen Morphologie der Vakuole führen, wurden beobachtet. In einigen Zellen führen diese Veränderungen zu einem Zusammenbruch des gesamten ER-Netzwerkes und der Vakuole und damit zum Zelltod. In transgenen *35S:DMP1-eGFP* Arabidopsispflanzen ist der Aufbau von ER und Vakuole nicht verändert. Wird *DMP1-eGFP* unter dem eigenen Promoter exprimiert, zeigt sich eine deutliche Aktivität von *DMP1* während der letzten Phasen sowohl der natürlichen als auch der dunkelinduzierten Seneszenz. Zunächst ist durch das eGFP die Ausbildung von Aggregaten im ER sowie die Aufspaltung des gesamten ERs in Vesikel zu beobachten. Anschließend fragmentiert die Vakuole. *DMP1* scheint also eine Rolle im programmierten Zelltod zu spielen, konkret im Abbau der Membranen von Vakuole und ER. Im Gegensatz dazu steht die Beobachtung, dass *DMP1* während der Vakuolenbiogenese im Cortex der Wurzelspitze, aktiv ist. *DMP1* scheint folglich auch bei Membranfusionen relevant zu sein. Wird *DMP1* transient in Tabak exprimiert, führen diese spezifischen Proteineigenschaften vermutlich zu den beobachteten dramatischen Membranveränderungen sowie zum Zelltod.

Kapitel Drei beschäftigt sich mit der subzellulären Lokalisation verschiedener DMP1-GFP-Fusionsproteine. Während DMP1-eGFP im Tonoplasten lokalisiert ist, befindet sich eGFP-DMP1 in der Plasmamembran. Daher wurden eine Reihe mutierter Fusionsproteine hergestellt und ihre Expression und subzelluläre Lokalisation sowohl in Tabak als auch *Arabidopsis* untersucht. Es zeigte sich, dass aufgrund eines alternativen Startcodons zwei Proteinisoformen, DMP1.1 und DMP1.2 translatiert werden. DMP1.1-eGFP wird zum Tonoplast geleitet, wohingegen DMP1.2-eGFP, dem 19 N-terminale Aminosäuren fehlen, zur Plasmamembran transportiert wird. Wenn die Aminosäuren zwei und drei mutiert oder die ersten vier N-terminalen Aminosäuren entfernt werden, ist auch DMP1.1-eGFP in der Plasmamembran lokalisiert. Diese Beobachtungen legen nahe, dass die Plasmamembran als „default“ pathway für DMP1 angesehen werden kann. Mittels eines DMP1-Antikörpers wurden sowohl DMP1.1 als auch DMP1.2 in Wildtyp-Arabidopsis nachgewiesen. Durch 5'-RACE-PCR und anschließende Sequenzierung wurde nachgewiesen, dass beide Proteinisoformen von demselben Transkript translatiert werden. Co-Expressionsstudien mit DMP1.1-eGFP und DMP1.2-mRFP zeigten, dass beide Isoformen miteinander interagieren. Die Dimerbildung wurde mit dem Split-Ubiquitin-System und durch chemisches Vernetzen *in planta* nachgewiesen. Demzufolge wird DMP1.2 durch die Interaktion mit DMP1.1. zur Vakuole umgeleitet. Damit konnte zum ersten Mal duales Targeting mit einer sogenannten „verfinsterten Verteilung“ bei einem pflanzlichen Membranprotein gezeigt werden.

In Kapitel Vier wurde mit Hilfe revers-genetischer Ansätze die Funktion von DMP1 untersucht. Dazu wurden Transkriptomanalysen durchgeführt und nach Proteininteraktoren gesucht. Sowohl die *dmp1* T-DNA Insertionsmutante (*dmp1-ko*) als auch *DMP1* Überexpressionspflanzen seneszieren

früher als der Wildtyp. Andere phänotypische Veränderungen konnten nicht beobachtet werden, was die Seneszenzspezifität von *DMP1* weiter untermauert. In einem Gel Blot Test mit *dmp1-ko* RNA wurden verkürzte Transkripte detektiert, die möglicherweise Vorlage für verkürzte und womöglich dysfunktionale Proteine sind. Da eine Abregulation der *DMP1* Expression durch künstliche microRNAs nicht zu einem *dmp1-ko* vergleichbaren Phänotyp führte, ist es denkbar, dass verkürzte Proteine Ursache des Knockoutphänotyps sind. Die Auswirkungen der *DMP1* Überexpression wurden mit Hilfe einer Transkriptomanalyse untersucht. *CYP94B3*, das an der Inaktivierung der biologisch aktivsten Form von Jasmonsäure (JA-Ile) beteiligt ist, zeigte interessanterweise die stärkste Abregulation. Dies könnte zu einer Akkumulation von JA-Ile und dadurch zu verfrühter Seneszenz führen. OPDA ist eine Vorstufe von Jasmonsäure und gilt als intrazelluläres Seneszenzmerkmal. Der OPDA-Gehalt wurde mittels GC-MS untersucht. Wie sich zeigte, ist die OPDA-Konzentration in den transgenen Pflanzen mehr als zweimal höher als im Wildtyp. Um weitere Einblicke in die Funktion von *DMP1* zu erhalten, wurde ein Split-Ubiquitin Screen in Hefe durchgeführt. Es zeigte sich, dass *DMP1* mit Bax Inhibitor-1 (BI-1) und den Cytochrom b5 Isoformen E und D interagiert. Diese Proteine wirken während des Zelltods zusammen, was eine mögliche Funktion von *DMP1* im programmierten Zelltod in der späten Seneszenz bekräftigt. Es wurde ferner demonstriert, dass die seneszenzspezifische Aktivierung von *DMP1* durch WRKY Transkriptionsfaktoren erfolgt. Wurden im *DMP1*-Promoter zwei Bindungsstellen von WRKY Proteinen, sogenannte W-Boxen, mutiert, konnte *DMP1* während der Blattalterung nicht mehr aktiviert werden.

General introduction

Senescence and leaf senescence, general characteristics

Senescence is a nearly universal feature of multicellular organisms (Hughes and Reynolds, 2005). The word *senescence* derives from the Latin word *senescere* which means “to grow old” and is considered as a synonym for *aging* (Gan, 2007). Two types of senescence are distinguished in plants: mitotic and postmitotic senescence (Guo and Gan, 2005). Mitotic senescence, also known as proliferative senescence (Hensel et al., 1994) occurs in germline-like cells that have lost their ability to undergo mitotic division and which will differentiate to form new organs such as leaves and flowers (Gan, 2007). The arrest of the shoot apical meristem is an example of mitotic senescence and is similar to replicative senescence in yeast and animal cell cultures. However, unlike replicative senescence, plant mitotic senescence is not controlled by telomere shortening (Gan, 2003). In contrast, postmitotic senescence is an active degenerative process which occurs in somatic cells of organs such as leaves and petals and is comparable to the senescence process which takes place in somatic tissues of an animal adult body (Gan, 2003). Post-mitotic senescence can occur at cellular, tissue, organ or organism level and ultimately leads to death (Nooden, 1988a).

Leaf senescence is a type of postmitotic senescence and constitutes the final stage of leaf development. It is an active process characterized by differential gene expression, changes in metabolism, deterioration of cell structures and recycling of nutrients (BuchananWollaston, 1997; Gan, 2003; Guo and Gan, 2005; Lim et al., 2007). The earliest and most visible sign of leaf senescence is yellowing which reflects degradation of chlorophyll and breakdown of chloroplasts. Carbon assimilation is replaced by catabolism of macromolecules such as proteins, lipids and nucleic acids. The nutrients released are exported to active growing parts of the plant such as new buds, young leaves, developing fruits and seeds. Thus, leaf senescence can be seen as an altruistic process contributing to whole plant fitness and ensuring optimal production of offspring (Lim et al., 2007). Leaf senescence is governed by developmental age. However, it can be accelerated or delayed by a range of internal and external signals and can therefore be regarded as evolutionary strategy contributing to plant survival under unfavorable environmental conditions (Munne-Bosch and Alegre, 2004). From an agricultural point of view, leaf senescence restricts the yield of crop plants by limiting their growth phase. Thus, deciphering the process of leaf senescence may help to improve agricultural traits of crop plants.

One of the major limitations of the study of developmental leaf senescence is its inherent asynchronicity. Within a single senescing leaf, cells are at many different developmental stages, the senescence process usually starting from tips and margins of leaves and proceeding towards the

General introduction

base. Mesophyll cells undergo final cell death earlier than other cell types (Lim et al., 2007) and the veins tend to remain active longer to maximize the export of nutrients. Methods consisting of inducing artificially leaf senescence by darkness, starvation, excision or by using cell suspension cultures which may lead to a more synchronous process have shown that induced and natural senescence have distinct gene expression profiles (Buchanan-Wollaston et al., 2005; Van der Graaff et al., 2006). Although they share large sets of genes, their distinct expression profiles highlight the complexity of the senescence regulatory network.

The terms senescence and programmed cell death (PCD) and their relationship have led to some confusion (van Doorn and Woltering, 2004). The two terms are used in the literature to describe similar, distinct or overlapping processes. In contrast to senescence, the term PCD is typically used to describe the process leading to cell death occurring during the hypersensitive response, pollen incompatibility, aleurone degeneration or formation of tracheary elements (Beers, 1997) which do not involve nutrient remobilization. Consequently, this definition considers senescence and PCD as mutually exclusive processes, completion of the senescence phase (including nutrient recycling) leading subsequently to PCD. This separation is based on the plasticity of the senescence program. Indeed, senescing tobacco and flax leaves have been shown to be able to regreen (Greening et al., 1982; Zavaleta-Mancera et al., 1999b; Zavaleta-Mancera et al., 1999a) implying reversal of chlorophyll degradation and redifferentiation of gerontoplasts to chloroplasts. Thus, according to this definition, senescence and PCD are separate processes, the former being reversible and the second committed. This definition excludes that organs such as roots, petals, stigmas or anthers undergo senescence since reversal of senescence has been observed only in leaves and shoots (van Doorn and Woltering, 2004). An alternative definition considers senescence as being the deterioration of organs and organisms while PCD concerns the degradative process at cellular level (Nooden et al., 1997; van Doorn and Woltering, 2004). Another definition implies that only photosynthetic tissues showing visible yellowing undergo senescence while all non-photosynthetic tissues undergo PCD (Nooden et al., 1997; van Doorn and Woltering, 2004, 2005). Finally, some authors use the terms senescence and PCD as synonyms, the former being a type of PCD. In this work, we will use the term senescence to describe the whole developmental program including changes in gene expression, metabolism and cell structure, nutrient remobilization and a terminal cell death phase. According to this conception, the term senescence is used to describe the trajectory before and after the point of no return marked by loss of the reversal capacity, the inherent PCD occurring after this point being therefore irreversible.

General introduction

Signals that regulate leaf senescence

Various internal and external factors control the onset and the progression of leaf senescence (Fig. 1). Internal factors include age, reproductive growth, sugar levels, phytohormones concentrations and reactive oxygen species. External factors comprise a range of abiotic and biotic stresses.

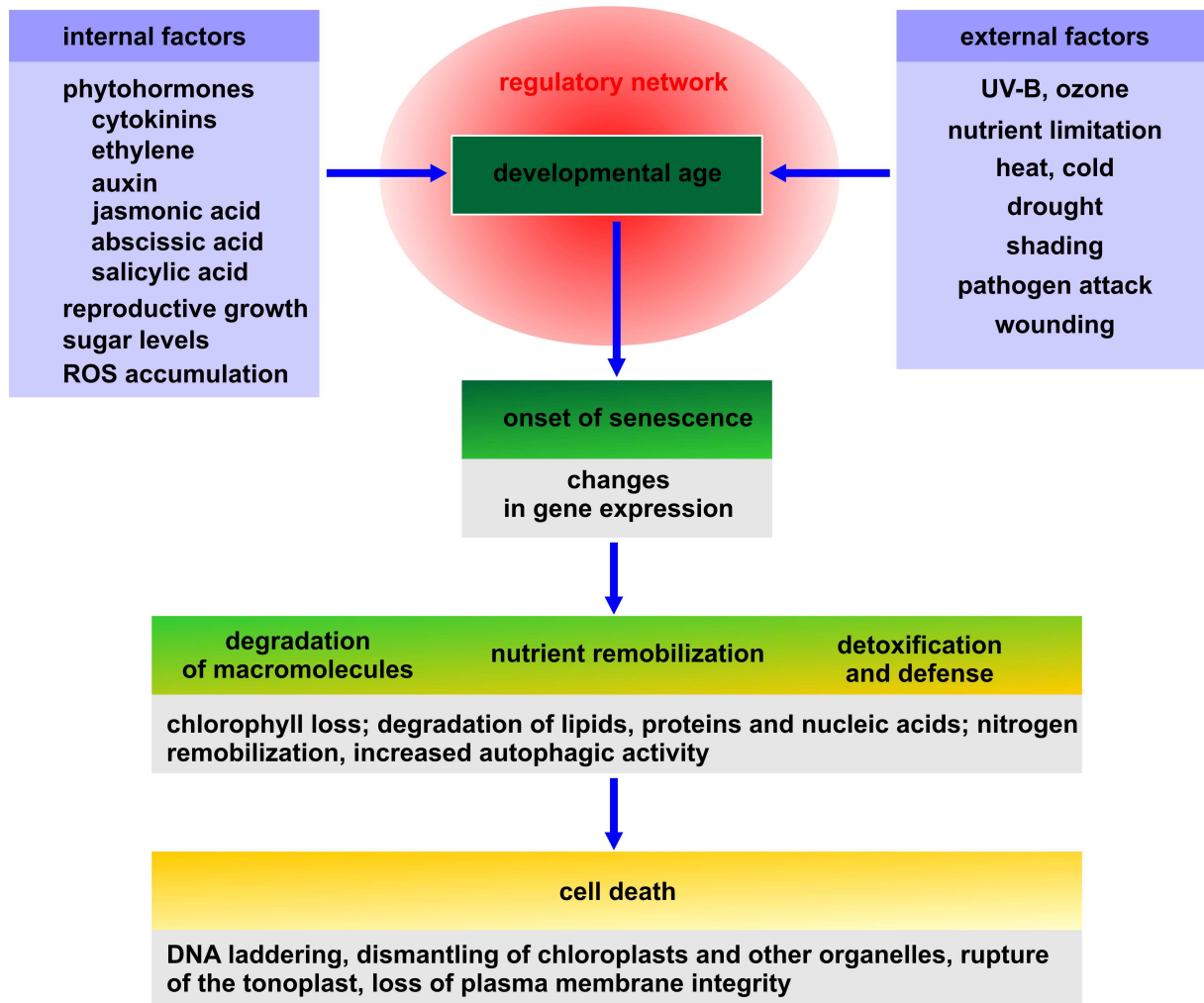


Fig. 1. Leaf senescence is a developmental age-dependent process which integrates internal and external signals via a regulatory network. This network activates large sets of senescence-associated genes responsible for the degeneration process, nutrient remobilization and final cell death. (Adapted from Lim et al. (2007))

Age and reproductive growth

When plants are grown in non-limiting nutrient conditions, away from pathogen attacks and free of abiotic stresses, leaf senescence will ultimately occur in an age-dependent manner (Hensel et al., 1993; Gan and Amasino, 1997; Quirino et al., 2000). How age initiates leaf senescence is still unclear. A decline of the photosynthetic activity with age has been suggested (Hensel et al., 1993).

General introduction

However, *Arabidopsis* and tobacco mutants with reduced photosynthetic activities display a delayed and not an early senescence (Miller et al., 2000; Woo et al., 2002).

Onset and regulation of senescence are correlated with reproductive development especially in monocarpic plants. The developing reproductive sink remobilizes nutrients from vegetative tissues and initiates the onset of senescence (Nooden, 1988b). Removal of flowers or fruits delays leaf senescence in various monocarpic plant species such as rice (Khan and Choudhuri, 1992), pea (Pic et al., 2002), soybean (Craftsbrandner and Egli, 1987) and sunflower (Sadras et al., 2000). Strikingly, the life span of pea plants is extended by 50 % when flowers are removed (Pic et al., 2002). Thus, monocarpic plant genomes appear to be optimized for reproduction which is determinant for the onset of leaf senescence. However, removing of flowers or fruits does not always lead to delayed senescence in monocarpic species. Removing of maize ear leads to either rapid or delayed leaf senescence depending on the genotype (Craftsbrandner and Egli, 1987). In *Arabidopsis*, leaf senescence is largely unaffected by reproductive growth (Nooden and Penney, 2001). The defined life span in optimal growth conditions is due to developmental programs (Hensel et al., 1993) and the onset of leaf senescence is triggered by age-related changes such as hormonal modulation, ROS accumulation and metabolic fluxes especially sugar and nitrogen signaling.

Sugars and metabolic fluxes

Sugars act as signaling molecules during various stage of plant development (Rolland et al., 2002; Rolland et al., 2006). Several studies suggest that increased sugar concentrations play a role during senescence and may be the most important factor initiating this process (Lim et al., 2007). First, increased sugar levels are higher in senescing leaves than in non-senescing leaves in *Arabidopsis* and tobacco (Masclaux et al., 2000). Second, expressing yeast invertase in the apoplast of *Arabidopsis*, tobacco and tomato plants leads to early senescence by accumulating sugars (Ding et al., 1993). Third, tomato plants overexpressing hexokinase (*HXK*) which acts as sugar sensor (Rolland et al., 2006) become more sensitive to sugars and display a precocious senescence phenotype (Dai et al., 1999). Inversely, knock-down of *AtHXK1* expression by stable ectopic overexpression of antisense *AtHXK1* transcripts leads to delayed senescence (Xiao et al., 2000). The role of sugars during senescence is further supported by genome-wide studies using microarrays. *SAG12* is induced 900-fold by glucose and enzymes involved in nitrogen assimilation such as the nitrate transporter *AtNRT2* and glutamine synthase *AtGLN1* are also upregulated (Pourtau et al., 2006). During natural senescence, key sugar-associated enzymes and transporters such as the high-affinity hexose transporter *STP13*, the monosaccharide transporter *SFP1* and *HXK* are all

General introduction

upregulated (Guo et al., 2004). It is important to note that the sugar-dependent regulation of senescence is highly complex, involves the coordination of various phytohormones (Guo and Gan, 2005) and is tightly associated with carbon and nitrogen availabilities (Leon and Sheen, 2003; Wingler et al., 2006).

Transition from anabolism to catabolism is a hallmark of leaf senescence (BuchananWollaston, 1997). Genes involved in catabolism are highly expressed during senescence and correlate with a drop in genes implicated in anabolism (Guo et al., 2004). Carbon and nitrogen availabilities are determinant for sugar accumulation and the regulation of metabolic fluxes and can lead to senescence. More precisely, the balance between carbon and nitrogen sources is crucial for sugar accumulation and signaling. High exogenous glucose concentrations (carbon source) induce early senescence in combination with low but not high nitrogen supply (Wingler et al., 2004). Senescence can be both accelerated and delayed by high CO₂ levels (Wingler et al., 2006). Nitrogen starvation also leads to early senescence possibly by influencing autophagic activity.

Reactive oxygen species (ROS) and nitric oxide (NO)

In contrast to animal PCD and the plant hypersensitive response (HR) where the mitochondria is the main generator of ROS, the chloroplast is mainly responsible for ROS production during leaf senescence (Quirino et al., 2000). The knock-out of *ndhF* which belongs to the Ndh complex involved in chlororespiratory electron transport chain results in delayed senescence in tobacco (Zapata et al., 2005). ROS are also generated via lipid oxidation (Mittler, 2002). The manipulation of *phospholipase D* and *SAG101* expression by antisense-suppression resulted in altered leaf senescence (Fan et al., 1997; He and Gan, 2002). Further reports indicate that defects in fatty acid biosynthesis pathways leads to senescence phenotypes (Mou et al., 2000; Wellesen et al., 2001) confirming that ROS are involved in leaf senescence. The cellular damages due to ROS accumulation during development possibly result in the onset of leaf development. Indeed, various delayed senescence mutants such as *ore1*, *ore3* and *ore9* show enhanced resistance to oxidative stress (Woo et al., 2004).

Nitric oxide (NO) has been shown to retard senescence. NO production is reduced and accompanied by strong down-regulation of NO synthase activity during senescence in pea leaves (Corpas et al., 2004). Exogenous application of NO offsets the senescing-inducing effects of abscisic acid and methyl-jasmonate in rice leaves. This antagonistic effect is abolished by the presence of an NO-specific scavenger (Hung and Kao, 2004). NO has the ability to remove ROS such as H₂O₂ in peroxisomes (del Rio et al., 2003). As ROS can induce senescence, NO counterbalances their senescence-inducing effects and has therefore an inhibitory effect on senescence.

General introduction

Hormonal control

Leaf senescence is influenced by several phytohormones. Ethylene and cytokinins have the most documented roles in inducing and delaying senescence respectively. Other hormones such as auxin, salicylic acid, jasmonic acid, abscisic acid and brassinosteroids also influence senescence. The effect of cytokinin and ethylene is conserved between plant species whereas the action of other hormones varies (Schippers et al., 2007). Investigation of the effect of single hormones is complex due to the significant overlap between the different signaling pathways. Three main ways to investigate hormonal responses in plants exist: by modifying hormone biosynthesis, perception or signaling. Hormones mutants have evidenced the role of phytohormones in leaf senescence. More recently, transcriptomic studies have highlighted changes in gene expression for the respective hormone biosynthesis, perception and signaling pathways as well as responsive genes during leaf senescence (Guo et al., 2004; Van der Graaff et al., 2006).

Exogenous stresses

Environmental stresses can be biotic, resulting from interaction with other organisms, or abiotic, resulting from chemical or physical changes in the environment compared to optimal conditions including extremes of light and temperature, radiation, drought, pathogen infection, oxidative stress, nutrient deficiency water stress and the presence of toxic material in the air, water or soil (Fig. 1). Expression of senescence-associated genes were reported in response to drought (Weaver et al., 1998; Pic et al., 2002), pathogen infection (Butt et al., 1998; Pontier et al., 1999), ozone treatment (Miller et al., 1999), UV-B treatment (John et al., 2001) and oxidative stress (Parlitz et al., ; Kleber-Janke and Krupinska, 1997; Weaver et al., 1998; Weaver and Amasino, 2001; Navabpour et al., 2003). Darkness is frequently used to induce senescence {Buchanan-Wollaston, 2005 #93; Lin and Wu, 2004; Roberts et al., 2006; Van der Graaff et al., 2006). Induced senescence, either in darkened attached or detached leaves, shares a high number of regulated genes with developmental senescence (Van der Graaff et al., 2006) as well as physiological and biochemical characteristics (Lers, 2007). In contrast, darkening of whole plants inhibits the senescence process (Weaver and Amasino, 2001). Senescence initiation induced by environmental stresses might be viewed as a defense response (Munne-Bosch and Alegre, 2004). Although senescence leads ultimately to cell death, it supports plants' survival during stress enabling plants to complete their life cycle and to produce viable seeds. Thus, induced senescence can be viewed as having adaptive significance since limited nutrients or water scarcity are frequent factors affecting plant development in various ecosystems. Strikingly, large sets of defense-related genes (Quirino et al., 2000; Gepstein et al., 2003; Guo et al., 2004; Lin and Wu, 2004) and pathogenesis-related genes (Quirino et al., 1999) are

General introduction

expressed during natural senescence. Thus, an extensive overlap between natural senescence and stress responses exists (Chen et al., 2002). However, it is still unclear whether defense-related genes are causes or consequences of senescence. Since stress-response pathways are triggered after the initiation of senescence, defense-related genes may function in detoxification and maintenance of cell viability during the whole senescence process (Guo et al., 2004).

Degradation processes and nutrient recycling

Chlorophyll degradation

As macroscopically illustrated by the yellowing of leaves, chlorophyll is degraded during senescence. The chlorophyll degradation pathway has been largely elucidated {Takamiya, 2000 #5; Berghold, 2002 #6}. The first steps take place in the chloroplast whereas the final reactions occur in the vacuole (Hörtensteiner, 2006). Cleavage of the tetrapyrrole ring leading to generation of the red chlorophyll catabolite (RCC) by Pheide *a* oxygenase (PaO) is the key step of this pathway (Hörtensteiner et al., 1998) which is therefore often referred to as the PaO pathway. Chlorophyll degradation is considered as a detoxification process to inactivate the phototoxic degradation intermediates since mutations or antisense expression of PaO and RCC reductase (RCCR) result in lesion mimic mutant phenotypes or cell death (Hörtensteiner, 2006). The final products of chlorophyll degradation, the non-fluorescent chlorophyll catabolites (NCCs) are deposited in the vacuole and not further degraded to remobilize the nitrogen they contain. However the chlorophyll-binding proteins which are released during dismantling of the pigment/chlorophyll binding proteins complexes are believed to be degraded and remobilized during senescence although the proteases involved in their breakdown remain to be characterized (Hörtensteiner, 2006).

Protein degradation

Functional analyses of SAGs have revealed three major protein degradation pathways occurring in senescing leaves: the ubiquitin/proteasome pathway, the autophagic/vacuolar pathway and the chloroplast degradation pathway (Liu et al., 2008).

Chloroplast proteins account for more than 70 % of total leaf proteins and represent a major source of nitrogen for mobilization (Hörtensteiner and Feller, 2002). Three types of chloroplast proteases (ClpP) have been categorized according to their subcellular compartments: stroma, thylakoid membrane and lumina (Adam and Clarke, 2002). They include the ATP-dependent Clp proteases (stroma), FtsH and Lon (thylakoid membrane) and the ATP-independent Deg (thylakoid-membrane and lumina). Chloroplast proteases are housekeeping proteins required for the turnover of chloroplast proteins and for the removal of damaged or mistargeted proteins (Adam and Clarke,

General introduction

2002). They are thought to be essential for the remobilization of free amino acids during senescence (Adam et al., 2006). In tobacco, the aspartic protease CND41 has been shown to be involved in this process (Kato et al., 2004). CND41 antisense tobacco plants showed delayed senescence. In vitro analysis using denatured Rubisco as substrate showed that CND41 has a proteolytic activity at physiological pH suggesting that CND41 is involved in Rubisco degradation allowing subsequent translocation of nitrogen during senescence. Moreover, chloroplasts isolated from mature pea leaves were shown to be able to degrade stromal proteins including Rubisco (Mitsuhashi and Feller, 1992; Roulin and Feller, 1998a). However, in senescing *Arabidopsis* leaves, no chloroplast protease has been clearly associated with degradation of stromal proteins such as Rubisco which represent about 50 % of total protein content in leaves from C₃ plants (Liu et al., 2008). It has often been suggested that Rubisco degradation may be initiated by ROS (Desimone et al., 1996; Ishida et al., 1998; Roulin and Feller, 1998b). A non-enzymatic cleavage of the large subunit of Rubisco induced by reactive oxygen has been reported (Ishida et al., 1997). A second pathway implying the formation of Rubisco-containing bodies (RCB), a kind of autophagic body, has been proposed for degradation of stromal proteins during senescence (Ishida et al., 2008; Izumi et al., 2010). In *Arabidopsis* senescing leaves, Ishida et al. (2008) showed using stroma-targeted GFP and DsRed and GFP-labeled Rubisco that Rubisco is released from chloroplasts into RCBs which are then taken up by the vacuole for degradation.

The ubiquitin-26S proteasome is required for targeted protein degradation during development and in response to environmental stresses (Sullivan et al., 2003). It involves three enzymes: E1, ubiquitin-activating enzyme; E2, ubiquitin-conjugating enzyme and E3, ubiquitin protein ligase.

More than 5 % of the proteome are components of the ubiquitin-26S proteasome pathway (Smalle and Vierstra, 2004). Several genes associated with this pathway are induced during senescence (Lin and Wu, 2004; Van der Graaff et al., 2006) indicating that this pathway is required for protein degradation during senescence. In *Arabidopsis*, the *ore9* mutant exhibits delayed senescence during developmental and hormone-modulated senescence (Woo et al., 2001). *ORE9* encodes an F-box protein which interact a component of the SCF complex that control selective ubiquitination and subsequent proteolysis of target proteins. Moreover, several ubiquitin-26S proteasome-associated genes have been detected in senescing wheat flag (Gregersen and Holm, 2007).

In contrast to the ubiquitin-26S proteasome machinery which predominantly degrades short-lived proteins, the autophagic/vacuolar pathway targets long-lived proteins, cytoplasmic components and entire organelles to the vacuole for degradation. In eukaryotes, autophagy is a universal mechanism for bulk degradation of cytosol and organelles to recycle nutrients and to degrade damaged and

General introduction

toxic components (Bassham, 2007). Two major autophagic pathways have been described in plants so far: microautophagy and macroautophagy (Bassham et al., 2006). Microautophagy involves engulfment of material directly by the vacuole through invagination of the tonoplast resulting in direct uptake of cytosolic components. In contrast, macroautophagy involves the sequestration of cytoplasm into double-membrane cup-shaped vesicles of unknown origin called autophagosomes. The outer membrane fuses with the tonoplast releasing an autophagic body consisting of the inner membrane and cargo into the lumen of the vacuole. Macroautophagy has been investigated in suspension cultures and whole plants during sucrose and nitrogen deprivation as well as during senescence for several plant species (Aubert et al., 1996; Moriyasu and Ohsumi, 1996; Doelling et al., 2002; Hanaoka et al., 2002). Almost all autophagy genes (*ATG*) in *Arabidopsis* are transcriptionally activated during developmental senescence and dark-induced senescence in detached and attached leaves (Van der Graaff et al., 2006). The autophagic pathway appears to be ubiquitous during development but the massive upregulation of almost every *ATG* gene during different types of senescence indicates an important role of the autophagic/vacuolar pathway in recycling and remobilization of nutrients during natural and induced senescence. Consistently, *Arabidopsis* knockout or RNAi mutants of *ATG4a/b*, *ATG5*, *ATG7*, *ATG9* and *ATG18a* display accelerated senescence and hypersensitivity to nutrient starvation (Doelling et al., 2002; Hanaoka et al., 2002; Yoshimoto et al., 2004; Thompson et al., 2005; Xiong et al., 2005). After transport into the vacuole through macroautophagy, substrate proteins are degraded by resident proteases such as cysteine proteases (*e.g.* SAG12), aspartic proteases, serine proteases, cathepsin B-like Cys proteases, papain-like proteases, peptidases, endopeptidases and aminopeptidases (Liu et al., 2008).

During the senescence of photosynthetic leaf cells from *Arabidopsis* and soybean, small senescence-associated vacuoles (SAVs) were observed in the cytoplasm (Otegui et al., 2005). SAVs exhibit intense proteolytic activity and contain dense aggregates which may consist of partially degraded cellular material reminiscent of late autophagic vacuoles. However, they are not derived from classical autophagosomes and their relationship to autophagy remains elusive. Moreover, the absence of γ -TIP in the membrane of SAVs suggests that they do not derive from fragmentation of the central vacuole. As they have been detected only in chloroplast-containing leaf cells, it has been proposed that they might be involved in the degradation of molecules released from chloroplasts (Otegui et al., 2005).

Lipid degradation

Membrane deterioration is an early and seminal feature of senescence and results from an enhanced catabolism of lipids (Thompson et al., 1998). Transcript levels of lipid-degrading enzymes

General introduction

including phospholipase D, phosphatidic acid phosphatase, lytic acyl hydrolase, lipoxygenase, α - and β -galactosidase and galactolipase are increased during senescence (Gepstein et al., 2003; Lin and Wu, 2004). Twenty-one out of 35 genes involved in fatty acid catabolism were shown by microarray analysis to be upregulated during senescence (Lin and Wu, 2004). Consistently, transgenic *Arabidopsis* plants with decreased levels of a senescence-induced lipase showed delayed leaf senescence (Thompson et al., 2000). Moreover, antisense suppression of *SAG101* which encodes an acyl hydrolase delayed the onset of leaf senescence whereas its overexpression induced premature senescence (He and Gan, 2002). Thus, degradation of lipids has senescence-promoting effects.

Nutrients recycling

Levels of C, N, P, S, K, Cu, Cr, Fe, Mo and Zn drop dramatically during leaf senescence in *Arabidopsis* indicating that these nutrients are mobilized from senescing leaves. Nitrogen remobilization is extremely efficient compared to phosphorus and sulfur remobilization. 90 % of the nitrogen and only 40 % of phosphorus and sulfur present in leaves are remobilized during senescence (Himelblau and Amasino, 2001). This remobilization involves the metabolization of proteins, nucleotides, lipids and polysaccharides. The majority of nitrogen remobilization is due to the hydrolysis of proteins to amino acids which are further catabolized, hydrolyzed, interconverted or exported without any modifications (Quirino et al., 2000; Hörtensteiner and Feller, 2002; Liu et al., 2008). Nucleic acid breakdown represents an important source of nitrogen, carbon and phosphorous. The nitrogen released is assimilated generally in the form of ammonium via the GS/GOGAT cycle which involves the concerted action of glutamine synthetase (GS) and glutamate synthase (GOGAT). Several cytosolic GSs are transcriptionally upregulated during senescence (Gepstein et al., 2003; Andersson et al., 2004; Van der Graaff et al., 2006). Glutamine is the major amino acid implicated in long-distance transport of nitrogen which occurs via the phloem (Tabuchi et al., 2007; Liu et al., 2008). Consistently, expression of GSs are predominantly restricted to the phloem (Edwards et al., 1990; Carvalho et al., 1992; Kamachi et al., 1992; Sakurai et al., 1996; Oliveira et al., 2002). Genes coding for enzymes related to the GS/GOGAT cycle including enzymes such as glutamate dehydrogenase, asparagine synthetase and aspartate aminotransferase are upregulated during senescence in *Arabidopsis* (Van der Graaff et al., 2006). The degradation of fatty acids of thylakoid membranes which represent the most abundant source of carbon in leaves and their possible may be subsequently converted into phloem-mobile sucrose through the gluconeogenesis pathway during senescence (Hopkins et al., 2007). Fatty acids originating from thylakoid membranes may be converted to acetyl-CoA by β -oxidation and respired by the TCA cycle to provide energy required for the metabolic reactions occurring during senescence (Chen et

General introduction

al., 2000; Charlton et al., 2005). Consistently, expression of key enzymes involved in these pathways such as the malate synthase, the isocitrate lyase and the pyruvate orthophosphate dikinase (PPDK) are enhanced during senescence (Guo et al., 2004). However, another pathway involving the PPDK but leading to the synthesis of asparagine serving as nitrogen carrier for nitrogen remobilization during senescence has been proposed (Lin and Wu, 2004; Liu et al., 2008).

Membrane dynamics and changes during senescence

On a weight basis, lipids are more efficient than carbohydrates and proteins as energy supplier (Thompson et al., 1998). Dismantling of membranes and organelles are metabolically coupled to energy production and remobilization of carbon, nitrogen and minerals to sink tissues (Matile, 1992). For that reason, cellular membranes are not degraded simultaneously, certain membranes retaining their structural integrity into late senescence. Ultrastructural analyses of senescing barley and maize leaves have revealed that thylakoids are the first membranes which are degraded. Deterioration of the internal mitochondrial membranes occurs only late during senescence (Kolodziejek et al., 2003).

The decline in structural and functional membrane integrity during senescence is clearly evident from permeability studies indicating increasing leakiness of membranes. Decrease in lipid fluidity during senescence is largely attributable to accelerated metabolism of membrane lipids leading to changes in the organization of the membrane bilayer and has been demonstrated in senescing petals, leaves, cotyledons and ripening fruits using fluorescence depolarization and electron spin resonance (Thompson et al., 1998). This decrease is due to an enrichment in free sterols which restrict the mobility of phospholipid chains (Shinitzky and Inbar, 1976). Moreover, this enrichment in free sterols is accompanied by an increase in the saturated-to-unsaturated fatty acid ratio due to depletion of polyunsaturated fatty acids from the senescing membranes (Fobel et al., 1987) which also leads to decreased bulk lipid fluidity. Changes in membrane fluidity have been shown to affect the function of membrane proteins such as transport (Grunze and Deuticke, 1974) or receptor function (Kirby and Green, 1980) by altering their conformation (Duxbury et al., 1991). Vertical displacement of membrane proteins towards membrane surfaces has been shown to occur following a decrease in membrane fluidity (Shinitzky et al., 1979; Shinitzky, 1984) rendering them prone to proteolysis (Hopkins et al., 2007). Indeed, a decrease in the level of membrane proteins in different senescing membranes has been reported (Layyee et al., 1992; Borochoy et al., 1994; Celikel and Vandoorn, 1995). Membrane proteins require a tight association with phospholipids which support their tertiary structure. Sterols are largely excluded from the phospholipid annulus surrounding membrane proteins (Warren et al., 1975). Thus, the enrichment in free sterols probably directly

General introduction

impacts on the tertiary structure of membrane proteins. Indeed, high sterol concentrations have been reported to induce membrane protein aggregation (Schneider et al., 1982).

Changes in membrane composition and permeability during senescence have also been evidenced by the occurrence of lipid phase separations shown by wide angle X-ray diffraction of isolated membrane fractions (Thompson et al., 1998). Membranes of non-senescent tissues are exclusively liquid-crystalline whereas membranes of senescing tissues have small domains of gel phase lipid (Leshem et al., 1984; Borochoy et al., 1987). The resulting mixture of liquid and gel phases in the lipid bilayer leads to leakiness of the senescing membrane due to packing imperfections at the phase boundaries (Barber and Thompson, 1980, 1983; Yamane et al., 1993). The emergence of gel-phase domains within senescing membranes is attributable to the accumulation of steryl and wax esters, free fatty acids, triacylglycerol and lipid catabolites (Yao et al., 1991a). However most of the lipid catabolites are also found in young membranes and result from membrane turnover (Thompson et al., 1998). These products phase separate within the bilayer forming domains that are released into the cytosol as lipid-protein particles probably by blebbing from the membrane surface (Yao et al., 1991b; Hudak et al., 1995). These particles have been isolated from the cytosol of different plant tissues and are enriched in free acids, steryl/wax esters and lipid and membrane protein catabolites compared to microsomal fractions (McKegney et al., 1995). These particles are believed to derive from all membranes accessible to the cytoplasm such as the plasma membrane, ER, mitochondria, tonoplast, Golgi and outer membranes of chloroplasts and mitochondria (Thompson et al., 1998). The formation of these lipid-protein particles is impaired during senescence leading to an accumulation of free acids, steryl/wax esters and lipid catabolites within the senescing membranes and subsequently to lipid phase separation and loss of membrane integrity (Thompson et al., 1998).

Changes in gene expression during senescence and senescence-associated transcription factors

Leaf senescence involves massive changes in gene expression. Approximately 2000 genes are upregulated during senescence whereas approximately 1500 genes are downregulated (Van der Graaff et al., 2006). The genes which undergo upregulation are commonly referred to as senescence-associated genes (*SAGs*). Although the function of many *SAGs* remains to be elucidated, *SAGs* can be classified into the following categories based on predicted or already assigned physiological functions: macromolecule degradation, lipid degradation, chlorophyll degradation, nucleic acid degradation, nutrient salvage and translocation, defense and detoxification genes and regulatory genes including transcription factors and signaling molecules (Kim et al., 2007).

Expression of 185 out of 1880 transcription factors was shown to change in *Arabidopsis* during senescence (Balazadeh et al., 2008). Forty-one were upregulated and 144 downregulated. The

General introduction

majority of them belong to NAC, WRKY, C2H2-type zinc finger, AP2/EREBP and MYB families. WRKY transcription factors are involved in plant-specific physiological programs including pathogen defense, trichome development and senescence (Eulgem et al., 2000). The cognate recognition sites for binding of WRKY transcription factors are called W-boxes (Fukuda and Shinshi, 1994; Rushton et al., 1996). Seventy-five and more than 100 WRKY transcription factors are found in *Arabidopsis thaliana* and *Oryza sativa* respectively (Zhang and Wang, 2005). More than 20 members are significantly upregulated during senescence in *Arabidopsis thaliana* (Van der Graaff et al., 2006). Among them, *WRKY53* and *-6* have been extensively investigated. *WRKY53* is expressed at early stages of leaf senescence and decreases at later stages indicating a regulatory role in early events of leaf senescence (Hinderhofer and Zentgraf, 2001). Targets of *WRKY53* include a range of SAGs, pathogenesis-related genes, stress-related genes and transcription factors including other *WRKY* factors (Miao et al., 2004). A *wrky53* knockout line exhibits a delayed senescence whereas ectopic overexpression leads to precocious senescence showing that *WRKY53* acts as a positive factor during leaf senescence (Miao et al., 2004). *WRKY6* is strongly induced during early to intermediate stages of leaf senescence and is a key regulator in plant-pathogen defense pathways (Robatzek and Somssich, 2001, 2002; Eulgem and Somssich, 2007). Targets of *WRKY6* have been identified and are mostly related to senescence and pathogen defense. They include the receptor-like kinase *SIRK*, the senescence-associated protein 1 *SENI* and the jasmonic acid regulatory protein *NAC2* (Robatzek and Somssich, 2002). Expression of several SAGs are altered in a *wrky6* knockout line which does not display an obvious senescence-related phenotype indicating potential functional redundancy (Robatzek and Somssich, 2002).

NAC proteins represent one of the largest plant-specific transcription factor family comprising 109 members in *Arabidopsis thaliana*. NAC transcription factors regulate embryo and shoot meristem development, auxin signaling, defense-response and senescence. One fifth of all NAC show increased transcript levels during senescence. *AtNAP* was the first NAC proteins whose role in the regulation of senescence was demonstrated (Guo and Gan, 2006). Overexpression of *AtNAP* triggers precocious senescence whereas a *nap* T-DNA knockout line shows a strongly delayed senescence. This phenotype could be complemented by *AtNAP* and orthologous genes from kidney bean and rice indicating a high degree of evolutionary conservation of *NAP* function in regulating senescence. *NTL9*, another NAC transcription factor has been shown to mediate osmotic stress signaling in leaf senescence (Yoon et al., 2008). It is membrane-bound in its dormant-state and becomes active following proteolytic cleavage. *NTL9* overexpression leads to premature activation of many SAGs which are in turn slightly down-regulated in the *ntl9* knockout line.

General introduction

Aim of the thesis

Plant senescence has been investigated in much detail at the morphological, physiological and genetic level. However, although intracellular reorganization during senescence is well documented, very little is known about senescence-associated membrane proteins. This thesis aims to unravel the function of a novel *Arabidopsis thaliana* membrane protein, AtDMP1 that is transcriptionally upregulated in leaf senescence and member of a strictly plant-specific protein family. The first chapter focuses on the characterization of the ten DMP family members of *Arabidopsis thaliana*. The phylogenetic distribution of DMP proteins, their expression, tissue-specificity and subcellular distribution were investigated. In chapter two, a possible implication of DMP1 in membrane remodeling, fusion and fission was revealed by examining the events triggered by DMP1-eGFP expression in tobacco and *Arabidopsis*. In chapter three, the mechanism that leads to the biosynthesis of two DMP1 isoforms targeted to different membrane systems was elucidated. In chapter four, DMP1 function and implication in senescence and cell death were further investigated by using *DMP1* knock-out and ectopic *DMP1* overexpressing lines, by *DMP1* promoter analysis and by isolating putative protein interactors.

References

- Adam, Z., and Clarke, A.K.** (2002). Cutting edge of chloroplast proteolysis. *Trends in Plant Science* **7**, 451-456.
- Adam, Z., Rudella, A., and van Wijk, K.J.** (2006). Recent advances in the study of Clp, FtsH and other proteases located in chloroplasts. *Current Opinion in Plant Biology* **9**, 234-240.
- Andersson, A., Keskitalo, J., Sjodin, A., Bhalerao, R., Sterky, F., Wissel, K., Tandre, K., Aspeborg, H., Moyle, R., Ohmiya, Y., Bhalerao, R., Brunner, A., Gustafsson, P., Karlsson, J., Lundeberg, J., Nilsson, O., Sandberg, G., Strauss, S., Sundberg, B., Uhlen, M., Jansson, S., and Nilsson, P.** (2004). A transcriptional timetable of autumn senescence. *Genome Biology* **5**.
- Aubert, S., Gout, E., Bligny, R., MartyMazars, D., Barrieu, F., Alabouvette, J., Marty, F., and Douce, R.** (1996). Ultrastructural and biochemical characterization of autophagy in higher plant cells subjected to carbon deprivation: Control by the supply of mitochondria with respiratory substrates. *Journal of Cell Biology* **133**, 1251-1263.
- Balazadeh, S., Riano-Pachon, D.M., and Mueller-Roeber, B.** (2008). Transcription factors regulating leaf senescence in *Arabidopsis thaliana*. *Plant Biol (Stuttg)* **10 Suppl 1**, 63-75.
- Barber, R.F., and Thompson, J.E.** (1980). Senescence-Dependent Increase in the Permeability of Liposomes Prepared from Bean Cotyledon Membranes. *Journal of Experimental Botany* **31**, 1305-1313.
- Barber, R.F., and Thompson, J.E.** (1983). Neutral Lipids Rigidify Unsaturated Acyl Chains in Senescing Membranes. *Journal of Experimental Botany* **34**, 268-276.
- Bassham, D.C.** (2007). Plant autophagy--more than a starvation response. *Curr Opin Plant Biol* **10**, 587-593.
- Bassham, D.C., Laporte, M., Marty, F., Moriyasu, Y., Ohsumi, Y., Olsen, L.J., and Yoshimoto, K.** (2006). Autophagy in development and stress responses of plants. *Autophagy* **2**, 2-11.

General introduction

- Beers, E.P.** (1997). Programmed cell death during plant growth and development. *Cell Death Differ* **4**, 649-661.
- Borochoy, A., Cho, M.H., and Boss, W.F.** (1994). Plasma-Membrane Lipid-Metabolism of Petunia Petals during Senescence. *Physiologia Plantarum* **90**, 279-284.
- Borochoy, A., Walker, M.A., Kendall, E.J., Pauls, K.P., and McKersie, B.D.** (1987). Effect of a freeze-thaw cycle on properties of microsomal membranes from wheat. *Plant Physiol* **84**, 131-134.
- Buchanan-Wollaston, V., Page, T., Harrison, E., Breeze, E., Lim, P.O., Nam, H.G., Lin, J.F., Wu, S.H., Swidzinski, J., Ishizaki, K., and Leaver, C.J.** (2005). Comparative transcriptome analysis reveals significant differences in gene expression and signalling pathways between developmental and dark/starvation-induced senescence in Arabidopsis. *Plant J* **42**, 567-585.
- BuchananWollaston, V.** (1997). The molecular biology of leaf senescence. *Journal of Experimental Botany* **48**, 181-199.
- Butt, A., Mousley, C., Morris, K., Beynon, J., Can, C., Holub, E., Greenberg, J.T., and Buchanan-Wollaston, V.** (1998). Differential expression of a senescence-enhanced metallothionein gene in Arabidopsis in response to isolates of *Peronospora parasitica* and *Pseudomonas syringae*. *Plant Journal* **16**, 209-221.
- Carvalho, H., Pereira, S., Sunkel, C., and Salema, R.** (1992). Detection of a Cytosolic Glutamine-Synthetase in Leaves of *Nicotiana-Tabacum-L* by Immunocytochemical Methods. *Plant Physiology* **100**, 1591-1594.
- Celikel, F.G., and Vandoorn, W.G.** (1995). Solute Leakage Lipid-Peroxidation and Protein-Degradation during the Senescence of Iris-Tepals (Vol 94, Pg 515, 1995). *Physiologia Plantarum* **95**, 326-326.
- Charlton, W.L., Johnson, B., Graham, I.A., and Baker, A.** (2005). Non-coordinate expression of peroxisome biogenesis, beta-oxidation and glyoxylate cycle genes in mature Arabidopsis plants. *Plant Cell Reports* **23**, 647-653.
- Chen, W., Provart, N.J., Glazebrook, J., Katagiri, F., Chang, H.S., Eulgem, T., Mauch, F., Luan, S., Zou, G., Whitham, S.A., Budworth, P.R., Tao, Y., Xie, Z., Chen, X., Lam, S., Kreps, J.A., Harper, J.F., Si-Ammour, A., Mauch-Mani, B., Heinlein, M., Kobayashi, K., Hohn, T., Dangl, J.L., Wang, X., and Zhu, T.** (2002). Expression profile matrix of Arabidopsis transcription factor genes suggests their putative functions in response to environmental stresses. *Plant Cell* **14**, 559-574.
- Chen, Z.H., Walker, R.P., Acheson, R.M., Tecsli, L.I., Wingler, A., Lea, P.J., and Leegood, R.C.** (2000). Are isocitrate lyase and phosphoenolpyruvate carboxykinase involved in gluconeogenesis during senescence of barley leaves and cucumber cotyledons? *Plant and Cell Physiology* **41**, 960-967.
- Corpas, F.J., Barroso, J.B., Carreras, A., Quiros, M., Leon, A.M., Romero-Puertas, M.C., Esteban, F.J., Valderrama, R., Palma, J.M., Sandalio, L.M., Gomez, M., and del Rio, L.A.** (2004). Cellular and subcellular localization of endogenous nitric oxide in young and senescent pea plants. *Plant Physiol* **136**, 2722-2733.
- Craftsbrandner, S.J., and Egli, D.B.** (1987). Modification of Seed Growth in Soybean by Physical Restraint - Effect on Leaf Senescence. *Journal of Experimental Botany* **38**, 2043-2049.
- Dai, N., Schaffer, A., Petreikov, M., Shahak, Y., Giller, Y., Ratner, K., Levine, A., and Granot, D.** (1999). Overexpression of Arabidopsis hexokinase in tomato plants inhibits growth, reduces photosynthesis, and induces rapid senescence. *Plant Cell* **11**, 1253-1266.
- del Rio, L.A., Corpas, F.J., Sandalio, L.M., Palma, J.M., and Barroso, J.B.** (2003). Plant peroxisomes, reactive oxygen metabolism and nitric oxide. *IUBMB Life* **55**, 71-81.
- Desimone, M., Henke, A., and Wagner, E.** (1996). Oxidative stress induces partial degradation of the large subunit of ribulose-1,5-bisphosphate carboxylase/oxygenase in isolated chloroplasts of barley. *Plant Physiology* **111**, 789-796.

General introduction

- Ding, B., Haudenschild, J.S., Willmitzer, L., and Lucas, W.J.** (1993). Correlation between arrested secondary plasmodesmal development and onset of accelerated leaf senescence in yeast acid invertase transgenic tobacco plants. *Plant J* **4**, 179-189.
- Doelling, J.H., Walker, J.M., Friedman, E.M., Thompson, A.R., and Vierstra, R.D.** (2002). The APG8/12-activating enzyme APG7 is required for proper nutrient recycling and senescence in *Arabidopsis thaliana*. *Journal of Biological Chemistry* **277**, 33105-33114.
- Duxbury, C.L., Legge, R.L., Paliyath, G., Barber, R.F., and Thompson, J.E.** (1991). Alterations in Membrane-Protein Conformation in Response to Senescence-Related Changes. *Phytochemistry* **30**, 63-68.
- Edwards, J.W., Walker, E.L., and Coruzzi, G.M.** (1990). Cell-Specific Expression in Transgenic Plants Reveals Nonoverlapping Roles for Chloroplast and Cytosolic Glutamine-Synthetase. *Proceedings of the National Academy of Sciences of the United States of America* **87**, 3459-3463.
- Eulgem, T., and Somssich, I.E.** (2007). Networks of WRKY transcription factors in defense signaling. *Curr Opin Plant Biol* **10**, 366-371.
- Eulgem, T., Rushton, P.J., Robatzek, S., and Somssich, I.E.** (2000). The WRKY superfamily of plant transcription factors. *Trends Plant Sci* **5**, 199-206.
- Fan, L., Zheng, S., and Wang, X.** (1997). Antisense suppression of phospholipase D alpha retards abscisic acid- and ethylene-promoted senescence of postharvest *Arabidopsis* leaves. *Plant Cell* **9**, 2183-2196.
- Fobel, M., Lynch, D.V., and Thompson, J.E.** (1987). Membrane Deterioration in Senescing Carnation Flowers - Coordinated Effects of Phospholipid Degradation and the Action of Membranous Lipoxygenase. *Plant Physiology* **85**, 204-211.
- Fukuda, Y., and Shinshi, H.** (1994). Characterization of a novel cis-acting element that is responsive to a fungal elicitor in the promoter of a tobacco class I chitinase gene. *Plant Mol Biol* **24**, 485-493.
- Gan, S.** (2003). Mitotic and postmitotic senescence in plants. *Sci Aging Knowledge Environ* **2003**, RE7.
- Gan, S.** (2007). Mitotic senescence in plants. In *Senescence processes in plants* (Blackwell Pub.), pp. 1-11.
- Gan, S., and Amasino, R.M.** (1997). Making Sense of Senescence (Molecular Genetic Regulation and Manipulation of Leaf Senescence). *Plant Physiol* **113**, 313-319.
- Gepstein, S., Sabeji, G., Carp, M.J., Hajouj, T., Neshner, M.F., Yariv, I., Dor, C., and Bassani, M.** (2003). Large-scale identification of leaf senescence-associated genes. *Plant J* **36**, 629-642.
- Greening, M.T., Butterfield, F.J., and Harris, N.** (1982). Chloroplast Ultrastructure during Senescence and Regreening of Flax Cotyledons. *New Phytologist* **92**, 279-&.
- Gregersen, P.L., and Holm, P.B.** (2007). Transcriptome analysis of senescence in the flag leaf of wheat (*Triticum aestivum* L.). *Plant Biotechnology Journal* **5**, 192-206.
- Grunze, M., and Deuticke, B.** (1974). Changes of Membrane-Permeability Due to Extensive Cholesterol Depletion in Mammalian Erythrocytes. *Biochimica Et Biophysica Acta* **356**, 125-130.
- Guo, Y., and Gan, S.** (2005). Leaf senescence: signals, execution, and regulation. *Curr Top Dev Biol* **71**, 83-112.
- Guo, Y., and Gan, S.** (2006). AtNAP, a NAC family transcription factor, has an important role in leaf senescence. *Plant J* **46**, 601-612.
- Guo, Y., Cai, Z., and Gan, S.** (2004). Transcriptome of *Arabidopsis* leaf senescence. *Plant Cell and Environment* **27**, 521-549.
- Hanaoka, H., Noda, T., Shirano, Y., Kato, T., Hayashi, H., Shibata, D., Tabata, S., and Ohsumi, Y.** (2002). Leaf senescence and starvation-induced chlorosis are accelerated by the disruption of an *Arabidopsis* autophagy gene. *Plant Physiology* **129**, 1181-1193.

General introduction

- He, Y.H., and Gan, S.S.** (2002). A gene encoding an acyl hydrolase is involved in leaf senescence in Arabidopsis. *Plant Cell* **14**, 805-815.
- Hensel, L.L., Grbic, V., Baumgarten, D.A., and Bleecker, A.B.** (1993). Developmental and age-related processes that influence the longevity and senescence of photosynthetic tissues in Arabidopsis. *Plant Cell* **5**, 553-564.
- Hensel, L.L., Nelson, M.A., Richmond, T.A., and Bleecker, A.B.** (1994). The fate of inflorescence meristems is controlled by developing fruits in Arabidopsis. *Plant Physiol* **106**, 863-876.
- Himelblau, E., and Amasino, R.M.** (2001). Nutrients mobilized from leaves of Arabidopsis thaliana during leaf senescence. *Journal of Plant Physiology* **158**, 1317-1323.
- Hinderhofer, K., and Zentgraf, U.** (2001). Identification of a transcription factor specifically expressed at the onset of leaf senescence. *Planta* **213**, 469-473.
- Hopkins, M., McNamara, L., Taylor, C., Wang, T.-W., and Thompson, J.** (2007). Membrane Dynamics and Regulation of Subcellular Changes During Senescence. In *Annual Plant Reviews Volume 26: Senescence Processes in Plants* (Blackwell Publishing Ltd), pp. 39-68.
- Hörtensteiner, S.** (2006). Chlorophyll degradation during senescence. *Annual Review of Plant Biology* **57**, 55-77.
- Hörtensteiner, S., and Feller, U.** (2002). Nitrogen metabolism and remobilization during senescence. *J Exp Bot* **53**, 927-937.
- Hörtensteiner, S., Wuthrich, K.L., Matile, P., Ongania, K.H., and Krautler, B.** (1998). The key step in chlorophyll breakdown in higher plants - Cleavage of pheophorbide alpha macrocycle by a monooxygenase. *Journal of Biological Chemistry* **273**, 15335-15339.
- Hudak, K., Yao, K.N., and Thompson, J.E.** (1995). Release of Fluorescent Peroxidized Lipids from Membranes in Senescing Tissue by Blebbing of Lipid-Protein Particles. *Hortscience* **30**, 209-213.
- Hughes, K.A., and Reynolds, R.M.** (2005). Evolutionary and mechanistic theories of aging. *Annu Rev Entomol* **50**, 421-445.
- Hung, K.T., and Kao, C.H.** (2004). Nitric oxide acts as an antioxidant and delays methyl jasmonate-induced senescence of rice leaves. *J Plant Physiol* **161**, 43-52.
- Ishida, H., Shimizu, S., Makino, A., and Mae, T.** (1998). Light-dependent fragmentation of the large subunit of ribulose-1,5-bisphosphate carboxylase/oxygenase in chloroplasts isolated from wheat leaves. *Planta* **204**, 305-309.
- Ishida, H., Nishimori, Y., Sugisawa, M., Makino, A., and Mae, T.** (1997). The large subunit of ribulose-1,5-bisphosphate carboxylase/oxygenase is fragmented into 37-kDa and 16-kDa polypeptides by active oxygen in the lysates of chloroplasts from primary leaves of wheat. *Plant Physiology* **114**, 1054-1054.
- Ishida, H., Yoshimoto, K., Izumi, M., Reisen, D., Yano, Y., Makino, A., Ohsumi, Y., Hanson, M.R., and Mae, T.** (2008). Mobilization of rubisco and stroma-localized fluorescent proteins of chloroplasts to the vacuole by an ATG gene-dependent autophagic process. *Plant Physiol* **148**, 142-155.
- Izumi, M., Wada, S., Makino, A., and Ishida, H.** (2010). The Autophagic Degradation of Chloroplasts via Rubisco-Containing Bodies Is Specifically Linked to Leaf Carbon Status But Not Nitrogen Status in Arabidopsis. *Plant Physiology* **154**, 1196-1209.
- John, C.F., Morris, K., Jordan, B.R., Thomas, B., and Mackerness, S.A.H.** (2001). Ultraviolet-B exposure leads to up-regulation of senescence-associated genes in Arabidopsis thaliana. *Journal of Experimental Botany* **52**, 1367-1373.
- Kamachi, K., Yamaya, T., Hayakawa, T., Mae, T., and Ojima, K.** (1992). Changes in Cytosolic Glutamine-Synthetase Polypeptide and Its Messenger-Rna in a Leaf Blade of Rice Plants during Natural Senescence. *Plant Physiology* **98**, 1323-1329.
- Kato, Y., Murakami, S., Yamamoto, Y., Chatani, H., Kondo, Y., Nakano, T., Yokota, A., and Sato, F.** (2004). The DNA-binding protease, CND41, and the degradation of ribulose-1,5-bisphosphate carboxylase/oxygenase in senescent leaves of tobacco. *Planta* **220**, 97-104.

General introduction

- Khan, R.I., and Choudhuri, M.A.** (1992). Influence of Reproductive-Organs on Plant Senescence in Rice and Wheat. *Biologia Plantarum* **34**, 241-251.
- Kim, H.J., Lim, P.O., and Nam, H.G.** (2007). Molecular Regulation of Leaf Senescence. In *Annual Plant Reviews Volume 26: Senescence Processes in Plants* (Blackwell Publishing Ltd), pp. 231-255.
- Kirby, C.J., and Green, C.** (1980). Erythrocyte-Membrane Cholesterol Levels and Their Effects on Membrane-Proteins. *Biochimica Et Biophysica Acta* **598**, 422-425.
- Kleber-Janke, T., and Krupinska, K.** (1997). Isolation of cDNA clones for genes showing enhanced expression in barley leaves during dark-induced senescence as well as during senescence under field conditions. *Planta* **203**, 332-340.
- Kolodziejek, I., Koziol, J., Waleza, M., and Mostowska, A.** (2003). Ultrastructure of mesophyll cells and pigment content in senescing leaves of maize and barley. *Journal of Plant Growth Regulation* **22**, 217-227.
- Layee, M., Stead, A.D., and Reid, M.S.** (1992). Flower Senescence in Daylily (*Hemerocallis*). *Physiologia Plantarum* **86**, 308-314.
- Leon, P., and Sheen, J.** (2003). Sugar and hormone connections. *Trends Plant Sci* **8**, 110-116.
- Lers, A.** (2007). Environmental Regulation of Leaf Senescence. In *Annual Plant Reviews Volume 26: Senescence Processes in Plants* (Blackwell Publishing Ltd), pp. 108-144.
- Leshem, Y.Y., Sridhara, S., and Thompson, J.E.** (1984). Involvement of Calcium and Calmodulin in Membrane Deterioration during Senescence of Pea Foliage. *Plant Physiology* **75**, 329-335.
- Lim, P.O., Kim, H.J., and Nam, H.G.** (2007). Leaf senescence. *Annual Review of Plant Biology* **58**, 115-136.
- Lin, J.F., and Wu, S.H.** (2004). Molecular events in senescing *Arabidopsis* leaves. *Plant J* **39**, 612-628.
- Liu, J., Wu, Y.H., Yan, J.J., Liu, Y.D., and Shen, F.F.** (2008). Protein degradation and nitrogen remobilization during leaf senescence. *J Plant Biol* **51**, 11-19.
- Masclaux, C., Valadier, M.H., Brugiere, N., Morot-Gaudry, J.F., and Hirel, B.** (2000). Characterization of the sink/source transition in tobacco (*Nicotiana tabacum* L.) shoots in relation to nitrogen management and leaf senescence. *Planta* **211**, 510-518.
- Matile, P.** (1992). Chloroplast senescence. In *Crop Photosynthesis: Spatial and Temporal Determinants* (Amsterdam: Elsevier Science B.V.), pp. 413-440.
- Mckegney, G., Yao, K.N., Ghosh, S., Huff, A., Mayak, S., and Thompson, J.E.** (1995). The Lipid-Composition of Cytosolic Particles Isolated from Senescing Bean Cotyledons. *Phytochemistry* **39**, 1335-1345.
- Miao, Y., Laun, T., Zimmermann, P., and Zentgraf, U.** (2004). Targets of the WRKY53 transcription factor and its role during leaf senescence in *Arabidopsis*. *Plant Molecular Biology* **55**, 853-867.
- Miller, A., Schlaghauser, C., Spalding, M., and Rodermel, S.** (2000). Carbohydrate regulation of leaf development: Prolongation of leaf senescence in Rubisco antisense mutants of tobacco. *Photosynth Res* **63**, 1-8.
- Miller, J.D., Arteca, R.N., and Pell, E.J.** (1999). Senescence-associated gene expression during ozone-induced leaf senescence in *Arabidopsis*. *Plant Physiology* **120**, 1015-1023.
- Mitsuhashi, W., and Feller, U.** (1992). Effects of Light and External Solutes on the Catabolism of Nuclear-Encoded Stromal Proteins in Intact Chloroplasts Isolated from Pea Leaves. *Plant Physiology* **100**, 2100-2105.
- Mittler, R.** (2002). Oxidative stress, antioxidants and stress tolerance. *Trends Plant Sci* **7**, 405-410.
- Moriyasu, Y., and Ohsumi, Y.** (1996). Autophagy in tobacco suspension-cultured cells in response to sucrose starvation. *Plant Physiology* **111**, 1233-1241.
- Mou, Z., He, Y., Dai, Y., Liu, X., and Li, J.** (2000). Deficiency in fatty acid synthase leads to premature cell death and dramatic alterations in plant morphology. *Plant Cell* **12**, 405-418.

General introduction

- Munne-Bosch, S., and Alegre, L.** (2004). Die and let live: leaf senescence contributes to plant survival under drought stress. *Funct. Plant Biol.* **31**, 203-216.
- Navabpour, S., Morris, K., Allen, R., Harrison, E., S, A.H.-M., and Buchanan-Wollaston, V.** (2003). Expression of senescence-enhanced genes in response to oxidative stress. *J Exp Bot* **54**, 2285-2292.
- Nooden, L.D.** (1988a). The phenomena of senescence and aging. In *Senescence and aging in plants*, L.D. Nooden and A.C. Leopold, eds (San Diego: Academic Press), pp. 1-50.
- Nooden, L.D.** (1988b). Whole plant senescence. In *Senescence and aging in plants*, L.D. Nooden and A.C. Leopold, eds (San Diego: Academic Press), pp. 391-439.
- Nooden, L.D., and Penney, J.P.** (2001). Correlative controls of senescence and plant death in *Arabidopsis thaliana* (Brassicaceae). *Journal of Experimental Botany* **52**, 2151-2159.
- Nooden, L.D., Guamet, J.J., and John, I.** (1997). Senescence mechanisms. *Physiologia Plantarum* **101**, 746-753.
- Oliveira, I.C., Brears, T., Knight, T.J., Clark, A., and Coruzzi, G.M.** (2002). Overexpression of cytosolic glutamine synthetase. Relation to nitrogen, light, and photorespiration. *Plant Physiology* **129**, 1170-1180.
- Otegui, M.S., Noh, Y.S., Martinez, D.E., Vila Petroff, M.G., Andrew Staehelin, L., Amasino, R.M., and Guamet, J.J.** (2005). Senescence-associated vacuoles with intense proteolytic activity develop in leaves of *Arabidopsis* and soybean. *Plant Journal* **41**, 831-844.
- Parlitz, S., Kunze, R., Mueller-Roeber, B., and Balazadeh, S.** Regulation of photosynthesis and transcription factor expression by leaf shading and re-illumination in *Arabidopsis thaliana* leaves. *J Plant Physiol* **168**, 1311-1319.
- Pic, E., de la Serve, B.T., Tardieu, F., and Turc, O.** (2002). Leaf senescence induced by mild water deficit follows the same sequence of macroscopic, biochemical, and molecular events as monocarpic senescence in pea. *Plant Physiology* **128**, 236-246.
- Pontier, D., Gan, S., Amasino, R.M., Roby, D., and Lam, E.** (1999). Markers for hypersensitive response and senescence show distinct patterns of expression. *Plant Mol Biol* **39**, 1243-1255.
- Pourtau, N., Jennings, R., Pelzer, E., Pallas, J., and Wingler, A.** (2006). Effect of sugar-induced senescence on gene expression and implications for the regulation of senescence in *Arabidopsis*. *Planta* **224**, 556-568.
- Quirino, B.F., Normanly, J., and Amasino, R.M.** (1999). Diverse range of gene activity during *Arabidopsis thaliana* leaf senescence includes pathogen-independent induction of defense-related genes. *Plant Mol Biol* **40**, 267-278.
- Quirino, B.F., Noh, Y.S., Himelblau, E., and Amasino, R.M.** (2000). Molecular aspects of leaf senescence. *Trends Plant Sci* **5**, 278-282.
- Robatzek, S., and Somssich, I.E.** (2001). A new member of the *Arabidopsis* WRKY transcription factor family, AtWRKY6, is associated with both senescence- and defence-related processes. *Plant J* **28**, 123-133.
- Robatzek, S., and Somssich, I.E.** (2002). Targets of AtWRKY6 regulation during plant senescence and pathogen defense. *Genes Dev* **16**, 1139-1149.
- Roberts, I.N., Passeron, S., and Barneix, A.J.** (2006). The two main endoproteases present in dark-induced senescent wheat leaves are distinct subtilisin-like proteases. *Planta* **224**, 1437-1447.
- Rolland, F., Moore, B., and Sheen, J.** (2002). Sugar sensing and signaling in plants. *Plant Cell* **14 Suppl**, S185-205.
- Rolland, F., Baena-Gonzalez, E., and Sheen, J.** (2006). Sugar sensing and signaling in plants: conserved and novel mechanisms. *Annu Rev Plant Biol* **57**, 675-709.
- Roulin, S., and Feller, U.** (1998a). Light-independent degradation of stromal proteins in intact chloroplasts isolated from *Pisum sativum* L. leaves: requirement for divalent cations. *Planta* **205**, 297-304.

General introduction

- Roulin, S., and Feller, U.** (1998b). Dithiothreitol triggers photooxidative stress and fragmentation of the large subunit of ribulose-1,5-bisphosphate carboxylase/oxygenase in intact pea chloroplasts. *Plant Physiology and Biochemistry* **36**, 849-856.
- Rushton, P.J., Torres, J.T., Parniske, M., Wernert, P., Hahlbrock, K., and Somssich, I.E.** (1996). Interaction of elicitor-induced DNA-binding proteins with elicitor response elements in the promoters of parsley PR1 genes. *Embo Journal* **15**, 5690-5700.
- Sadras, V.O., Echarte, L., and Andrade, F.H.** (2000). Profiles of leaf senescence during reproductive growth of sunflower and maize. *Ann Bot-London* **85**, 187-195.
- Sakurai, N., Hayakawa, T., Nakamura, T., and Yamaya, T.** (1996). Changes in the cellular localization of cytosolic glutamine synthetase protein in vascular bundles of rice leaves at various stages of development. *Planta* **200**, 306-311.
- Schippers, J.H.M., Jing, H.-C., Hille, J., and Dijkwel, P.P.** (2007). Developmental and Hormonal Control of Leaf Senescence. *Senescence processes in plants* **26**, 170.
- Schneider, H., Hochli, M., and Hackenbrock, C.R.** (1982). Relationship between the Density Distribution of Intramembrane Particles and Electron-Transfer in the Mitochondrial Inner Membrane as Revealed by Cholesterol Incorporation. *Journal of Cell Biology* **94**, 387-393.
- Shinitzky, M.** (1984). *Physiology of membrane fluidity* (CRC Press), pp. 1-52.
- Shinitzky, M., and Inbar, M.** (1976). Microviscosity Parameters and Protein Mobility in Biological-Membranes. *Biochimica Et Biophysica Acta* **433**, 133-149.
- Shinitzky, M., Skornick, Y., and Haran-Ghera, N.** (1979). Effective tumor immunization induced by cells of elevated membrane-lipid microviscosity. *Proc Natl Acad Sci U S A* **76**, 5313-5316.
- Smalle, J., and Vierstra, R.D.** (2004). The ubiquitin 26S proteasome proteolytic pathway. *Annu Rev Plant Biol* **55**, 555-590.
- Sullivan, J.A., Shirasu, K., and Deng, X.W.** (2003). The diverse roles of ubiquitin and the 26S proteasome in the life of plants. *Nature Reviews Genetics* **4**, 948-958.
- Tabuchi, M., Abiko, T., and Yamaya, T.** (2007). Assimilation of ammonium ions and reutilization of nitrogen in rice (*Oryza sativa* L.). *Journal of Experimental Botany* **58**, 2319-2327.
- Thompson, A.R., Doelling, J.H., Suttangkakul, A., and Vierstra, R.D.** (2005). Autophagic nutrient recycling in Arabidopsis directed by the ATG8 and ATG12 conjugation pathways. *Plant Physiology* **138**, 2097-2110.
- Thompson, J., Taylor, C., and Wang, T.W.** (2000). Altered membrane lipase expression delays leaf senescence. *Biochemical Society Transactions* **28**, 775-777.
- Thompson, J.E., Froese, C.D., Madey, E., Smith, M.D., and Hong, Y.W.** (1998). Lipid metabolism during plant senescence. *Progress in Lipid Research* **37**, 119-141.
- Van der Graaff, E., Schwacke, R., Schneider, A., Desimone, M., Flugge, U.I., and Kunze, R.** (2006). Transcription analysis of arabidopsis membrane transporters and hormone pathways during developmental and induced leaf senescence. *Plant Physiology* **141**, 776-792.
- van Doorn, W.G., and Woltering, E.J.** (2004). Senescence and programmed cell death: substance or semantics? *J Exp Bot* **55**, 2147-2153.
- van Doorn, W.G., and Woltering, E.J.** (2005). Many ways to exit? Cell death categories in plants. *Trends Plant Sci* **10**, 117-122.
- Warren, G.B., Houslay, M.D., Metcalfe, J.C., and Birdsall, N.J.M.** (1975). Cholesterol Is Excluded from Phospholipid Annulus Surrounding an Active Calcium-Transport Protein. *Nature* **255**, 684-687.
- Weaver, L.M., and Amasino, R.M.** (2001). Senescence is induced in individually darkened Arabidopsis leaves but inhibited in whole darkened plants. *Plant Physiology* **127**, 876-886.
- Weaver, L.M., Gan, S.S., Quirino, B., and Amasino, R.M.** (1998). A comparison of the expression patterns of several senescence-associated genes in response to stress and hormone treatment. *Plant Molecular Biology* **37**, 455-469.

General introduction

- Wellesen, K., Durst, F., Pinot, F., Benveniste, I., Nettesheim, K., Wisman, E., Steiner-Lange, S., Saedler, H., and Yephremov, A.** (2001). Functional analysis of the LACERATA gene of *Arabidopsis* provides evidence for different roles of fatty acid omega -hydroxylation in development. *Proc Natl Acad Sci U S A* **98**, 9694-9699.
- Wingler, A., Mares, M., and Pourtau, N.** (2004). Spatial patterns and metabolic regulation of photosynthetic parameters during leaf senescence. *New Phytologist* **161**, 781-789.
- Wingler, A., Purdy, S., MacLean, J.A., and Pourtau, N.** (2006). The role of sugars in integrating environmental signals during the regulation of leaf senescence. *J Exp Bot* **57**, 391-399.
- Woo, H.R., Kim, J.H., Nam, H.G., and Lim, P.O.** (2004). The delayed leaf senescence mutants of *Arabidopsis*, *ore1*, *ore3*, and *ore9* are tolerant to oxidative stress. *Plant Cell Physiol* **45**, 923-932.
- Woo, H.R., Goh, C.H., Park, J.H., Teyssendier de la Serve, B., Kim, J.H., Park, Y.I., and Nam, H.G.** (2002). Extended leaf longevity in the *ore4-1* mutant of *Arabidopsis* with a reduced expression of a plastid ribosomal protein gene. *Plant J* **31**, 331-340.
- Woo, H.R., Chung, K.M., Park, J.H., Oh, S.A., Ahn, T., Hong, S.H., Jang, S.K., and Nam, H.G.** (2001). ORE9, an F-box protein that regulates leaf senescence in *Arabidopsis*. *Plant Cell* **13**, 1779-1790.
- Xiao, W.Y., Sheen, J., and Jang, J.C.** (2000). The role of hexokinase in plant sugar signal transduction and growth and development. *Plant Molecular Biology* **44**, 451-461.
- Xiong, Y., Contento, A.L., and Bassham, D.C.** (2005). AtATG18a is required for the formation of autophagosomes during nutrient stress and senescence in *Arabidopsis thaliana*. *Plant Journal* **42**, 535-546.
- Yamane, K., Abiru, S., Fujishige, N., Sakiyama, R., and Ogata, R.** (1993). Export of Soluble Sugars and Increase in Membrane-Permeability of *Gladiolus* Florets during Senescence. *Journal of the Japanese Society for Horticultural Science* **62**, 575-580.
- Yao, K., Paliyath, G., Humphrey, R.W., Hallett, F.R., and Thompson, J.E.** (1991a). Identification and Characterization of Nonsedimentable Lipid Protein Microvesicles. *Proceedings of the National Academy of Sciences of the United States of America* **88**, 2269-2273.
- Yao, K.N., Paliyath, G., and Thompson, J.E.** (1991b). Nonsedimentable Microvesicles from Senescing Bean Cotyledons Contain Gel Phase-Forming Phospholipid Degradation Products. *Plant Physiology* **97**, 502-508.
- Yoon, H.K., Kim, S.G., Kim, S.Y., and Park, C.M.** (2008). Regulation of leaf senescence by NTL9-mediated osmotic stress signaling in *Arabidopsis*. *Mol Cells* **25**, 438-445.
- Yoshimoto, K., Hanaoka, H., Sato, S., Kato, T., Tabata, S., Noda, T., and Ohsumi, Y.** (2004). Processing of ATG8s, ubiquitin-like proteins, and their deconjugation by ATG4s are essential for plant autophagy. *Plant Cell* **16**, 2967-2983.
- Zapata, J.M., Guera, A., Esteban-Carrasco, A., Martin, M., and Sabater, B.** (2005). Chloroplasts regulate leaf senescence: delayed senescence in transgenic *ndhF*-defective tobacco. *Cell Death Differ* **12**, 1277-1284.
- Zavaleta-Mancera, H.A., Thomas, B.J., Thomas, H., and Scott, I.M.** (1999a). Regreening of senescent *Nicotiana* leaves II. Redifferentiation of plastids. *Journal of Experimental Botany* **50**, 1683-1689.
- Zavaleta-Mancera, H.A., Franklin, K.A., Ougham, H.J., Thomas, H., and Scott, I.M.** (1999b). Regreening of senescent *Nicotiana* leaves I. Reappearance of NADPH-protochlorophyllide oxidoreductase and light-harvesting chlorophyll a/b-binding protein. *Journal of Experimental Botany* **50**, 1677-1682.
- Zhang, Y.J., and Wang, L.J.** (2005). The WRKY transcription factor superfamily: its origin in eukaryotes and expansion in plants. *Bmc Evolutionary Biology* **5**, -.

General introduction

Chapter 1

Expression, localization and phylogeny of a novel family of plant-specific membrane proteins

A. Kasaras & R. Kunze

Address:

Freie Universität Berlin, Institut für Biologie - Angewandte Genetik, Dahlem Centre of Plant Sciences (DCPS)

Keywords: *Arabidopsis thaliana*; senescence; DUF679; membrane protein; tonoplast; endoplasmic reticulum; cell death

Correspondence: R. Kunze, Freie Universität Berlin, Institut für Biologie - Angewandte Genetik, Dahlem Centre of Plant Sciences, Albrecht-Thaer-Weg 6, D-14195 Berlin, Germany.

Email: rkunze@zedat.fu-berlin.de

Abstract

In a screen for senescence-associated genes in *Arabidopsis thaliana* a novel highly upregulated membrane protein was identified. It is a member of an uncharacterized, strictly plant specific gene family and was named *AtDMP1* (*Arabidopsis thaliana* DUF679 domain membrane protein 1). The AtDMP proteins are predicted to have four transmembrane spans with cytosolic amino- and carboxy-termini. In this study, we investigated the phylogenetic distribution of DMP proteins, their tissue-specific expression and subcellular localization in *Arabidopsis thaliana*. The *Chlamydomonas reinhardtii* and *Physcomitrella patens* genomes contain only a single *DMP* gene copy, whereas in dicots 5 to 13 and in monocots 11 to 16 *DMP* genes are found, many of which supposedly result from recent gene duplications. The ubiquitous occurrence of DMP proteins in green plants and their absence in other kingdoms suggest a role in plant-specific processes. In *A. thaliana* expression of nine out of ten *DMP* genes was detected. The expression patterns were found to be markedly tissue- and development-specific. Thus, functional redundancy of most proteins is unlikely. The occurrence of several AtDMPs in tissues undergoing senescence (*AtDMP1*, -3, -4), dehiscence (*AtDMP1*) or abscission (*AtDMP1*, -2, -4, -7) suggests an involvement of DMPs in different types of programmed cell death. AtDMP-eGFP fusion proteins were found to localize either to the endoplasmic reticulum, the tonoplast or, under certain conditions, to both membrane systems. Further investigations are in progress to elucidate the functions of the AtDMP proteins.

Introduction

The terminal developmental phase in the life cycle of plant leaves and other tissues is senescence. In this phase with the exception of the cell wall the vast majority of macromolecular cellular compounds are degraded and exported from the cells for recycling as nutrients in sink tissues (Hill, 1980; Himelblau & Amasino, 2001). The transition from the photosynthetically active phase to senescence is a slow, genetically regulated developmental process that involves reprogramming of the cellular metabolism and is accompanied by changes in cell morphology, metaplasia of plastids and conversion of vacuoles and other membrane-engulfed vesicles (Noodén *et al.*, 1997; Thomas *et al.*, 2003). In chloroplasts, chlorophyll is degraded and the final catabolites are sequestered in the vacuole, which involves the activity of the senescence-associated ABC transporter MRP2 (Frelet-Barrand *et al.*, 2008; Lu *et al.*, 1998). Autophagy is a major and conserved mechanism for the bulk degradation of intracellular proteins and organelles in the vacuoles (Bassham, 2007). It was recently shown that whole chloroplasts can be transported into the vacuole by autophagy (Wada *et al.*, 2009). Other compartments associated with leaf senescence are 'senescence-associated vacuoles' (Otegui *et al.*, 2005). However, the genealogy of senescence-associated membrane-engulfed vesicles is not well known.

In spite of the critical role of membranes and membrane proteins in senescence, only few senescence-associated membrane proteins and transporters have been reported. In a genome-wide expression analysis of natural and induced leaf senescence in *Arabidopsis thaliana* the novel senescence-associated protein DMP1 (DUF679 domain membrane protein 1) was identified (van der Graaff *et al.*, 2006). DMP1 belongs to a hitherto unknown plant-specific protein family with ten members in *Arabidopsis*. All DMP proteins have four transmembrane spans and none has any sequence similarity to a known transporter, channel or other membrane protein in any kingdom. Furthermore most *DMP* genes are absent from micro-array chips leading to an incomplete picture of the distribution of the *DMPs* on whole plant level. The lack of informations concerning the transcription profile of the *DMPs* and the absence of conserved domains or any similarity to other known proteins led us to investigate the whole gene/protein family at different levels. We investigated the expression patterns on organ level by semi-quantitative RT-PCR, the tissue-specificity by promoter-GUS fusion and the subcellular localization by DMP-eGFP fusion. We show that *DMPs* exhibit unique expression patterns in different plant organs. Several *DMPs* might be involved in various programmed cell death programs including senescence in rosette/cauline leaves and siliques, dehiscence in siliques and abscission of floral organs and siliques. However the occurrence of several *DMPs* in tissues not undergoing obvious programmed cell death such as root hairs, pollen grains or stomata indicate an implication of *DMPs* in other cellular processes. The phylogenetic analysis reveals that the *DMP* family is specific for green plants, suggesting a yet

Chapter 1

unknown plant-specific function. The DMP-eGFP fusion proteins showed predominant localization to the tonoplast and the ER excluding implication in processes which take place in organelles such as the chloroplast or the mitochondrion.

Material and methods

Plant material, growth conditions and plant transformation

Arabidopsis thaliana ecotype Columbia 0 and *Nicotiana benthamiana* plants were grown on soil in the greenhouse at 22°C under long day conditions (16-h light/8-h dark cycle). Five to six weeks old *Arabidopsis* plants were used for *Agrobacterium tumefaciens*-mediated transformation by floral dipping (Clough & Bent, 1998). Transgenic plants were selected on 0,8 % agar plates containing ½ MS medium supplemented with 50 µg/ml kanamycin for 10 days. Four weeks old tobacco plants (*Nicotiana benthamiana*) were used for *Agrobacterium tumefaciens*-mediated transient expression of the different *35S:DMP-eGFP* and *35S:eGFP-DMP* fusions (Bendahmane *et al.*, 2000).

Generation of binary vectors

All PCR reactions described were performed with *Pfu* polymerase (MBI Fermentas, St-Leon-Rot, Germany) and all PCR products were verified by sequencing (Macrogen, Seoul, Korea and GATC, Konstanz, Germany). The binary vector pUTkan3, a JH212 derivative carrying the *uidA* gene was used for the generation of all *DMP_{pro}:uidA* constructs. The 10 *DMP* promoter regions were PCR-amplified from genomic *Arabidopsis* Col-0 DNA using primer pairs listed in supplementary Table S1. The amplicates were then digested with *XbaI-PstI* (*DMP1_{pro}* and *DMP3_{pro}*) or *KpnI-PstI* (*DMP2_{pro}*, *DMP4_{pro}*, *DMP5_{pro}*, *DMP6_{pro}*, *DMP7_{pro}*, *DMP8_{pro}*, *DMP9_{pro}* and *DMP10_{pro}*) and ligated to *XbaI-PstI* or *KpnI-PstI* digested pUTkan3 to generate the 10 different *DMP_{pro}:uidA* constructs.

The binary vector pGTkan3, a pJH212 derivative containing a promoterless *eGFP* gene was used to generate *DMP-eGFP* fusions (C-terminal fusions). To express the fusion proteins from the CaMV 35S promoter, pPGTkan3 was generated. The 35S promoter was amplified from pPTkan3 (pJH212 derivative) by PCR using the primers 5'-gagaggtaccAATTCGGTCCCCAGATTAGCC and 5'-ggctctagaGTCCCCCGTGTCTCTCCAAA. The resulting PCR product was digested with *KpnI-XbaI* and ligated to *KpnI-XbaI* digested pGTkan3 to generate pPGTkan3. The open reading frames (ORF) of DMP1 and 3 lacking the stop codon were amplified with the primer pairs listed in Table S2. The amplicates were digested with *XbaI-PstI* and ligated to *XbaI-PstI* digested pPGTkan3 to generate *35S:DMP1-eGFP* and *35S:DMP3-eGFP*. The other *35S:DMP-eGFP* fusions were originally generated in the vector pA7-GFP (Hong *et al.*, 1999) for transient expression in protoplasts. The ORFs of *DMP2*, -4, -5, -6, -7, -8, -9, -10 were amplified by RT-PCR on total RNA

Chapter 1

from *Arabidopsis* rosettes with the primers listed in Table S2. The PCR products were digested with *XhoI-SpeI* and ligated to *XhoI-SpeI* digested pA7-GFP to generate the eight different *DMP-eGFP* fusions. For further analyses of the fusions proteins in stably transformed *Arabidopsis thaliana* plants and transiently infiltrated tobacco epidermal cells binary vectors were created. The eight *DMP-eGFP(-6His-Nos3')* fusions were released out of pA7-GFP by *XhoI-EcoRI* digestion, the overhangs of the fragments were filled in with T4 DNA polymerase (MBI Fermentas, St-Leon-Rot, Germany) and ligated to *XbaI-SpeI*-linearized and T4 DNA polymerase filled-in pCB302-3 (Xiang *et al.*, 1999).

For the construction of N-terminal fusions of DMP2, -6, -7 and 10 with eGFP, the eGFP ORF lacking the stop codon was amplified from pGTkan3 with the primer pair 5'-**gtggtacc**ATGGTGAGCAAGGGCGAGGAG-3'/5'-**cggctctaga**CTTGTACAGCTCGTCCATGCC-3'. The PCR product was digested with *KpnI-XbaI* and ligated to *KpnI-XbaI* digested pGTkan3 to create pNGTkan3. The *DMP* ORFs were amplified with the primers listed in Table S3. The PCR products were digested with *XbaI-XhoI* and ligated to *XbaI-XhoI* digested pNGTkan3 to generate *35S:eGFP-DMP* fusions. Expression of all *35S:eGFP-DMP* and *35S:DMP-eGFP* constructs was analyzed by laser scanning confocal microscopy (LSCM) in transiently infiltrated tobacco leaves and in stably transformed *Arabidopsis thaliana* plants (only C-terminal fusions).

The tonoplast marker 'TPK1-mRFP' (Latz *et al.*, 2007) was PCR amplified from plasmid pPily with the primers 5'-**gtggtacc**ATGTCGAGTGATGCAGCTCGT-3' and 5'**gagactcgag**TTAGGCGCCGGTGGAGTGGCG-3'. The PCR product was digested with *KpnI-XhoI* and ligated to *KpnI-XhoI*-linearized pPTkan3 to generate *35S:TPK1-mRFP* in a binary vector. The ER marker 'mCherry-HDEL' consists of mCherry with an N-terminally fused signal peptide of AtWAK2 and the C-terminally fused ER retention motif HDEL (Nelson *et al.*, 2007). The plasma membrane marker 'mRFP-MUB2' (Downes *et al.*, 2006) was generated by amplifying mRFP from pPily with the primers 5'-**acggctctaga**ATGGCCTCCTCCGAGGACGTC-3' and 5'**GCGCGCCGGTGGAGTGGCG**-3' and MUB2 from genomic *Arabidopsis* DNA with the primers 5'-**gccgagggccgcccactccaccggcgcc**ATGGCAGAGGTGAAGGATCAA-3' and 5'-**gagactcgag**TTAACAACGAGCTCCAAAACA-3'. By overlapping PCR using the two amplicates and the external primers 5'-**acggctctaga**ATGGCCTCCTCCGAGGACGTC-3' and 5'-**gagactcgag**TTAACAACGAGCTCCAAAACA-3' 'mRFP-MUB2' was generated. This amplicate was *XbaI-XhoI* digested and ligated into *XbaI-XhoI* linearized pPTkan3 to generate '*35S:mRFP-MUB2*'.

Chapter 1

Histochemical Localization of GUS Activity

Twenty-four independent transgenic lines for each of the 10 *DMP_{pro}:uidA* constructs were assayed by GUS staining in the T1 generation. For each construct, 3 independent lines exhibiting representative GUS patterns were chosen for further investigation. Plant tissues were fixed in 90% acetone for 1 hour at -20 °C, washed twice with 50 mM NaPO₄ buffer pH 7.0 and vacuum-infiltrated with X-Gluc solution (50 mM NaPO₄ buffer pH 7.0, 0.1% Triton X-100, 10 mM potassium ferricyanide, 10 mM potassium ferrocyanide and 0,5 mg/ml 5-bromo-4-chloro-3-indolyl-β-D-glucuronide) overnight at 37°C. Identical staining conditions were used for all GUS expression experiments. Stained tissues were cleared with an ethanol series.

Confocal microscopy

Fluorescence images were acquired with a Leica TCS-SP5 laser scanning confocal microscope. GFP was visualized by excitation with the 488 nm line of the argon laser. Emission was detected with a spectral detector set between 505 nm and 560 nm. Water immersion objectives 20x and 63x with numerical apertures values of 0.7 and 1.20 respectively were used. Post-acquisition image processing was performed with the Leica LAS AF software.

GUS staining image acquisition

Photographs of all GUS stained tissues except for root and pollen were taken with a Leica Z16 APO A macroscope equipped with a Leica DFC420C camera. Images of root and pollen were obtained with a Zeiss Axioskop 2 plus equipped with an AxioCam ICc3 camera. The Plan-Apochromat 20x/0.8 objective and the software AxioVision Rel. 4.6 were used for image acquisition and processing.

DNA and protein sequence sources and analyses

AtDMP promoter and ORF sequences were retrieved from The *Arabidopsis* Information Resource release 9 (www.Arabidopsis.org). Primers were designed using QuantPrime (<http://www.quantprime.de>). All PCR products for subsequent cloning steps were verified by sequencing. Protein sequences from other plants with homology to AtDMP1 (At3g21520) were retrieved from the Phytozome comparative genomics database version 4.1 (www.phytozome.net). For display in Figure 3 the sequences were renamed. The original designations used in the Phytozome database are provided in supplementary Table S5. Protein sequences were aligned with Clustal X 2.0 (Larkin *et al.*, 2007). Three of the 122 AtDMP1-homologous sequences clustered in Phytozome 4.1 were excluded from the alignment because they are presumably incomplete (*Arabidopsis lyrata* scaffold_702583.1, *Medicago truncatula* AC146553_19 and *Oryza sativa* 12012.m06167). Phylogenetic trees were constructed by the Neighbor Joining algorithm

Chapter 1

implemented in Clustal X 2.0. Due to the high divergence between the sequences alignment positions with gaps could not be excluded during tree building. Confidence values for the groupings in the tree were derived by bootstrap analysis with 1000 trials. Trees (cladograms) were drawn with the FigTree program developed by Andrew Rambaut (<http://tree.bio.ed.ac.uk/>).

RNA isolation and semi-quantitative RT-PCR

Total RNA was extracted from different *Arabidopsis* tissues as described (Downing *et al.*, 1992). The tissues tested included young (20 DAS), mature (34 DAS) and senescing rosette leaves (51 DAS), green and senescing cauline leaves, green and senescent siliques, young and old stems, flowers and roots. Seeds were removed from both green/non-dehiscent siliques and senescent/dehiscent siliques before harvest. The young stems harvested included exclusively the upper part of main inflorescence stems without floral organs and siliques. The old stems included only brown parts of the stems underneath the first node. Roots were harvested from plants grown on soil to avoid light effects.

Total RNA was treated with DNase to remove DNA contamination. First strand cDNA was synthesized on 2 µg total RNA with poly(dT)₂₃VN primer by SuperScriptIII reverse transcriptase (Invitrogen, Karlsruhe, Germany). Gene expression of the ten *AtDMPs* was determined by semi-quantitative RT-PCR. PCR reactions were 2 min at 95 °C initial denaturation followed by 24, 30 or 36 cycles of 30 sec 95 °C, 30 sec 58 °C, 40 sec 72 °C. *ACT2* (At3g18780) was used as internal control and *SAG12* (At5g45890) as senescence marker. To be able to control for DNA contamination, *ACT2* and *SAG12* primer pairs flank an intron on genomic DNA. The *DMP1*, -2, -3, -5, -7, -10 primer pairs were designed to amplify the complete open reading frames. For the highly similar gene pairs *DMP4* - *DMP6* and *DMP8* - *DMP9* internal primers were used to prevent cross-amplification. The sizes of the resulting amplicates are listed in Table S4.

Results

The DMP protein family

In a screen for senescence-associated genes in *Arabidopsis* a novel senescence-upregulated membrane protein gene, termed *AtDMP1* (DUF679 domain membrane protein 1), was discovered. *AtDMP1* belongs to a novel uncharacterized gene family with ten members in *Arabidopsis*. The protein alignment (Fig. 1) reveals that the AtDMP proteins are divergent in their amino-terminal parts, but conserved from the first transmembrane (TM) domain to the C-terminus. This conserved part of the proteins is annotated in the NCBI-CDD database as the DUF679 domain of unknown function (www.ncbi.nlm.nih.gov/Structure/cdd/cddsrv.cgi?uid=113833). According to the consensus TM span calculation tool of the ARAMEMNON plant membrane protein database

Chapter 1

(<http://aramemnon.botanik.uni-koeln.de/>; Schwacke *et al.*, 2003) with the exception of DMP7 the DMP proteins are predicted to contain four TM spans. In the conceptual DMP7 amino acid sequence the N-terminal two TM spans are lacking due to an incorrect gene model. The cDNA sequence reveals that DMP7 has four TM spans and is homologous along its whole sequence to the other family members. In addition to the TM spans, highly conserved sequence motifs are located in inter-TM loops and the short carboxy-termini extending into the cytoplasm (Fig. 1).

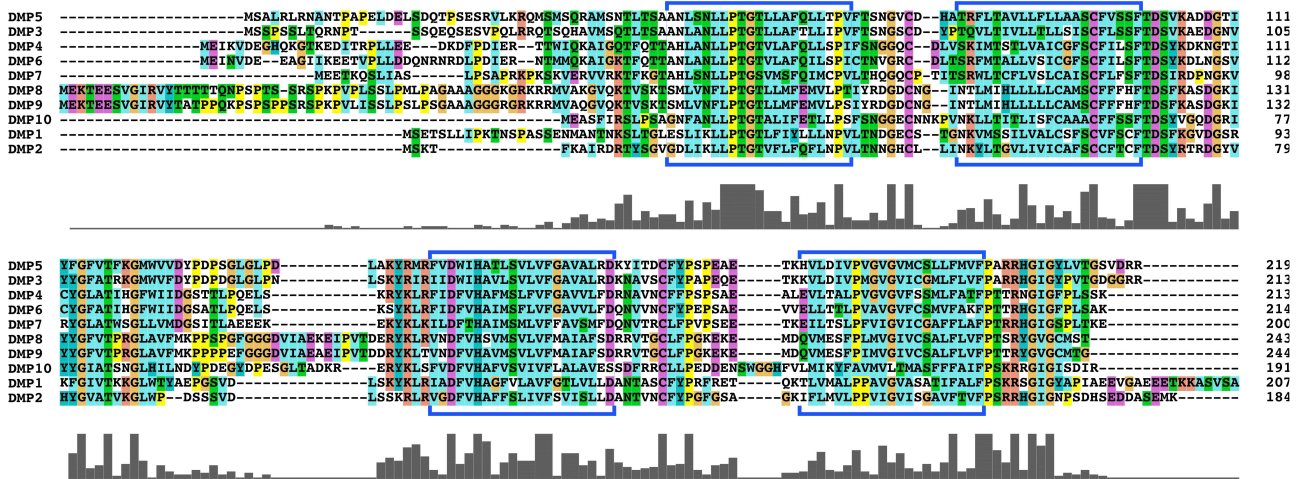


Figure 1: AtDMP protein alignment. The ten AtDMP proteins were aligned using Clustal X 2.0. The blue frames indicate the TM spans. The height of the columns underneath each amino acid position indicates a conservation score. The background coloration highlights the consensus chemical character at the respective amino acid position (Clustal X 2 default coloration scheme). Blue/cyan: non-polar; green: polar; magenta: negative charge; red: positive charge.

An unrooted tree constructed from the aligned DMP protein sequences can be divided in six clades, four of which contain a pair of two similar proteins each (Fig. 2). A FASTA (v3) pairwise similarity search (www.ebi.ac.uk/Tools/fasta33/) calculates 43% identity between AtDMP1 and AtDMP2 with 80% sequence coverage. AtDMP3 and AtDMP5 are 65% identical (91% sequence coverage), AtDMP4 and AtDMP6 are 73% identical (100% coverage) and AtDMP8 and AtDMP9 are 90% identical (100% coverage). It is likely that the gene pairs result from gene duplications in the *Arabidopsis* genome.

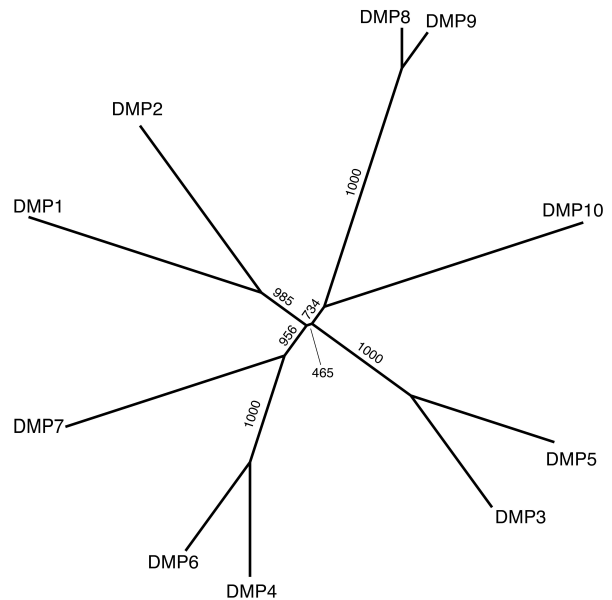


Figure 2: Unrooted N-J tree of AtDMP proteins. DMP1: At3g21520; DMP2: At3g21550; DMP3: At4g24310; DMP4: At4g18425; DMP5: At3g02430; DMP6: At5g46090; DMP7: At4g28485; DMP8: At1g09157; DMP9: At5g39650; DMP10: At5g27370. Bootstrap values (1000 trials) are indicated above branches.

Chapter 1

BLAST(-PSI) searches for DMP homologous proteins did not reveal any related amino acid motifs in animals, fungi, prokaryotes or archae. However, DMP homologs occur in all higher plants, mosses and in *Chlamydomonas reinhardtii*. The Phytozome database (version 4.1; www.phytozome.net) lists 122 orthologous and paralogous genes of AtDMP1 in 14 green plant (*Viridiplantae*) genomes. Figure 3 shows a cladogram of the N-J tree generated from the alignment of 119 of these genes (three genes were excluded from the tree because their sequences are supposedly incomplete). The single celled green alga *C. reinhardtii* has one single DMP homolog (Cr7g13767) that differs from the bulk of green plant DMP proteins by an extended cytoplasmic C-terminus (>100 amino acids) and branches off near the center of the tree. The bryophyte moss *Physcomitrella patens* also has only one DMP homolog. Interestingly, this protein is more similar to an angiosperm clade including AtDMP1 and AtDMP2 than to the algae or lycophyte orthologs. The lycophyte *Selaginella* has two, 67% identical DMP proteins that are most similar to a clade that splits into a small subclade formed by only three dicot proteins including AtDMP10 and a large subclade that includes 22 orthologs from monocotyledons. The four monocotyledonous plants *Brachypodium distachyon*, sorghum, maize and rice contain 11 to 16 DMP homologs, whereas in dicotyledons the number of DMPs varies from 5 (*Medicago truncatula*) to 13 (*Glycine max*). With the exception of AtDMP8, for each *A. thaliana* DMP protein the most closely related orthologous protein is found in *Arabidopsis lyrata*.

Organ- and age-dependent expression of DMP genes

In an earlier microarray-based screen for senescence-associated *Arabidopsis* membrane protein genes *DMP1* was found to be ~70fold upregulated in rosette leaf no. 6 between the fully expanded stage 6 weeks after sowing and a progressed senescence stage ~12 days later with approximately 75% of the leaf surface showing chlorophyll degradation (van der Graaff *et al.*, 2006). To investigate the age-dependent expression of all *DMP* genes in other *Arabidopsis* organs and tissues, the public expression data repositories are only of limited use because only four of the ten family members are represented on the Agilent 'Arabidopsis 2' and Affymetrix 'ATH1' microarrays (*DMP1*, -2, -3, -9 and *DMP1*, -2, -4, -9, respectively). We therefore investigated the expression of all *DMP* genes by semi-quantitative RT-PCR in young (20 DAS), mature (34 DAS) and senescing rosette leaves (51 DAS), green and senescing cauline leaves, green and senescent siliques, young and old stems and in flowers and roots (Fig. 4). *SAG12* was used as senescence marker and *ACT2* as internal control.

DMP1 expression increases massively during senescence in rosette leaves, cauline leaves and siliques following the same expression pattern as *SAG12*. *DMP1* expression was also detected in roots, thus confirming microarray data (van der Graaff *et al.*, 2006; Winter *et al.*, 2007) where

Chapter 1

DMP1 was found to be expressed in senescing rosette leaves and roots. Although expressed at a much lower level than *DMP1*, *DMP3* and *-4* are also upregulated in senescing rosette leaves, cauline leaves and siliques which might indicate a similar or overlapping function during senescence. However, no transcriptional upregulation was detected for *DMP1*, *-3*, *-4* and *SAG12* in old stems, indicating that stems might not undergo a senescence program comparable to those in leaves and siliques which have several features in common on the transcriptional level (Wagstaff *et al.*, 2009). *DMP3* and *-4* transcripts were additionally detected in roots and flowers respectively. Whereas *DMP2*, *-6* and *-7* were detected in all organs tested, *DMP8*, *-9* and *-10* were detected exclusively in flowers. *DMP5* could not be detected in any organ tested. Table 1 shows an overview of the expression and localization data presented below for all DMP proteins.

Unexpectedly, double bands of variable intensity were obtained with *DMP6* and *-7* in all organs tested. Sequencing of these bands showed that both *DMP6* bands were specific amplicates, the lower band lacking nucleotides 89 to 169, which would lead to a protein lacking 27 amino acids, from position 30 to 56 (Fig. S1). No intron-exon borders are present at these positions which would indicate an alternative splicing leading to two different proteins. However, perfect consensus intron/exon boundaries exist at these positions on the complementary, non-coding DNA strand, suggesting that transcripts might be synthesized in the antisense orientation. The neighboring gene downstream of *DMP6*, *At5g46100*, encoding a protein of unknown function, is located on the opposite strand and the stop codons of the *DMP6* and *At5g46100* ORFs are separated by only 184 bp. The sequence of *At5g46100* full length transcripts is not known, but it is conceivable that antisense transcripts of *DMP6* derive from this gene. Further investigations are required to show the presence of *DMP6* antisense transcripts in the cell which might have a regulatory function on *DMP6*.

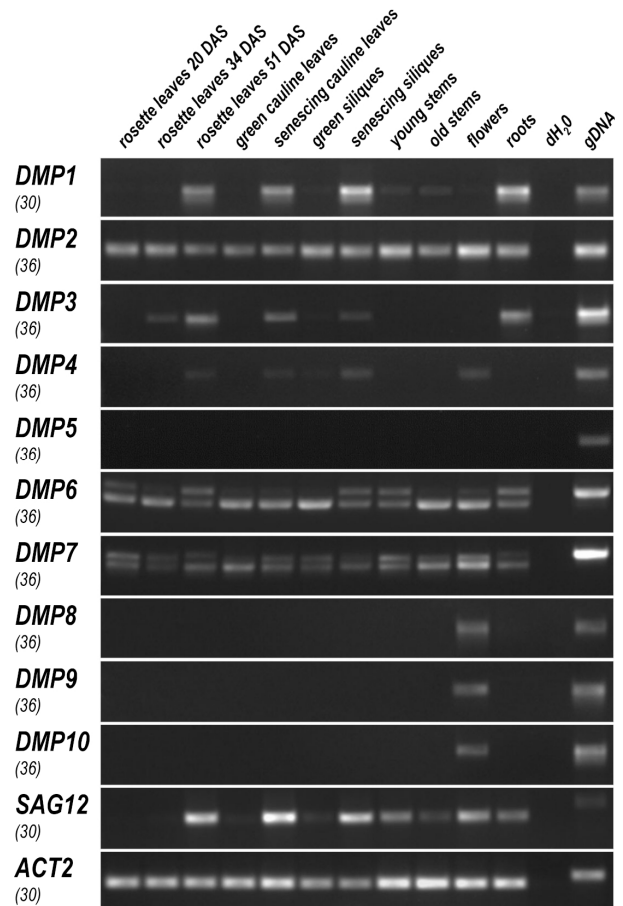


Figure 4: Semi-quantitative RT-PCR expression analysis of *DMP1* to *-10* in rosette leaves (20, 34 and 51 DAS), green and senescing cauline leaves, green and senescing siliques, young and old stems, flowers and roots. *SAG12* was used as senescence maker and *ACT2* as internal control. Numbers in brackets on the left side indicate the number of PCR cycles. The water control reactions were performed without cDNA or genomic DNA (gDNA). The gDNA reaction served as positive control and as size reference.

Chapter 1

Table 1. Expression data, promoter activities and subcellular localization of DMP fusion proteins.

	Semi-quantitative RT-PCR	Tissue specificity (<i>DMP_{pro}:uidA</i> fusions)	Subcellular localization
<i>DMP1</i>	senescing rosette and cauline leaves; senescing siliques; roots; stems	irregular patches on senescing rosette and cauline leaves; silique dehiscence and abscission zones; senescing silique wall; roots	tonoplast; ER
<i>DMP2</i>	all organs tested	stomata and vascular tissue of leaves, siliques, stems and sepals; roots; floral organ abscission zone	tonoplast; ER
<i>DMP3</i>	senescing rosette and cauline leaves; senescing siliques; roots	regular patches on senescing rosette and cauline leaves; root hairs	ER
<i>DMP4</i>	senescing rosette and cauline leaves; senescing siliques; flowers	local patches on senescing rosette and cauline leaves; vascular tissue of the whole plant; anthers; floral organ abscission zone	tonoplast
<i>DMP5</i>	not detected	not detected	ER
<i>DMP6</i>	all organs tested	root hairs	tonoplast
<i>DMP7</i>	all organs tested	vasculature of leaves, sepals, petals and roots; silique and floral organ abscission zones, silique tips	ER
<i>DMP8</i>	flowers	not detected	tonoplast; ER
<i>DMP9</i>	flowers	pollen	tonoplast; ER
<i>DMP10</i>	flowers	not detected	not detected

In the case of *DMP7*, the upper band was shown to be an unspecific amplificate. Optimized PCR conditions failed to improve specificity. *DMP7* is the only *DMP* gene predicted to contain two short introns. However, sequencing of the lower band showed that only the second intron is spliced, which leads to a protein of 200 amino acids in length with 4 predicted transmembrane spans (Fig. 1). Translation of the predicted processed transcript would lead to a shorter protein of 165 amino acids with a very divergent N-terminal part lacking the two first transmembrane spans (Fig. S1). No shorter transcripts deriving from the removal of two introns which would lead to such a protein were detected by PCR. These data suggest that *DMP6* and *DMP7* are present in the cells as unique proteins without isoforms.

The RT-PCR experiments indicate striking differences in the transcription patterns of *DMP* genes: *DMP1* and to a certain extent *DMP3* and *-4* show senescence-specific expression. *DMP2*, *-6* and *-7* are ubiquitously expressed in the organs tested and *DMP8*, *-9* and *-10* are expressed only in floral organs. To obtain a more detailed picture of the tissue-specificity of the *DPMs*, transcriptional fusions of the ten *DPM* promoters with the GUS coding sequence were constructed. The size of the promoter regions amplified to generate the ten *DMP_{pro}:uidA* constructs are listed in supplementary Table S1. Rosette and cauline leaves, siliques, stems, flowers and roots of homozygous transgenic *DMP1-10_{pro}:uidA* plants were systematically subjected to GUS staining. As GUS staining turned

out to be inefficient in yellow, late senescent leaves, leaves at the onset of senescence were used for these experiments.

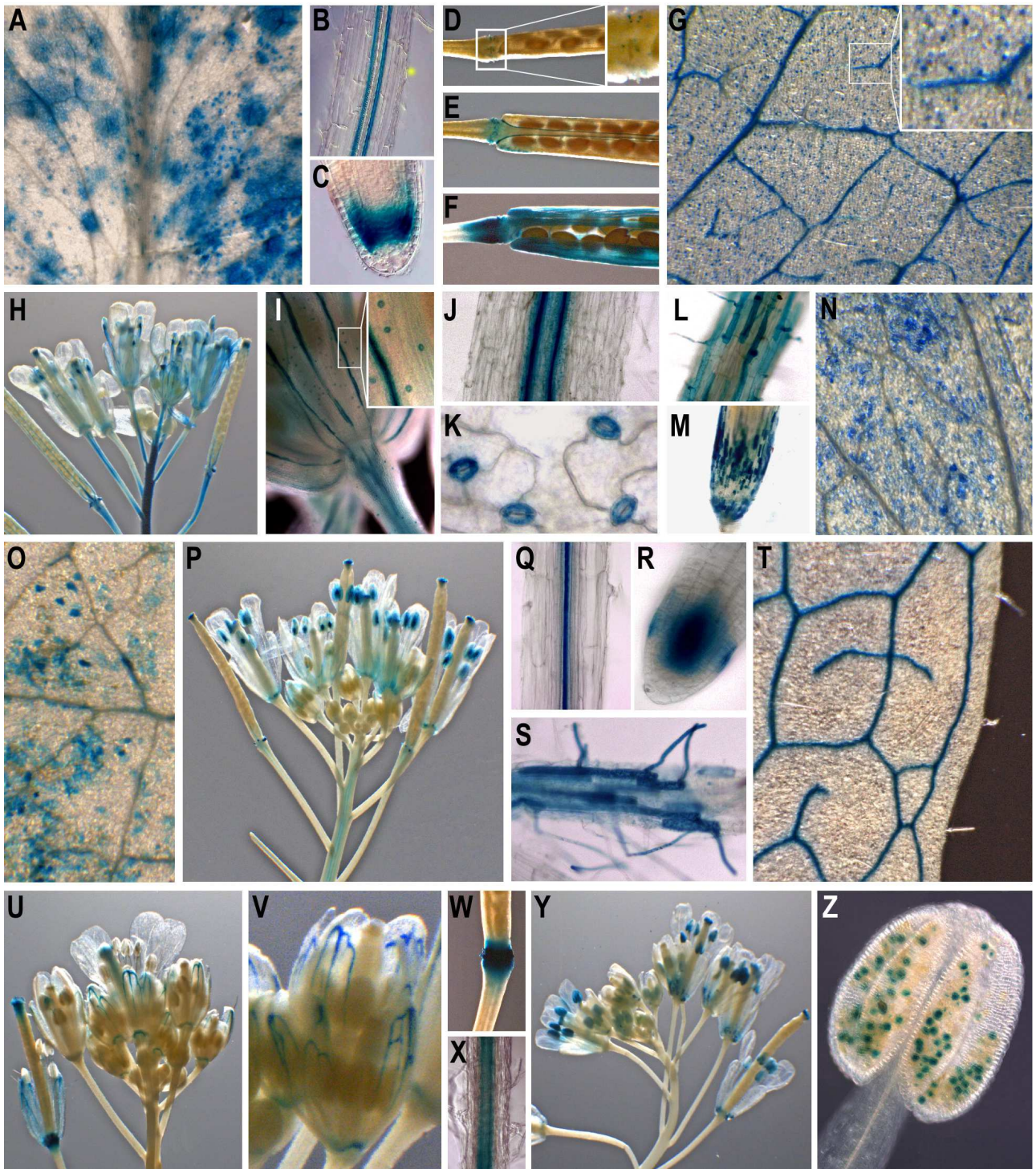


Figure 5: Histochemical analysis of GUS expression in transgenic *Arabidopsis thaliana* plants carrying DMP promoter:GUS fusions. *DMP1_{pro}:uidA* expression in mature/early senescing rosette leaf (A), root (B), root tip (C) and during silique development (D-F). *DMP2_{pro}:uidA* expression in vascular tissues and stomata of leaves (G, K), sepals and stems (H,I), siliques (H), and expression in root (J). *DMP3_{pro}:uidA* expression in root hairs (L), root tip (M) and mature/early senescing rosette leaves (N). *DMP4_{pro}:uidA* expression in mature/early senescing rosette leaf (O), inflorescence (P), root (Q) and root tip (R). Expression of *DMP6_{pro}:uidA* in root hairs (S). *DMP7_{pro}:uidA* expression in vasculature of leaves (T), inflorescence (U, V), silique tip (U,W) and root vasculature (X). *DMP9_{pro}:uidA* expression in floral organs (Y) is restricted to pollen (Z). Note the promoter activity of *DMP2*, 4 and 7 in the floral organ abscission zone (H, P, U and V).

Chapter 1

DMP1_{pro} was shown to be active in mature/early senescing rosette leaves (Fig. 5A), in the phloem bundles of roots (Fig. 5B), in root tips (Fig. 5C) and in siliques (Fig. 5D-F) confirming the expression data. Interestingly, the expression in leaves is restricted to tissue patches varying in size and staining intensity, but tends to be associated with vascular tissue. This expression pattern is somewhat reminiscent of patterns observed in lesion mimic mutants (Morita-Yamamuro *et al.*, 2005). It was observed in all transgenic plants tested and was reproduced over 3 generations. A comparable pattern was observed in senescing cauline leaves (data not shown). In siliques, the promoter exhibits a senescence-associated activity. It is weakly active in little patches at the abscission zone of young fully expanded siliques (Fig. 5D), becomes more active upon development at the abscission and dehiscence zones (Fig. 5E) and is strongly active in all tissues of senescing and dehiscent siliques with the exception of the seeds (Fig. 5F).

Expression of *DMP2_{pro:uidA}* was detected in all organs tested, reflecting the data obtained by semi-quantitative RT-PCR. The vascular tissues and stomata of leaves (Fig. 5G), siliques (Fig. 5H), sepals (Fig. 5I-K) and stems (Fig. 5H-I), the floral organ abscission zone (Fig. 5H) and the phloem bundles of roots (Fig. 5J) exhibited *DMP2* promoter activity. The promoter of *DMP3* is weakly active in mature/early senescing rosette leaves and exhibits a quite regular patchy pattern over the whole leaf area, but is never associated with vascular tissue or stomata (Fig. 5N). The same pattern was observed in cauline leaves (data not shown). *DMP3_{pro}* was also found to be expressed in root hairs (Fig. 5L) and in root tips (Fig. 5M). Promoter activity of *DMP4* was hardly detectable in mature/early senescing rosette and cauline leaves. It was observed at some local spots and in vascular tissue (Fig. 5O). Weak promoter activity of *DMP4* was observed in some local spots of mature/early senescing rosette and cauline leaves and in vascular tissue throughout the whole plant (Fig. 5O, P). Stronger *DMP4* expression was observed in anthers, the floral organ abscission zone (Fig. 5P), in stele tissues of roots (Fig. 5Q) and in root tips (Fig. 5R). *DMP6_{pro}* expression was detected exclusively in root hairs (Fig. 5S), whereas by RT-PCR low *DMP6* expression was detected also in other organs (Fig. 4). In *DMP7_{pro:uidA}* transgenic plants, GUS staining was observed in vascular tissues of leaves, sepals, petals (Fig. 5T-V) and roots (Fig. 5X), in the floral organ abscission zone (Fig. 5U-V) and in the tip and abscission zone of siliques (Fig. 5U, W). *DMP9_{pro}* activity was exclusively detected in pollen (Fig. 5Y-Z). The GUS staining observed at the base of floral organs on Fig. 5Y are pollen grains and not staining of floral organ abscission zones. No activity could be detected with *DMP5_{pro}*, *DMP8_{pro}* and *DMP10_{pro}* in any of the tested organs, although low levels of *DMP8* and *10* transcripts were detected by RT-PCR in flowers. Altogether, these data indicate a wide spectrum of expression patterns and levels of the *DMP* genes, which excludes functional redundancy of DMP proteins in most tissues.

Subcellular localization of DMP proteins

To test if the DMP proteins target to the same intracellular membrane in the different tissues, the subcellular localization was investigated. DMP protein localization was first estimated by using the plant membrane protein database ARAMEMNON (release 6.1) which uses up to 17 individual prediction programs to generate consensus predictions (<http://aramemnon.botanik.uni-koeln.de>). The consensus localization prediction method indicates a weak to moderate chloroplast targeting signal for six DMP proteins (DMP1, -3, -5, -7, -8 and -9). The four other proteins (DMP2, -4, -6, -10) are predicted to enter the secretory pathway with weak to moderate probability. The absence of clear target signals led us to investigate the subcellular localization of all DMP proteins by using eGFP as reporter. C-terminal (DMP-eGFP) fusions expressed from the CaMV 35S promoter were generated and investigated both in transiently infiltrated tobacco epidermal cells and stably transformed *Arabidopsis* plants. For the proteins which did not lead to fluorescence signals (DMP6, -7 and -10), N-terminal fusion proteins (eGFP-DMP) were generated and investigated in transiently infiltrated tobacco epidermal cells. Different fluorescence markers localizing to the tonoplast (TPK1-mRFP), the ER (mCherry-HDEL) and the plasma membrane (mRFP-MUB2) were used in colocalization experiments to confirm subcellular localization of the different DMP-eGFP and eGFP-DMP fusion proteins (Fig. 6). DMP10 was the only protein which did not lead to any fluorescence signal when fused either N-terminally or C-terminally to eGFP. DMP3-eGFP, DMP5-eGFP and DMP7-eGFP clearly labeled the ER as shown in colocalization experiments with the ER marker mCherry-HDEL (Fig. 6. C, E, G). DMP1-eGFP, DMP2-eGFP, DMP4-eGFP, eGFP-DMP6, DMP8-eGFP and DMP9-eGFP labeled the tonoplast as shown with the tonoplast marker TPK1-mRFP in colocalization experiments (Fig. 6A, B, D, F, H and I respectively). To unambiguously distinguish between tonoplast and plasma membrane localization, all proteins were also coexpressed with a plasma membrane marker (mRFP-MUB2) in tobacco epidermal cells. As an example, coexpression of DMP1-eGFP and mRFP-MUB2 is shown in Fig. 6J. Moreover, specific features of the tonoplast, namely the labeling of transvacuolar strands (Reisen *et al.*, 2005; Ruthardt *et al.*, 2005), tonoplastic invaginations (termed "bulbs" by Saito *et al.*, 2002) and the engulfment of the nucleus and plastids on the side facing the vacuole confirm tonoplast localization (see legend of Fig. 6). However, we observed that subcellular localization of DMP2-eGFP, DMP8-eGFP and DMP9-eGFP was variable. Two to three days after infiltration we observed localization of these three proteins in the ER and in some vesicles of approximately 1 μm diameter which could be Golgi bodies, transvacuolar Golgi network (TGN) or prevacuolar compartment (PVC) (Fig. 6L). After five days, the fluorescent proteins clearly labeled the tonoplast (Fig. 6B, H, I). These changes in subcellular localization may reflect slow movement of these fusion proteins through the secretory pathway but may also reflect mistargeting due to overexpression or the use of fusion proteins.

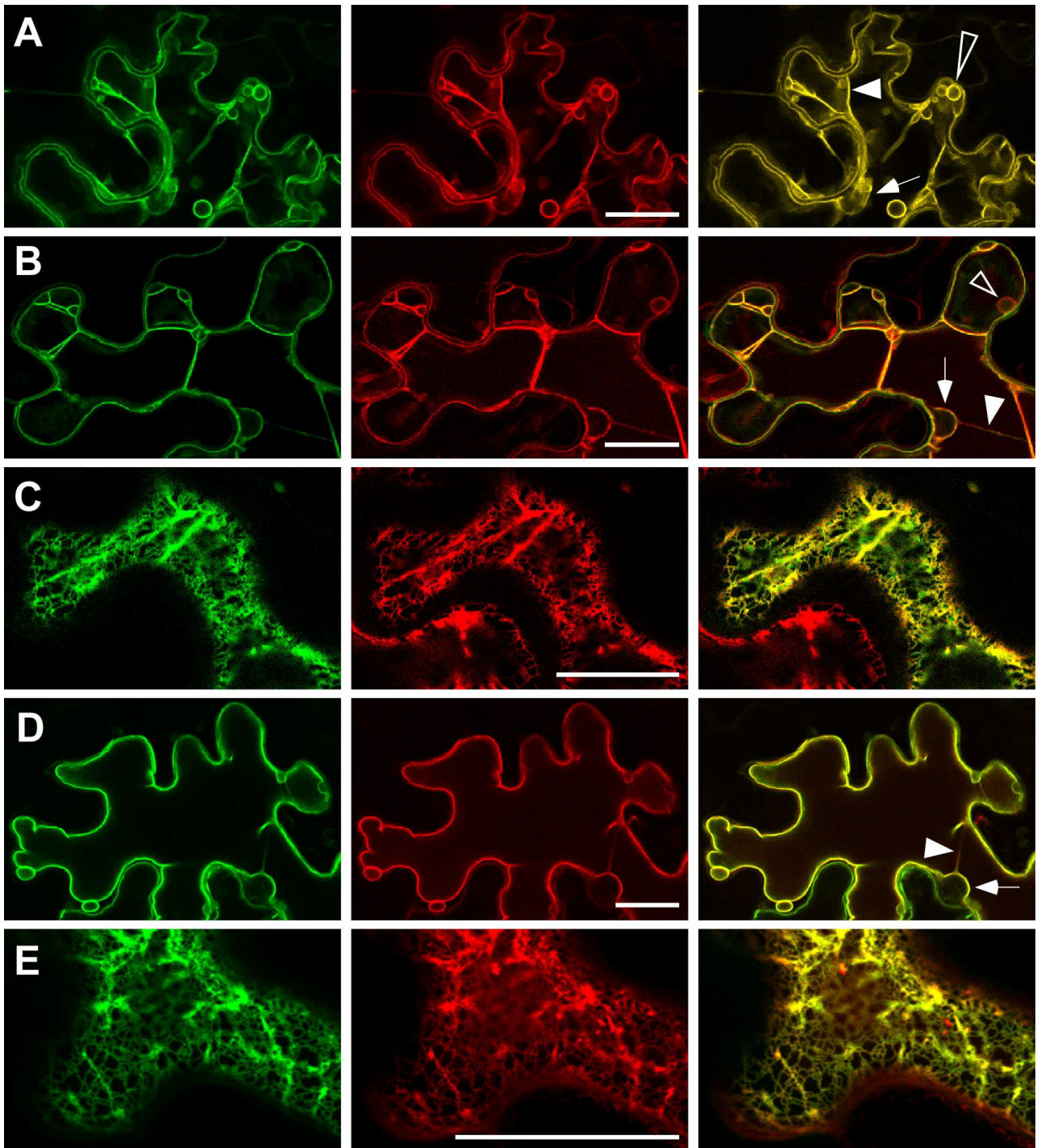


Figure 6. Colocalisation experiments between *Arabidopsis* DMP proteins fused either N- or C-terminally to eGFP and different membrane markers fused to mRFP or mCherry. (A): Colocalisation of DMP1-eGFP on the left panel (lp) with the tonoplast marker TPK1-mRFP on the middle panel (mp) and the overlay of both fluorescence signals on the right panel (rp). (B): DMP2-eGFP (lp), TPK1-mRFP (mp) and overlay (rp). (C): DMP3-eGFP (lp), mCherry-HDEL (endoplasmic reticulum marker) (mp) and overlay (rp). (D): DMP4-eGFP (lp), TPK1-mRFP (mp) and overlay (rp). (E): DMP5-eGFP (lp), mCherry-HDEL (mp) and overlay (rp). (F): eGFP-DMP6 (lp), TPK1-mRFP (mp) and overlay (rp). (G): eGFP-DMP7 (lp), mCherry-HDEL (mp) and overlay (rp). (H): DMP8-eGFP (lp), TPK1-mRFP (mp) and overlay (rp). (I): DMP9-eGFP (lp), TPK1-mRFP (mp) and overlay (rp). (J): Coexpression of DMP1-eGFP and the plasma membrane marker mRFP-MUB2. (K): DMP8-eGFP fluorescence pattern in stably transformed *Arabidopsis*. (L) DMP8-eGFP fluorescence pattern shown three days after infiltration. All fusion proteins are expressed from the CaMV 35S promoter. All images were taken in transiently infiltrated tobacco epidermal cells with the exception of (K). Filled arrowheads (A, B, D, F, H, I) show transvacuolar strands, open arrowheads (A, B, F, J) show tonoplast invaginations called “bulbs”, arrows (A, B, D, F, H) indicate the nucleus and the open circle (L) indicates a small vesicle. Scale bars are 30 μm .

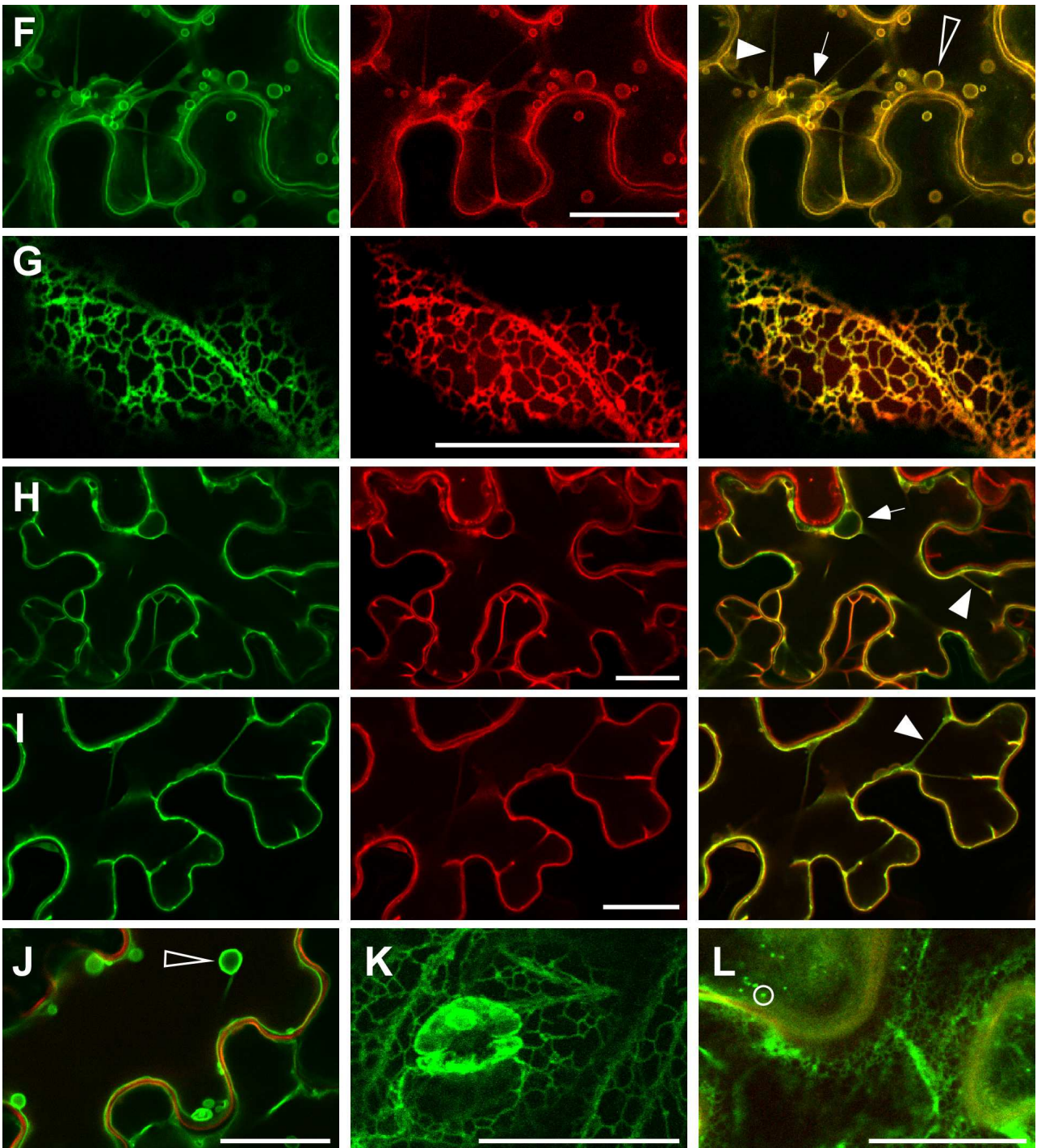


Figure 6. Continued.

However overexpression of DMP2-eGFP, DMP8-eGFP and DMP9-eGFP in stably transformed *Arabidopsis* plants led to signals labeling the ER membrane and not the tonoplast as shown for DMP8-eGFP in Fig. 6K. Moreover, overexpression of DMP1-eGFP in stably transformed *Arabidopsis* plants showed that, besides strongest fluorescence signals in the tonoplast, a fraction of the fusion proteins was also observed in the ER (data not shown), whereas in tobacco infiltrated leaves only the tonoplast was labeled at any time after infiltration (Fig. 6A). Investigation of

Chapter 1

DMP1-eGFP expressed from the native promoter in stably transformed *Arabidopsis* shed more light on this dual localization: depending on the cell type and the developmental stage DMP1-eGFP targets either to the ER or the tonoplast. A tissue- and developmental stage-dependent targeting may also explain the different or dual localizations observed upon overexpression of DMP2-eGFP, DMP8-eGFP and DMP9-eGFP in tobacco and *Arabidopsis*.

In summary, these observations suggest that none of the DMP proteins are targeted to chloroplasts as is predicted for some of them, but predominantly locate at two different membranes: the tonoplast and the ER.

Discussion

AtDMP1 was discovered in a screen for senescence-associated genes in *Arabidopsis thaliana*. It encodes a novel, unknown membrane protein with four TM spans that has no similarity to any functionally assigned protein domain in any organism. The DMP proteins have only short N- and C-terminal cytoplasmic ends and loops protruding from the membrane and they have no similarity with transporters or channels. A search for related sequences revealed that *AtDMP1* belongs to a strictly plant-specific gene family which is represented in all green algae and green plants for that ESTs or genome sequences are available at NCBI. A TBLASTN search with *AtDMP1* and *AtDMP9* proteins against the NCBI EST database identifies in addition to the 119 DMP sequences of the 14 species represented in the cladogram (Fig. 3) 100 orthologs in 42 other plants (data not shown).

In *Arabidopsis thaliana* and *Arabidopsis lyrata* some DMP proteins occur as closely related pairs (Fig. 3; *AtDMP1/2* - Aly_302570/302573; *AtDMP4/6* - Aly_702582/7.3458; *AtDMP3/5* - Aly_7.1852/300181; *AtDMP8/9*). The corresponding gene pairs supposedly result from gene duplications that must have happened before the separation of *A. thaliana* and *A. lyrata*, which took place approximately 5 million years ago (reviewed in Clauss & Koch, 2006). *A. lyrata* has an ortholog of *AtDMP9*, but not of *AtDMP8*. *AtDMP9* and Aly_7.1 have the same length (244 aa) and are 98% identical, whereas *AtDMP8* and *AtDMP9* are only 90% identical and *AtDMP8* is one amino acid shorter. This suggests that either the *AtDMP8* ortholog in *A. lyrata* was lost after the speciation of *A. thaliana* and *A. lyrata*, or *AtDMP8* resulted from an *AtDMP9* duplication after the separation from *A. lyrata* and its sequence evolved very quickly due to a lack of selective pressure. It argues for the latter scenario that a *DMP8* ortholog is dispensable for *A. lyrata*, no *DMP8* expression was detected in *A. thaliana* by semi-quantitative RT-PCR and no *AtDMP8* promoter activity was detected in any plant tissue. On the other hand, *A. lyrata* has two orthologs of *AtDMP5* (Aly_300181 and Aly_5.1; Fig. 3). With the same length of 219 amino acids and only 5 substitutions, four of which are conservative, Aly_300181 is 98% identical to *AtDMP5*. The second

Chapter 1

ortholog Aly_5.1 is lacking 10 amino acids within the N-terminus and 18 amino acids from the 2nd TM span and has a 19 amino acid insertion upstream of the penultimate TM span, but is otherwise 95% identical to Aly_300181. This suggests that either Aly_5.1 derived from Aly_300181 by duplication after the separation of *A. thaliana* and *A. lyrata* and subsequently mutated rapidly in the absence of selective pressure, or the Aly_5.1 ortholog in *A. thaliana* was deleted.

The RT-PCR experiments showed that *DMP1* and, at much lower levels, *DMP3* and *DMP4* are transcriptionally activated in senescing rosette and cauline leaves and senescing siliques (see Table 1 for overview). Interestingly, only these three genes exhibit a patchy expression pattern in mature/early senescing leaves. *DMP1* is highly active in patches variable in size and shape and often associated with vascular tissue whereas *DMP3* is weakly expressed in more regular patches not associated with vascular tissue and *DMP4* is only faintly expressed in some local spots and in vasculature. These patchy expression patterns possibly indicate partially overlapping tissue-specificity and related functions of *DMP1*, -3 and -4 during leaf senescence.

Furthermore, five out of seven *DMP* promoters led to detectable GUS expression in tissues undergoing different types of programmed cell death. *DMP1* is expressed in silique dehiscence and abscission zones, *DMP7* in the silique abscission zone and *DMP2*, *DMP4* and *DMP7* in the floral organ abscission zone. *DMP8* and *DMP10* transcription was detected by RT-PCR in flowers, but no promoter activity was observed in transgenic *DMP8_{pro:uidA}* and *DMP10_{pro:uidA}* *Arabidopsis* plants. One possible explanation for this discrepancy is that the 920 bp *DMP8* and 2021 bp *DMP10* fragments upstream of the ATG start codons do not represent the complete promoter, as it is possible that downstream regions also contribute to transcription regulation. Indeed, downstream regulatory sequences were reported for several *Arabidopsis* genes (Curie *et al.*, 1993; Larkin *et al.*, 1993; Moreno-Fonseca & Covarrubias, 2001). A discrepancy between the RT-PCR experiment and the promoter activity was also observed with *DMP6*. As discussed above, it cannot be excluded that the 1954 bp promoter fragment lacks regulatory sequences. However, in case of the *DMP6* gene it is tempting to speculate that its activity is modulated by the formation of double stranded RNA with the 3' end of the *At5g46100* mRNA. *DMP5* expression could neither be detected by RT-PCR in any *Arabidopsis* tissue nor by promoter-GUS fusions. It remains unclear if *DMP5* is expressed at levels below the detection limit, becomes only conditionally activated or if it is non-functional.

The investigation of the subcellular localization of the different DMP-eGFP and eGFP-DMP fusion proteins expressed from the CaMV 35S promoter showed predominant localization at two membranes in the cell: the tonoplast and the ER. *DMP3*-eGFP, *DMP5*-eGFP and eGFP-*DMP7* were always retained in the ER and never decorated the tonoplast in tobacco epidermal cells and *Arabidopsis*. These three proteins share a di-arginine motif three residues behind the last TM domain and *DMP3* and *DMP5* contain an additional di-arginine motif at their very C-termini (Fig.

Chapter 1

1). Di-arginine motifs have been reported to function as ER retention/retrieval signals at cytosolic N- and C-termini and in cytosolic loops of plant membrane proteins (Boulaflous *et al.*, 2009; Michelsen *et al.*, 2005; Schutze *et al.*, 1994; Teasdale & Jackson, 1996). However, to clarify the contribution of the di-arginine and other di-basic motifs in targeting DMP3, -5 and -7 to the ER requires mutant analyses, as similar motifs also occur in other DMP proteins that do not localize in the ER.

When expressed by the CaMV 35S promoter in tobacco epidermal cells, DMP1-eGFP, DMP2-eGFP, DMP4-eGFP, DMP6-eGFP, DMP8-eGFP and DMP9-eGFP enter the secretory pathway and decorate the vacuolar membrane. DMP1-eGFP, DMP4-eGFP and DMP6-eGFP exclusively accumulate in the tonoplast whereas DMP2-eGFP, DMP8-eGFP and DMP9-eGFP apparently move slowly along the secretory pathway, labeling first the ER and later the tonoplast. In stably transformed *Arabidopsis*, these proteins accumulate exclusively in the ER. whereas DMP1-eGFP show dual ER/tonoplast localization. Expression of DMP1-eGFP from the native promoter in transgenic *Arabidopsis* revealed that subcellular localization is cell type- and development-dependent. Thus, it is conceivable that dual localization of DMP1-eGFP, DMP2-eGFP, DMP8-eGFP and DMP9-eGFP in the same cell, temporal changes in localization and discrepancies between localization in tobacco and *Arabidopsis* may reflect intrinsic properties of the proteins. The use of the DMP gene native promoters for fusion protein expression and immunogold labeling of the native DMP proteins may be necessary to unequivocally determine the intracellular localization. The function of the DMP proteins at the ER membrane and the tonoplast is still elusive, but their exclusive and ubiquitous occurrence in green plants indicates a role in plant-specific processes. Several DMP proteins are expressed in senescing organs (*DMP1*, -3, -4) or tissues that will stall later in development (*DMP1*, -2, -4, -7). These expression patterns strongly suggest an involvement of several *DMPs* in various programmed cell death processes including senescence, dehiscence and abscission. However, the activities of several *DMP* promoters in various tissues lacking programmed cell death indicate that DMP proteins are also involved in other cellular processes. Further investigations using mutants and transgenic plants with altered *DMP* expression are required to elucidate the function of the *DMPs*.

Acknowledgements

The binary vectors pUTkan3, pGTkan3 and pPTkan3 were kindly provided by Guillaume Pilot (Virginia Tech, Blacksburg). pA7 was a gift of Karin Czempinski (University of Potsdam, Germany) and TPK1-mRFP1/pPily a gift of Dirk Becker (University of Würzburg, Germany). A.K. and this project were supported by the priority programm 1108 of the Deutsche Forschungsgemeinschaft (DFG).

References

- Bassham D.C. (2007) Plant autophagy--more than a starvation response. *Current Opinion in Plant Biology*, **10**, 587-593.
- Bendahmane A., Querci M., Kanyuka K., Baulcombe D.C. (2000) Agrobacterium transient expression system as a tool for the isolation of disease resistance genes: application to the Rx2 locus in potato. *Plant Journal*, **21**, 73-81.
- Boulaflous A., Saint-Jore-Dupas C., Herranz-Gordo M.C., Pagny-Salehabadi S., Plasson C., Garidou F., Kiefer-Meyer M.C., Ritzenthaler C., Faye L., Gomord V. (2009) Cytosolic N-terminal arginine-based signals together with a luminal signal target a type II membrane protein to the plant ER. *BMC Plant Biology*, **9**, 144.
- Clauss M.J., Koch M.A. (2006) Poorly known relatives of *Arabidopsis thaliana*. *Trends in Plant Science*, **11**, 449-459.
- Clough S.J., Bent A.F. (1998) Floral dip: a simplified method for *Agrobacterium*-mediated transformation of *Arabidopsis thaliana*. *Plant Journal*, **16**, 735-743.
- Curie C., Axelos M., Bardet C., Atanassova R., Chaubet N., Lescure B. (1993) Modular organization and development activity of an *Arabidopsis thaliana* EF-1 alpha gene promoter. *Molecular & General Genetics*, **238**, 428-436.
- Downes B.P., Saracco S.A., Lee S.S., Crowell D.N., Vierstra R.D. (2006) MUBs, a family of ubiquitin-fold proteins that are plasma membrane-anchored by prenylation. *The Journal of Biological Chemistry*, **281**, 27145-27157.
- Downing W.L., Mauxion F., Fauvarque M.O., Reviron M.P., de Vienne D., Vartanian N., Giraudat J. (1992) A *Brassica napus* transcript encoding a protein related to the Kunitz protease inhibitor family accumulates upon water stress in leaves, not in seeds. *Plant Journal*, **2**, 685-693.
- Frelet-Barrand A., Kolukisaoglu H.Ü., Plaza S., Rüffer M., Azevedo L., Hörtensteiner S., Marinova K., Weder B., Schulz B., Klein M. (2008) Comparative mutant analysis of *Arabidopsis* ABCC-type ABC transporters: AtMRP2 contributes to detoxification, vacuolar organic anion transport and chlorophyll degradation. *Plant and Cell Physiology*, **49**, 557-569.
- Hill J. (1980) The Remobilization of Nutrients from Leaves. *Journal of Plant Nutrition*, **2**, 407-444.
- Himelblau E., Amasino R.M. (2001) Nutrients mobilized from leaves of *Arabidopsis thaliana* during leaf senescence. *Journal of Plant Physiology*, **158**, 1317-1323.
- Hong B., Ichida A., Wang Y., Gens J.S., Pickard B.G., Harper J.F. (1999) Identification of a calmodulin-regulated Ca²⁺-ATPase in the endoplasmic reticulum. *Plant Physiology*, **119**, 1165-1176.
- Larkin J.C., Oppenheimer D.G., Pollock S., Marks M.D. (1993) *Arabidopsis* GLABROUS1 Gene Requires Downstream Sequences for Function. *The Plant Cell*, **5**, 1739-1748.
- Larkin M.A., Blackshields G., Brown N.P., Chenna R., McGettigan P.A., McWilliam H., Valentin F., Wallace I.M., Wilm A., Lopez R., Thompson J.D., Gibson T.J., Higgins D.G. (2007) Clustal W and Clustal X version 2.0. *Bioinformatics*, **23**, 2947-2948.
- Latz A., Becker D., Hekman M., Muller T., Beyhl D., Marten I., Eing C., Fischer A., Dunkel M., Bertl A., Rapp U.R., Hedrich R. (2007) TPK1, a Ca²⁺-regulated *Arabidopsis* vacuole two-pore K(+) channel is activated by 14-3-3 proteins. *Plant Journal*, **52**, 449-459.

Chapter 1

- Lu Y.P., Li Z.S., Drozdowicz Y.M., Hortensteiner S., Martinoia E., Rea P.A. (1998) AtMRP2, an Arabidopsis ATP binding cassette transporter able to transport glutathione S-conjugates and chlorophyll catabolites: functional comparisons with AtMRP1. *The Plant Cell*, **10**, 267-282.
- Michelsen K., Yuan H., Schwappach B. (2005) Hide and run. Arginine-based endoplasmic-reticulum-sorting motifs in the assembly of heteromultimeric membrane proteins. *EMBO reports*, **6**, 717-722.
- Moreno-Fonseca L.P., Covarrubias A.A. (2001) Downstream DNA sequences are required to modulate Pvlea-18 gene expression in response to dehydration. *Plant Molecular Biology*, **45**, 501-515.
- Morita-Yamamuro C., Tsutsui T., Sato M., Yoshioka H., Tamaoki M., Ogawa D., Matsuura H., Yoshihara T., Ikeda A., Uyeda I., Yamaguchi J. (2005) The Arabidopsis gene CAD1 controls programmed cell death in the plant immune system and encodes a protein containing a MACPF domain. *Plant and Cell Physiology*, **46**, 902-912.
- Nelson B.K., Cai X., Nebenfuhr A. (2007) A multicolored set of in vivo organelle markers for colocalization studies in Arabidopsis and other plants. *Plant Journal*, **51**, 1126-1136.
- Noodén L.D., Guiamét J.J., John I. (1997) Senescence mechanisms. *Physiologia Plantarum*, **101**, 746-753.
- Otegui M.S., Noh Y.S., Martinez D.E., Vila Petroff M.G., Andrew Staehelin L., Amasino R.M., Guiamet J.J. (2005) Senescence-associated vacuoles with intense proteolytic activity develop in leaves of Arabidopsis and soybean. *Plant Journal*, **41**, 831-844.
- Reisen D., Marty F., Leborgne-Castel N. (2005) New insights into the tonoplast architecture of plant vacuoles and vacuolar dynamics during osmotic stress. *BMC Plant Biology*, **5**, 13.
- Ruthardt N., Gulde N., Spiegel H., Fischer R., Emans N. (2005) Four-dimensional imaging of transvacuolar strand dynamics in tobacco BY-2 cells. *Protoplasma*, **225**, 205-215.
- Saito C., Ueda T., Abe H., Wada Y., Kuroiwa T., Hisada A., Furuya M., Nakano A. (2002) A complex and mobile structure forms a distinct subregion within the continuous vacuolar membrane in young cotyledons of Arabidopsis. *Plant Journal*, **29**, 245-255.
- Schutze M.P., Peterson P.A., Jackson M.R. (1994) An N-terminal double-arginine motif maintains type II membrane proteins in the endoplasmic reticulum. *The EMBO Journal*, **13**, 1696-1705.
- Schwacke R., Schneider A., van der Graaff E., Fischer K., Catoni E., Desimone M., Frommer W.B., Flügge U.I., Kunze R. (2003) ARAMEMNON, a Novel Database for Arabidopsis Integral Membrane Proteins. *Plant Physiology*, **131**, 16-26.
- Teasdale R.D., Jackson M.R. (1996) Signal-mediated sorting of membrane proteins between the endoplasmic reticulum and the golgi apparatus. *Annual Review of Cell and Developmental Biology*, **12**, 27-54.
- Thomas H., Ougham H.J., Wagstaff C., Stead A.D. (2003) Defining senescence and death. *Journal of Experimental Botany*, **54**, 1127-1132.
- van der Graaff E., Schwacke R., Schneider A., Desimone M., Flügge U.I., Kunze R. (2006) Transcription analysis of Arabidopsis membrane transporters and hormone pathways during developmental and induced leaf senescence. *Plant Physiology*, **141**, 776-792.
- Wada S., Ishida H., Izumi M., Yoshimoto K., Ohsumi Y., Mae T., Makino A. (2009) Autophagy plays a role in chloroplast degradation during senescence in individually darkened leaves. *Plant Physiology*, **149**, 885-893.

Chapter 1

- Wagstaff C., Yang T.J., Stead A.D., Buchanan-Wollaston V., Roberts J.A. (2009) A molecular and structural characterization of senescing *Arabidopsis* siliques and comparison of transcriptional profiles with senescing petals and leaves. *Plant Journal*, **57**, 690-705.
- Winter D., Vinegar B., Nahal H., Ammar R., Wilson G.V., Provart N.J. (2007) An "Electronic Fluorescent Pictograph" browser for exploring and analyzing large-scale biological data sets. *PLoS ONE*, **2**, e718.
- Xiang C., Han P., Lutziger I., Wang K., Oliver D.J. (1999) A mini binary vector series for plant transformation. *Plant Molecular Biology*, **40**, 711-717.

Supporting Information

Table S1: Primers used for the amplification of the 10 *DMP* promoter regions. For each primer pair, the size of the promoter region amplified is indicated. The restriction sites are shown in boldface and the sequences corresponding to the promoter regions are put in uppercase.

Primer name	Sequence	Size of amplified promoter fragment
DMP1 _{pro} -F	5'- cgg tctaga GAGAACAAAATCCTCCGTATC-3'	2364 bp
DMP1 _{pro} -R	5'- aactgcag GAGCTTGAACCTTAGAGTTAG-3'	
DMP2 _{pro} -F	5'- gtg tacc CAACCGAAGATTTTGAAC TTG-3'	1945 bp
DMP2 _{pro} -R	5'- gtctgcag TTTTTTGTTCTTCTTTTGTA A-3'	
DMP3 _{pro} -F	5'- cgg tctaga AGT TGGACTCTTGCCAGTTTA-3'	685 bp
DMP3 _{pro} -R	5'- aactgcag ATTCTTTTCGTTTTTCTTATTT-3'	
DMP4 _{pro} -F	5'- gtg tacc GCTTTGGTTTTGTTGTATTGG-3'	1792 bp
DMP4 _{pro} -R	5'- gtctgcag ATCTTTGAAGTTGTTTCCTTTG-3'	
DMP5 _{pro} -F	5'- gtg tacc CGCAATTTTCTTCAACCGCTG-3'	632 bp
DMP5 _{pro} -R	5'- gtctgcag CTTTTTAGTTTTGATTCTTTTC-3'	
DMP6 _{pro} -F	5'- gtg tacc TGATCTAAACTAGTGTTC AAC-3'	1954 bp
DMP6 _{pro} -R	5'- gtctgcag AATACTCGAGATTC AAATCTC-3'	
DMP7 _{pro} -F	5'- gtg tacc CTTTGGATTTGTGAATAAAAC-3'	1844 bp
DMP7 _{pro} -R	5'- gtctgcag CTTCAATTGTTTTTTCGTTAA-3'	
DMP8 _{pro} -F	5'- gtg tacc TTCCATCATTTCCTCAGCATC-3'	920 bp
DMP8 _{pro} -R	5'- gtctgcag TCTCTCTGTGTTTTGTGACTC-3'	
DMP9 _{pro} -F	5'- gtg tacc CCTCAA AATTCGGATTAACAA-3'	1995 bp
DMP9 _{pro} -R	5'- gtctgcag TTTCGTGTGTTTCTCTCTGTT-3'	
DMP10 _{pro} -F	5'- gtg tacc CCTATTTTCATTTCA TTCAT-3'	2021 bp
DMP10 _{pro} -R	5'- gtctgcag TTTCGTAATTTGATCGGAAGTG-3'	

Table S2: Primers used for the amplification of the 10 *DMP* open reading frames (ORF) to generate the C-terminal DMP-eGFP fusions. All *DMPs* were amplified on gDNA. Thus, DMP7 contains an intron. For each primer pair, the size of the ORF amplified is indicated. The restriction sites are shown in boldface and the sequences corresponding to the open reading frames are put in uppercase.

Primer name	Sequence	Size of ORF amplified
DMP1 _{ORF_C} -F	5'- cgg tctaga ATGTCCGAAACTTCTTTGCTC-3'	621 bp
DMP1 _{ORF_C} -R	5'- aactgcag cGGCAGAGACCGAGGCTTTC-3	
DMP2 _{ORF_C} -F	5'- gtctcgag ATGTCGAAAACATTC AAAGCC-3'	552 bp
DMP2 _{ORF_C} -R	5'- gactagt ccTTTCATCTCGGAAGCATCATC-3'	
DMP3 _{ORF_C} -F	5'- cgg tctaga ATGTCTTCACCATCTTCCCTA-3'	639 bp
DMP3 _{ORF_C} -R	5'- aactgcag cACGACGACCCCGTCTCCGG-3'	
DMP4 _{ORF_C} -F	5'- gtctcgag ATGGAGATCAAAGTTGACGAA-3'	639 bp
DMP4 _{ORF_C} -R	5'- gactagt ccTTTACTAGAAAGTGGAAAACC-3'	
DMP5 _{ORF_C} -F	5'- gtctcgag ATGTCTGCCCTTCGGCTAAGA-3'	657 bp
DMP5 _{ORF_C} -R	5'- gactagt ccTCGGCGATCTACGCTACCGGT-3'	
DMP6 _{ORF_C} -F	5'- gtctcgag ATGGAGATTAATGTTGATGAA-3'	642 bp
DMP6 _{ORF_C} -R	5'- gactagt ccTTTAGCAGAGAGGGGAAAACC-3'	
DMP7 _{ORF_C} -F	5'- gtctcgag ATGGAGGAGACGAAGCAGTCA-3'	600 bp
DMP7 _{ORF_C} -R	5'- gactagt ccTTCTTTGGTAAGGGGAGATCC-3'	
DMP8 _{ORF_C} -F	5'- gtctcgag ATGGAGAAAACAGAGGAAAGC-3'	729 bp
DMP8 _{ORF_C} -R	5'- gactagt ccTGTAGACATGCATCCGACACC-3'	
DMP9 _{ORF_C} -F	5'- gtctcgag ATGGAGAAAACAGAGGAAAGC-3'	732 bp
DMP9 _{ORF_C} -R	5'- gactagt ccACCAGTCATGCAACCAAC-3'	
DMP10 _{ORF_C} -F	5'- gtctcgag ATGGAGGCGTTCATTAGA-3'	573 bp
DMP10 _{ORF_C} -R	5'- gactagt ccACGAATGTCTGAAATTCGGAT-3'	

Chapter 1

Table S3: Primers used for the amplification of the *DMP6*, -7 and -10 open reading frames (ORF) to generate the N-terminal eGFP-DMP fusions. All *DMPs* were amplified on gDNA. Thus, *DMP7* contains an intron. For each primer pair, the size of the ORF amplified is indicated. The restriction sites are shown in boldface and the sequences corresponding to the open reading frames are put in uppercase.

Primer name	Sequence	Size of ORF amplified
DMP6 _{ORF_N} -F	5'-acggt ctaga ATGGAGATTAATGTTGATGAA-3'	645 bp
DMP6 _{ORF_N} -R	5'-gagact cgag TCATTTAGCAGAGAGGGGAAA-3'	
DMP7 _{ORF_N} -F	5'-acggt ctaga ATGGAGGAGACGAAGCAGTCA-3'	600 bp
DMP7 _{ORF_N} -R	5'-gagact cgag TTATTCTTTGGTAAGGGGAGA-3'	
DMP10 _{ORF_N} -F	5'-acggt ctaga TGGAGGCGTCGTTCATTAGA-3'	576 bp
DMP10 _{ORF_N} -R	5'-gagact cgag TCAACGAATGTCTGAAATTCC-3'	

Table S4: Primers used for semi-quantitative RT-PCR analyses.

Primer name	Sequence	Size of amplificate (bp) cDNA/gDNA
DMP1 _{RT-PCR} -F	5'-ATGTCCGAAACTTCTTTGCTC-3'	624/624
DMP1 _{RT-PCR} -R	5'-TTAGGCAGAGACCGAGGCTTTC-3'	
DMP2 _{RT-PCR} -F	5'-ATGTGCGAAAACATTCAAAGCC-3'	555/555
DMP2 _{RT-PCR} -R	5'-TCATTTTCATCTCGGAAGCATC-3'	
DMP3 _{RT-PCR} -F	5'-ATGTCTTCACCATCTTCCCTA-3'	642/642
DMP3 _{RT-PCR} -R	5'-CTAACGACGACCCCGTCTCC-3'	
DMP4 _{RT-PCR} -F	5'-CAAAGTTGACGAAGGTCATCA-3'	627/627
DMP4 _{RT-PCR} -R	5'-CTAGAAAGTGGAAAACCAATC-3'	
DMP5 _{RT-PCR} -F	5'-ATGTCTGCCCTTCGGCTAAGA-3'	660/660
DMP5 _{RT-PCR} -R	5'-TCATCGGCGATCTACGCTACC-3'	
DMP6 _{RT-PCR} -F	5'-TAATGTTGATGAAGAAGCTGG-3'	630/630
DMP6 _{RT-PCR} -R	5'-GCAGAGAGGGGAAAACCAATA-3'	
DMP7 _{RT-PCR} -F	5'-ATGGAGGAGACGAAGCAGTCA-3'	603/691
DMP7 _{RT-PCR} -R	5'-TTATTCTTTGGTAAGGGGAGA-3'	
DMP8 _{RT-PCR} -F	5'-GAGTTTACACGACGACAACGA-3'	698/698
DMP8 _{RT-PCR} -R	5'-TGTAGACATGCATCCGACACC-3'	
DMP9 _{RT-PCR} -F	5'-GAGTTTACACGGCGACTCCGC-3'	701/701
DMP9 _{RT-PCR} -R	5'-ACCAGTCATGCAACCAACACCG-3'	
DMP10 _{RT-PCR} -F	5'-ATGGAGGCGTCGTTCATTAGA-3'	576/576
DMP10 _{RT-PCR} -R	5'-TCAACGAATGTCTGAAATTCC-3'	
SAG12 _{RT-PCR} -F	5'-GGCTATTGAAGGAGCAACACA-3'	397/544
SAG12 _{RT-PCR} -R	5'-CGCAGTTACTGCATGATCAAG-3'	
ACT2 _{RT-PCR} -F	5'-CTTCCCTCAGCACATTCCAG-3'	407/496
ACT2 _{RT-PCR} -R	5'-AACATTGCAAAGAGTTTCAAGGT-3'	

Chapter 1

Table S5. Gene designations used in Figure 3 and in the Phytozome database

Phytozome 4.1 designation	designation Fig. 3	Species	Notes
scaffold_300181.1.aly.16047632	Aly_300181	Arabidopsis lyrata	
scaffold_302570.1.aly.16041876	Aly_302570	Arabidopsis lyrata	
scaffold_302573.1.aly.16056165	Aly_302573	Arabidopsis lyrata	
fgenesh2_kg.5_288_AT3G02430.1.aly.16056908	Aly_5.1	Arabidopsis lyrata	
scaffold_602905.1.aly.16048741	Aly_6.1	Arabidopsis lyrata	
fgenesh2_kg.7_3458_AT5G39650.1.aly.16050206	Aly_7.1	Arabidopsis lyrata	
Al_scaffold_0007_1275.aly.16062784	Aly_7.1275	Arabidopsis lyrata	
fgenesh2_kg.7_1852_AT4G24310.1.aly.16044399	Aly_7.1852	Arabidopsis lyrata	
scaffold_800229.1.aly.16058422	Aly_7.3458	Arabidopsis lyrata	
scaffold_702582.1.aly.16046999	Aly_702582	Arabidopsis lyrata	
scaffold_702583.1.aly.16043620		Arabidopsis lyrata	77 aa*incomplete
AT1G09157.1.ath.15599734	At1g09157	Arabidopsis thaliana	
AT3G02430.1.ath.15612548	At3g02430	Arabidopsis thaliana	
AT3G21520.1.ath.15615052	At3g21520	Arabidopsis thaliana	
AT3G21550.1.ath.15615055	At3g21550	Arabidopsis thaliana	
AT4G18425.1.ath.15620827	At4g18425	Arabidopsis thaliana	
AT4G24310.1.ath.15621604	At4g24310	Arabidopsis thaliana	
AT4G28485.1.ath.15622164	At4g28485	Arabidopsis thaliana	
AT5G27370.1.ath.15626837	At5g27370	Arabidopsis thaliana	
AT5G39650.1.ath.15627581	At5g39650	Arabidopsis thaliana	
AT5G46090.1.ath.15628411	At5g46090	Arabidopsis thaliana	
Bradi1g57240.1.bdi.16478175	Bdi1g57240	Brachypodium distachyon	
Bradi1g61470.1.bdi.16478677	Bdi1g61470	Brachypodium distachyon	
Bradi1g67550.1.bdi.16479479	Bdi1g67550	Brachypodium distachyon	
Bradi2g13280.1.bdi.16482455	Bdi2g13280	Brachypodium distachyon	
Bradi2g13290.1.bdi.16482456	Bdi2g13290	Brachypodium distachyon	
Bradi2g16640.1.bdi.16482830	Bdi2g16640	Brachypodium distachyon	
Bradi2g46210.1.bdi.16486042	Bdi2g46210	Brachypodium distachyon	
Bradi2g56950.1.bdi.16487458	Bdi2g56950	Brachypodium distachyon	
Bradi3g10870.1.bdi.16489609	Bdi3g10870	Brachypodium distachyon	
Bradi3g37160.1.bdi.16492384	Bdi3g37160	Brachypodium distachyon	
Bradi3g43480.1.bdi.16493189	Bdi3g43480	Brachypodium distachyon	
evm.model.supercontig_113.49.cpa.16406060	Cpa_113	Carica papaya	
evm.model.supercontig_140.48.cpa.16408894	Cpa_140.48	Carica papaya	
evm.model.supercontig_16.78.cpa.16410115	Cpa_16.78	Carica papaya	
evm.TU.contig_32101.2.cpa.16430061	Cpa_32101	Carica papaya	
evm.model.supercontig_66.114.cpa.16424558	Cpa_66.114	Carica papaya	
evm.model.supercontig_83.95.cpa.16427239	Cpa_83	Carica papaya	
chromosome7_g13767.t1	Cr7g13767	Chlamydomonas reinhardtii	
Glyma02g08330.1.gma.16247392	Gm02g08330	Glycine max	
Glyma06g44280.1.gma.16265136	Gm06g44280	Glycine max	
Glyma07g32210.1.gma.16268470	Gm07g32210	Glycine max	
Glyma07g38360.1.gma.16269144	Gm07g38360	Glycine max	
Glyma07g38370.1.gma.16269145	Gm07g38370	Glycine max	
Glyma09g37210.1.gma.16277497	Gm09g37210	Glycine max	

Chapter 1

Glyma13g24350.1.gma.16291409	Gm13g24350	Glycine max	
Glyma13g28350.1.gma.16291863	Gm13g28350	Glycine max	
Glyma13g30840.1.gma.16292158	Gm13g30840	Glycine max	
Glyma16g27410.1.gma.16303080	Gm16g27410	Glycine max	
Glyma17g02400.1.gma.16304143	Gm17g02400	Glycine max	
Glyma18g11220.1.gma.16308557	Gm18g11220	Glycine max	
Glyma18g11430.1.gma.16308578		Glycine max	removed in phytozome 4.1
Glyma18g11450.1.gma.16308580	Gm18g11450	Glycine max	
AC158497_10.mtr.16440477	Mtr_2.1	Medicago truncatulata	
AC158497_16.mtr.16466061	Mtr_2.2	Medicago truncatulata	
CT027665_1.mtr.16433839	Mtr_5.1	Medicago truncatulata	
AC140025_43.mtr.16444166	Mtr_7.1	Medicago truncatulata	
AC146553_19		Medicago truncatulata	116 aa*incomplete
12001.m09137.osa.1162425	Os01g26896	Oryza sativa	
12001.m09139.osa.1162424	Os01g26904	Oryza sativa	
12001.m09163.osa.1162394	Os01g27120	Oryza sativa	
12001.m09254.osa.1162301		Oryza sativa	removed in phytozome 4.1
12001.m09361.osa.1162175	Os01g29240	Oryza sativa	
12001.m09365.osa.1162171	Os01g29280	Oryza sativa	
12001.m09370.osa.1162166	Os01g29330	Oryza sativa	
12001.m43407.osa.1158133	Os01g65992	Oryza sativa	
12002.m07924.osa.1168957	Os02g27800	Oryza sativa	
1_2003.m07892.osa.1173156	Os03g25440	Oryza sativa	
12005.m08955.osa.1190421	Os05g48840	Oryza sativa	
12006.m07100.osa.1193430	Os06g24490	Oryza sativa	
12007.m06536.osa.1198489	Os07g22510	Oryza sativa	
12007.m08728.osa.1201014	Os07g45080	Oryza sativa	
12008.m04301.osa.1201663	Os08g01530	Oryza sativa	
12012.m06071.osa.1221438	Os12g22270	Oryza sativa	
12012.m06167.osa.1221541		Oryza sativa	108 aa*incomplete
e_gw1.5.155.1.ppa.1911453	Ppa_5	Physcomitrella patens	
eugene3.01240091.ptr.1096907	Ptr_124	Populus trichocarpa	
gw1.150.213.1.ptr.1091951	Ptr_150	Populus trichocarpa	
fgenes4_pg.C_scaffold_41000052.ptr.1105591	Ptr_41.1	Populus trichocarpa	
gw1.64.526.1.ptr.1114406	Ptr_64	Populus trichocarpa	
gw1.86.53.1.ptr.1098298	Ptr_86	Populus trichocarpa	
fgenes4_pg.C_LG_IV000479.ptr.1106057	Ptr_IV.1	Populus trichocarpa	
fgenes4_pg.C_LG_VIII000758.ptr.1103102	Ptr_VIII.1	Populus trichocarpa	
eugene3.00081073.ptr.1089016	Ptr_VIII.2	Populus trichocarpa	
fgenes4_pg.C_LG_X001516.ptr.1087267	Ptr_X.1	Populus trichocarpa	
eugene3.00100249.ptr.1067698	Ptr_X.2	Populus trichocarpa	
estExt_fgenes4_pm.C_LG_XIII0118.ptr.1116033	Ptr_XIII.1	Populus trichocarpa	
Sb01g034360.1.sbi.1953235	Sb01g034360	Sorghum bicolor	
Sb02g041170.1.sbi.1959625	Sb02g041170	Sorghum bicolor	
Sb03g011250.1.sbi.1961378	Sb03g011250	Sorghum bicolor	
Sb03g027410.1.sbi.1962404	Sb03g027410	Sorghum bicolor	
Sb03g027420.1.sbi.1962405	Sb03g027420	Sorghum bicolor	
Sb03g041810.1.sbi.1964141	Sb03g041810	Sorghum bicolor	
Sb04g019010.1.sbi.1966451	Sb04g019010	Sorghum bicolor	
Sb07g000680.1.sbi.1974618	Sb07g000680	Sorghum bicolor	
Sb09g028420.1.sbi.1981842	Sb09g028420	Sorghum bicolor	
Sb10g008180.1.sbi.1983158	Sb10g008180	Sorghum bicolor	

Chapter 1

Sb10g008530.1.sbi.1983205	Sb10g008530	Sorghum bicolor	
Sb10g010790.1.sbi.1983480	Sb10g010790	Sorghum bicolor	
Sb10g021060.1.sbi.1983937	Sb10g021060	Sorghum bicolor	
gw1.7.1319.1.smo.1857759	Smo_7.1319	Selaginella moellendorffii	
gw1.7.1321.1.smo.1857774	Smo_7.1321	Selaginella moellendorffii	
GSVIVT00003045001.vvi.1705101	Vvi_10.1	Vitis vinifera	
GSVIVT00018646001.vvi.1719597	Vvi_12.1	Vitis vinifera	
GSVIVT00035393001.vvi.1736344	Vvi_12.2	Vitis vinifera	
GSVIVT00020980001.vvi.1721931	Vvi_14.1	Vitis vinifera	
GSVIVT00001767001.vvi.1703823	Vvi_18.1	Vitis vinifera	
GSVIVT00019862001.vvi.1720813	Vvi_5.1	Vitis vinifera	
GSVIVT00001645001.vvi.1703701	Vvi_Un	Vitis vinifera	
GRMZM2G052463_T01.zma.16558175	Zm_187076	Zea mays	
AC188714.3_FGT044.zma.16505876	Zm_188714	Zea mays	
AC196465.3_FGT023.zma.16510251	Zm_196465	Zea mays	
AC200144.4_FGT052.zma.16512625	Zm_200144	Zea mays	
GRMZM2G036585_T01.zma.16547755	Zm_200873	Zea mays	
GRMZM2G116041_T01.zma.16600006	Zm_204886	Zea mays	
GRMZM2G098182_T01.zma.16588150	Zm_205243	Zea mays	
GRMZM2G111920_T01.zma.16597329	Zm_206162	Zea mays	
GRMZM2G140842_T01.zma.16616302	Zm_210048	Zea mays	
GRMZM2G002568_T01.zma.16525510	Zm_210869	Zea mays	
AC211372.4_FGT037.zma.16519750	Zm_211372	Zea mays	
GRMZM2G061939_T01.zma.16564415	Zm_215227	Zea mays	
GRMZM2G078050_T01.zma.16575032	Zm_225342	Zea mays	
GRMZM2G070013_T01.zma.16569728	Zm_199043	Zea mays	
GRMZM2G040175_T01.zma.16550073	Zm_208715	Zea mays	

A

L29 P30 L56 P57

DMP6 \triangleright 5' - TTA CCT ----- TTA CCT - 3'

3' - AAT Gga ----- aat gGA - 5' \triangleleft At5g46100

B

	10	20	30	40	50	60	70	80	90
DMP7 predicted	MEEETKQSLIASLPSAPRKEKSKVERVVSVPSPVAGSPASSSPVAPSASSSPLPTLEHOTA-----								
DMP7	MEEETKQSLIASLPSAPRKEKSKVERVVRKVFKGTAHLSNLLPTGSMVMSFQIMCPVLTHQGCPTTISRWLTCFLVSLCAISCFLFSFDSDS								
	100	110	120	130	140	150	160	170	180
DMP7 predicted	-----RYGLATWSGLLVMDGSIHLTEEEKKPKYKLLDPIHAIMSMLVFFAVSMFDQNVTRCLFPVPSSEETKEILLTSLEFVIGVICG								
DMP7	IRDPNGKVRVYGLATWSGLLVMDGSIHLTEEEKKPKYKLLDPIHAIMSMLVFFAVSMFDQNVTRCLFPVPSSEETKEILLTSLEFVIGVICG								
	190	200							
DMP7 predicted	AFFLAFPTRRHGIGSPLTKE								
DMP7	AFFLAFPTRRHGIGSPLTKE								

Figure S1. A: The top strand shows part of the AtDMP6 sequence, with the encoded amino acids above in grey letters. The complementary strand is the presumed 3' UTR of the *At5g46100* gene with the putative intron that is lacking in the sequence of the smaller *DMP6* RT-PCR product in Fig. 4. B: The top line shows the *DMP7* amino acid sequence according to the TAIR gene model. The bottom line shows the *DMP7* amino acid sequence translated from the sequence of the smaller *DMP7* cDNA product in Fig. 4.

Chapter 2

***Arabidopsis* DMP1-eGFP induces membrane remodeling and proliferation at the ER and the tonoplast**

Alexis Kasaras¹, Michael Melzer² and Reinhard Kunze¹

Address:

¹Freie Universität Berlin, Institut für Biologie - Angewandte Genetik, Dahlem Centre of Plant Sciences (DCPS), Albrecht-Thaer-Weg 6, D-14195 Berlin, Germany, ²Institute of Plant Genetics and Crop Plant Research (IPK), Corrensstraße 3, D-06466 Gatersleben, Germany

Keywords: tonoplast, endoplasmic reticulum, membrane remodeling, fusion, fission, membrane protein, green fluorescent protein, senescence

The work presented in this chapter has been submitted for publication to BMC Plant Biology

Abstract

Background: *Arabidopsis* DMP1 was discovered in a genome wide screen for senescence-associated membrane proteins. DMP1 is a member of a novel plant-specific membrane protein family of unknown function. In rosette leaves *DMP1* expression increases from very low background level several 100fold during senescence progression.

Results: Overexpression of AtDMP1-eGFP in *Nicotiana benthamiana* triggers a complex process of succeeding membrane fusion and fission events changing the structure of the endoplasmic reticulum (ER) and the vacuole. Induction of spherical structures (“bulbs”), changes in the architecture of the ER from tubular to cisternal elements, expansion of smooth ER, formation of crystalloid ER, and emergence of vacuolar membrane sheets and foamy membrane structures inside the vacuole are proceeding in this order. In a fraction of cells it can be observed that the process culminates in cell death after breakdown of the entire ER network and the vacuole. The integrity of the plasma membrane, nucleus and Golgi vesicles are retained until this stage. The possible biological relevance and partially artificial nature of these events are discussed. Stable overexpression of AtDMP1-eGFP in *Arabidopsis thaliana* does not perturb ER and vacuole morphology. In contrast, expression by the native *DMP1* promoter visualizes formation of aggregates (“boluses”) and vesiculation of the entire ER network preceding disintegration of the central vacuole during the latest stage of natural senescence (NS) in siliques, rosette and cauline leaves and in darkened rosette leaves. In roots tips, *DMP1* is strongly expressed in the cortex undergoing vacuole biogenesis.

Conclusions: Our data suggest that DMP1 is directly or indirectly involved in membrane fission during breakdown of the ER and the tonoplast during leaf senescence and in membrane fusion during vacuole biogenesis in roots. We propose that these properties of DMP1, exacerbated by transient overexpression, may cause or contribute to the dramatic membrane remodeling events which lead to cell death in infiltrated tobacco leaves.

Background

DMP1 (DUF679 Membrane Protein 1) is a short membrane protein of 207 amino acids with four transmembrane spans and belongs to a small, strictly plant-specific protein family comprising ten members in *Arabidopsis thaliana* [1]. *DMP1* is transcriptionally up-regulated during developmental senescence (NS) in siliques, rosette and cauline leaves, during dark induced senescence in attached (DIS) and detached leaves (DET) and it is expressed in the phloem bundles of roots and the cortex of root tips [2]. In all three senescence programs, *DMP1* expression increases from the onset until the very late stages of senescence. This suggests conserved functions during developmental and induced senescence as well as an involvement during the entire senescence program. *DMP1* is also expressed in the dehiscence and abscission zones of siliques [1], which indicates a role in programmed cell death (PCD).

In metazoans, based on cell morphology apoptosis, autophagy and necrosis are distinguished as the three main PCD forms. In plants “autolytic” and “non-autolytic” PCD are differentiated [3]. Non-autolytic PCD is marked by the absence of rapid cytoplasm clearance [3], as is observed e.g. in hypersensitive response and endosperm degeneration. Autolytic PCD is characterized by rupture of the tonoplast and subsequent rapid cytoplasm clearance and occurs e.g. in tracheary element differentiation and senescence, although the relationship between senescence and PCD is still controversial [4-6]. In the present study, we use the term PCD for the terminal stage of leaf senescence. The earliest detectable alterations during leaf senescence are changes in the ultrastructure of chloroplasts. In the course of senescence eventually all organelles are degraded. In *Iris* and carnation petal senescence, ER and attached ribosomes, Golgi bodies and mitochondria have been reported to be degraded during senescence before vacuolar collapse [7]. Ultrastructural, biochemical and gene expression data indicate that large-scale autophagy is involved in these degradation processes [8]. However, the fate of organelles has been almost exclusively investigated by electron microscopy using fixed cells. Investigations of ultrastructural changes of organelles undergoing senescence using fluorescence tags in living cells are scarce.

Here we present an extensive characterization of the complex cellular processes induced by the senescence-associated DMP1 protein fused to eGFP in *Nicotiana benthamiana* and *Arabidopsis thaliana* by confocal fluorescence and electron microscopy. In tobacco, DMP1-eGFP overexpression triggers membrane remodeling, expansion, fusion and fission events at the tonoplast and the ER. We classified the successive remodeling events into five stages and showed that they ultimately can lead to cell death by extensive fragmentation of the ER and the vacuole. We note the formation of a “second” ER-network that we propose to be proliferating smooth ER. To our

knowledge, this is the first observation of a clear separation of rough and smooth ER of the cortical ER in tobacco using fluorescent tags. Thus, overexpression of DMP1-eGFP might induce a differentiation of the cortical ER. In *Arabidopsis* we investigated DMP1-eGFP fluorescence patterns in tissues undergoing NS or DIS as well as the response to whole plant darkening, a treatment that does not induce senescence [9]. We found that in all tissues and senescence types DMP1-eGFP illuminates vesiculation events of the ER and the tonoplast and the formation of aggregates ("boluses") within the ER. The formation of boluses, which suggest altered protein flow and the vesiculation of the entire ER network, has not been reported during senescence yet. We suggest that rupture of the tonoplast, a hallmark of autolytic PCD in the terminal senescence stage, may be accompanied or preceded by fragmentation of the vacuole. The effects of DMP1-eGFP expression in tobacco and *Arabidopsis* suggest that DMP1 regulates membrane folding and is involved in tonoplast and ER membrane fusion and fission reactions.

Results

Overexpression of DMP1-eGFP in *Nicotiana benthamiana* epidermis cells induces membrane remodeling

To investigate intracellular targeting of DMP1 we agroinfiltrated a *35S:DMP1-eGFP* construct into tobacco leaves. Unexpectedly, the fusion protein displayed a highly dynamic and temporally changing fluorescence pattern (Fig. 1). Two to three days post infiltration (dpi), the first fluorescence signals became visible and labeled the boundaries of the cells and spherical structures inside the lumen of the central vacuole (Fig. 1A). Until five dpi the fluorescence pattern changed and the cells underwent membrane remodeling to various degrees (Fig. 1B). Two days later the majority of cells exhibited severely remodeled endomembranes, giving the cells a "foamy" appearance (Fig. 1C). These membrane remodeling patterns and time courses were highly

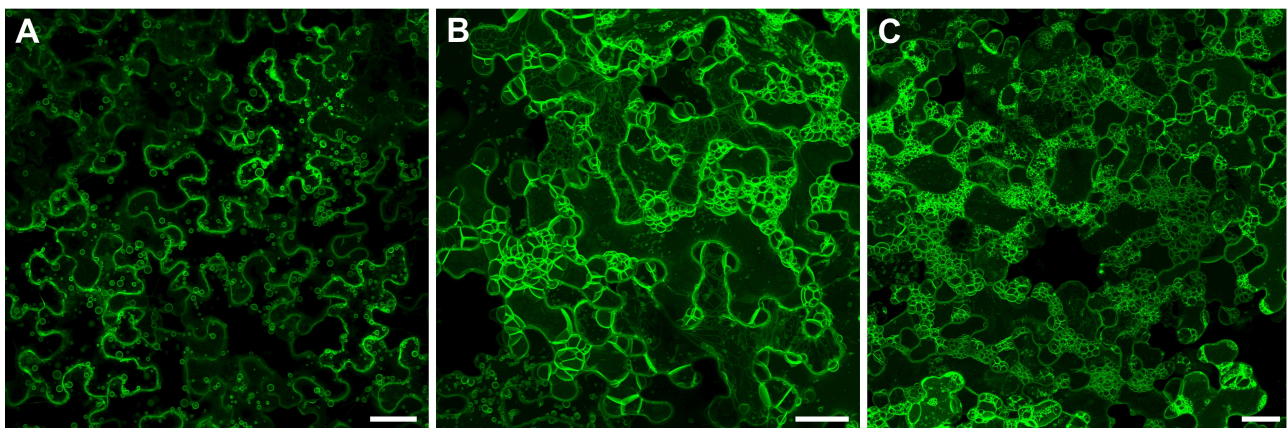


Figure 1. Temporal dynamics of DMP1-eGFP fluorescence patterns in tobacco epidermis cells. Representative overviews of tobacco epidermis cells expressing DMP1-eGFP at 2 dpi (A), 5 dpi (B) and 7 dpi (C). Scale bar, 40 μm

Chapter 2

reproducible with only little fluctuation in severity. Expression of DMP1-eGFP by the *DMP1* promoter induced a comparable but somewhat weaker membrane remodeling phenotype.

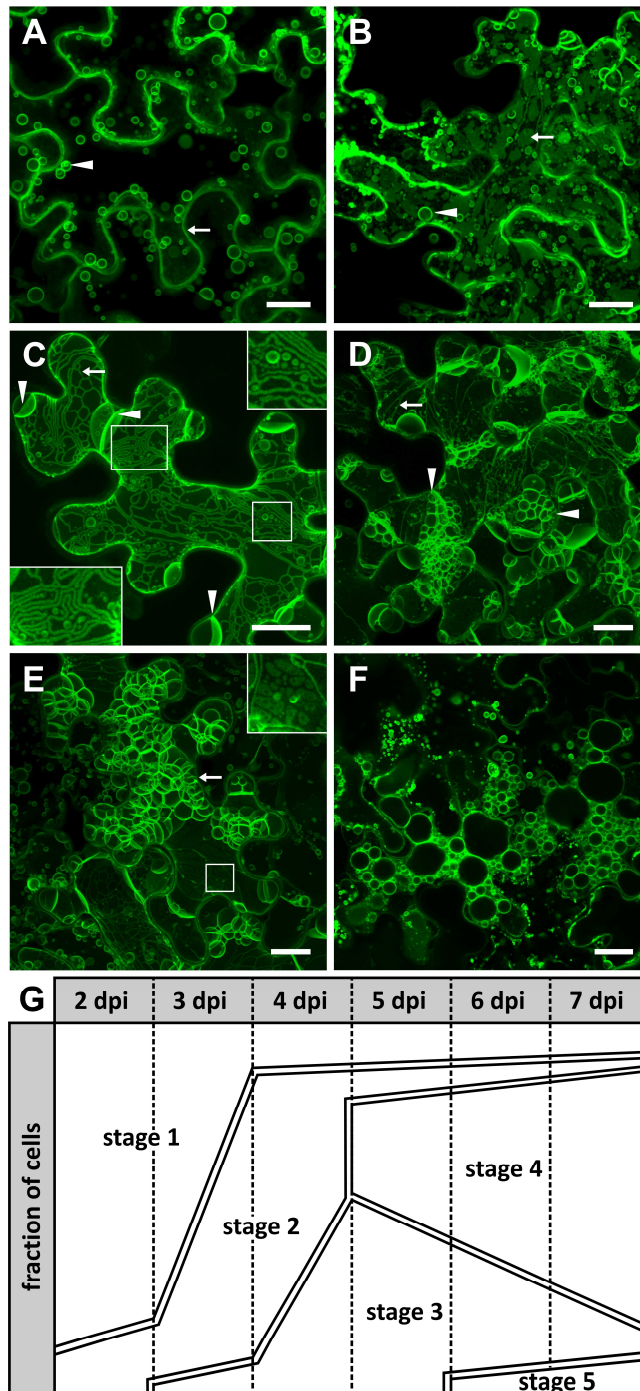


Figure 2. DMP1-eGFP induces membrane remodeling in *Nicotiana benthamiana*. Transient overexpression of DMP1-eGFP in tobacco epidermis cells results in distinct fluorescence patterns classified into five stages: stage 1 (A), stage 2 (B), stage 3 (C), stage 3 to stage 4 transition (D), stage 4 (E) and stage 5 (F). (G) Schematic of the dynamic alteration in DMP1-eGFP fluorescence patterns from stage 1 to stage 5. Scale bar, 20 μ m.

We classified the course of endomembrane remodeling into five stages. Stage 1 is characterized by well-defined fluorescence signals along the cell walls (Fig. 2A, arrow) and at spherical structures located inside the lumen of the vacuole (Fig. 2A, arrowhead). Three to four days dpi the cells

Chapter 2

typically enter stage 2 where they begin to display extended membrane sheets within the cytoplasm reminiscent of ER cisternae (Fig. 2B, arrow) and bulbs (Fig. 2B, arrowhead). Stage 3 is distinguished by large tubular and reticulated structures forming a network reminiscent of cortical ER (Fig. 2C, arrow). Also spherical bodies are visible (Fig. 2C, insets), but unlike the spherical structures in stages 1 and 2 they appear to be located in the cytoplasm, and large membrane sheets crossing and thereby compartmentalizing the central vacuole emerge (Fig. 2C, arrowheads). Fig. 2D shows a cell in transition from stage 3 with its distinctive tubular structures (Fig. 2D, arrow) to stage 4 with its typical "foamy" membrane meshwork (Fig. 2D, arrowheads). In stage 4 a great deal of the central vacuole is filled with this "foamy" membrane mesh (Fig. 2E, arrow). Some residual tubular structures are still present, and occasionally enigmatic, sponge-like structures appear (Fig. 2E, inset). In the terminal stage 5 the vacuole breaks down by vesiculation (Fig. 2F). This stage was rarely observed because the cells appear to die rapidly after vacuole disintegration and only a minor fraction of stage 4 cells enters stage 5. Interestingly, in spite of strong membrane remodeling the cells seem to stay viable for a prolonged period of time without entering vesiculation. Figure 2G shows the approximate fractions of cells in stages 1 to 5 at different times after infiltration.

To characterize the membrane structures labeled by DMP1-eGFP we subsequently performed colocalization experiments with various membrane markers.

Stage 1: The tonoplast located DMP1-eGFP induces the formation of bulbs

The first DMP1-eGFP fluorescence signals were observed at the cell periphery and in spherical structures two days after infiltration (Fig. 3A). Upon co-infiltration DMP1-eGFP clearly colocalized with the tonoplast marker TPK1-mRFP (Fig. 3BC, arrowheads), but not with the plasma membrane marker mRFP-MUB2 (supplementary Fig. S1). TPK1-mRFP was largely excluded from the spherical structures (Fig. 3BC, arrows) which supposedly are identical to the "bulbs" reported by [10] as they are comparable in size, motility and fluorescence intensity. Overlap between DMP1-eGFP and TPK1-mRFP fluorescence at the bulbs was extremely rare and only partial. Some regions of the bulbs were labeled with either DMP1-eGFP or TPK1-mRFP (Fig. 3D, arrows), suggesting different membrane properties and rapid exclusion of TPK1-mRFP from the bulbs. As γ -TIP-mCherry did not lead to proper fluorescence signals in tobacco [1] it could not be used as an alternative tonoplast/bulb marker. We therefore studied DMP1-eGFP infiltrated tobacco leaf epidermis cells by transmission electron microscopy. In DMP1-eGFP expressing epidermis cells we observed a significantly higher number of bulbs (Fig. 3L) than in mock-transformed cells, supporting the notion that overexpression of DMP1-eGFP induces formation of bulbs. DMP1-eGFP was never observed in Golgi vesicles (Fig. 3E, G, H) and was largely excluded from the ER (Fig.

3E, F, H) which had a normal tubular morphology. The same result was obtained by using the integral fusion protein RFP-p24 instead of the luminal YFP-HDEL as ER marker (supplementary Fig. S2).

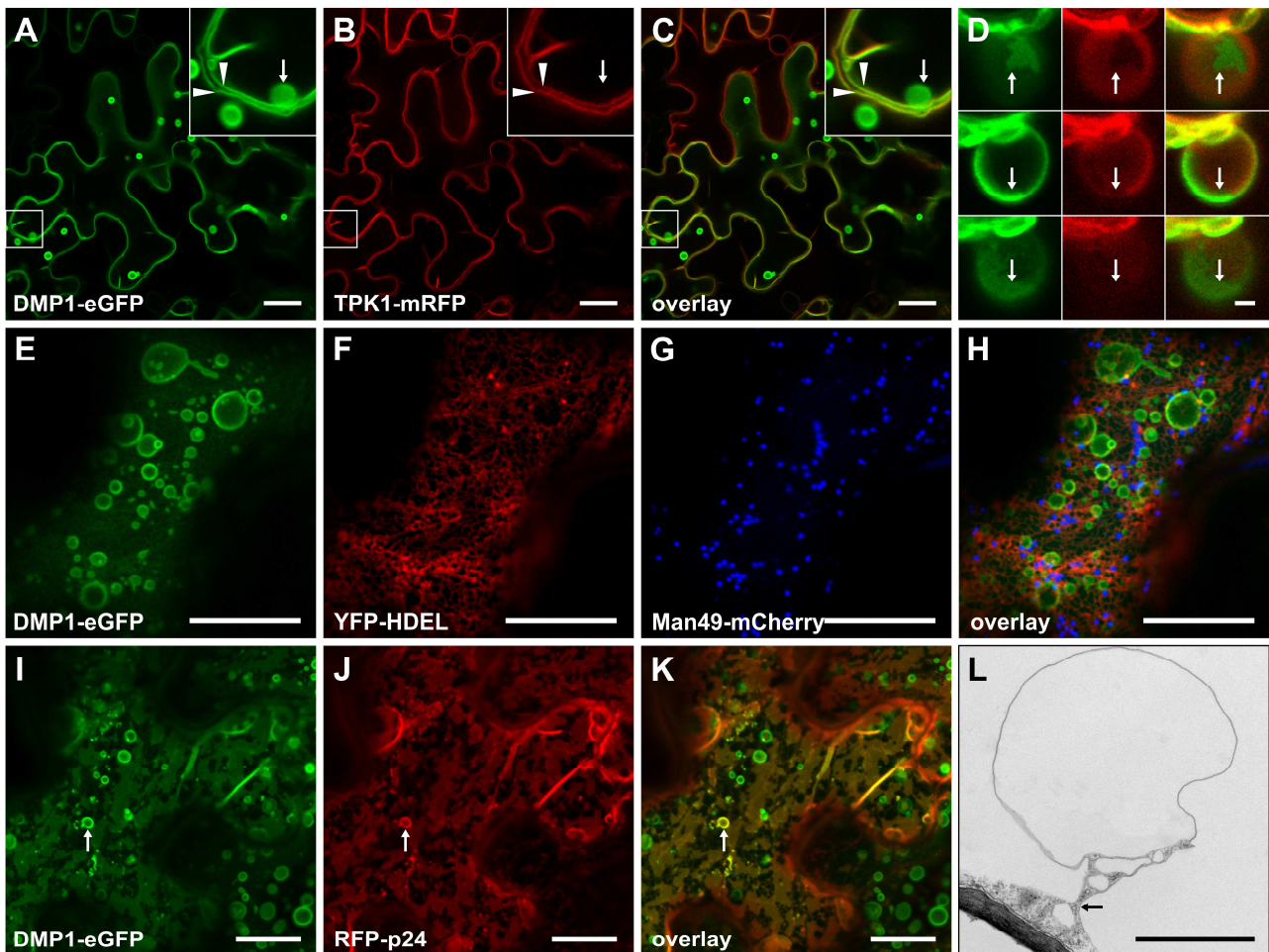


Figure 3. Stage 1 and 2. Co-expression of DMP1-eGFP (A) and the tonoplast marker TPK1-mRFP (B) shows in stage 1 colocalization at the vacuolar membrane (C) and occasional partial overlap at bulbs (D). Co-expression in stage 1 of DMP1-eGFP (E), YFP-HDEL labeling the ER lumen (F) and Man49-mCherry decorating Golgi vesicles (G) shows no localization of DMP1-eGFP in Golgi vesicles and no or only weak signals in the ER (H). Co-expression during stage 2 of DMP1-eGFP (I) and the ER membrane marker RFP-p24 (J) shows colocalization in the ER that exhibits cisternal morphology (K). Bulbs in tobacco epidermis cells visualized by electron microscopy (L). Scale bar, 20 μm except D, 2 μm

Stage 2: Reorganization of the ER - transition from tubular elements to cisternae

Stage 2 is characterized by the appearance of bulky cisternae in the cytoplasm that strongly resemble cortical ER observed under certain conditions (see Discussion), while the bulbs and tonoplast labeling from stage 1 are still retained (Fig. 1B). The ER localization of DMP1-eGFP was verified by co-expression with RFP-p24 (Fig. 3I, J, K). We also occasionally observed RFP-p24 signals in bulbs (Fig 3J, K, arrows). This might either indicate mislocalization of the ER marker due to overexpression or some dysfunction of the ER during stage 2.

Stage 3: *De novo* formation of a cortical ER-derived network inside the cytoplasm and vacuolar sheets inside the vacuole

Stage 3 is marked by different membrane remodeling events. Most conspicuously the labeling of novel tubular structures which did not colocalize with the different markers used. In stage 2 DMP1-eGFP and RFP-p24 both decorate the whole ER network composed principally of cisternae (Fig. 4A, B, C). DMP1-eGFP additionally decorates another tubular mesh from which RFP-p24 is excluded (Fig. 4A, B, C, insets). However, both networks share the same overall pattern, indicating either physical connection or differential labeling of the same entity. Strikingly, over time DMP1-eGFP and RFP-p24 progressively segregate. While DMP1-eGFP initially colocalizes with RFP-p24 in the ER cisternae (Fig. 4D, E, F, arrowhead), the tubular structures mostly dissociate from the ER network (Fig. 4D, E, F, insets). In late stage 3, when first vacuolar sheets and "foamy" structures emerge (Fig. 2C and 4G, arrows), DMP1-eGFP is almost undetectable in the ER network labeled by YFP-HDEL (Fig. 4G, H). This time course suggests that the tubular structures derive directly from the ER and coincide with a progressive exclusion of DMP1-eGFP from the ER. The tubules labeled only by DMP1-eGFP form an interconnected network throughout the cytoplasm (Fig. 4A, G, K and L), are homogeneous in diameter and show a smooth and relaxed appearance (Fig. 4A, D, G, K, L and 2C), and are - in contrast to the repetitive polygonal structure of the cortical ER network - often tightly packed and peculiarly folded (Fig. 2C, insets and 4L, inset). Large swollen spherical formations reminiscent of ER cisternae are often observed at the intersection of DMP1-eGFP-labeled tubules (Fig. 4G and K, arrows and inset). In late stage 3, isolated tubules are also found (Fig. 4G, arrowheads and K, arrowhead) whose occurrence coincides with the presence of cytosol-located vesicles (Fig. 4G, empty arrowhead, K, inset and L). These vesicles and the isolated tubules likely derive from the DMP1-eGFP-labeled network by fission events.

As mentioned above, vacuolar sheets crossing the lumen of the vacuole and first "foamy" membranes appear in stage 3 and accumulate gradually (Fig. 2C). The density of vacuolar sheets correlates with a progressive loss of the DMP1-eGFP labeled network. Moreover, the tubules were occasionally found tightly associated with these vacuolar sheets (supplementary Fig. S3). These observations suggest a connection between these two structures. Golgi vesicles appeared to be unaffected during stage 3 (Fig. 4I) suggesting proper ER-Golgi transport despite high remodeling of the ER.

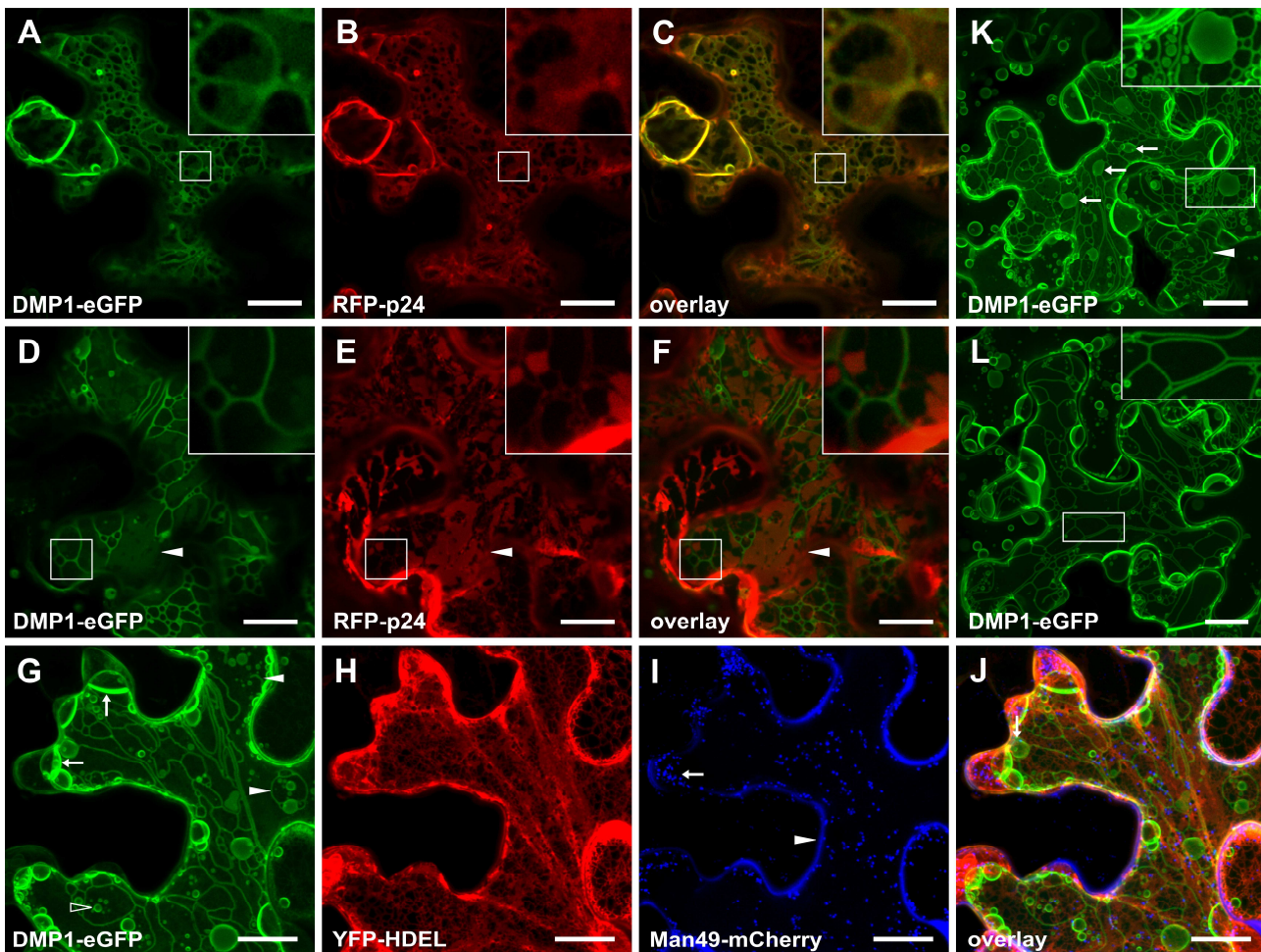


Figure 4. Stage 3. Co-expression of DMP1-eGFP and ER markers during stage 3 shows cells with partial colocalization (A-C and D-F) and cells lacking colocalization (G-J). Accordingly, in cells expressing DMP1-eGFP alone, ER with cisternal morphology can be distinguished in the background in some of them (K) but not in others (L). Co-expression of DMP1-eGFP (A) and RFP-p24 (B) shows colocalization with the ER network (C) except for tubular structures where RFP-p24 is excluded (insets A-C). Tubular network dissociating from the ER (D-F). Weak residual DMP1-eGFP signals in the cisternal ER network (D-F, arrows). Vacuolar sheet formation inside the vacuole occurs preferentially at the periphery of cells (G, arrows) that still exhibit a DMP1-labeled tubular network and cytosolic vesicles which are either connected to this network (K, inset) or suspended in the cytosol (K, inset, and G, arrow). Tubules are often closely spaced but unconnected (K, inset). DMP1-eGFP (G) and YFP-HDEL (H, false-colored) do not colocalize (J) and Golgi vesicles labeled by Man49-mCherry are intact (I false-colored, arrow). Man49-mCherry accumulates to some extent in the apoplast (I, arrowhead). Scale bar, 20 μm

Stage 4: Formation of "foamy" membrane structures inside the vacuole

Transition from stage 3 to 4 is indicated by the appearance of "foamy" membrane formations that coincide with a decrease in tubular structures (Fig. 2D). The "foamy" membranes likely derive from accumulation of vacuolar sheets. At this time no DMP1-eGFP signals are detected in the ER anymore (Fig. 5A, C, D and E, G, H₁) which appears to be compressed into interstices (Fig. 5C, G, arrows) and junctions of the "foamy" membranes (Fig. 5C G, arrowheads). The junctions contain different organelles such as peroxysomes or mitochondria (Fig. 5I, arrowhead and K) as found in transvacuolar strands [11]. Confocal fluorescence microscopy (Fig. 5H₁) and electron microscopy

Chapter 2

(Fig. 5I, J, K) consistently revealed that the vacuolar sheets and "foamy" membranes are double membranes. DMP1-eGFP (Fig. 5E) and TPK1-mRFP (Fig. 5F) do not perfectly colocalize as shown by separation of the two fluorescence signals (Fig. 5H₁ and H₂). The distance between the two fluorescence peaks is about 200 nm to 300 nm (Fig. 5H₁ and 5H₂ membrane segments 1, 2 and 3) which would allow small organelles to pass through. The double-membrane topology is corroborated by the observation of ER squeezed between the two membranes of a membrane sheet (supplementary Fig. S4). Occasionally however, perfect colocalization is observed which might indicate localization of both fusion proteins at both membranes (Fig. 5H₁ and 5H₂ membrane segment 4). Under electron microscopy the double membranes appear more closely stacked (Fig. 5I and K). However, this may be a fixation artefact and not reflect the situation *in vivo*. Membrane sheets consisting of a single membrane were never observed by EM. In 70 nm thin cross-sections the double membranes completely crossed the lumen of the vacuole, confirming that they correspond to the vacuolar sheets and not to transvacuolar strands (TVS) as the latter are unlikely straight and oriented in parallel to the section cut across the whole vacuole. TPK1-mRFP is often excluded from regions within foamy membrane structures (supplementary Fig S5). Interestingly, these areas are located at contact zones between adjacent sheets within foamy membrane structures.

During stage 4 intriguing sponge-like flat structures arise (Fig. 2E, inset, supplementary Fig. S6). TPK1-mRFP is excluded from these areas (Fig. S6) reminiscent of the observations in individual bulbs (Fig. 3D) and within foamy structures (Fig S5). We hypothesize that these sponge-like structures represent residual TPK1-mRFP-free membrane domains derived from bulbs and vacuolar sheets. Additionally we observed the formation of crystalloid ER (Fig. 5J₁J₂).

Stage 5: Vesiculation of the vacuole and the ER leading to cell death

Six days post infiltration some cells with severe vesiculation of endomembranes also display overall intracellular disintegration, indicating the onset of cell death (Fig. 2F). As in stage 4, DMP1-eGFP only labels the tonoplast and foamy membrane formations but not the ER (Fig. 5L, M, N). The ER is not reticulated but highly vesiculated (Fig 5M, N, O, arrow). The vacuolar and foamy membranes also appear to vesiculate more heavily than in stage 4 and form smaller vesicles (Fig. 5O, arrow and P). Despite the obvious breakdown of the ER, the integrity of the nuclear membrane (Fig. 5M, arrowhead and O) and Golgi vesicles (Fig. 5Q) is still retained. The Golgi marker which also is partially secreted to the apoplast (Fig. 4I) indirectly indicates in Fig. 5P that the plasma membrane, not labeled by DMP1-eGFP, is still intact (Fig. 5P, Q, R, arrows). The massive vesiculation of endomembranes was confirmed by electron microscopy (Fig. 5S).

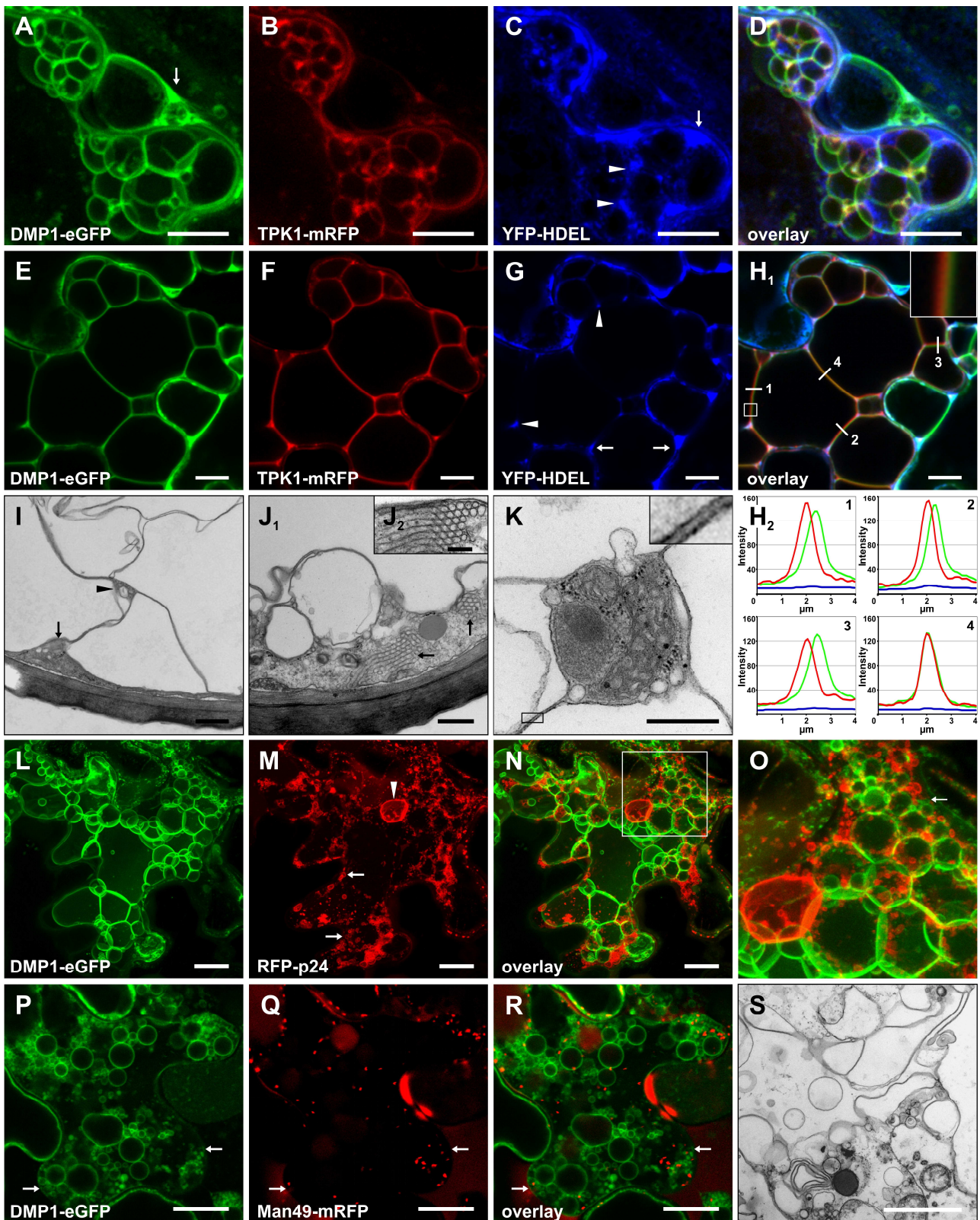


Figure 5. Stage 4 and 5. Co-expression of DMP1-eGFP (A), TPK1-mRFP (B) and YFP-HDEL (C, false-colored) shows colocalization of DMP1-eGFP and TPK1-mRFP and dissociation from the ER (D). The ER is compressed into interstices and junctions formed by foamy membrane structures (C and G, arrows and arrowheads respectively). On single plane images (E-H₁) but not maximum projection (A-D), the colocalization between DMP1-eGFP (E) and TPK1-mRFP (F) appears incomplete (H₁). In the majority of membrane segments analysed the fluorescence signal peaks are shifted between 200 nm and 300 nm (H₂, panels 1-3), suggesting a double membrane structure, one membrane being labeled by DMP1-eGFP and the other with TPK1-mRFP. In some membrane segments the fluorescence peaks match perfectly, indicating colocalization (H₁ and H₂, segment and panel 4 respectively). Vacuolar sheets and foamy

Figure 5 (continued)

membrane formations have double membranes (I and K). Interstices and membrane junctions contain cytoplasm and trapped organelles (I, arrow and arrowhead). Crystalloid ER in a late stage 4 cell (J_1 and J_2). Cells displaying foamy vacuolar membrane structures (L) and labeling of the whole tonoplast (P) enter cell death by vesiculation of the entire ER network (M, arrows) except for the nuclear envelope (M, arrowhead). DMP1-eGFP (L) and RFP-p24 (M) were fully dissociated (N, magnified in O) as in stage 4. The Golgi vesicles remain unaffected in these cells (Q and R). This process was visualized by EM (S). Scale bar, A-H₁ and S, 10 μm ; I, J_1 and K, 0,5 μm ; L-N and P-R, 20 μm ; J_2 , 0,1 μm

Overexpression of DMP1-eGFP in transgenic *Arabidopsis thaliana* shows dual ER/tonoplast localization

To determine if dual tonoplast/ER localization and induction of membrane remodeling by DMP1 overexpression is conserved in transgenic plants, we transformed *Arabidopsis thaliana* with *35S:DMP1-eGFP* and investigated the subcellular localization of the fusion protein. Seven days after sowing (DAS), bulbs and tonoplast localization is observed in young cotyledons (Fig. 6A). Five days later (12 DAS) the number of bulbs decreases (Fig. 6B) and at 18 DAS the bulbs disappear (Fig. 6C). This time course of bulb development is consistent with previous observations using γ -TIP as marker [10]. In addition to accumulation in bulbs strong DMP1-eGFP signals are observed in the ER as well as in ER bodies in all these stages (Fig. 6A, B, C, arrows and inset). The ER bodies vanish as the cotyledons age, corroborating earlier observations [12]. Accordingly, in cotyledons of *Arabidopsis* DMP1-eGFP is dually targeted to the ER and the tonoplast, but overexpression of DMP1-eGFP does not affect the morphology and development of the ER and the tonoplast in this organ. ER bodies are also labeled by DMP1-eGFP in hypocotyl cells somewhat later in development (Fig. 6G). In rosette leaves, we observe an intense, leaf-age independent accumulation of DMP1-eGFP in the ER (Fig. 6D). In addition, protoplasts prepared from rosette leaves also show some tonoplast localization, confirming the dual localization seen in cotyledons (data not shown). During developmental leaf senescence and even more pronounced during dark induced leaf senescence (Fig. 6H), individual cells or leaf areas show massive vesiculation

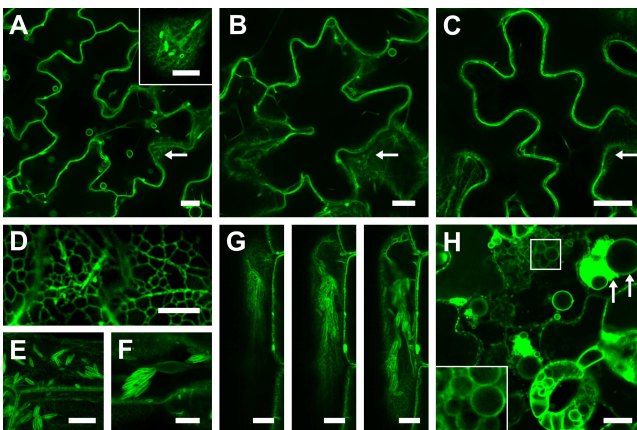


Figure 6. Dual ER/tonoplast localization of DMP1-eGFP in stably transformed *A. thaliana* plants. Overexpression of DMP1-eGFP in young emerging *Arabidopsis* cotyledons (7 DAS) leads to labeling of the tonoplast and bulbs (A), the ER network (A, arrow and inset) and ER bodies (A, inset). In 12 DAS cotyledons the number of bulbs decreases (B) and at 18 DAS bulbs are no longer visible (C). In rosette leaves intense ER labeling is observed (D). In hypocotyls the ER is associated with single ER bodies (E), with ER body clusters (F), or with large ER body aggregates extending across the whole cell (G). Massive vesiculation of endomembranes occurs during dark induced senescence (H). Scale bar, 10 μm

Chapter 2

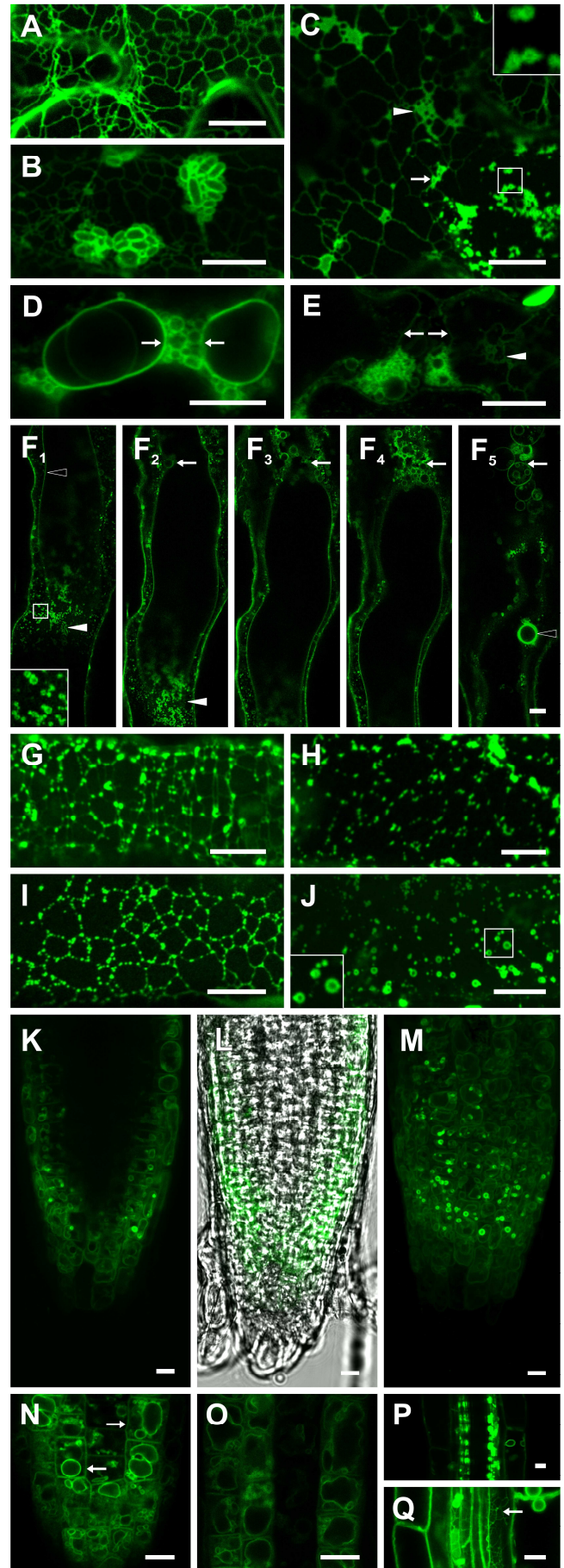
reminiscent of the cellular breakdown process during stage 5 in tobacco. Thus, DMP1-eGFP in *Arabidopsis* leaves is supposedly associated in a similar way in disintegration of the ER and the vacuole by vesiculation as in tobacco (Fig. 6H, arrows).

Expression of DMP1-eGFP from the *DMP1* promoter in *Arabidopsis* highlights formation of boluses within the ER and fragmentation of the ER and the tonoplast during senescence

To scrutinize whether dual localization in *Arabidopsis* is an artifact by overexpression of DMP1-eGFP by the *CaMV 35S* promoter, we expressed the same fusion protein from the native *DMP1* promoter in transgenic plants. In accordance with the senescence-associated activity of the *DMP1* promoter [1], DMP1-eGFP fluorescence is only detectable in mature, early and late senescing rosette leaves, senescing cauline leaves, senescing silique walls and roots (Fig. 7). In mature-to-early senescing rosette leaves, DMP1-eGFP strongly accumulates in the ER and to a lesser extent in the tonoplast. However, the tonoplast signals are hardly distinguishable from the ER signals (Fig. 7A). ER bodies are occasionally observed (Fig. 7B). Formation of boluses resembling the eponymous protein aggregates reported by Griffing (2011) and vesiculation events are observed in rosette leaves (Fig. 7C, E, F), cauline leaves (Fig. 7G) and silique walls (Fig. 7H) undergoing natural senescence. Darkening of single rosette leaves (Fig. 7I) or whole plants (Fig. 7D and J) lead to similar events. In individual cells disintegration of the ER is occasionally recognizable (Fig. 7C). In these cells the junctions of the ER tubules seem to swell (arrow) and to vesiculate (arrowhead). We suggest that bolus formation precedes vesiculation of the ER, though it cannot be excluded that the two processes represent two different fates for cells undergoing senescence. Indeed, supplementary Fig. S7 shows that neighboring cells of the same type undergoing induced senescence can display different degrees of bolus formation and vesiculation. In other cells, fragmentation of the tonoplast is obvious (Fig. 7D and E, arrows) with occasional persistence of residual ER network (Fig. 7E, arrowhead), suggesting a close succession of the two vesiculation processes. Figures 7F₁-F₅ show ER which already underwent vesiculation (arrowheads) and fragmentation/vesiculation of the tonoplast (arrow), indicating that ER breakdown precedes tonoplast breakdown. Tonoplast vesiculation is more rarely observed than ER vesiculation during developmental or dark induced senescence. Tonoplast breakdown is presumably only a short-lived phase as it rapidly and irreversibly leads to cell death. The persistence of the nuclear membrane (Fig. 7F₅, open arrowhead) in spite of progressed ER breakdown is reminiscent of the events in tobacco during stage 5. Finally, in roots vacuolar localization of DMP1-eGFP is obvious in the cortex of root tips (Fig. 7K-O). In accordance with the current view of vacuole biogenesis, the emerging cells near the root tip contain several vacuoles differing in size (Fig. 7D) whereas the older cells in the elongation zone have fewer vacuoles or a single central vacuole (Fig. 7O). In these

cells the plasma membrane is also labeled (Fig. 7N, arrows), which is due to a truncated isoform of DMP1 (to be published elsewhere). In the phloem bundles, the subcellular localization could not be determined because of the small size of cells (Fig. 7P). The ER network was also visible in roots, highlighting once more the ability of DMP1-eGFP to target multiple subcellular membrane systems (Fig. 7Q).

Figure 7. DMP1-eGFP fluorescence patterns during development in *A. thaliana*. In mature/early senescing rosette leaves DMP1-eGFP expressed from the native *DMP1* promoter localizes in the ER (A) and occasionally in ER bodies (B). Vesiculation of the ER in rosette leaves during late NS (C). Vesiculation of the vacuole in rosette leaves during late NS (D, E). Vesiculation of the ER and the vacuole in rosette leaves during late NS (F₁-F₅). F₁-F₅ are individual pictures of a Z-stack through vesiculated ER (F₁ and F₂) and the central vacuole undergoing fragmentation (F₂-F₅, arrows). The integrity of the nuclear envelope is retained at this stage (F₅, empty arrowhead). Bolus formation in cauline leaves during late NS (G). Bolus formation in silique walls during late NS (H). Bolus formation in rosette leaves of darkened whole plants (I). Vesiculation of the ER in rosette leaves during DIS (J). The polygonal architecture of the ER is still visible despite strong bolus formation and punctate distribution of fluorescence signals (G-I) or vesiculation (J). DMP1-eGFP is strongly expressed in the cortex of root tips (K-O), in phloem bundles (P), and weakly expressed in other cell layers of the root (Q). In the cortex DMP1-eGFP localizes to the tonoplast, highlighting vacuole biogenesis (K, single picture, M maximal projection and L, light transmission). Magnification of the region near the root tip (N) shows multiple vacuoles of different size and shape which tend to form a central vacuole in the root elongation zone (O). Subcellular localization in the phloem bundle could not be determined but strong fluorescence signals in structures which might be ER boluses were observed (P). ER localization in roots is shown in (Q, arrow). Scale bar, 10 μ m



Discussion

DMP1-eGFP shows dual intracellular targeting and induces membrane remodeling

Transient overexpression of DMP1-eGFP in tobacco epidermis cells revealed dynamic targeting of the protein to the tonoplast and the ER. This may indicate that DMP1 possesses competitive tonoplast targeting and ER retention signals, as has been found in proteins that are dually targeted to different compartments such as mitochondria and chloroplasts [13]. The most striking effect of DMP1-eGFP overexpression is the complex remodeling and the formation of novel membrane structures at the tonoplast and the ER. Shortly after transfection DMP1-eGFP induces the formation of bulbs (stage 1) resembling those first described in young cotyledons. Formation of these bulbs is believed to be independent of the cytoskeleton [11] as they disappear as cell expansion progresses. It was initially suggested that they might serve as membrane reservoirs during rapid cell and vacuole expansion [10]. More recently Saito et al. (2011) reported that bulbs emerge in germinating seeds by fusion of small vacuoles. Bulbs were found in numerous tissues, at various developmental stages, under stress conditions and in different plant species, suggesting additional functions [14-21]. Specific functions of the bulbs differing from the remaining tonoplast are also indicated in our study by the segregation of DMP1-eGFP and TPK1-mRFP at bulb membranes. A similar case was made by Saito et al. (2002) who showed that though γ -TIP-GFP and GFP-AtRab7c were both located at the tonoplast, only γ -TIP-GFP was present at the bulbs.

In stage 2 DMP1-eGFP mostly localizes in the ER, which undergoes severe reorganization during that stage. As the cortical ER has in stage 1 a tubular morphology and contains almost no DMP1-eGFP, it is likely that the protein induces reorganization of the ER to large cisternae during stage 2. Similarly, induction of ER cisternae formation has been observed by overexpression of GFP fused to the transmembrane domain of calnexin [22, 23]. Transition from tubular to cisternal architecture of the ER has been reported in response to various abiotic and biotic stresses and presumably reflects modification in ER functions. The tubule-to-cisternae transition may be correlated to the integrity of the actin cytoskeleton, which precisely overlies the ER network [24], as its disassembly as well as myosin inhibition both lead to loss of the tubular structure and the formation of large cisternae [25].

The DMP1-eGFP-labeled tubules, which appear at the beginning of stage 3, form a network that matches the cortical ER (Fig. 4 A-C). Towards the end of stage 3 the DMP1-eGFP-labeled network dissociates from the cortical ER network (Fig. 4D-F). In contrast to a differentiation of the ER into distinct subregions with different protein content, e.g. reticulons which accumulate at edges of ER sheets [26, 27], we observe a segregation of the DMP1-eGFP-labeled structures from the ER,

Chapter 2

resulting in two physically disconnected membrane networks (Fig. 4D-F and G-J). As the DMP1-eGFP-labeled network appears more relaxed and less reticulated than the ER network associated with the GFP-HDEL and RFP-p24 markers, we propose that it consists of smooth ER whereas the latter rather is rough ER. This scenario raises the question whether the smooth ER network was originally present in the cell but not labeled by DMP1-eGFP, GFP-HDEL and RFP-24 or if accumulation of DMP1-eGFP in the rough ER during stage 2 led to expansion of smooth ER. We observed the presence of crystalloid ER in the infiltrated cells consisting exclusively of smooth ER (Fig. 5J₁ and J₂) as has also been described in other studies [28-34]. As crystalloid ER has not been found in WT tobacco epidermis cells before, an expansion of the smooth ER triggered by DMP1-eGFP seems plausible.

The transition from stage 3 to 4 is accompanied by the disappearance of the smooth ER and accumulation of vacuolar membrane sheets. We cannot distinguish whether the two events are independent processes or if the tubules and vesicles that appear in early stage 3 fuse later with the tonoplast to form the vacuolar sheets. The formation of crystalloid ER rather suggests that they occur independently of each other.

Vacuolar membrane sheets have been proposed to be bulbs which lost their spherical shape and adopted a sheet-like configuration [11, 19]. This model is supported by our observation that the local separation of DMP1-eGFP and TPK1-mRFP signals in stage 1-bulbs (Fig. 3A-D) re-emerges somewhat later in the foamy stage 3-vacuolar sheets (Fig. 4E-H₂). The sponge-like structures observed during late stage 3 and stage 4 may represent residual membrane islands originating from bulbs and vacuolar sheets.

Despite severe membrane remodeling, stage 4-cells appear to remain viable for several days, suggesting that the essential physiological functions of the cells are still intact. Stage 5 presumably represents the fate of cells which have passed a developmental point of no return and undergo cell death.

In *Arabidopsis* DMP1 highlights dynamic restructuring of the ER and vacuole late in developmental and induced senescence.

The fate of the ER during senescence is largely enigmatic yet. It has been reported to disappear like other organelles during petal senescence [7] and even less is known about its destiny during developmental (NS) or induced leaf senescence (DIS). We discovered that the first morphological alteration during NS and DIS affecting the whole ER is the formation of aggregates termed 'boluses'. DMP1-eGFP expression by its native, senescence-associated promoter illuminates the

Chapter 2

formation of boluses in all studied organs undergoing NS or DIS (rosette leaves, cauline leaves and siliques). Comparable aggregations within the ER have been shown by overexpressing reticulons, a class of ER proteins with membrane curvature-inducing properties, in tobacco epidermis cells. The luminal protein GFP-HDEL displays a punctate repartition within the ER network when coexpressed with RTNLB13 and RNTLB1-4 [27]. It was suggested that overexpression of reticulons induces constrictions of the ER tubules creating luminal pockets in which soluble proteins accumulate. A formation of boluses resembling those in our study was also observed within the lumen and at membranes of the ER subdomain that associates with the chloroplast upon expression of a luminal, GFP-HDEL, and a trans-membrane protein, YFP-RHD3 (Griffing, 2011). Our study yields for the first time evidence that bolus formation at the ER network occurs during plant development and concerns the whole ER network within a cell. We assume that bolus formation reflects a restrained protein mobility and motion within the ER as a consequence of fading ER integrity and function during late senescence. The timing of membrane reorganization suggests that the subsequent stage in ER network degradation is a brief vesiculation phase (Fig. 7C). The fate of these vesicles is unclear. Possibly they are taken up by the vacuole for further degradation.

Bolus formation and ER fragmentation are most prominent in darkened plants, as this treatment probably synchronizes cells and subsequent cell death. Vacuole disorganization is even more rarely observed than ER vesiculation. van Doorn et al. (2011) describes that autolytic cell death is marked by an increase of vacuole size by fusion of smaller vacuoles, accompanied by a decrease in cytoplasm. Either the situation is different in epidermis cells in which the central vacuole already occupies more than 90 % of the cell volume or this process is very brief or may even be concomitant with rupture of the tonoplast leading to cell death.

A function of DMP1 in membrane fusion and fission events during development?

The molecular function of DMP1 is still unknown. However, as from stage 2 all phases of membrane remodeling in tobacco cells overexpressing DMP1-eGFP are associated with membrane fusion or fission, it is tempting to speculate that DMP1 might be actively involved in these processes. In stage 1, the formation of bulbs results from invagination of the tonoplast forming a double-membrane inside the vacuole [10, 19] and may thus not require membrane fusion or fission. During stage 2, ER reorganization from tubular to cisternal elements requires membrane fusion. Apparent segregation of smooth ER from the cortical ER network can only be explained by membrane fission and membrane expansion. The emergence of free tubules and small vesicles in the cytosol that obviously originate from the smooth ER-network requires membrane fission.

Chapter 2

Formation of vacuolar sheets and foamy membrane structures in stage 4 likely needs membrane fission and fusion, and eventually vesiculation of the vacuole during stage 5 necessitates membrane fission. Also in *Arabidopsis* the location of DMP1-eGFP suggests a close connection to membrane fission/fusion events. In root tips undergoing central vacuole biogenesis, known to take place by fusion of smaller vacuoles and vesicles, DMP1-eGFP is no longer expressed in the cortex layer as soon as the central vacuole is established. This strongly argues for a participation of DMP1 in vacuole biogenesis in this cell layer. During senescence, the protein is associated rather with the reverse reaction, i.e. the fragmentation of the ER and the tonoplast by membrane fission. It is conspicuous that DMP1 shares a similar overall architecture with the reticulons, which have been shown to shape ER tubules by membrane bending [35, 36]. The members of both protein families possess four transmembrane domains. In reticulons these are arranged in two long hydrophobic "hairpins" leading to a wedge-like topology with very short loops 1 and 3 and a longer loop 2 facing the cytosol [27]. The DMP proteins have also short loops 1 and 3 and a longer loop 2 [1]. Whether DMP1 is directly, e.g. by enforcing membrane distortion, or indirectly, e.g. by interaction and cooperation with other proteins, responsible for the membrane remodeling phenomena reported in this study remains to be elucidated.

Conclusions

Our data suggest that DMP1 possesses intrinsic membrane fusion, fission and remodeling properties. (1) Overexpression of DMP1-eGFP in tobacco led to temporally ordered remodeling events of the ER (tubules-to-sheets transition, proliferation of smooth ER, formation of crystalloid ER) and the tonoplast (formation of bulbs, vacuolar sheets, "foamy" structures). (2) Stable expression in *Arabidopsis* by the native promoter demonstrated for the first time the occurrence of boluses and vesiculation of the ER during developmental and induced senescence. (3) In root tips of *Arabidopsis* plants DMP1 is associated with vacuole biogenesis.

Methods

Generation of constructs

35S:DMP1-eGFP and *mRFP-MUB2* [37] expression vectors were generated as described [1]. *TPK1-mRFP* [38] was modified as described in Kasaras and Kunze (2010). *RFP-p24* [39] and *YFP-HDEL* were provided by David Robinson (University of Heidelberg, Germany) and Chris Hawes (Oxford Brookes University, UK) respectively. *DMP1p:DMP1-eGFP* was generated by amplifying a 2364 bp *DMP1promoter:624 bp DMP1* ORF fragment on genomic *Arabidopsis* Col-0 DNA with the primers 5'-CGGTCTAGAGAGAACAAAATCCTCCGTATC-3' and 5'-

Chapter 2

AACTGCAGCGGCAGAGACCGAGGCTTTC-3', digestion of the PCR product with *XbaI/PstI* and ligation into *XbaI/PstI* digested binary vector pGTkan3 [1].

Plant material, growth conditions and plant transformation

Arabidopsis thaliana Col-0 and *Nicotiana benthamiana* plants were grown and transformed as described [1]. All *Agrobacterium* cultures were resuspended to $OD_{600} = 0,05$ prior to tobacco infiltration. To reduce silencing of the transgenes, all constructs were co-infiltrated with the silencing suppressor p19 [40].

Confocal microscopy

Confocal microscopy was performed on a Leica TCS-SP5 AOBS (acousto-optical beam splitter) confocal laser scanning microscope (Leica Microsystems) equipped with water immersion objectives (20x with numerical aperture of 0.7 and 63x with numerical aperture of 1,20). Excitation / emission wavelengths were: eGFP: 488 nm (argon laser) / 495 nm - 510 nm; YFP: 514 nm (argon laser) / 525 nm - 555 nm; mRFP and mCherry: 561 nm (diode-pumped solid-state (DPSS) laser) / 585 nm - 655 nm. Multi-color imaging of cells co-expressing eGFP, YFP and mRFP (or mCherry) was performed by sequential scanning to prevent crosstalk. Post-acquisition image processing was performed with the Leica LAS AF software (Leica Microsystems). Depending on the structure either single pictures or maximum projections resulting from z-stacks are shown. Following pictures result from maximum projections: Fig. 1B and C; Fig. 2B-E; Fig. 3I-K; Fig. 4A-C, G-J, K and L; Fig. 5A-D, L-O and M; Fig. 7M; supplementary Fig. S7.

Transmission Electron Microscopy

For fixation, substitution and embedding of one mm² leaf sections (see Table T1 for protocol) a laboratory microwave (PELO BioWave® 34700-230, Ted Pella, Inc., Redding CA, USA) was used. For analysis in a Tecnai G2 Sphera transmission electron microscope (FEI Company, Eindhoven, Netherlands) at 120 kV, ~70 nm ultra thin sections were cut with a diamond knife and contrasted with uranyl acetate and lead citrate prior to examination.

Authors' contributions

AK conceived the study, carried out all experiments, performed data analysis and interpretation, prepared the figures and wrote the manuscript. MM carried out the transmission electron microscopy. RK conceived the study and wrote the manuscript.

Acknowledgements

We thank David Robinson (University of Heidelberg, Germany) and Chris Hawes (Oxford Brookes University, UK) for providing constructs *RFP-p24* and *YFP-HDEL*, respectively. A.K. and this project were supported by priority programme 1108 of the Deutsche Forschungsgemeinschaft (DFG).

References

1. Kasaras A, Kunze R: **Expression, localisation and phylogeny of a novel family of plant-specific membrane proteins.** *Plant Biol (Stuttg)* 2010, **12 Suppl 1**:140-152.
2. Van der Graaff E, Schwacke R, Schneider A, Desimone M, Flugge UI, Kunze R: **Transcription analysis of arabidopsis membrane transporters and hormone pathways during developmental and induced leaf senescence.** *Plant Physiology* 2006, **141**:776-792.
3. van Doorn WG: **Classes of programmed cell death in plants, compared to those in animals.** *J Exp Bot* 2011.
4. Thomas H, Ougham HJ, Wagstaff C, Stead AD: **Defining senescence and death.** *Journal of Experimental Botany* 2003, **54**:1127-1132.
5. van Doorn WG, Woltering EJ: **Senescence and programmed cell death: substance or semantics?** *J Exp Bot* 2004, **55**:2147-2153.
6. Nooden LD: **Introduction.** In: **NoodenLD. Plant cell death processes.** *Amsterdam: Elsevier* 2004:1-18.
7. van Doorn WG, Woltering EJ: **Physiology and molecular biology of petal senescence.** *J Exp Bot* 2008, **59**:453-480.
8. Thompson AR, Vierstra RD: **Autophagic recycling: lessons from yeast help define the process in plants.** *Current Opinion in Plant Biology* 2005, **8**:165-173.
9. Weaver LM, Amasino RM: **Senescence is induced in individually darkened Arabidopsis leaves but inhibited in whole darkened plants.** *Plant Physiology* 2001, **127**:876-886.
10. Saito C, Ueda T, Abe H, Wada Y, Kuroiwa T, Hisada A, Furuya M, Nakano A: **A complex and mobile structure forms a distinct subregion within the continuous vacuolar membrane in young cotyledons of Arabidopsis.** *Plant J* 2002, **29**:245-255.
11. Oda Y, Higaki T, Hasezawa S, Kutsuna N: **Chapter 3. New insights into plant vacuolar structure and dynamics.** *Int Rev Cell Mol Biol* 2009, **277**:103-135.
12. Matsushima R, Hayashi Y, Kondo M, Shimada T, Nishimura M, Hara-Nishimura I: **An endoplasmic reticulum-derived structure that is induced under stress conditions in Arabidopsis.** *Plant Physiol* 2002, **130**:1807-1814.
13. Karniely S, Pines O: **Single translation--dual destination: mechanisms of dual protein targeting in eukaryotes.** *EMBO Rep* 2005, **6**:420-425.
14. Beebo A, Thomas D, Der C, Sanchez L, Leborgne-Castel N, Marty F, Schoefs B, Bouhidel K: **Life with and without AtTIP1;1, an Arabidopsis aquaporin preferentially localized in the apposing tonoplasts of adjacent vacuoles.** *Plant Mol Biol* 2009, **70**:193-209.
15. Escobar NM, Haupt S, Thow G, Boevink P, Chapman S, Oparka K: **High-throughput viral expression of cDNA-Green fluorescent protein fusions reveals novel subcellular addresses and identifies unique proteins that interact with plasmodesmata.** *Plant Cell* 2003, **15**:1507-1523.

Chapter 2

16. Hicks GR, Rojo E, Hong S, Carter DG, Raikhel NV: **Geminating pollen has tubular vacuoles, displays highly dynamic vacuole biogenesis, and requires VACUOLESS1 for proper function.** *Plant Physiol* 2004, **134**:1227-1239.
17. Reisen D, Marty F, Leborgne-Castel N: **New insights into the tonoplast architecture of plant vacuoles and vacuolar dynamics during osmotic stress.** *Bmc Plant Biology* 2005, **5**:-
18. Saito C, Uemura T, Awai C, Tominaga M, Ebine K, Ito J, Ueda T, Abe H, Morita MT, Tasaka M, Nakano A: **The occurrence of bulbs, a complex configuration of the vacuolar membrane, is affected by mutations of vacuolar SNARE and phospholipase in Arabidopsis.** *Plant J* 2011.
19. Uemura T, Yoshimura SH, Takeyasu K, Sato MH: **Vacuolar membrane dynamics revealed by GFP-AtVam3 fusion protein.** *Genes to Cells* 2002, **7**:743-753.
20. Gao XQ, Li CG, Wei PC, Zhang XY, Chen J, Wang XC: **The dynamic changes of tonoplasts in guard cells are important for stomatal movement in Vicia faba.** *Plant Physiol* 2005, **139**:1207-1216.
21. Kutsuna N, Hasezawa S: **Morphometrical study of plant vacuolar dynamics in single cells using three-dimensional reconstruction from optical sections.** *Microsc Res Tech* 2005, **68**:296-306.
22. Irons SL, Evans DE, Brandizzi F: **The first 238 amino acids of the human lamin B receptor are targeted to the nuclear envelope in plants.** *J Exp Bot* 2003, **54**:943-950.
23. Runions J, Brach T, Kuhner S, Hawes C: **Photoactivation of GFP reveals protein dynamics within the endoplasmic reticulum membrane.** *J Exp Bot* 2006, **57**:43-50.
24. Boevink P, Oparka K, Santa Cruz S, Martin B, Betteridge A, Hawes C: **Stacks on tracks: the plant Golgi apparatus traffics on an actin/ER network.** *Plant J* 1998, **15**:441-447.
25. Quader H, Zachariadis M: **The Morphology and Dynamics of the ER.** In *The Plant Endoplasmic Reticulum. Volume 4*: Springer Berlin / Heidelberg; 2006: 1-23: *Plant Cell Monographs*].
26. Shibata Y, Shemesh T, Prinz WA, Palazzo AF, Kozlov MM, Rapoport TA: **Mechanisms determining the morphology of the peripheral ER.** *Cell* 2010, **143**:774-788.
27. Sparkes I, Tolley N, Aller I, Svozil J, Osterrieder A, Botchway S, Mueller C, Frigerio L, Hawes C: **Five Arabidopsis Reticulon Isoforms Share Endoplasmic Reticulum Location, Topology, and Membrane-Shaping Properties.** *Plant Cell* 2010, **22**:1333-1343.
28. Anderson RG, Orci L, Brown MS, Garcia-Segura LM, Goldstein JL: **Ultrastructural analysis of crystalloid endoplasmic reticulum in UT-1 cells and its disappearance in response to cholesterol.** *J Cell Sci* 1983, **63**:1-20.
29. Bassot JM: **A microtubular and a paracrystalline form in the endoplasmic reticulum of the photocytes of annelids, Polynoinae.** *J Cell Biol* 1966, **31**:135-158.
30. Chin DJ, Luskey KL, Anderson RG, Faust JR, Goldstein JL, Brown MS: **Appearance of crystalloid endoplasmic reticulum in compactin-resistant Chinese hamster cells with a 500-fold increase in 3-hydroxy-3-methylglutaryl-coenzyme A reductase.** *Proc Natl Acad Sci U S A* 1982, **79**:1185-1189.
31. Kochevar DT, Anderson RG: **Purified crystalloid endoplasmic reticulum from UT-1 cells contains multiple proteins in addition to 3-hydroxy-3-methylglutaryl coenzyme A reductase.** *J Biol Chem* 1987, **262**:10321-10326.
32. Orci L, Brown MS, Goldstein JL, Garcia-Segura LM, Anderson RG: **Increase in membrane cholesterol: a possible trigger for degradation of HMG CoA reductase and crystalloid endoplasmic reticulum in UT-1 cells.** *Cell* 1984, **36**:835-845.
33. Pathak RK, Luskey KL, Anderson RG: **Biogenesis of the crystalloid endoplasmic reticulum in UT-1 cells: evidence that newly formed endoplasmic reticulum emerges from the nuclear envelope.** *J Cell Biol* 1986, **102**:2158-2168.

Chapter 2

34. Yamamoto A, Masaki R, Tashiro Y: **Formation of crystalloid endoplasmic reticulum in COS cells upon overexpression of microsomal aldehyde dehydrogenase by cDNA transfection.** *J Cell Sci* 1996, **109 (Pt 7)**:1727-1738.
35. Frigerio L, Tolley N, Sparkes I, Craddock CP, Eastmond PJ, Runions J, Hawes C: **Transmembrane domain length is responsible for the ability of a plant reticulon to shape endoplasmic reticulum tubules in vivo.** *Plant Journal* 2010, **64**:411-418.
36. Shibata Y, Hu J, Kozlov MM, Rapoport TA: **Mechanisms shaping the membranes of cellular organelles.** *Annu Rev Cell Dev Biol* 2009, **25**:329-354.
37. Downes BP, Saracco SA, Lee SS, Crowell DN, Vierstra RD: **MUBs, a family of ubiquitin-fold proteins that are plasma membrane-anchored by prenylation.** *Journal of Biological Chemistry* 2006, **281**:27145-27157.
38. Latz A, Becker D, Hekman M, Mueller T, Beyhl D, Marten I, Eing C, Fischer A, Dunkel M, Bertl A, et al: **TPK1, a Ca²⁺-regulated Arabidopsis vacuole two-pore K⁺ channel is activated by 14-3-3 proteins.** *Plant Journal* 2007, **52**:449-459.
39. Lerich A, Langhans M, Sturm S, Robinson DG: **Is the 6 kDa tobacco etch viral protein a bona fide ERES marker?** *J Exp Bot* 2011, **62**:5013-5023.
40. Voinnet O, Rivas S, Mestre P, Baulcombe D: **An enhanced transient expression system in plants based on suppression of gene silencing by the p19 protein of tomato bushy stunt virus.** *Plant J* 2003, **33**:949-956.

Additional files

Table T1. Fixation, substitution and embedding solutions for transmission electron microscopy

Process	Chemical	Power [W]	Time	Vacuum [mm Hg]
Primary fixation	2.0% (v/v) glutaraldehyde and 2.0% (w/v) formaldehyde in 50 mM cacodylate buffer	150	1 min	15
		0	1 min	15
		150	1 min	15
		0	1 min	15
		150	1 min	15
		0	1 min	15
Wash	1x with 50 mM cacodylate buffer (pH 7.3) and 2x aqua dest.	150	45 sec	0
		0	45 sec	0
Secondary fixation	1% (v/v) osmiumtetroxide in aqua dest.	0	1 min	15
		80	2 min	15
		0	1 min	15
		80	2 min	15
Wash	2 x aqua dest. 1 x aqua dest.	150	45 sec	0
		0	15 min	0
Dehydration	Ethanol series: 30%, 40%, 50%, 60%, 75%, 90%, 2x 100% and 1 x Propylenoxide	150	45 sec	0
Resin infiltration	Spurr resin in propylenoxide: 25%, 50%, 75%, 2x 100% 1 x 100% Spurr resin	250	3 min	0
		--	1 h	--
Polymerisation	70°C in a heating cabinet	--	24 h	--

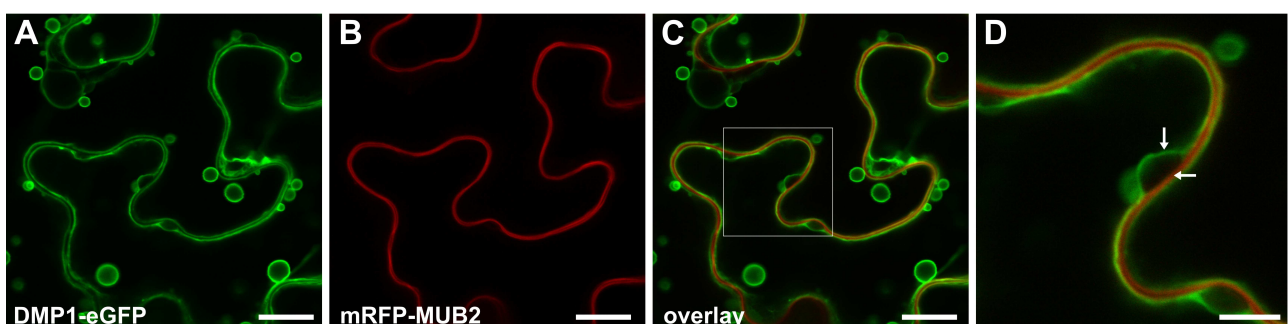


Figure S1. DMP1-eGFP does not localize to the plasma membrane. Coexpression of DMP1-eGFP (A) and the plasma membrane associated fusion protein mRFP-MUB2 (B) shows clear separation of the fluorescence signals (C, detail in D). Scale bar, 20 μ m

Chapter 2

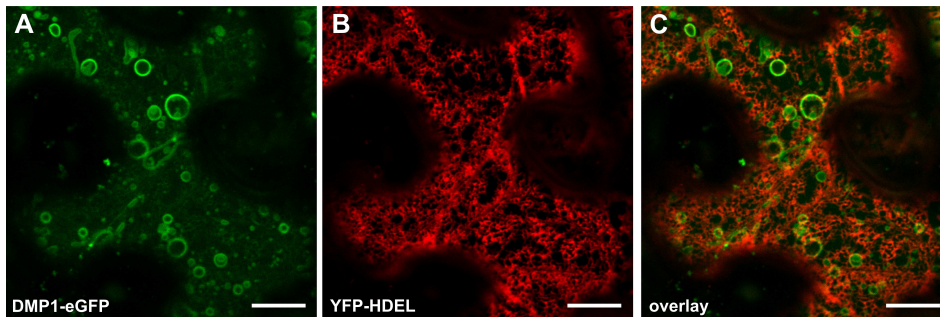


Figure S2. DMP1-eGFP does not localize to the ER during stage 1. Coexpression of DMP1-eGFP (A) and YFP-HDEL (B) labeling the lumen of the ER shows separation of the fluorescence signals (C). In some cells hardly discernible DMP1-eGFP signals show up which presumably are non-specific background (A). Scale bar, 10 μm

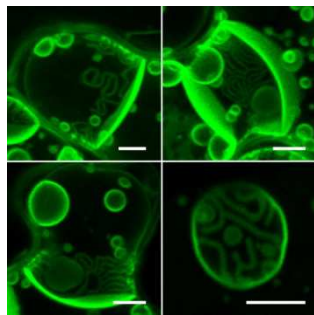


Figure S3. Tight association between DMP1-eGFP-labeled tubules and vacuolar sheets. DMP1-eGFP labeled tubules appear occasionally in tight association with vacuolar sheets, suggesting vacuolar uptake of the tubules. Scale bar, 5 μm

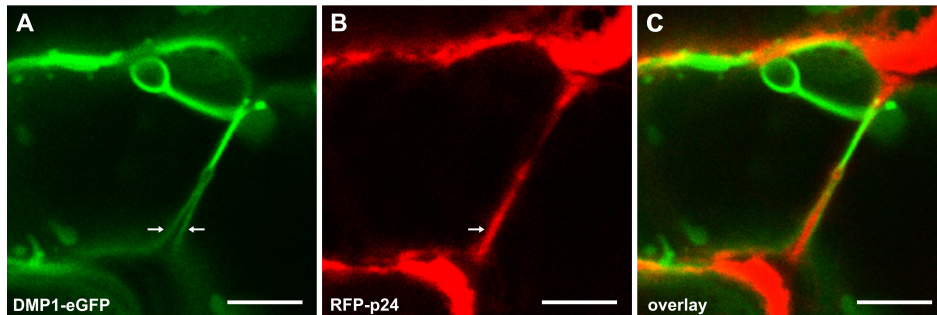


Figure S4. The vacuolar sheets are double membranes. Coexpression of DMP1-eGFP (A) and RFP-p24 (B) shows ER squeezed between the two membranes (C) forming a vacuolar sheet (arrows). Scale bar, 20 μm

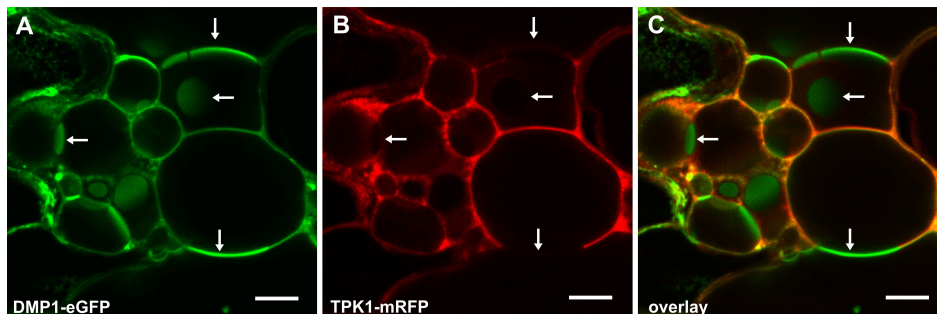


Figure S5. Exclusion of TPK1-mRFP at contact zones within foamy membrane structures. In areas where DMP1-eGFP strongly accumulates (A) TPK1-mRFP is frequently excluded, indicating inhomogeneous membrane composition. The signals appear to exclude each other (C, arrows). These areas are often round shaped and found at contact zones of adjacent sheets (A-C, arrows). Scale bar, 10 μm

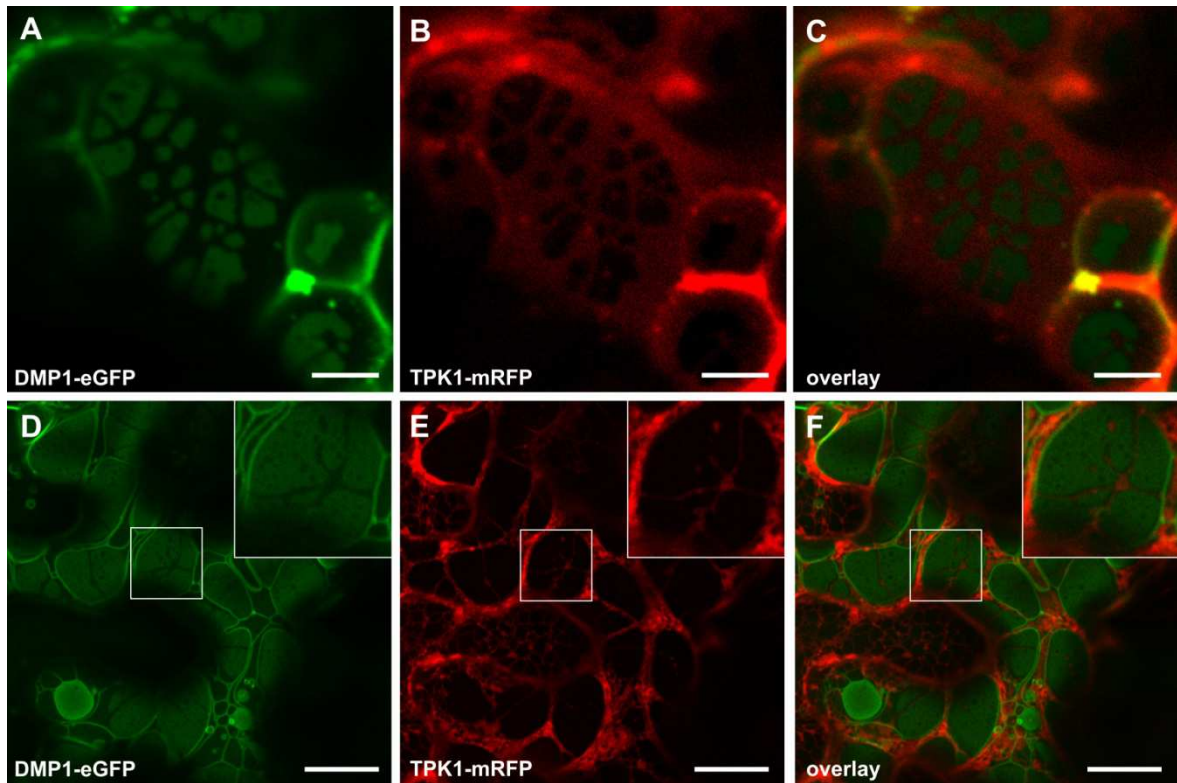


Figure S6. The sponge-like structures are tonoplast domains. Coexpression of DMP1-eGFP (A) and TPK1-mRFP (B) demonstrates separation of the fluorescence signals during stages 3 and 4 (C). The signals appear at the same confocal plane, indicating tonoplast areas with different membrane properties. Occasionally, sponge-like structures extend throughout the whole cell (D). In these cells, the ER labeled with RFP-p24 (E) as well as the tubular network labeled with DMP1-eGFP (A) appear to be compacted in spaces lacking sponge-like structures (F) suggesting spatial proximity between the tonoplast and the plasma membrane. Scale bar, A-C, 5 μm ; D-F, 20 μm

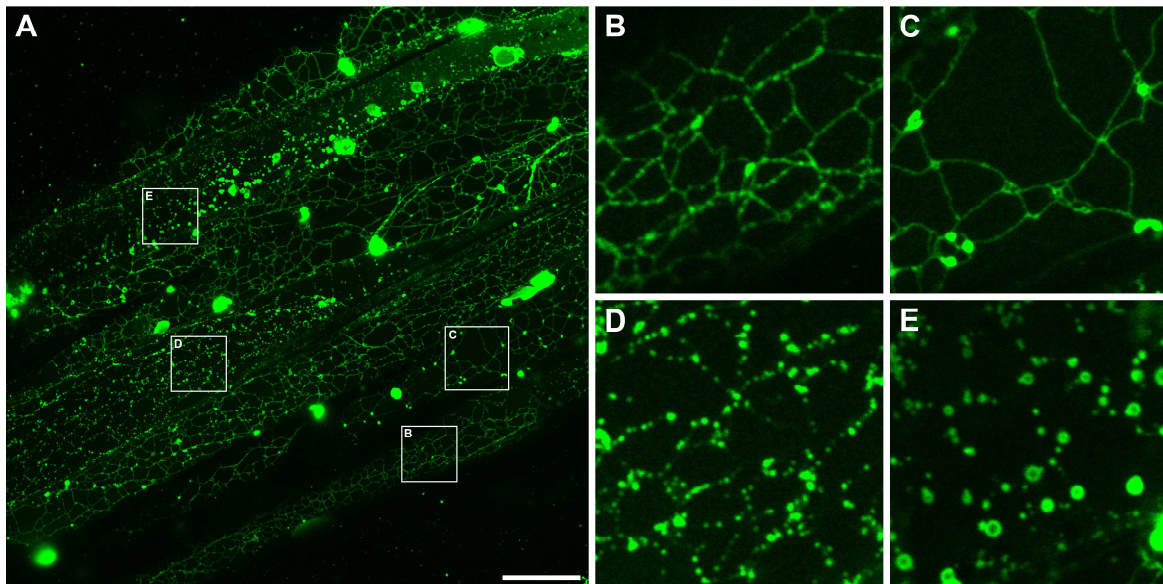


Figure S7. Bolus formation and vesiculation of the ER occur asynchronously within a tissue. Epidermis cells along a leaf vein of a rosette leaf after darkening of the whole plant for 7 days (A). Magnification of individual cells from panel A (B-E). ER network showing low background bolus formation (B). ER network with apparent loss of reticulation and boluses concentrated at tubule junctions (C). Intense bolus formation with the fluorescence signals exhibiting a punctate distribution (D). Vesiculation of the entire ER network (E). Scale bar, 30 μm

Chapter 2

Chapter 3

The amino-terminus is responsible for differential targeting of DMP1 protein isoforms to the tonoplast and the plasma membrane

Alexis Kasaras and Reinhard Kunze

Address:

Freie Universität Berlin, Institut für Biologie - Angewandte Genetik, Dahlem Centre of Plant Sciences (DCPS)

Keywords: dual targeting, protein isoforms, leaky ribosome scanning, eclipsed distribution, tonoplast, endoplasmic reticulum, plasma membrane, membrane protein, protein-protein interaction

The work presented in this chapter is in preparation for publication

Abstract

DMP1 is a senescence-associated gene of unknown function encoding a small membrane protein containing four transmembrane spans. Previous studies have highlighted a complex subcellular distribution of DMP1-eGFP in *Nicotiana benthamiana* and *Arabidopsis thaliana*. Dual-localization at the tonoplast and the endoplasmic reticulum (ER) as well as an additional, developmental-dependent localization at the plasma membrane (PM) were monitored. In this study, we focused on the elucidation of the mechanisms governing the different subcellular localizations, especially the tonoplast and PM targeting, by analyzing novel fusion proteins (eGFP-DMP1 and DMP1_{loop2}-eGFP) as well as various DMP1-eGFP fusion proteins carrying different mutations or truncations. eGFP-DMP1 and DMP1-eGFP fusions showed divergent distribution of the two proteins to the PM and the tonoplast, respectively. Translation of DMP1-eGFP leads to the formation of two protein isoforms, DMP1.1-eGFP and DMP1.2-eGFP, due to leaky ribosome scanning. The occurrence of DMP1.1 and DMP1.2 was also detected in *Arabidopsis* WT plants. Second translation initiation leading to expression of DMP1.2 was abolished in tobacco by mutating position +4 within the kozak sequence of DMP1.1. Additionally, mutation of the first AUG^{START} codon or the second in-frame AUG^{START} codon resulted in translation loss of DMP1.1 or DMP1.2 respectively. 5'-RACE-PCR and sequencing confirmed that the two protein isoforms are translated from a single transcript. By expressing both isoforms separately, we showed that DMP1.1-eGFP is targeted to the tonoplast whereas DMP1.2-eGFP, like eGFP-DMP1, is found in the PM. By investigating mutated DMP1-eGFP fusions, we showed that targeting of DMP1.1 to the tonoplast is determined by several factors. The properties of the amino acids in position 2 and to a lesser extent 3, overall length of the N-terminus, integrity of the first transmembrane domain and accessibility of the N-terminus are critical for proper targeting. Localization of DMP1.2 to the PM results from lack of the first 19 N-terminal amino acids and suggests that the PM represents the default pathway. However, the N-terminus of DMP1.1 is insufficient to direct soluble proteins to the lumen of the vacuoles or to redirect integral PM-located proteins to the tonoplast. DMP1.2-eGFP subcellular localization in the PM is largely undetectable when coexpressed with DMP1.1-eGFP. Using the heterologous split-ubiquitin system and chemical crosslinking, we showed that DMP1 is able to dimerize in yeast and to form homodimers and -tetramers *in planta* respectively. By competition experiments in tobacco using different fluorophores, we observed a fraction of DMP1.2 at the tonoplast in the presence of DMP1.1. We propose that DMP1.2 is at least partially delivered to the vacuole upon protein-protein interaction with DMP1.1. This is the first report of tonoplast/PM dual targeted membrane protein isoforms displaying an “eclipsed” distribution where the isoform lacking the positive targeting signal (DMP1.2) is redirected by the second isoform (DMP1.1) upon protein-protein interaction.

Introduction

DMP1 is a membrane protein of 207 amino acids (aa) containing four predicted transmembrane domains (TMD). It belongs to a plant-specific gene family comprising ten members in *Arabidopsis thaliana* (Kasaras and Kunze, 2010). DMP1 appears to be involved in senescence-associated membrane remodeling in tobacco and *Arabidopsis* (Kasaras and Kunze, submitted), but the biological function of DMP1 and the other DMP proteins is still unknown. We investigated the subcellular localization of all DMP proteins in transiently transfected *Nicotiana benthamiana* epidermis cells and in stably transformed *Arabidopsis thaliana* using eGFP as fluorescence tag. All DMP proteins are distributed between two membranes, the tonoplast and the ER, with the exception of DMP10 which was not detected (Kasaras and Kunze, 2010). DMP1, -2, -8 and -9 were found in both the tonoplast and the ER suggesting that they may contain competitive tonoplast targeting signals and ER retention/retrieval signals. However, overexpression may lead to mislocalization and not reflect subcellular localization at physiological expression level and in the native tissues. DMP1-eGFP expression by the CaMV 35S promoter in tobacco leaves results in complex and dynamically changing localization due to strong membrane remodeling at the tonoplast and the ER. A somewhat different distribution of the fusion protein is observed in stably transformed *Arabidopsis* expressing it from the native promoter. DMP1-eGFP shows dual localization at the tonoplast and the ER in root tips, senescing rosette and cauline leaves and senescing siliques. Interestingly a third localization at the plasma membrane (PM) was observed in root tip cells undergoing vacuole biogenesis. These apparently inconsistent results prompted us to investigate the targeting signals of DMP1.

The number of dual-targeted proteins increased in the last years suggesting that dual-targeting is a common mechanism used by the cell to place identical activities in different compartments (Karniely and Pines, 2005). In plants, dual targeting to chloroplasts and mitochondria is common. At least 50 proteins are targeted to both compartments (Carrie et al., 2009a). These activities are mainly related to DNA and RNA maintenance, translation components and cellular defense responses (Mackenzie, 2005). Systematic investigation of organellar aminoacyl-tRNA synthetases in *Arabidopsis* have shown that dual-targeting is the rule for this class of proteins as 17 members are shared between mitochondria and plastids and five between the cytosol and mitochondria (Duchene et al., 2005). Dual-targeted proteins in plants are shared between mitochondria and plastids, mitochondria and peroxysomes, mitochondria and nucleus, cytosol and mitochondria, tonoplast and ER. The molecular mechanisms leading to dual-targeting in eukaryotes are diverse. They include transcripts from two genes with one lacking the targeting sequence, alternative transcription initiations from a single gene, occurrence of spliced and non-spliced mRNA,

Chapter 3

alternative translation initiations, competitive signals on the same polypeptides, presence of ambiguous signals, partial inaccessibility to signals due to folding, protein binding or protein modifications and partial or reverse translocation from organelles. (Duchene et al., 2005; Karniely and Pines, 2005; Mackenzie, 2005; Regev-Rudzki and Pines, 2007; Carrie et al., 2009a; Carrie et al., 2009b). Regev-Rudzki and Pines (2007) have proposed the term “eclipsed” proteins to describe uneven distribution of dual-targeted proteins between compartments, the detection of one isoform by standard biochemical and visualization methods being impaired or masked by the presence of the overrepresented one. They suggest that eclipsed distribution is probably more common than currently recognized.

In the present study, we aimed to identify the mechanisms leading to the complex subcellular distribution of DMP1 and to the occurrence of two DMP1 protein isoforms. The generation and investigation of novel fusion proteins, eGFP-DMP1 and DMP1_{loop2}-eGFP, showed that eGFP-DMP1 is localized to the PM whereas DMP1_{loop2}-eGFP was targeted to the tonoplast like DMP1-eGFP. This discrepancy was paralleled by different protein bands on protein gel blots. To unravel this conundrum we analyzed intracellular targeting and electrophoretic mobility of mutated DMP1-eGFP fusion proteins. We found that DMP1 transcripts are translated into two protein isoforms, DMP1.1 and the shorter DMP1.2 which lacks 19 amino acids of the amino terminus. DMP1.1 localizes to the tonoplast whereas DMP1.2 is found at the PM, indicating that the 19 N-terminal residues include the tonoplast targeting sequence. However, DMP1.2 is partially redirected to the tonoplast by interaction with DMP1.1.

Results

As we showed in our previous study (chapter 2), ER localization of DMP1-eGFP in tobacco is mainly observed during “stage” 2 and 3. As we mainly focused on the dual tonoplast/PM localization in this study, we investigated the localization of the mutated proteins predominantly at 2-3dpi (stage 1) where only the tonoplast localization is observed with DMP1-eGFP.

Position effects of eGFP on DMP1 subcellular localization

To clarify the complex subcellular localization of DMP1-eGFP, we generated and analyzed two novel fusion proteins expressed from the 35S promoter: eGFP-DMP1 (N terminal fusion) and DMP1_{loop2}-eGFP, which contains the fluorescent tag within the second loop. The second loop was chosen because it represents the longest cytosolic part of the protein (38 aa) even longer than the N- and C-termini, consisting of 30 and 29 aa respectively (Fig. 1A). The first and third loops were considered

Chapter 3

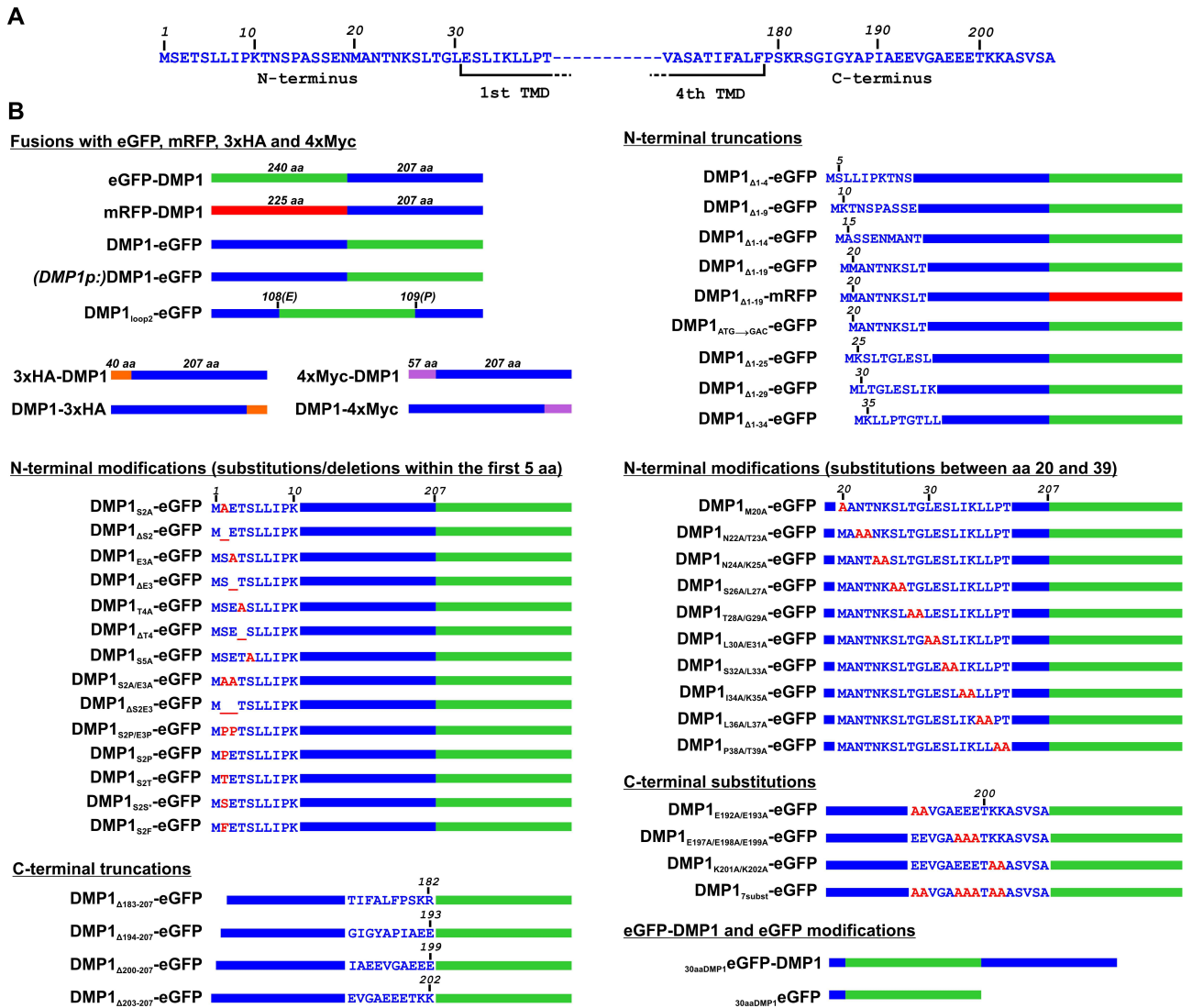


Figure 1. Fusion proteins used in this study. (A) Primary structure of DMP1 N- and C-termini. Beginning of the first TMD and ending of the last TMD are represented. (B) Schematic representations of all fusion proteins generated for this study. Amino acids substitutions and deletions are highlighted in red. All proteins are expressed from the 35S promoter with the exception of DMP1-eGFP which is expressed either from the 35S or the native promoter (*DMP1p*). Fusion proteins are classified according to the position of their modifications.

as inappropriate for eGFP insertion due to their short length (10 and 16 aa respectively). To reduce the risk to impair protein function, eGFP was inserted between amino acid 108 (glutamic acid) and 109 (proline) (Fig. 1B), a highly divergent region within the second loop throughout the whole DMP protein family (Kasaras and Kunze, 2010). Both constructs were investigated in transiently transformed tobacco (Fig. 2A, B, D and E) and stably transformed *Arabidopsis* (Fig. 2C and I) and compared with DMP1-eGFP (Fig. 2G-H). Both in tobacco and *Arabidopsis*, DMP1_{loop2}-eGFP and DMP1-eGFP exhibited comparable fluorescence patterns. Two days post infiltration (dpi), the tonoplast and tonoplast invaginations called bulbs (Saito et al., 2002) were labeled by DMP1_{loop2}-eGFP and DMP1-eGFP (Fig. 2D and G). At later stages both fusion proteins triggered drastic remodeling of the tonoplast (Fig. 2E and H) leading to the formation of foamy membrane structures

Chapter 3

as described in our previous study (chapter 2). In *Arabidopsis*, both fusion proteins labeled the tonoplast and bulbs in young cotyledons (Fig. 2F and I). Thus, DMP1-eGFP and DMP1_{loop2}-eGFP localized to the same membrane. Surprisingly eGFP-DMP1 exhibited a complete different fluorescence pattern. Sharp continuous fluorescence signals along the cell walls were observed (Fig. 2A). This fluorescence pattern did not change upon time (Fig. 2C) and was conserved in stably transformed *Arabidopsis*. Additionally eGFP-DMP1 labeled small vesicles inside the cytosol comparable to Golgi vesicles in terms of size which were observed in both tobacco (Fig. 2A, inset) and *Arabidopsis* (Fig. 2C, arrows and inset). The divergent fluorescence patterns clearly indicate that eGFP-DMP1 and DMP1-eGFP/DMP1_{loop2}-eGFP localized to distinct membranes. Since DMP1-eGFP and DMP1_{loop2}-eGFP displayed a comparable fluorescence pattern, eGFP-DMP1 is likely to be mistargeted in *Nicotiana benthamiana* and *Arabidopsis thaliana* due to the N-terminal fusion of eGFP.

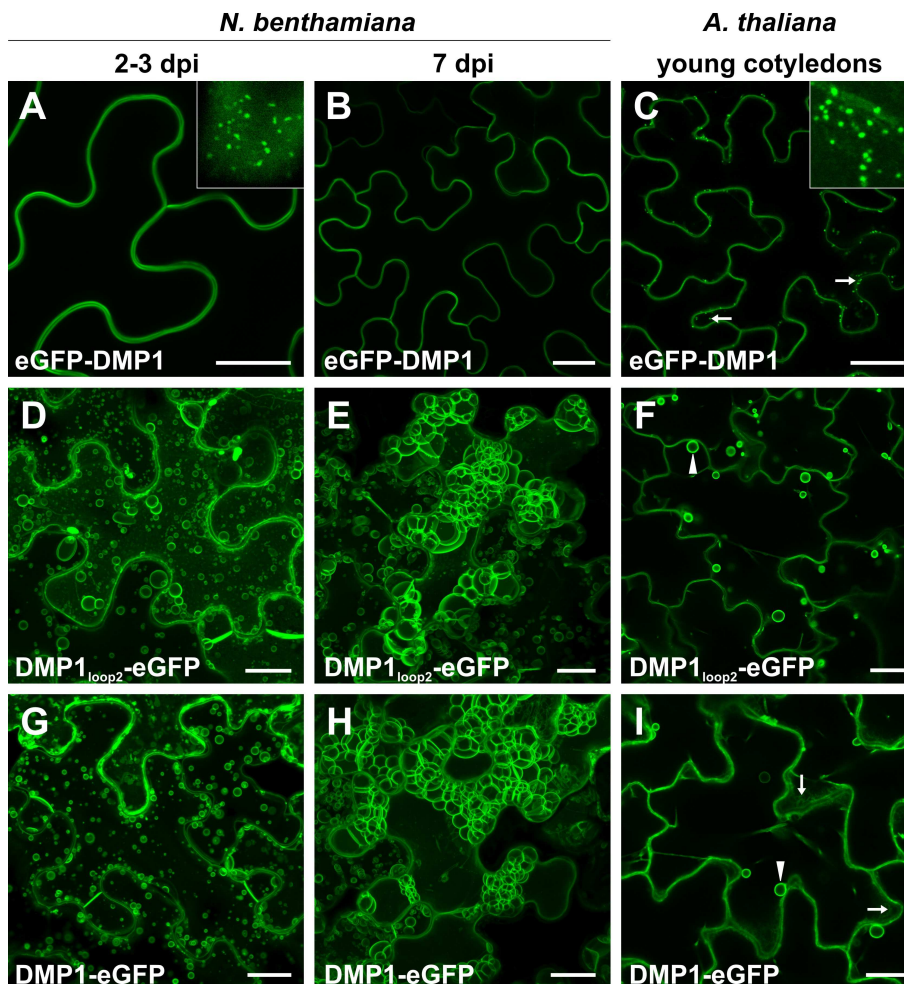


Figure 2. Position effect of eGFP on subcellular localization of the different fusion proteins. Fluorescence pattern of eGFP-DMP1 in *Nicotiana benthamiana* at 2-3 dpi (A), 7dpi (B) and in young cotyledons of *Arabidopsis thaliana* (C). Additional punctate structures labeled with eGFP-DMP1 are highlighted in the insets (A and C) and shown with arrows (C). Respective fluorescence patterns of DMP1_{loop2}-eGFP and DMP1-eGFP in tobacco are shown in (D) and (G) at 2-3 dpi, in (E) and (H) at 7 dpi and in *Arabidopsis thaliana* in (F) and (I). Scale bar, 20 μ m

eGFP-DMP1 localizes to the plasma membrane and to endosomes

To define the subcellular localization of eGFP-DMP1, we performed colocalization experiments with different markers. To distinguish between the PM and the tonoplast, we used mRFP-MUB2 as PM marker (Downes et al., 2006; Kasaras and Kunze, 2010) and TPK1-mRFP as tonoplast marker (Latz et al., 2007; Kasaras and Kunze, 2010). eGFP-DMP1 (Fig. 3A and D) clearly colocalized with mRFP-MUB2 (Fig. 3B and overlay 3C) but not with TPK1-mRFP (Fig. 3E and overlay 3F). Thus, eGFP-DMP1 localized to the PM. To identify the nature of the small vesicles, we tested several markers in colocalization experiments: Man49-mCherry localizing in Golgi vesicles (Saint-Jore-Dupas et al., 2006; Nelson et al., 2007) and mRFP-ARA7 localizing to the prevacuolar compartment (PVC) (Lee et al., 2004). Both Man49-mCherry (Fig. 3H) and mRFP-ARA7 (Fig. 3K) did not colocalize with eGFP-DMP1 (Fig. 3G and J, and the overlays 3I and L respectively). However, the vesicles labeled by eGFP-DMP1 and Man49-mCherry were often observed in close association (Fig. 3I, insets) and appeared to move sometimes as single units, suggesting physical connection (data not shown). Such associations were never observed between the vesicles labeled by eGFP-DMP1 and mRFP-ARA7 (Fig. 3L and data not shown). To further test if the trans-Golgi network (TGN) is the compartment containing eGFP-DMP1. Therefore we constructed several fusion proteins known to locate to the TGN: SYP41-mRFP, SYP43-mRFP and VTI11-mRFP (Uemura et al., 2004) but unfortunately in our hands, they did not function in transiently transfected tobacco epidermis cells. However due to the occasional tight associations between Golgi vesicles and the vesicles labeled by eGFP-DMP1 and the exclusion of eGFP-DMP1 signals from PVC, the trans-Golgi network is likely the compartment eGFP-DMP1 localized in.

Position effects of different tags on protein occurrence

Detection of eGFP-DMP1 and DMP1-eGFP on Western blot showed unexpected different banding patterns. Whereas eGFP-DMP1 showed a single band, two bands were detected with DMP1-eGFP (Fig. 4C). The upper band of the double band detected was of the same size as the single band detected with eGFP-DMP1 which indicates that this protein is probably the full length fusion protein and the lower one a truncated form. Thus, the discrepancy observed between the subcellular localizations of eGFP-DMP1 and DMP1-eGFP is reflected in the occurrence of one or two proteins. The same pattern was observed in stably transformed *Arabidopsis* (Fig. 4A) once more pointing to a conserved mechanism between these two species. A double band was also detected with DMP1_{loop2}-eGFP in tobacco and *Arabidopsis* (data not shown) reinforcing the hypothesis that eGFP-DMP1 is the mistargeted fusion protein. To further test the impact of a tag on the occurrence of one or two proteins, we fused two other tags, 3xHA and 4xMyc, N- and C-terminally to DMP1 (Fig. 1B).

Chapter 3

These tags are much smaller than eGFP (40 and 57 aa respectively to 240 aa for eGFP) and might potentially less interfere with different mechanisms such as proper targeting or post-translational maturation which might explain the occurrence of one or two proteins. Comparable pattern were obtained with these tags (Fig. 4D and E). Whereas both N-terminal fusions 3xHA-DMP1 and 4xMyc-DMP1 led to the detection of one protein, two proteins were detected with the two C-terminal fusions DMP1-3xHA and DMP1-4xMyc. Thus, fusion of a tag, independently of its size, to the amino terminus of DMP1 prevents the occurrence of the smaller fusion protein.

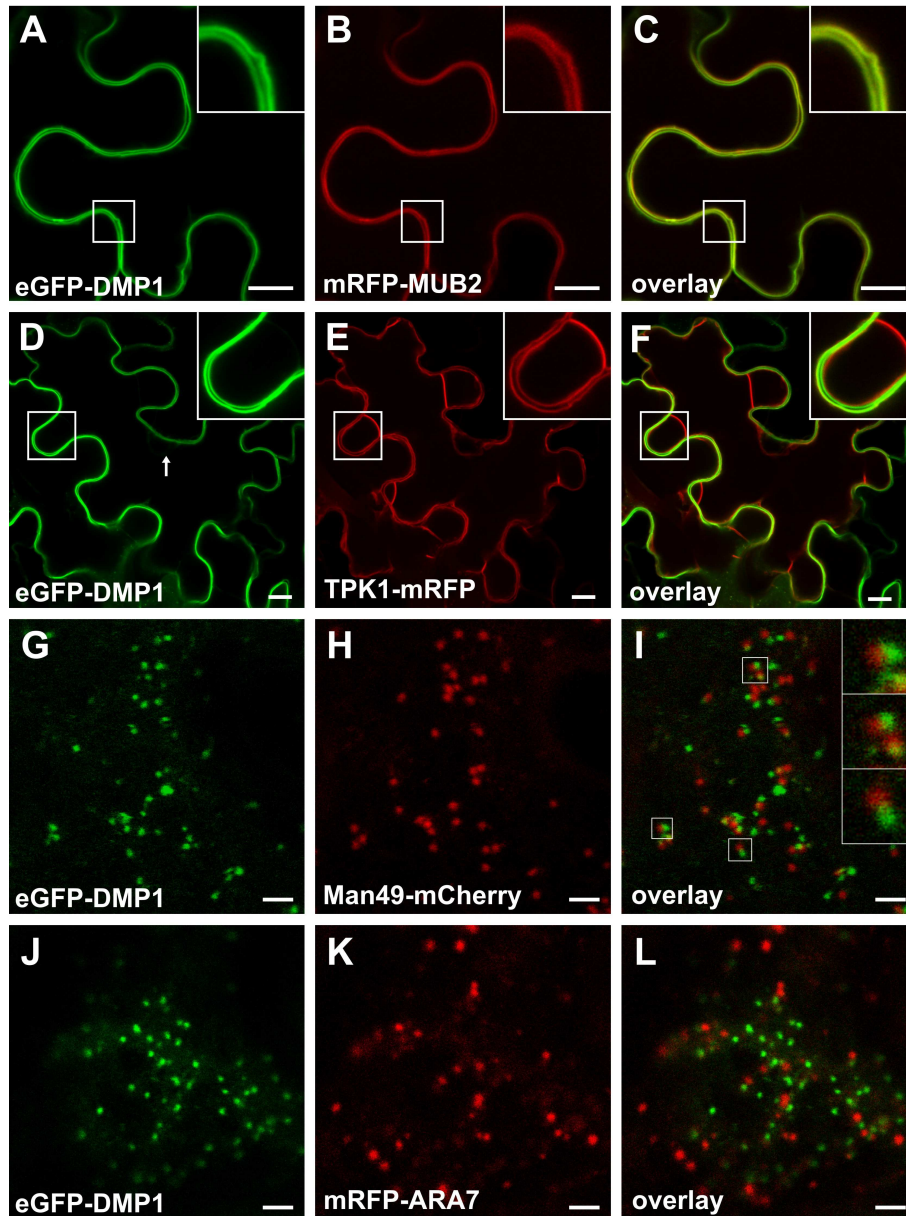


Figure 3. Determination of eGFP-DMP1 subcellular localization in co-localization experiments. eGFP-DMP1 (A and D) co-expressed with mRFP-MUB2 (B) and TPK1-mRFP (E) shows perfect colocalization of the fluorescence signals at the PM (C) but not at the tonoplast (F). The small punctate structures labeled with eGFP-DMP1 (G and J) does not colocalize with the Golgi-associated fusion protein Man49-mCherry (H and overlay I) and with mRFP-ARA7 (K and overlay L) illuminating the PVC. Scale bar, A-F; 10 μ m, G-L; 3 μ m

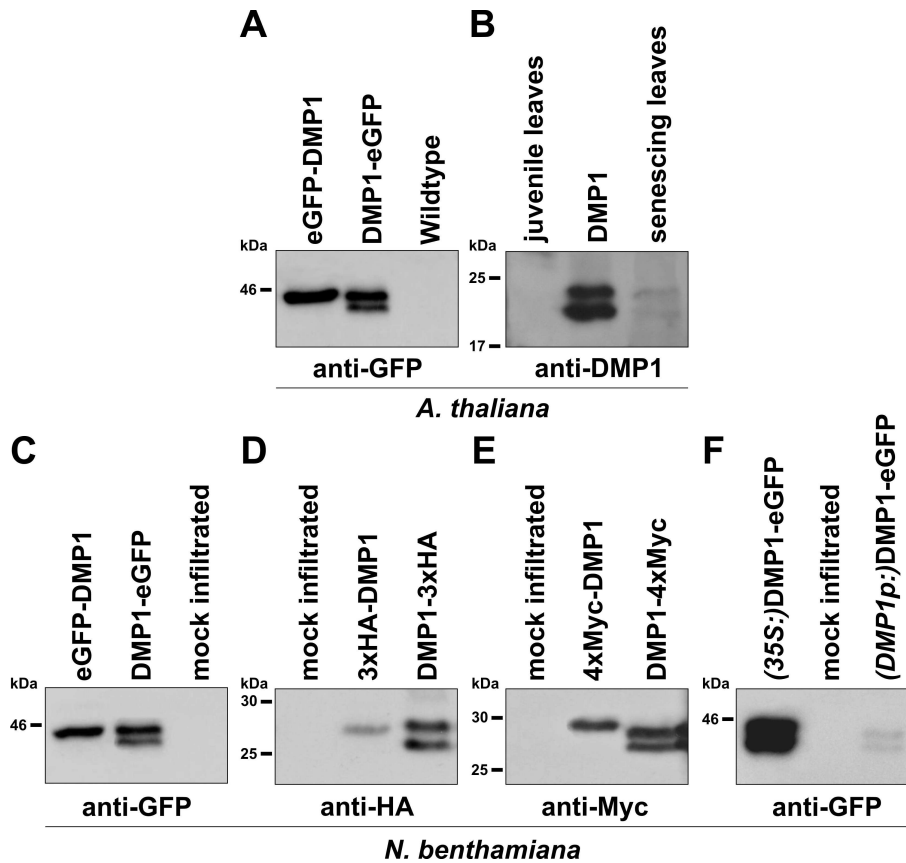


Figure 4. Differential protein patterns due to position of the tags. Fusion proteins were detected using anti-GFP (A, C and F), anti-HA (D) and anti-Myc (E). DMP1 were detected in WT senescing *Arabidopsis* plants and in transgenic line *DMP1-OE1* using anti-DMP1 (B). Membrane fractions were enriched by microsome purification prior to detection. *Arabidopsis* leaves expressing eGFP-DMP1, DMP1-eGFP (A) and DMP1 (B) and juvenile WT leaves were harvested at 18 DAS. The senescing WT leaves were harvested at 43 DAS. All N-terminal fusions lead to detection of single proteins whereas all C-terminal as well as the unfused DMP1 shows two proteins.

Occurrence of the two DMP1-eGFP fusion proteins does not result from overexpression

We further tested if the occurrence of the two DMP1-eGFP forms might be an artifact due to overexpression. To do so, we expressed DMP1-eGFP from the native promoter. We directly amplified *DMP1p:DMP1* from genomic DNA in a single PCR reaction to keep the native 5'UTR avoiding the presence of artificial nucleotides upstream of the translation start. Expression of *DMP1p:DMP1-eGFP* in tobacco clearly led to detection of two distinct proteins (Fig. 4F). Despite the fact that the promoter of *DMP1* is senescence-specific in *Arabidopsis* leaves, it promoted transcription to a level sufficient to detect the resulting two fusion proteins in transiently transformed tobacco leaves. Thus, the occurrence of two fusion proteins is not due to overexpression and to the promoter used.

Two distinct DMP1 proteins are found in *Arabidopsis*

To fully exclude any effects of eGFP on the occurrence of the two distinct fusion proteins, we investigated the protein patterns of unfused DMP1 expressed from either the 35S promoter or the native one with the help of an antibody raised against DMP1. In both cases, the double band pattern was detected (Fig. 4B). DMP1 was detected only in senescing rosette leaves paralleling the senescence-specificity shown on transcription level (Kasaras and Kunze, 2010). Thus, two DMP1 isoforms of approximately 2-3 kDa difference in a 1:1 ratio occur in *Arabidopsis* WT plants.

Protein occurrence and subcellular localization are independent events

Given the fact that the discrepancy between the subcellular localization of eGFP-DMP1 and DMP1-eGFP was accompanied by the occurrence of one or two proteins respectively, we tried to elucidate if these events were linked by generating an N-terminal truncation series of DMP1-eGFP (Fig. 1B). The truncation of the four, nine, 14 and 19 first aa resulted in either single fusion proteins as eGFP-DMP1 (Fig. 5C) or double fusion proteins all localizing to the PM (Fig. 5M and N and Table 1). Thus, the occurrence of two proteins does not correlate with tonoplast subcellular localization. Moreover, the first four aa appears to be crucial for proper tonoplast targeting since DMP1 Δ 1-4-eGFP localized in the PM (Fig. 5M). The truncation of additional aa (DMP1 Δ 1-25-eGFP, DMP1 Δ 1-29-eGFP, DMP1 Δ 1-34-eGFP) resulted in ER retention (Fig. 5O and Table 1). Only DMP1 Δ 1-25-eGFP could be clearly detected on WB and showed a one-band-pattern similar (Fig. 5C).

The N-terminal truncation series suggested a crucial role for the first four aa in targeting the proteins either to the tonoplast or the PM. To elucidate which amino acid(s) is/are essential for proper targeting and protein occurrence, we substituted amino acids S2, E3, T4, S5 to alanines respectively and deleted individually S2, E3, T4 (fig. 1B). All individual substitutions or deletions did not affect subcellular localization (Fig. 5F and G and Table 1). All showed tonoplast/bulbs localization at 3 dpi and were all able to induce strong membrane remodeling with time (data not shown) as the non-modified DMP1-eGFP (Fig. 2G and H; chapter 2). The substitution of E3, T4, S5 or deletion of E3 and T4 did not affect protein banding pattern, two proteins were detected (Fig. 5A). In contrast, the deletion and the substitution of aa S2 both led to a single protein, the smaller one being lacking. This identifies S2 as crucial position for the occurrence of one or two proteins but not for targeting to the vacuole. Thus, the presence of one or two proteins does not reflect subcellular localization.

Chapter 3

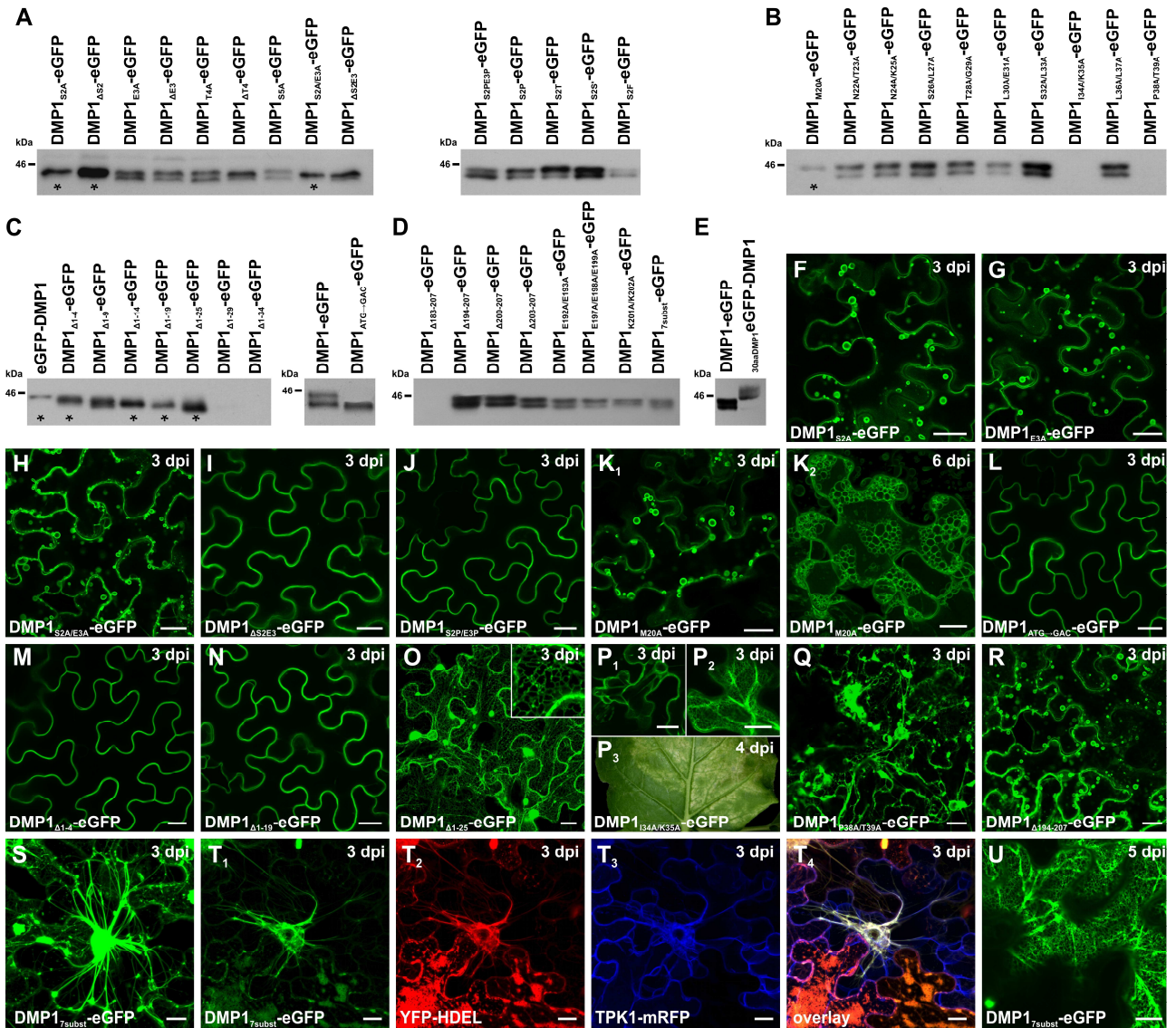


Figure 5. Effect of the different mutations generated on DMP1-eGFP subcellular localization correlated with the respective protein patterns on WB. (A) Detection of DMP1-eGFP carrying mutations within the first five amino acids (A), between position M20 and T39 (B), lacking different N-terminal segments (C) or being C-terminally modified (D). (E) Protein pattern of DMP1 N-terminus fused to eGFP-DMP1 compared to eGFP-DMP1. All protein detections (A-E) were performed using anti-GFP. Single bands are highlighted with asterisks. Substitutions S2A (F), E3A (G), S2A/E3A (H), M20A (K_{1,2}), and Δ 194-207 truncation (R) do not affect targeting of DMP1-eGFP to the tonoplast and labeling of bulbs. Mutations Δ S2E3 (I), S2P/E3P (J) and Δ 1-4 (M) are sufficient to abolish tonoplast targeting, the respective proteins locating to the PM. Expression of the shorter isoform DMP1.2 alone were achieved by mutating the first start codon (L) and by truncating the 19 first amino acids (N). Both fusion proteins show clear location to the PM. Larger N-terminal truncation (Δ 1-25) leads to retention in the ER (O). Substitution P38A/T39A within the first TMD leads to strong protein aggregates within the ER (Q). Substitution I34A/K35A within the first TMD induces rapid cell death (P₃), the fusion protein being located both to the tonoplast (P₁) and the ER (P₂). Substitution of the seven charged aa within the C-terminus of DMP1 leads to abnormal subcellular localization at 3 dpi (S) which tend to disappear and to display a strong ER labeling at 5 dpi (U). Co-expression of DMP1_{7subst}-eGFP (T₁), the soluble ER marker YFP-HDEL red false-colored (T₂) and the tonoplast fusion protein TPK1-mRFP blue false-colored (T₃) show DMP1-eGFP labeling perinuclear ER exhibiting aberrant architecture (T₄). Subcellular localization of all mutant DMP1-eGFP fusion proteins are given in Table 1. Scale bar, 20 μ m

DMP1-eGFP targeting to the tonoplast depends on the sequence and length of the DMP1 amino terminus

Deletion of S2 alone resulted in a single protein located to the tonoplast/bulbs but deletion of S2E3T4 at once (DMP1 $_{\Delta 1-4}$ -eGFP) resulted in a single protein localizing to the PM. To investigate the mechanism underlying proper targeting of DMP1, we deleted S2E3 at once or substituted them to alanines (Fig. 1B). Interestingly, both the patterns on WB and the subcellular localization differed between DMP1 $_{\Delta S2E3}$ -eGFP and DMP1 $_{S2A/E3A}$ -eGFP. DMP1 $_{S2A/E3A}$ -eGFP localized to the tonoplast and bulbs (Fig. 5H) and displayed one band on WB (Fig. 5A) whereas DMP1 $_{\Delta S2E3}$ -eGFP localized to the PM (Fig. 5I) and displayed two bands (Fig. 5A) confirming that protein occurrence and subcellular localization are not linked events. The fact that DMP1 $_{S2A/E3A}$ -eGFP and DMP1 $_{\Delta 1-4}$ -eGFP both led to loss of tonoplast targeting and PM localization suggest that length of the N-terminal part of DMP1 is crucial for proper targeting. However the properties of the first amino acids also appeared to be determining. Indeed, mutation of S2E3 to prolines (DMP1 $_{S2P/E3AP}$ -eGFP) was sufficient to prevent targeting to the vacuole. Even the single substitution of S2 to a proline (DMP1 $_{S2P}$ -eGFP) appeared to largely redirect the fusion protein to the PM (data not shown). However DMP1 $_{S2P}$ -eGFP mainly exhibited an eGFP-DMP1-like fluorescence pattern but a non-negligible fluorescence fraction was found at the tonoplast and bulbs suggesting that tonoplast targeting was not fully impaired by the S2P mutation. Thus, nature of the amino acids at position 2 and to a lesser extent at position 3 appears to be crucial for proper targeting to the tonoplast.

The shorter DMP1 protein isoform is translated at a second translation initiation site

Deletion and substitution of aa S2 both resulted in lack of the smaller fusion protein. The difference between both proteins was estimated around 2-3 kDa on WB. We hypothesized that this difference may be due to a post-translational cleavage between aa 20 to 30, E31 being predicted to be the first aa within the first TMD (Kasaras and Kunze, 2010). If so, aa S2 would be essential for recognition and/or downstream cleavage. We further hypothesized that the smaller protein may be translated from a second in-frame AUG^{START} codon which leads to a methionine in position 20 in the full length protein. To test these two hypotheses we generated a mutation series between aa 20 and 31 (Fig. 1B). DMP1 $_{M20A}$ -eGFP was the only mutated fusion protein which exhibited a single band on WB, the smaller one being lacking (Fig. 5B). Thus, the smaller DMP1 protein results from a second translation initiated in position M20 and not from a post-translational maturation. We will refer to them hereafter as DMP1.1 and DMP1.2, DMP1.2 being the shorter isoform. DMP1 $_{M20A}$ -eGFP exhibited the same fluorescence pattern as DMP1-eGFP (Fig. 5K₁) leading to strong remodeling of the tonoplast with time (Fig. 5K₂) indicating that the truncated DMP1.2 is not required for

Chapter 3

membrane remodeling. The fusion protein DMP1 Δ_{1-19} -eGFP generated in the N-terminal truncation series (Fig. 1B) corresponds to DMP1.2-eGFP and was found in the PM (Fig. 5N). Thus, DMP1.1 is targeted to the tonoplast upon recognition of the first amino acids. DMP1.2 which lack the first 19 aa escapes tonoplast targeting. Thus, the PM appears to be a default pathway. However, as already mentioned, truncation of 6 additional aa (DMP1 Δ_{1-25} -eGFP) impairs localization to the PM, the fusion proteins being retained in the ER (Fig. 5O). Thus, a certain length of the amino terminus is required for transit through the secretory pathway to the PM. We further confirmed that the lower band observed on WB is due to a second translation initiation by mutating the first AUG^{START} to GAC (35S:DMP1_{ATG→GAC}-eGFP) (Fig. 1B and Table 1). Only the lower band was observed on WB (Fig. 5C) corresponding to DMP1.2-eGFP.

The PM is the default pathway for DMP1.2 and DMP1.1

By coexpressing DMP1.2 fused to mRFP (DMP1 Δ_{1-19} -mRFP, Fig. 6B) and eGFP-DMP1 (Fig. 6A), we confirmed that they both colocalized in the PM (Fig. 6C). Thus, DMP1.1 is indeed mistargeted to the PM when fused N-terminally to eGFP. This indicates that the first amino acids especially S2 are not recognized by the tonoplast targeting machinery if they are not located at the very end of the N-terminus. Thus both truncation of DMP1 N-terminus (DMP1.2) and N-terminal addition of a tag resulted in localization in the PM. This strongly indicates that the PM is the default pathway for DMP1.2 but also DMP1.1.

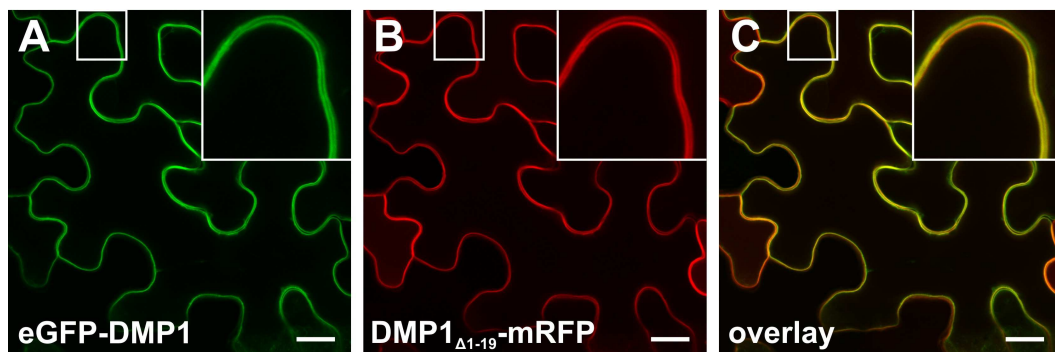


Figure 6. DMP1.1 is mistargeted to the PM and colocalizes with DMP1.2 when fused N-terminally to eGFP. Co-expression of eGFP-DMP1 (A) and DMP1 Δ_{1-19} -mRFP (B) show perfect colocalization of the fluorescence signals at the PM (C). Scale bar, 20 μ m

Suboptimal Kozak sequence in position +4 is responsible for leaky ribosome scanning leading to translation of DMP1.2

By mutating M20 to alanine, we identified this position as AUG^{START} codon for translation of DMP1.2. We also showed that the mutation and deletion of S2 prevented translation of DMP1.2

Chapter 3

suggesting a link between these two events. We suggested that a leaky ribosome scanning mechanism (Kozak, 2002) might be this link. Indeed, a closer look at the context surrounding the start codon revealed that in all the constructs which did not lead to the translation of the smaller fusion protein (Table 1) the thymine in position +4 had been exchanged to guanine. Guanine and to a lesser extent alanine are conserved nucleotides in position +4 in *Arabidopsis* (Rangan et al., 2008) responsible for efficient translation initiation. Thus, the native thymine in position +4 represents a suboptimal context for translation initiation allowing ribosome to stop and initiate at the first start codon but also to bypass it allowing scanning until the second start codon. *35S:DMP1_{S2P}-eGFP* carries a cytosine in position +4 which is even rarely found in this position than thymine (Rangan et al., 2008). The leaky ribosome scanning was not affected, *DMP1_{S2P}-eGFP* led to the presence of two proteins (Fig. 5A). We further exchange position +4 to adenine (*35S:DMP1_{S2T}-eGFP*, Fig. 1B) which did not modify leaky ribosome scanning at the first start codon (Fig. 5A). Thus, mutation of thymine in position +4 to guanine but not to cytosine or adenine improved the translation context at the first ATG and prevented translation of DMP1.2. The only exception was *35S:DMP1_{A1-4}-eGFP* which carries a thymine in position +4 like *DMP1-eGFP* but led to a single fusion protein (Table 1 and Fig. 5C) suggesting improved context at the first start codon. *35S:DMP1_{A1-4}-eGFP* has a thymine in position +6 instead of a cytosine as in *35S:DMP1-eGFP* (Table 1). We tested if positions +5 and +6 might also be determinant for translation efficiency. We therefore generated *35S:DMP1_{S2F}-eGFP* and *35S:DMP1_{S2S*}-eGFP* (Fig. 1B and Table 1) which carry mutations in position +5 and +6 respectively. Both led to translation of two proteins suggesting that these positions are not important for translation efficiency in this context. Thus other positions upstream of position +6 might improve translation efficiency at the first ATG in *35S:DMP1_{A1-4}-eGFP*. We did not further modified positions downstream of position +1 within the 5'-UTR especially position -3, known to influence translation initiation efficiency (Kozak, 2002). Indeed, these positions are completely divergent in the 35S promoter and *DMP1p* (Fig. 7D) but both led to the translation of two proteins suggesting that these positions are not influencing translation efficiency in this context.

All proteins are translated from single transcripts

To confirm that the occurrence of the two DMP1 isoforms is related to leaky ribosome scanning and to invalidate the possibility of the occurrence of two distinct mRNA due to alternative transcription start, we amplified the 5' end of the cDNA by 5'-RACE-PCR (Fig. 7C). We tested several constructs leading either to one (*35S:DMP1_{A1-4}-eGFP*, *35S:DMP1_{M20A}-eGFP*, *35S:DMP1_{S2A/E3A}-eGFP*) or two proteins (*35S:DMP1-eGFP*, *DMP1p:DMP1-eGFP*, *35S:DMP1_{S2A}-eGFP*, *35S:DMP1_{E3A}-eGFP*, *35S:DMP1_{A52E3}-eGFP*) in tobacco (Fig. 7A). Additionally, we tested

transgenic *Arabidopsis* plants expressing *35S:DMP1-eGFP* and *35S:DMP1* as well as WT plants (Fig. 7B). In all cases, single transcripts were amplified (Fig. 7A and B). Sequencing was used to confirm their identity and to exclude the presence of two transcripts which might not have been separated by electrophoresis (data not shown).

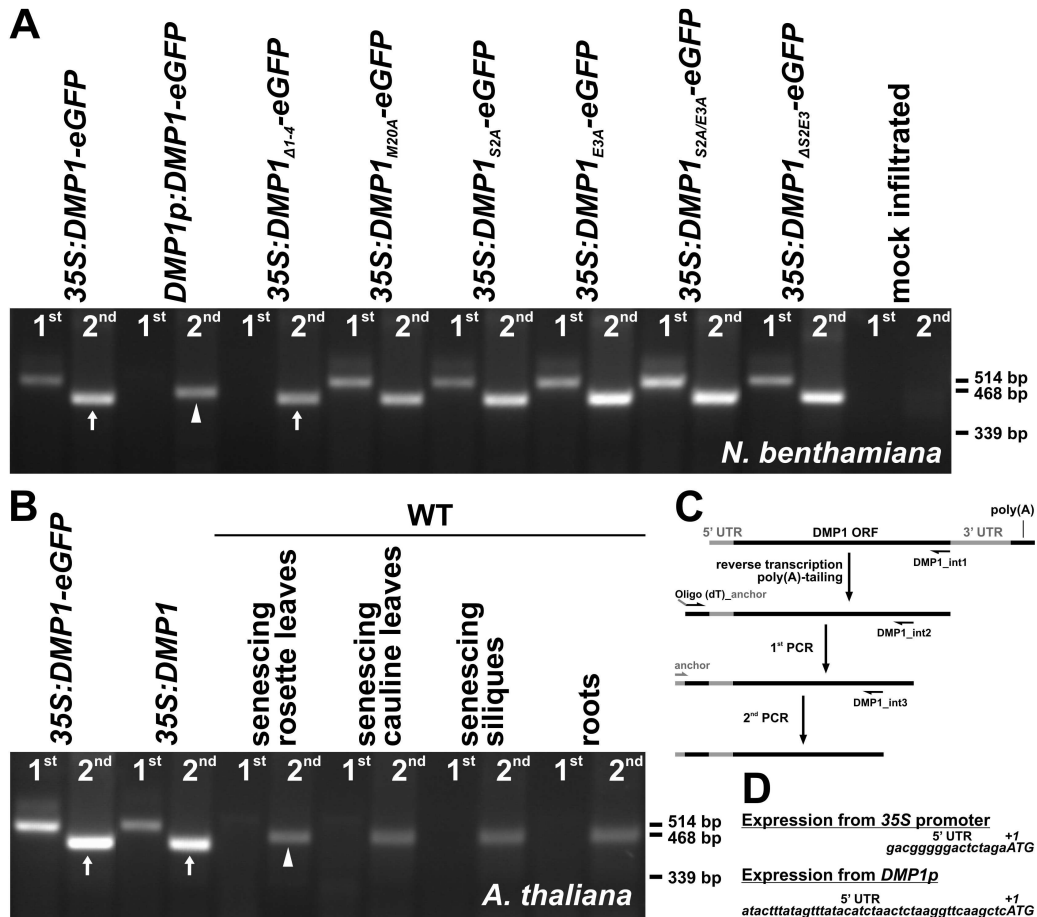


Figure 7. DMP1.1 and DMP1.2 are translated from the same transcript. 5'-RACE-PCR were performed as schematically represented (C). Total RNA from *Nicotiana benthamiana* infiltrated leaves expressing DMP1-eGFP from the native or 35S promoter and DMP1-eGFP carrying the modifications $\Delta 1-4$, M20A, S2A, E3A, S2A/E3A and $\Delta S2E3$ (A) was used. Similarly total RNA from *Arabidopsis* plants stably transformed with *35S:DMP1-eGFP* and *35S:DMP1* as well as different tissues expressing *DMP1* were used. In all cases, single transcripts were amplified. Slight shift between products amplified from transcripts deriving from the 35S promoter (arrows) and *DMP1p* (arrowheads) were observed (A and B). Sequencing showed that transcripts deriving from *DMP1p* have a longer 5'UTR than those deriving from 35S (D).

DMP1 N-terminus is not sufficient to target soluble proteins to the vacuole and to redirect integral PM-localized proteins to the tonoplast

Since the N-terminal part of DMP1 was shown to be responsible for targeting of DMP1.1 to the tonoplast, we asked the question if it might be sufficient to target soluble proteins to the vacuole. We therefore fused the whole soluble N-terminus of DMP1 consisting of 30 aa to eGFP (Fig. 1A). The fluorescence signals observed (Fig. 8B) were similar to those observed with free eGFP (Fig.

Chapter 3

8A), labeling the nucleus and the entire cytosol but not the lumen of the central vacuole. Thus, the N-terminal part of DMP1 cannot target soluble proteins to the vacuole. Several constructs has been generated at the end of the redaction of this phd thesis in order to test if DMP1 N-terminus could serve as tonoplast targeting motif for integral plasma membrane proteins. Indeed, the PM is likely the default pathway for most membrane proteins (Bassham et al., 2008). Thus, the addition of DMP1 N-terminus might target them to the tonoplast. To do so, we screened the publicly available database SUBA II (<http://suba.plantenergy.uwa.edu.au/>) for membrane proteins which has already been shown to localize only to the PM both by GFP fusion and MS/MS assays. We chose proteins which possess an N-terminus of approximately the same size that that of DMP1. We cloned the ammonium transporter AMT2 (Sohlenkamp et al., 2002), the inositol transporter INT2 (Schneider et al., 2007) and the equilibrative nucleoside transporter ENT6 (Wormit et al., 2004). Since we did know if the N-terminus of DMP1 alone would be sufficient, we amplified both the N-terminus alone and the N-terminus containing the first TMD from DMP1. We exchanged them for the N-termini alone or containing the first TMD of AMT2, INT2 and ENT6 respectively. All these chimeric constructs were already tested in tobacco. Unfortunately, targeting to the tonoplast could not be achieved. PM localization was largely altered but the chimeric proteins appeared to be largely retained within the ER or led to fluorescence pattern which could not be assigned precisely to one membrane. Thus, the N-terminus of DMP1 with or without the first TMD is not sufficient to target integral PM proteins to the tonoplast. This indicates that other factors play a role in tonoplast targeting of DMP1.1.

The N-terminus of DMP1.1 fused to the mistargeted eGFP-DMP1 does not restore targeting to the tonoplast

We showed that eGFP-DMP1 was mistargeted due to the presenece of eGFP at the amino terminus. position effects of eGFP fused to the N-terminus of DMP1.1. We then investigated if the N-terminus of DMP1 would be sufficient to restore proper targeting of eGFP-DMP1 to the tonoplast. We therefore fused the N-terminus of DMP1 to eGFP-DMP1 (Fig. 1B). ${}_{30\text{aaDMP1}}\text{eGFP-DMP1}$ decorated the PM like eGFP-DMP1 (Fig. 8C). This suggests that the position of the first TMD and thus, the overall size of the N-terminus are required to target DMP1.1 to the tonoplast. The fact that $\text{DMP1}_{\text{loop2}}\text{-eGFP}$ is properly targeted to the tonoplast (Fig. 2D-F) is in agreement with this assumption.

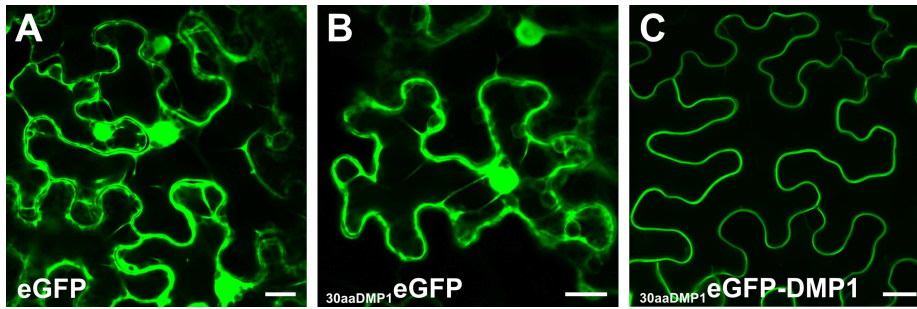


Figure 8. DMP1 N-terminus does not target eGFP to the vacuole and does not restore tonoplast targeting to eGFP-DMP1. eGFP (A), $_{30aaDMP1}$ eGFP (B) and $_{30aaDMP1}$ eGFP-DMP1 (C) were expressed individually in tobacco epidermis cells. Pictures were taken at 3 dpi. Scale bar, 20 μ m

The integrity of the first TMD is required for proper targeting of DMP1-eGFP to the vacuole

As we generated the mutation series between aa 20 and 39 (see above and Fig. 1B), we showed that M20 is responsible for translation of DMP1.2. The other mutations within the N-terminus (N22A/T23A, N24A/K25A, S26A/L27A and T28A/G29A) as well as three mutation pairs within the first TMD (L30A/E31A, S32A/L33A and L36A/L37A) did not affect subcellular localization (Table 1) and protein occurrence (Fig. 5D). In contrast the mutation pair I34A/K35A led rapidly to necrotic-like lesions after 3-4 dpi (Fig. 5P₃) and death of the infiltrated area. Fluorescence signals were extremely weak (Fig. 5P₁ and P₂) and proteins could not be detected on WB (Fig. 5B). Mutation pair P38A/T39A led to large protein aggregates (Fig. 5Q). Thus mutations within the first TMD even using the hydrophobic aa alanine as substitute appears to dramatically affect protein localization.

DMP1.2 partially localizes to the tonoplast upon interaction with DMP1.1 in tobacco

In chapter 2, we showed in *Arabidopsis* root tips that DMP1-eGFP is also found at the PM in addition to the tonoplast location. The PM-localization is likely imputable to DMP1.2. However, we also showed that expression of DMP1-eGFP (i.e. DMP1.1-eGFP + DMP1.2-eGFP) in tobacco and *Arabidopsis* led to labeling of the tonoplast but not of the PM (chapter 2, Fig. 2 and Fig. 9 E, H and K). Due to the strong fluorescence intensities observed with the two isoforms expressed individually (DMP1_{M20A}-eGFP, Fig. 5K₁₋₂ and DMP1 _{Δ 1-19}-eGFP, Fig. 5N) and taking into account DMP1 predicted topology, eGFP is likely to be cytosolic when fused C-terminally to DMP1.1 and DMP1.2. Since DMP1.1 and DMP1.2 are found at approximate equimolar levels when DMP1-eGFP is expressed (Fig. 4A and 5C), significant protein turnovers are excluded. Thus, PM and tonoplast fluorescence signals should be approximately of the same intensity. We next hypothesized if DMP1.2 might interact with DMP1.1 and be directed to the tonoplast as a consequence. We tested DMP1 dimerization by different methods. We used the heterologous split-ubiquitin system in

Chapter 3

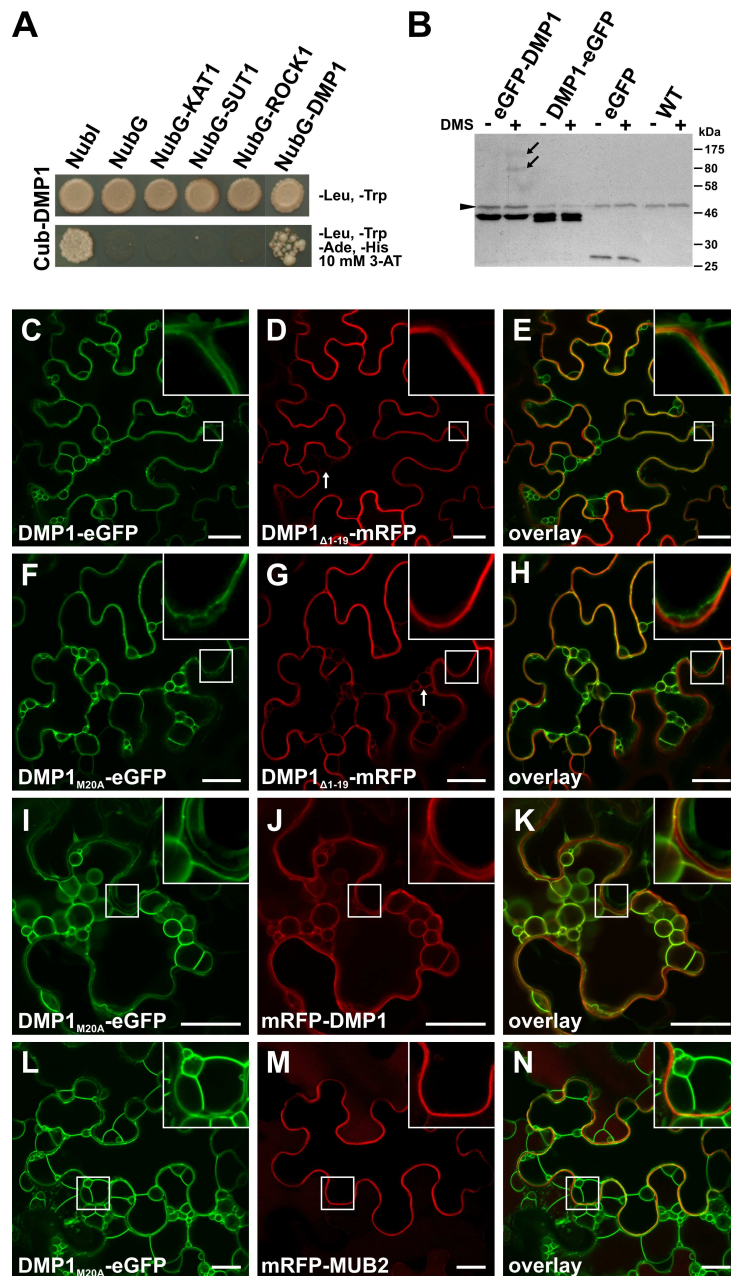


Figure 9. DMP1 dimerizes in yeast and *in planta*. (A) The split-ubiquitin system in yeast was used to test DMP1 dimerization. Interaction between Cub-DMP1 used as bait and the prey NubG-DMP1 were detected. Orientation of DMP1 was verified by coexpressing Cub-DMP1 and the positive control Nubi. Growth was observed showing that Cub and therefore the N-terminus of DMP1 were cytosolic. The soluble negative control NubG as well as the unrelated integral protein NubG-KAT1, NubG-SUT1 and NubG-ROCK1 did not interact with Cub-DMP1. 10 mM 3-AT was added to lower background growth to an acceptable level. For vector selection, leucine and tryptophane were not present in the media. For detection of protein-protein interactions, adenine and histidine were additionally lacking in the media. Crosslinking experiments using DMS were carried out to detect DMP1 protein-protein interaction in *planta* (B). Tobacco lower epidermis cells were transformed with *35S:DMP1-eGFP*, *35S-eGFP-DMP1* and *35S:eGFP*. Microsomes were purified five days after infiltration. Crosslinking experiments were performed on the microsomal fractions for eGFP-DMP1 and DMP1-eGFP and on the soluble fraction for eGFP. Two additional bands were detected in the presence of DMS for eGFP-DMP1. The size of these bands fits with the size of eGFP-DMP1 homodimers and – tetramers. The band highlighted with an arrowhead is unspecific and was detected in all samples including non-infiltrated WT tobacco plants (B). Co-expression of DMP1-eGFP (C) and DMP1 $_{\Delta 1-19}$ -mRFP (D) show clear dissociation of the fluorescence signals at the PM (E, inset) and weak location of DMP1 $_{\Delta 1-19}$ -mRFP to the tonoplast (D, arrow). Co-expression of DMP1 $_{M20A}$ -eGFP (F) and DMP1 $_{\Delta 1-19}$ -mRFP (G) or mRFP-DMP1 (J) show clear dissociation of the fluorescence signals at the PM (H and K, inset) and moderate to substantial location of DMP1 $_{\Delta 1-19}$ -mRFP and mRFP-DMP1 to the tonoplast (J and G, arrow and overlays H and K). Exclusion of the PM from the foamy membranes structures was shown by co-expressing DMP1 $_{M20A}$ -eGFP (L) and mRFP-MUB2 (M). Clear segregation of the fluorescence signals were observed (N).

Chapter 3

yeast (Fig. 9A), the crosslinker DMS to show interaction *in planta* (Fig. 9B) and performed competition experiments *in planta* (Fig. 9C-N). DMP1 clearly dimerized in yeast (Fig. 9A). Crosslinker experiments using DMS on microsomes containing either eGFP-DMP1 or DMP1-eGFP showed protein-protein interaction only in the case of eGFP-DMP1 (Fig. 9B). Additionally to eGFP-DMP1 (46 kDa on gel, 49 kDa calculated), we detected proteins at approximately 85 and 170 kDa which would correspond to homodimers and -tetramers (Fig. 9B). Thus, DMP1 appears to be able to interact *in planta*. The fact that we could not detect protein interactions with DMP1-eGFP might be due to a technical problem. It could also indicate that DMP1 has not exactly the same topology regarding the membrane it is located to. Indeed DMS requires a distance of 11 Å between primary amines of lysine residues of interacting proteins due to its 8-atoms spacer arm. Thus this prerequisite might be present with eGFP-DMP1 but not DMP1-eGFP. We next investigated protein-protein interaction by competition experiments (Fig. 9C-N). We coexpressed DMP1-eGFP (Fig. 9C) or DMP1_{M20A}-eGFP (Fig. 9F) with DMP1_{Δ1-19}-mRFP (Fig. 9D and G) in tobacco. By careful observation of a large number of cells and following independent infiltrations, we observed in average a larger fraction of DMP1_{Δ1-19}-mRFP localizing in the tonoplast when co-expressed with DMP1_{M20A}-eGFP than with DMP1-eGFP (Fig. 9C-H). It suggests that DMP1.2 can indeed interact with DMP1.1 and localize at least partially in the tonoplast. By coexpressing DMP1_{M20A}-eGFP (Fig. 9I) and mRFP-DMP1 (Fig. 9J), we could show that DMP1.1 is also able to interact with itself since a considerable fraction of mRFP-DMP1 was found associated with the tonoplast (Fig. 9K). To exclude the fact that the PM could be involved in these foamy membrane structures and therefore be responsible for colocalization of DMP1_{Δ1-19}-mRFP with DMP1_{M20A}-eGFP, we coexpressed DMP1_{M20A}-eGFP (Fig. 9L) with mRFP-MUB2 (Fig. 9N) and showed clear dissociation of the fluorescence signals (Fig. 9N). Thus, DMP1.2 is targeted to the tonoplast, at least to a certain extent, through protein-protein interaction with DMP1.1 itself recognized by the tonoplast targeting machinery.

Mutations of the charged di-KK, di-EE and tri-EEE motifs within the C-terminus impair DMP1-eGFP ER export

We hypothesized in our previous study (chapter 2) that competitive signals within DMP1 might be responsible for the dual ER/tonoplast targeting observed in stably transformed *Arabidopsis* and during membrane remodeling in tobacco. In the present study, we showed that the very end of the N-terminus and its length are required for proper targeting to the tonoplast. We next investigated which residues may be responsible for ER retention or retrieval. DMP1 has the longest C-terminus among all DMP members (Kasaras and Kunze, 2010). It encompasses 29 aa compared to DMP3 and -5 (18 aa), DMP10 (15 aa), DMP4,-6 and -7 (14 aa), DMP8 and -9 (12 aa), and DMP2 (22 aa).

Chapter 3

DMP1 is the only protein to have a di-lysine motif in its C-terminus known to promote ER retrieval of membrane proteins from the Golgi upon interaction with the coatomer (COPI) (Jackson et al., 1990; Cosson and Letourneur, 1994; Gaynor et al., 1994; Letourneur et al., 1994; Gomord et al., 1997; Gomord et al., 1999; Pagny et al., 1999). However this motif is located in position -6/-7 and would be unusual. The classical retrieval signal is K(x)Kxx at the very end of the carboxy-terminus. A di-acidic and a tri-acidic motif (EE and EEE) are also present in DMP1 C-terminus which are absent in all other DMPs. Di-acidic motifs, composed of two acidic residues separated by one amino acid (D/ExD/E), have been shown to act as ER export motifs in various species including yeast, human and plants (Ma et al., 2001; Malkus et al., 2002; Wang et al., 2004; Hanton et al., 2005; Mikosch et al., 2006; Sieben et al., 2008; Mikosch et al., 2009). The diacidic dipeptide EE has also been identified as lysosome targeting signal (Piguet et al., 1999). Despite the fact that EE and EEE motifs in plants has not been reported as ER retention signals in contrast to di-lysines motifs, the fact that D/ExD/E signals play a role in export from the ER prompted us to investigate the effect of their respective mutations on DMP1-eGFP subcellular localization. We performed following mutations: E192A/E193A, E197A/E198A/E199A, K201A/K202A (Fig. 1B). We generated additionally DMP1_{7subst}-eGFP which carries all substitutions (Fig. 1). Similarly to the N-terminal truncation series, we generated a C-terminal truncation series lacking various carboxy segments: Δ 183-207, Δ 194-207, Δ 200-207 and Δ 203-207 (Fig. 1B). DMP1 Δ 183-207-eGFP was found in the ER and in aggregates (Table 1) suggesting that too large C-terminal truncations may impede proper folding and ER export. Proteins were not detected on WB (Fig. 5D) suggesting that translation termination may also be affected. The three other C-terminal truncations as well as the independent substitutions did not alter fluorescence pattern and protein banding pattern on WB (Table 1, Fig. 5R and D). However, we did not investigate the subcellular localization of these proteins in stably transformed *Arabidopsis* where the ER localization may be altered. Interestingly, DMP1_{7subst}-eGFP induced strong and chaotic membrane remodeling at 3dpi whose overall pattern somehow resembled “swollen” actin filaments with extremely intense signals in the perinuclear region (Fig. 5S). Colocalization experiments between DMP1_{7subst}-eGFP (Fig. 5T₁), YFP-HDEL (Fig. 5T₂) and TPK1-mRFP (Fig. 5T₃) showed that DMP1 was localized in the ER undergoing drastic remodeling (Fig. 5T₄). We did not observe colocalization between DMP1-eGFP and TPK1-mRFP except in the perinuclear region (Fig. 5T₄) and bulbs were rarely observed (data not shown) indicating that tonoplast targeting of DMP1 was impaired. This may be interpreted as impaired ER export which would be dominant over tonoplast targeting. At 5 dpi, the ER largely regained normal architecture (Fig. 5U). Tonoplast and bulbs labeling were almost absent (not shown). Thus, the simultaneous mutation of seven charged amino acids within DMP1 carboxy-terminus impaired ER export.

Chapter 3

Table 1. Overview of the different fusion proteins used in this study with their corresponding N-terminal sequence, protein occurrence (bands on Western blot) and subcellular localization in tobacco epidermis cells at 2-3 dpi. PM, plasma membrane, ER, endoplasmic reticulum; N.D., not detected; n.d., not determined.

Proteins	N-term	protein occurrence	subcellular localization	
(35S)DMP1 (DMP1p)DMP1	ATG TCC	two (DMP1.1 and DMP1.2)	n.d.	
DMP1-eGFP fusions				
eGFP-DMP1	-	one	PM	
DMP1-eGFP (DMP1p)DMP1-eGFP DMP1 _{loop2} -eGFP	ATG TCC	two	tonoplast/bulbs	
N-terminal modifications				
DMP1 _{S2A} -eGFP	ATG GCC	one	tonoplast/bulbs	
DMP1 _{ΔS2} -eGFP	ATG GAA			
DMP1 _{E3A} -eGFP	ATG TCC	two		
DMP1 _{ΔE3} -eGFP				
DMP1 _{T4A} -eGFP				
DMP1 _{ΔT4} -eGFP				
DMP1 _{S5A} -eGFP	ATG GCC	one		
DMP1 _{S2A/E3A} -eGFP	ATG ACT	two		PM
DMP1 _{ΔS2E3} -eGFP	ATG CCC			
DMP1 _{S2P/E3P} -eGFP	ATG CCC			
DMP1 _{S2P} -eGFP	ATG ACC			
DMP1 _{S2T} -eGFP	ATG TCT			
DMP1 _{S2S*} -eGFP	ATG TTC			
DMP1 _{S2F} -eGFP	ATG TCC		one	tonoplast/bulbs
DMP1 _{M20A} -eGFP				
DMP1 _{N22A/T23A} -eGFP				
DMP1 _{N24A/K25A} -eGFP				
DMP1 _{S26A/L27A} -eGFP				
DMP1 _{T28A/G29A} -eGFP				
DMP1 _{L30A/E31A} -eGFP				
DMP1 _{S32A/L33A} -eGFP				
DMP1 _{L36A/L37A} -eGFP				
DMP1 _{I34A/K35A} -eGFP		N.D.	ER/tonoplast (slow cell death) ER + aggregates	
DMP1 _{P38A/T39A} -eGFP				
N-terminal truncations				
DMP1 _{Δ1-4} -eGFP	ATG TCT	one	PM	
DMP1 _{Δ1-9} -eGFP	ATG AAA	two		
DMP1 _{Δ1-14} -eGFP	ATG GCT	one		
DMP1 _{Δ1-19} -eGFP	ATG ATG			
DMP1 _{ATG→GAC} -eGFP	ATG GCA			
DMP1 _{Δ1-25} -eGFP	ATG TCC	N.D.	ER + aggregates	
DMP1 _{Δ1-29} -eGFP	ATG CTA			
DMP1 _{Δ1-34} -eGFP	ATG AAG			
C-terminal modifications				
DMP1 _{E192A/E193A} -eGFP	ATG TCC	two	tonoplast/bulbs	
DMP1 _{E197A/E198A/E199A} -eGFP				
DMP1 _{K201A/K202A} -eGFP				
DMP1 _{7subst} -eGFP				
C-terminal truncations				
DMP1 _{Δ183-207} -eGFP	ATG TCC	N.D.	ER + aggregates	
DMP1 _{Δ194-207} -eGFP				
DMP1 _{Δ200-207} -eGFP		two	tonoplast/bulbs	
DMP1 _{Δ203-207} -eGFP				

Discussion

Improvement DMP1 translation initiation site abolishes translation of DMP1.2

The majority of proteins showing multiple distributions which are described in the literature result from multiple transcripts from a single gene or multiple genes (Karniely and Pines, 2005). In our cases, we clearly showed using 5'-RACE-PCR and sequencing that DMP1.1 and DMP1.2 derive from single transcripts. Mutation of the first AUG^{START} codon and the second in-frame AUG^{START} codon clearly showed that a leaky ribosome scanning is responsible for the generation of the two isoforms. Moreover, mutation of the second AUG^{START} codon clearly excluded that DMP1.2 translation is initiated alternatively at a non-AUG codon which has been reported in different cases of multiple-targeted proteins (Kobayashi et al., 2001; Christensen et al., 2005; Sunderland et al., 2006; Wamboldt et al., 2009). Effect of overexpression on ribosome scanning was excluded as DMP1.1 and DMP1.2 were detected in tobacco and in *Arabidopsis* expressing DMP1-eGFP from the native promoter. The scanning model implies that the ribosome binds first to the 5' end of a transcript and migrates linearly until it encounters the first AUG where it stops (Kozak, 1986). DMP1.2 translation could also be abolished by modifying and improving translation efficiency at the first translation initiation site (TIS). Based on 28382 sequences, aaaaaaa(A/G)(A/C)aAUGGcgaataata has been determined as consensus sequence in *Arabidopsis* (Rangan et al., 2008). Positions -3 and +4 are strong determinants of TIS in plants (Joshi et al., 1997; Rangan et al., 2008) and mammals (Kozak, 2002) and are suggested to have synergistic effect on initiation of translation (Pisarev et al., 2006). TIS lacking both purines in position -3 and G in position +4 are described as weak context enabling leaky scanning (Kozak, 2002). DMP1.1 TIS has a C in position -3 and a T in position +4 (CAAGCTCAUGTCCGAA) which is the third rarest combination in *Arabidopsis* found in only 1,54 % of all transcripts (Rangan et al., 2008). Interestingly, expression from the 35S promoter which contains a different 5' UTR did not influence translation efficiency although an A is found in position -3 (Fig. 7D). Only additional substitution of T in position +4 to G (mutations S2A, ΔS2, S2A/E3A) abolished translation of DMP1.2 and thus, probably forced the ribosome to stop at the first TIS. Substitution to A (mutations ΔS2E3) or C (mutations S2P, S2P/E3P) did not influence translation of DMP1.2 at the second TIS. Thus, only the conserved combination A in -3 and G in +4 which is found in 25,53 % of all transcripts in *Arabidopsis* (Rangan et al., 2008) appears to stop scanning at the first TIS leading to translation of only DMP1.1. Interestingly, the second TIS (AAAACAUGGCAAA) leading to translation of DMP1.2 has a much more conserved context than DMP1.1 with A in -3 and G in +4. The fact that we did never observed two bands with N-terminal fusion proteins independently of the tag used (eGFP, 3xHA, 4xMyc) is directly linked with the fact that DMP1.1

Chapter 3

TIS is not used as first TIS. The TIS of the respective tags might promote efficient translation preventing further scanning until DMP1.1 TIS. The latter may be too distant from the first TIS in these constructs despite putative leaky scanning. To further confirm skipping ribosome scanning we performed *in vitro* transcription and translation of DMP1 using rabbit reticulocyte lysates and a cell-free system (Schwarz et al., 2008). Unfortunately both approaches failed and were finally abandoned. All in all our data obtained with the different mutations are clearly in agreement with the ribosome scanning model.

The PM is the default pathway for DMP1.1 and DMP1.2

In tobacco, we showed that DMP1.1-eGFP (DMP1_{M20A}-eGFP and the mutated forms DMP1_{S2A}-eGFP, DMP1_{ΔS2}-eGFP and DMP1_{S2A/E3A}-eGFP) is targeted to the tonoplast and that DMP1.2-eGFP (DMP1_{Δ1-19}-eGFP, DMP1_{Δ1-19}-mRFP and DMP1_{ATG→GAC}-eGFP) is found at the PM and endosomes. It indicates that lack of the 19 first aa is responsible for targeting to the tonoplast. Thus, a positive signal likely targets DMP1.1 to the tonoplast and location at the PM of DMP1.2 appears to be directly due to the absence of this signal. In other terms, the PM is likely the default pathway for DMP1.2. The fact that we observed endosomes, probably the TGN with DMP1.2-eGFP and not with DMP1.1-eGFP strongly suggest that they take two different routes along the secretory pathway. Our extensive analysis using different mutated fusion proteins allowed us to confine the targeting sequence at the very end of the amino terminus. We found that position S2 and to a lesser extend position E3 are crucial for targeting to the vacuole. Indeed, we showed that mutation S2P largely but not totally redirected DMP1-eGFP whereas mutations S2P/E3P was only found in the PM. However, S and E are not indispensable aa in these positions since the mutations S2A, ΔS2, E3A, ΔE3 and S2A/E3A did not alter proper targeting to the tonoplast. Thus, certain amino acids can substitute for the native ones without affecting targeting while others cannot like proline. In contrast, deletion of these aa (ΔS2E3) redirected the fusion protein to the PM suggesting that the overall length of the N-terminus is also required for proper targeting. The mutation Δ1-4, which corresponds to ΔS2E3T4 is also found at the PM, confirmed this hypothesis. Indeed, this deletion “restitutes” a serine in position 2 and places a leucine in position 3 (originally in positions 5 and 6 respectively). Thus, the deletion itself is responsible for loss of tonoplast targeting and not the nature of the aa in these positions. All larger deletions (Δ1-9, Δ1-14 and Δ1-19 (DMP1.2)) show the same subcellular localization at the PM. Thus length of the N-terminus is critical for proper targeting. Similarly, the length of the N-terminal soluble longin domain of R-SNAREs is required for vacuolar targeting. Truncation of this domain leads to loss of tonoplast localization and redirection to the PM and endosomes, likely the TGN (Uemura et al., 2005). Even larger deletions of DMP1 N-terminus (Δ1-25 and Δ1-29) however led to ER retention, indicating that a certain

Chapter 3

length of the N-terminus is nevertheless required for transit to the PM. We did not modify the length of the first TMD. It has been reported for single-pass membrane proteins that it is responsible for retention in a specific compartment along the secretory pathway in yeast, animals and plants (Pedrazzini et al., 1996; Rayner and Pelham, 1997; Yang et al., 1997; Brandizzi et al., 2002). Brandizzi et al. (2002) showed using chimeras that successive deletions within the TMD from 23 aa to 20 aa and to 17 aa resulted in a relocation from the PM to Golgi vesicles and ER membranes respectively. Thus, length of the TMD appears to be a crucial sorting parameter for single-pass membrane proteins and was proposed to be linked with an increase of membrane thickness along the secretory pathway. To our knowledge, a similar process has not been reported to date for multiple-spanning membrane protein. However, we showed that certain mutations within the first TMD (P38A/T39A) abolished proper targeting to the tonoplast and induced aggregates within the ER. Substitutions I34A/K35A even induced cell death for an unknown reason. This mutated protein was found to be weakly detectable but localized to both the ER and the tonoplast, two membranes where DMP1 is natively found in. Thus, it is unlikely that it induces artificial effects due to its function in a foreign membrane as we observed for DMP3 and -5 (chapter 4). Indeed, N-terminal fusion of eGFP to DMP3 and -5 induced an accumulation of these proteins, which are normally found at ER membranes, in Golgi vesicles inducing rapid cell death obviously due to their mislocalization. In the case of mutations within DMP1 first TMD, they likely impaired proper folding and topology or altered putative interactions with the other TMDs within the membrane.

The accessibility of the N-terminus also appears to be required. Indeed, the N-terminal fusion eGFP-DMP1 is “mistargeted” although the whole targeting information is still present. eGFP likely masked the signal which became inaccessible for cytosolic proteins targeting ultimately the proteins to the tonoplast. Some studies dealing with mitochondrial-targeting showed comparable events where removing from or adding aa to the N-terminus altered mitochondrial targeting (Chaumont et al., 1994; de Castro Silva Filho et al., 1996; Rudhe et al., 2002; Bonke et al., 2003; Carrie et al., 2009b). eGFP-DMP1 corresponds to eGFP-DMP1.1. If DMP1.1 is not targeted to the tonoplast anymore, it transits to the PM where it perfectly colocalized with DMP1.2. Thus, absence of the targeting signal or masking by additional aa direct the proteins to the PM which suggest that the PM represents the default pathway for both DMP1.1 and DMP1.2 isoforms. Thus, the very end of the N-terminus of DMP1, especially position 2, its overall length and its accessibility are all required for proper targeting to the tonoplast. Fusion of DMP1 N-terminus to the mistargeted eGFP-DMP1 ($_{30\text{aaDMP1}}\text{eGFP-DMP1}$) did not restore tonoplast targeting despite accessibility of the N-terminus suggesting that not only the length of the N-terminus but also the relative position of the latter to the

Chapter 3

first TMD is critical for proper targeting. DMP1_{loop2}-eGFP proper targeting to the tonoplast corroborates this assumption. DMP1 N-terminus was also shown to be insufficient to target soluble proteins to the lumen of the vacuole as well as unrelated integral PM proteins to the tonoplast.

Does DMP1 contain an ER export site?

We showed that the C-terminus of DMP1 is not directly involved in tonoplast targeting as most truncations (Δ 194-207, Δ 200-207 and Δ 203-207) and all individual substitutions (E192A/E193A, E197A/E198A/E199A and K201A/K202A) did not affect targeting. Similarly to the N-terminal truncations, the largest truncation (Δ 183-207) was retained in the ER and was not detected on WB which suggests impairment of proper translation termination, protein folding or translocation. However, substitutions of the di-KK, di-EE and tri-EEE motifs at once (DMP1_{7subst}-eGFP) led to predominant retention in the ER and induced strong membrane remodeling which tended to disappear with time. However DMP1_{7subst}-eGFP remained associated with ER membranes and did not reach the vacuole suggesting that ER export was impaired. Whether the three motifs act synergistically as ER export signals is speculative. The substitutions for alanines may have created a hydrophobic C-terminus impairing proper folding and affecting DMP1 function. The drastic remodeling may be seen as illustration for an altered protein function and confirm DMP1 inherent properties to induce membrane remodeling (chapter 2).

Protein-protein interaction directs DMP1.2 to the tonoplast

DMP1.1-eGFP is targeted to the tonoplast whereas DMP1.2-eGFP is found at the PM when expressed independently. Expression of DMP1-eGFP leads to the expression of both isoforms at once due to leaky ribosome scanning. Both isoforms were found in more or less equimolar concentrations when DMP1 was expressed as unfused protein, fused to different tags or carrying various mutations which did not affect ribosome skipping (Fig. 4A, B, C, D, E and F and 5A, B, C, D and E). However, fluorescence signals at the PM in the presence of both isoforms expressed from the same construct were largely undetectable. eGFP fluorescence intensity would be strongly reduced if eGFP faced the vacuolar lumen (Tamura et al., 2003) or the apoplast due to the acidic environment. Since protein topology is retained during migration through the secretory pathway, the C-terminus of both DMP1.1 and DMP1.2, and thus eGFP reside in the cytosol. Therefore, eGFP fluorescence intensity should be equal when associated to the PM or the tonoplast. Moreover, a prerequisite of the split-ubiquitin system is that the terminus to which the C-terminal ubiquitin half Cub is fused, has to be cytosolic to allow release of the synthetic transcription factor and activation of the reporter gene after migration into the nucleus (Stagljar et al., 1998). Both Cub-DMP1 and DMP1-Cub was found to function as bait (chapter 4) indicating that both N- and C-termini are

Chapter 3

cytosolic in yeast. The fact that the PM localization is hardly visible in the presence of both isoforms is reminiscent of the notion of “eclipsed” protein isoforms where one location is not or only hardly detectable due to uneven membrane distribution (Regev-Rudzki et al., 2005; Regev-Rudzki and Pines, 2007). We provided evidences that DMP1 is able to dimerize in yeast. eGFP-DMP1 was found to form homodimers and tetramers in tobacco using chemical crosslinking. Thus, DMP1.1 mistargeted to the PM can still interact with itself. Our competition experiments using DMP1-eGFP (i.e. DMP1.1-eGFP + DMP1.2-eGFP) or DMP1_{M20A}-eGFP (i.e. DMP1.1-eGFP alone) coexpressed with DMP1_{Δ1-19}-mRFP (DMP1.2-mRFP) showed that the DMP1.2-mRFP fraction found at the tonoplast was greater when coexpressed with DMP1_{M20A}-eGFP than with DMP1-eGFP, so in the absence of DMP1.2-eGFP. This suggests competition of DMP1.2-eGFP and DMP1.2-mRFP for interaction with DMP1.1-eGFP. However determination of the respective expression level at cell level could not be achieved directly but only indirectly by investigating cells showing approximately equal fluorescence signals for both fluorophores at given settings. We made the same observations using mRFP-DMP1 instead of DMP1_{Δ1-19}-mRFP confirming that DMP1.1 can interact not only with DMP1.2 but also with itself. Thus the domain responsible for dimerization or higher oligomerization is not located within the 19 first aa of the N-terminus.

We observed fluorescence signals at endosomes only when DMP1.2 was expressed alone. Expression of DMP1-eGFP leading to translation of both isoforms did not lead to the labeling of these structures. This further indicates that the isoforms take two independent routes along the secretory pathway when expressed independently and that DMP1.2 is largely redirected to the tonoplast in the presence of DMP1.1. This is reminiscent of ZmPIP1s and ZmPIP2s membrane distribution. When expressed independently, ZmPIP2s were found in the PM whereas ZmPIP1s were retained in the ER. Coexpressed, ZmPIP1s were relocated to the PM (Zelazny et al., 2007). The authors showed that this relocation was due to interaction between ZmPIP1s and ZmPIP2s using FRET/FLIM imaging microscopy. The trafficking to the PM of two ZmPIP2s (ZmPIP2;4 and ZmPIP2;5) was then shown to result from the presence of a diacidic motif acting as ER export site (Zelazny et al., 2009).

Since the function of DMP1 is still unknown, it is complicated to speculate about the biological relevance of DMP1 membrane distribution and DMP1.2 additional occurrence. However a comparable distribution was observed with the tonoplastic intrinsic proteins TIP3;1 and TIP3;2 which additionally to their tonoplast localization showed developmentally regulated PM- and to a lesser extend ER localization (Gattolin et al., 2011). They were found to localize at the tonoplast, the PM and ER membranes in embryos during seed maturation and during the early stages of seed germination and not in the other tissues they were expressed in. The authors speculated that they

Chapter 3

may compensate for the absence or low concentration of PIPs during these developmental stages. However, the molecular mechanism behind this development-dependent membrane distribution was only monitored but not investigated.

Outlook

The distribution of DMP1 isoforms will be further investigated by microsome fractionation on sucrose gradient. eGFP-specific and DMP1-specific antibodies will be used to discriminate between both DMP1 isoforms and antibodies against ER-, PM- and tonoplast-specific membrane proteins will allow to determine their subcellular distribution in transgenic lines overexpressing either DMP1-eGFP, eGFP-DMP1 (Kasaras and Kunze, 2010) or unfused DMP1 (chapter 4). Fractionation in the presence or absence of Mg^{2+} which stabilize or dissociate ribosomes from the ER respectively will be used to unequivocally show DMP1 localization in the ER. Eclipsed occurrence of DMP1.2 at the PM would be manifested in identical membrane distribution of both isoforms in the same fractions and absence of DMP1.2 in the fraction containing the PM-derived microsomes. DMP1 capacity to interact with itself would be corroborated.

Material and methods

Generation of constructs

All PCR reactions were performed with *Pfu* polymerase (MBI Fermentas) or Phusion® High-Fidelity DNA Polymerase (New England Biolabs) and the sequences of all PCR products were verified by sequencing (GATC). The primers used for the generation of the different constructs described in this study are listed in Table S1. *35S:DMP1-eGFP* and *DMP1pro-DMP1-eGFP* were generated as described in Kasaras and Kunze, 2010 and Kasaras et al, 2011 respectively.

The open reading frame of DMP1 was amplified from gDNA with *XbaI*_DMP1_{ORF}_F and *PstI*_DMP1_{ORF}_R and the resulting PCR product was digested with *XbaI-PstI* and ligated to *XbaI-PstI* digested pNGTkan3 to generate *35S:eGFP-DMP1*. Similarly *35S:DMP1* was generated by using the same digested PCR amplificate but by ligating it to *XbaI-PstI* digested pPTkan3. The generation of *35S:DMP1_{loop2}-eGFP* required several steps: *eGFP* was amplified from pGTkan3 with the primers *XhoI/Gly₄/eGFP_F* and *NcoI/Gly-Ala₂-Gly/eGFP_R* and in parallel two DMP1 halves were generated. The first half was amplified using the primer pair *XbaI_DMP1_{ORF1}_F/ XhoI_DMP1_{ORF1}_R* corresponding to amino acids 1-108 of DMP1 and the second using *NcoI_DMP1_{ORF2}_F/ PstI_DMP1_{ORF2}_R* representing amino acids 109-207. By successive digestions/ligations, the two DMP1 halves were fused to eGFP leading to DMP1_{ORF1}-eGFP-DMP1_{ORF2}, DMP1_{ORF1} and eGFP being separated by a Gly₄-linker and eGFP and DMP1_{ORF2} by a

Chapter 3

Gly-Ala₂-Gly-linker. DMP1_{ORF1}-eGFP-DMP1_{ORF2} was then digested with *XbaI-PstI* and ligated to *XbaI-PstI* digested pPTkan3 to generate 35S:DMP1_{loop2}-eGFP. 35S:mRFP-DMP1 was generated by amplifying mRFP was amplified from 35S:mRFP-MUB2 using the primer pair listed in Table S1. The resulting amplificate was digested with *KpnI-XbaI* and ligated to *KpnI-XbaI* digested pPTkan3 already containing DMP1 (i.e. construct 35S:DMP1) to generate 35S:mRFP-DMP1.

The N-terminal truncations series including the constructs 35S: DMP1_{Δ1-4}-eGFP, 35S: DMP1_{Δ1-9}-eGFP, 35S:DMP1_{Δ1-14}-eGFP, 35S:DMP1_{Δ1-19}-eGFP, 35S:DMP1_{Δ1-25}-eGFP, 35S:DMP1_{Δ1-29}-eGFP, 35S:DMP1_{Δ1-34}-eGFP as well as the constructs containing substitutions or deletions within the first five N-terminal amino acids (35S:DMP1_{S2A}-eGFP, 35S:DMP1_{ΔS2}-eGFP, 35S:DMP1_{E3A}-eGFP, 35S:DMP1_{ΔE3}-eGFP, 35S:DMP1_{T4A}-eGFP, 35S:DMP1_{ΔT4}-eGFP, 35S:DMP1_{S5A}-eGFP, 35S:DMP1_{S2A/E3A}-eGFP, 35S:DMP1_{ΔS2E3}-eGFP, 35S:DMP1_{S2P}-eGFP, 35S:DMP1_{S2T}-eGFP, 35S:DMP1_{S2F}-eGFP, 35S:DMP1_{S2S*}-eGFP, 35S:DMP1_{S2P/E3P}-eGFP) were generated by using specific forward primers, a unique reverse primer (see Table S1) and 35S:DMP1-eGFP as template. All PCR products were digested with *XbaI-PstI* and ligated to *XbaI-PstI* digested pPGTkan3. 35S:DMP1_{Δ1-19}-mRFP was generated by amplifying DMP1_{Δ1-19} using the primer listed in Table S1, digesting the resulting amplificate with *XbaI-XhoI* and by ligating it to *XbaI-XhoI*-digested pPRTkan3.

35S:DMP1_{M20A}-eGFP, 35S:DMP1_{N22A/T23A}-eGFP, 35S:DMP1_{N24A/K25A}-eGFP, 35S:DMP1_{S26A/L27A}-eGFP, 35S:DMP1_{T28A/G29A}-eGFP, 35S:DMP1_{L30A/E31A}-eGFP, 35S:DMP1_{S32A/L33A}-eGFP, 35S:DMP1_{I34A/K35A}-eGFP, 35S:DMP1_{L36A/L37A}-eGFP, 35S:DMP1_{P38A/T39A}-eGFP were all generated in two distinct PCR reactions using the construct 35S:DMP1-eGFP as template and a subsequent overlapping PCR with the two first PCR products as template. The first PCR products were generated using a unique forward primer (towardsMCS_F) located on the vector just upstream of the 35S promoter and a second specific reverse primer containing the desired mutation (see Table S1). The second PCR products were generated with a specific forward primer corresponding to the reverse complement sequence of the specific reverse primers used in the first reactions and a unique reverse primer (eGFP-Gen5') binding in the eGFP sequence (see Table S1). As 35S:DMP1-eGFP was used as template all first PCR products contained the original *XbaI* restriction site and the second ones, the original *PstI* restriction site. The overlaps of the respective two PCR products created by the complementary primers used in the first two PCRs allowed the generation of single PCR products containing the mutations in final overlapping PCR reactions with towardsMCS_F and eGFP-Gen5' as external primers. These PCR products were then digested with *XbaI-PstI* and ligated to *XbaI-PstI* digested pPGTkan3.

Chapter 3

DMP1_{E192A/E193A}-eGFP, *DMP1_{E197A/E198A/E199A}-eGFP*, *DMP1_{K201A/K202A}-eGFP*, *DMP1_{7subst}-eGFP* were generated in a comparable cloning strategy with two distinct PCR reactions and subsequent overlapping PCR reactions. *35S:DMP1-eGFP* was used as template and the unique external primers (35S-towardsGene and RBCS_term) as well as the specific internal primers are listed in Table S1. The resulting PCR products were digested with *XbaI-PstI* and ligated to *XbaI-PstI* digested pPGTkan3.

The C-terminal truncation series (*DMP1_{Δ183-207}-eGFP*, *DMP1_{Δ194-207}-eGFP*, *DMP1_{Δ200-207}-eGFP*, *DMP1_{Δ203-207}-eGFP*) was generated by using a unique forward primer, specific reverse primers (see Table S1) and *35S:DMP1-eGFP* as template. The PCR products were then digested with *XbaI-PstI* and ligated to *XbaI-PstI* digested pPGTkan3.

35S:DMP1-3xHA, *35S:3xHA-DMP1*, *35S:DMP1-4xMyc* and *35S:4xMyc-DMP1* were generated via LR reaction (GATEWAY cloning technology) between DMP1-pDONR222 (Entry Clone) and the destination vectors pGWB14, 15, 17 and 18 respectively. DMP1-pDONR222 was created via BP reaction between a PCR product consisting of DMP1 flanked by the attB1 and attB2 sites (amplified with the primer pair attB1-DMP1_F/attB2-DMP1_R, see Table S1) and pDONR222.

35S:mRFP-ARA7 (ref) was reamplified by PCR with *XbaI-mRFP-Ara7/mRFP-Ara7-XhoI* (see Table S1), digested with *XbaI-XhoI* and ligated to *XbaI-XhoI* digested pPTkan3. *35S:TPK1-mRFP* and *35S:mRFP-MUB2* are described in (Kasaras and Kunze, 2010) and *35S:Man49-mCherry* (G-rb, CD3-968) in (Nelson et al., 2007).

Plant material, growth conditions and plant transformation

Arabidopsis thaliana ecotype Columbia 0 and *Nicotiana benthamiana* plants were grown and transformed as described in (Kasaras and Kunze, 2010). All *Agrobacterium* cultures were resuspended to OD_{600nm}=0,05 prior to tobacco infiltration.

Microsome purification, Western blotting and antibodies

For each extraction, 1 g grinded plant material was resuspended in 3 ml extraction buffer (50 mM HEPES pH 6,5; 10 % sucrose; 5 mM EDTA; 1 mM DTT; protease inhibitor cocktail). Lysates were filtered through a double layer of Miracloth and centrifuged for 5 min at 4 °C, 2500 g. Supernatants were ultracentrifuged for 45 min at 4 °C, 100000 g. The pellets representing the membrane fractions were resuspended in 350 µl extraction buffer.

10 µl of the membrane fractions were denaturated for 10 min with Laemmli buffer at 95 °C, separated onto SDS/PAGE gels, blotted onto PVDF membrane (Immobilon-P, Millipore,

Chapter 3

Schwalbach, Germany) and detected by chemiluminescence (Pierce ECL Western Blotting Substrate).

Detection was achieved with following antibodies: mouse anti-HA (Covance), mouse anti-Myc (Millipore), rabbit anti-GFP-HRP (Santa Cruz) and rabbit anti-DMP1 (Pierce). As secondary antibodies, goat anti-mouse or anti-rabbit IgG-HRP (Santa Cruz) were used. To obtain anti-DMP1, rabbit anti-serum was raised against the DMP1 C-terminal peptide (KRSGIGYAPIAEEVGAE) corresponding to amino acids 181 to 197. Anti-serum was directly used without purification as 1:5000 dilution for detection.

Chemical crosslinking

Crosslinking experiments were performed directly after microsome purification. Microsomal fractions were incubated with 5 mM Dimethyl Suberimidate•2 HCl (DMS) (Thermo Scientific) for one hour at room temperature prior to denaturation and loading on protein gel as described above.

5' RACE-PCR

RNA was isolated from *Nicotiana benthamiana* infiltrated leaves using TRIsure (Bioline) and from *Arabidopsis thaliana* (senescing tissues and roots) as previously described (Downing et al., 1992). 2 µg total RNA of each sample were used to transcribe mRNA into first-strand cDNA using the RevertAidTM Reverse Transcriptase possessing RNase H activity (MBI Fermentas) and a DMP1 specific primer (DMP1-int1, see Table S1). The cDNA were column-purified (Macherey-Nagel) and subjected to poly(A)-tailing by Terminal Deoxynucleotidyl Transferase (MBI Fermentas). d(A)-tailed cDNA were column-purified and used in a first PCR reaction. An Oligo dT primer fused to a linker (Oligo d(T)-anchor_F), an internal DMP1 primer (DMP1-int2), Taq DNA Polymerase (MBI Fermentas) and following cycling conditions were used: 2 min at 94 °C initial denaturation followed by 35 cycles of 25 sec 94 °C, 25 sec 58 °C, 45 sec 72 °C and 5 min at 72 °C final elongation. PCR products were diluted 1/20 and used as template in a second PCR reaction (nested PCR) with the primer pair anchor_F/DMP1_int3 (see Table S1) and the same cycling conditions as above. PCR products of both PCR rounds were separated by gel electrophoresis and verified by sequencing (GATC).

References

- Bassham, D.C., Brandizzi, F., Otegui, M.S., and Sanderfoot, A.A.** (2008). The Secretory System of Arabidopsis. The Arabidopsis Book, e0116.
- Bonke, M., Thitamadee, S., Mahonen, A.P., Hauser, M.T., and Helariutta, Y.** (2003). APL regulates vascular tissue identity in Arabidopsis. Nature **426**, 181-186.

- Brandizzi, F., Frangne, N., Marc-Martin, S., Hawes, C., Neuhaus, J.M., and Paris, N.** (2002). The destination for single-pass membrane proteins is influenced markedly by the length of the hydrophobic domain. *Plant Cell* **14**, 1077-1092.
- Carrie, C., Giraud, E., and Whelan, J.** (2009a). Protein transport in organelles: Dual targeting of proteins to mitochondria and chloroplasts. *FEBS J* **276**, 1187-1195.
- Carrie, C., Kuhn, K., Murcha, M.W., Duncan, O., Small, I.D., O'Toole, N., and Whelan, J.** (2009b). Approaches to defining dual-targeted proteins in Arabidopsis. *Plant J* **57**, 1128-1139.
- Chaumont, F., Silva Filho Mde, C., Thomas, D., Leterme, S., and Boutry, M.** (1994). Truncated presequences of mitochondrial F1-ATPase beta subunit from *Nicotiana plumbaginifolia* transport CAT and GUS proteins into mitochondria of transgenic tobacco. *Plant Mol Biol* **24**, 631-641.
- Christensen, A.C., Lyznik, A., Mohammed, S., Elowsky, C.G., Elo, A., Yule, R., and Mackenzie, S.A.** (2005). Dual-domain, dual-targeting organellar protein presequences in Arabidopsis can use non-AUG start codons. *Plant Cell* **17**, 2805-2816.
- Cosson, P., and Letourneur, F.** (1994). Coatamer interaction with di-lysine endoplasmic reticulum retention motifs. *Science* **263**, 1629-1631.
- de Castro Silva Filho, M., Chaumont, F., Leterme, S., and Boutry, M.** (1996). Mitochondrial and chloroplast targeting sequences in tandem modify protein import specificity in plant organelles. *Plant Mol Biol* **30**, 769-780.
- Downes, B.P., Saracco, S.A., Lee, S.S., Crowell, D.N., and Vierstra, R.D.** (2006). MUBs, a family of ubiquitin-fold proteins that are plasma membrane-anchored by prenylation. *Journal of Biological Chemistry* **281**, 27145-27157.
- Downing, W.L., Mauxion, F., Fauvarque, M.O., Reviron, M.P., de Vienne, D., Vartanian, N., and Giraudat, J.** (1992). A Brassica napus transcript encoding a protein related to the Kunitz protease inhibitor family accumulates upon water stress in leaves, not in seeds. *Plant J* **2**, 685-693.
- Duchene, A.M., Giritch, A., Hoffmann, B., Cognat, V., Lancelin, D., Peeters, N.M., Zaepfel, M., Marechal-Drouard, L., and Small, I.D.** (2005). Dual targeting is the rule for organellar aminoacyl-tRNA synthetases in Arabidopsis thaliana. *Proc Natl Acad Sci U S A* **102**, 16484-16489.
- Gattolin, S., Sorieul, M., and Frigerio, L.** (2011). Mapping of tonoplast intrinsic proteins in maturing and germinating Arabidopsis seeds reveals dual localization of embryonic TIPs to the tonoplast and plasma membrane. *Mol Plant* **4**, 180-189.
- Gaynor, E.C., te Heesen, S., Graham, T.R., Aebi, M., and Emr, S.D.** (1994). Signal-mediated retrieval of a membrane protein from the Golgi to the ER in yeast. *J Cell Biol* **127**, 653-665.
- Gomord, V., Wee, E., and Faye, L.** (1999). Protein retention and localization in the endoplasmic reticulum and the Golgi apparatus. *Biochimie* **81**, 607-618.
- Gomord, V., Denmat, L.A., FitchetteLaine, A.C., SatiatJeunemaitre, B., Hawes, C., and Faye, L.** (1997). The C-terminal HDEL sequence is sufficient for retention of secretory proteins in the endoplasmic reticulum (ER) but promotes vacuolar targeting of proteins that escape the ER. *Plant Journal* **11**, 313-325.
- Hanton, S.L., Renna, L., Bortolotti, L.E., Chatre, L., Stefano, G., and Brandizzi, F.** (2005). Diacidic motifs influence the export of transmembrane proteins from the endoplasmic reticulum in plant cells. *Plant Cell* **17**, 3081-3093.
- Jackson, M.R., Nilsson, T., and Peterson, P.A.** (1990). Identification of a consensus motif for retention of transmembrane proteins in the endoplasmic reticulum. *EMBO J* **9**, 3153-3162.
- Joshi, C.P., Zhou, H., Huang, X.Q., and Chiang, V.L.** (1997). Context sequences of translation initiation codon in plants. *Plant Molecular Biology* **35**, 993-1001.
- Karniely, S., and Pines, O.** (2005). Single translation--dual destination: mechanisms of dual protein targeting in eukaryotes. *EMBO Rep* **6**, 420-425.

- Kasaras, A., and Kunze, R.** (2010). Expression, localisation and phylogeny of a novel family of plant-specific membrane proteins. *Plant Biol (Stuttg)* **12 Suppl 1**, 140-152.
- Kobayashi, Y., Dokiya, Y., and Sugita, M.** (2001). Dual targeting of phage-type RNA polymerase to both mitochondria and plastids is due to alternative translation initiation in single transcripts. *Biochem Biophys Res Commun* **289**, 1106-1113.
- Kozak, M.** (1986). Point mutations define a sequence flanking the AUG initiator codon that modulates translation by eukaryotic ribosomes. *Cell* **44**, 283-292.
- Kozak, M.** (2002). Pushing the limits of the scanning mechanism for initiation of translation. *Gene* **299**, 1-34.
- Latz, A., Becker, D., Hekman, M., Mueller, T., Beyhl, D., Marten, I., Eing, C., Fischer, A., Dunkel, M., Bertl, A., Rapp, U.R., and Hedrich, R.** (2007). TPK1, a Ca²⁺-regulated Arabidopsis vacuole two-pore K⁺ channel is activated by 14-3-3 proteins. *Plant Journal* **52**, 449-459.
- Lee, G.J., Sohn, E.J., Lee, M.H., and Hwang, I.** (2004). The Arabidopsis Rab5 homologs Rha1 and Ara7 localize to the prevacuolar compartment. *Plant and Cell Physiology* **45**, 1211-1220.
- Letourneur, F., Gaynor, E.C., Hennecke, S., Demolliere, C., Duden, R., Emr, S.D., Riezman, H., and Cosson, P.** (1994). Coatamer is essential for retrieval of dilysine-tagged proteins to the endoplasmic reticulum. *Cell* **79**, 1199-1207.
- Ma, D., Zerangue, N., Lin, Y.F., Collins, A., Yu, M., Jan, Y.N., and Jan, L.Y.** (2001). Role of ER export signals in controlling surface potassium channel numbers. *Science* **291**, 316-319.
- Mackenzie, S.A.** (2005). Plant organellar protein targeting: a traffic plan still under construction. *Trends Cell Biol* **15**, 548-554.
- Malkus, P., Jiang, F., and Schekman, R.** (2002). Concentrative sorting of secretory cargo proteins into COPII-coated vesicles. *J Cell Biol* **159**, 915-921.
- Mikosch, M., Kaberich, K., and Homann, U.** (2009). ER export of KAT1 is correlated to the number of acidic residues within a triacidic motif. *Traffic* **10**, 1481-1487.
- Mikosch, M., Hurst, A.C., Hertel, B., and Homann, U.** (2006). Diacidic motif is required for efficient transport of the K⁺ channel KAT1 to the plasma membrane. *Plant Physiol* **142**, 923-930.
- Nelson, B.K., Cai, X., and Nebenfuhr, A.** (2007). A multicolored set of in vivo organelle markers for co-localization studies in Arabidopsis and other plants. *Plant Journal* **51**, 1126-1136.
- Pagny, S., Lerouge, P., Faye, L., and Gomord, V.** (1999). Signals and mechanisms for protein retention in the endoplasmic reticulum. *Journal of Experimental Botany* **50**, 157-164.
- Pedrazzini, E., Villa, A., and Borgese, N.** (1996). A mutant cytochrome b5 with a lengthened membrane anchor escapes from the endoplasmic reticulum and reaches the plasma membrane. *Proc Natl Acad Sci U S A* **93**, 4207-4212.
- Piguet, V., Gu, F., Foti, M., Demaurex, N., Gruenberg, J., Carpentier, J.L., and Trono, D.** (1999). Nef-induced CD4 degradation: a diacidic-based motif in Nef functions as a lysosomal targeting signal through the binding of beta-COP in endosomes. *Cell* **97**, 63-73.
- Pisarev, A.V., Kolupaeva, V.G., Pisareva, V.P., Merrick, W.C., Hellen, C.U., and Pestova, T.V.** (2006). Specific functional interactions of nucleotides at key -3 and +4 positions flanking the initiation codon with components of the mammalian 48S translation initiation complex. *Genes Dev* **20**, 624-636.
- Rangan, L., Vogel, C., and Srivastava, A.** (2008). Analysis of context sequence surrounding translation initiation site from complete genome of model plants. *Molecular Biotechnology* **39**, 207-213.
- Rayner, J.C., and Pelham, H.R.** (1997). Transmembrane domain-dependent sorting of proteins to the ER and plasma membrane in yeast. *EMBO J* **16**, 1832-1841.
- Regev-Rudzki, N., and Pines, O.** (2007). Eclipsed distribution: a phenomenon of dual targeting of protein and its significance. *Bioessays* **29**, 772-782.

- Regev-Rudzki, N., Karniely, S., Ben-Haim, N.N., and Pines, O.** (2005). Yeast aconitase in two locations and two metabolic pathways: seeing small amounts is believing. *Mol Biol Cell* **16**, 4163-4171.
- Rudhe, C., Clifton, R., Whelan, J., and Glaser, E.** (2002). N-terminal domain of the dual-targeted pea glutathione reductase signal peptide controls organellar targeting efficiency. *J Mol Biol* **324**, 577-585.
- Saint-Jore-Dupas, C., Nebenfuhr, A., Boulaflous, A., Follet-Gueye, M.L., Plasson, C., Hawes, C., Driouich, A., Faye, L., and Gomord, V.** (2006). Plant N-glycan processing enzymes employ different targeting mechanisms for their spatial arrangement along the secretory pathway. *Plant Cell* **18**, 3182-3200.
- Saito, C., Ueda, T., Abe, H., Wada, Y., Kuroiwa, T., Hisada, A., Furuya, M., and Nakano, A.** (2002). A complex and mobile structure forms a distinct subregion within the continuous vacuolar membrane in young cotyledons of *Arabidopsis*. *Plant J* **29**, 245-255.
- Schneider, S., Schneidereit, A., Udvardi, P., Hammes, U., Gramann, M., Dietrich, P., and Sauer, N.** (2007). *Arabidopsis* INOSITOL TRANSPORTER2 mediates H⁺ symport of different inositol epimers and derivatives across the plasma membrane. *Plant Physiol* **145**, 1395-1407.
- Schwarz, D., Dotsch, V., and Bernhard, F.** (2008). Production of membrane proteins using cell-free expression systems. *Proteomics* **8**, 3933-3946.
- Sieben, C., Mikosch, M., Brandizzi, F., and Homann, U.** (2008). Interaction of the K(+) channel KAT1 with the coat protein complex II coat component Sec24 depends on a di-acidic endoplasmic reticulum export motif. *Plant J* **56**, 997-1006.
- Sohlenkamp, C., Wood, C.C., Roeb, G.W., and Udvardi, M.K.** (2002). Characterization of *Arabidopsis* AtAMT2, a high-affinity ammonium transporter of the plasma membrane. *Plant Physiol* **130**, 1788-1796.
- Stagljar, I., Korostensky, C., Johnsson, N., and te Heesen, S.** (1998). A genetic system based on split-ubiquitin for the analysis of interactions between membrane proteins in vivo. *Proc Natl Acad Sci U S A* **95**, 5187-5192.
- Sunderland, P.A., West, C.E., Waterworth, W.M., and Bray, C.M.** (2006). An evolutionarily conserved translation initiation mechanism regulates nuclear or mitochondrial targeting of DNA ligase 1 in *Arabidopsis thaliana*. *Plant J* **47**, 356-367.
- Tamura, K., Shimada, T., Ono, E., Tanaka, Y., Nagatani, A., Higashi, S., Watanabe, M., Nishimura, M., and Hara-Nishimura, I.** (2003). Why green fluorescent fusion proteins have not been observed in the vacuoles of higher plants. *Plant Journal* **35**, 545-555.
- Uemura, T., Sato, M.H., and Takeyasu, K.** (2005). The longin domain regulates subcellular targeting of VAMP7 in *Arabidopsis thaliana*. *FEBS Lett* **579**, 2842-2846.
- Uemura, T., Ueda, T., Ohniwa, R.L., Nakano, A., Takeyasu, K., and Sato, M.H.** (2004). Systematic analysis of SNARE molecules in *Arabidopsis*: Dissection of the post-Golgi network in plant cells. *Cell Structure and Function* **29**, 49-65.
- Wamboldt, Y., Mohammed, S., Elowsky, C., Wittgren, C., de Paula, W.B., and Mackenzie, S.A.** (2009). Participation of leaky ribosome scanning in protein dual targeting by alternative translation initiation in higher plants. *Plant Cell* **21**, 157-167.
- Wang, X., Matteson, J., An, Y., Moyer, B., Yoo, J.S., Bannykh, S., Wilson, I.A., Riordan, J.R., and Balch, W.E.** (2004). COPII-dependent export of cystic fibrosis transmembrane conductance regulator from the ER uses a di-acidic exit code. *J Cell Biol* **167**, 65-74.
- Wormit, A., Traub, M., Florchinger, M., Neuhaus, H.E., and Mohlmann, T.** (2004). Characterization of three novel members of the *Arabidopsis thaliana* equilibrative nucleoside transporter (ENT) family. *Biochem J* **383**, 19-26.
- Yang, M., Ellenberg, J., Bonifacino, J.S., and Weissman, A.M.** (1997). The transmembrane domain of a carboxyl-terminal anchored protein determines localization to the endoplasmic reticulum. *J Biol Chem* **272**, 1970-1975.

Chapter 3

- Zelazny, E., Micielica, U., Borst, J.W., Hemminga, M.A., and Chaumont, F.** (2009). An N-terminal diacidic motif is required for the trafficking of maize aquaporins ZmPIP2;4 and ZmPIP2;5 to the plasma membrane. *Plant J* **57**, 346-355.
- Zelazny, E., Borst, J.W., Muylaert, M., Batoko, H., Hemminga, M.A., and Chaumont, F.** (2007). FRET imaging in living maize cells reveals that plasma membrane aquaporins interact to regulate their subcellular localization. *Proc Natl Acad Sci U S A* **104**, 12359-12364.

Table T1 (continued)

forward primer	sequence	reverse primer	sequence	destination vector
XbaI_DMP1 _{10ref} _F	CGG TCTAGA ATG TCC GAA ACT TCT TTTG CTC	PstI-DMP1 _{KR182}	AA CTGCAG C TCGTTT GCTGGAAACAAGC	pPGTkan3
		PstI-DMP1 _{HEE193}	AA CTGCAG C CTCCTCAGCAATTGGCGCGTA	
		PstI-DMP1 _{HEE199}	AA CTGCAG C CTCCTCTTCAGCACCTACCTC	
		PstI-DMP1 _{KK202}	AA CTGCAG C TTTCTGGTCTCTCTTCAGC	
35S-lowardsGene	GGA AGT TCA TTT CAT TTG GAG	PIA _{AA} VGA _{EEET} KK _{ASVA} _R	CGCCCGCAACAATTGGCGGTACCC	
PIA _{AA} VGA _{EEET} KK _{AS}	GGGTACCGCCCAATTGCTCGCGGGTAGGTCTGAAGAGGAG	RBCS_1 _{term}	AATGCCATAATACTCAAACTC	
35S-lowardsGene	siehe oben	PIA _{EEV} GAA _{AAAT} KK _{ASVA} _R	CGCCCGCCAGCACCTACCTCTCAGC	
PIA _{EEV} GAA _{AAAT} KK _{AS}	GCTGAGGAGGTAGGTGCTCGCGGGCGACCAAGAAAGCCCTCGGTC	RBCS_1 _{term}	siehe oben	
35S-lowardsGene	siehe oben	PIA _{EEV} GAA _{EEET} AAA _{SVA} _R	CGCCCGGGTCTCTCTTCAGCACCC	pPGTkan3
PIA _{EEV} GAA _{EEET} AAA _S	GGTCTGTAAGAGGAGACCGGGCGGCTCGGTCTCTGCC	RBCS_1 _{term}	siehe oben	
35S-lowardsGene	siehe oben	AAVGA _{AAAT} AAA _{SVA} _R	GGCGGGCGGGTGGCGGGCGAGCACTACCGCCAGCAATTGGCGCGTA	
AAVGA _{AAAT} AAA _{SVA}	GCCGCCGCCACCCTCGCCGCTCGGTCTCTGCCGCTGCAG	RBCS_1 _{term}	siehe oben	
atB1-DMP1_F	GGGGACAAGTTTGTACAAA AAA GCA GGC TTG ATG TCC GAA ACT TCT TTG CTC	atB2-DMP1_R	GGGGACCAGTTTGTACAAA AAG CTGGGT T GGC AGA GAC CGA GGC TTT C	
XbaI-mRFP-Ava7	ACGG TCTAGA ATGGCTCTCTCGAGGAGGTC	mRFP-Ava7-XhoI	TAGA CTGGAG CTAAGACACAACAATGAGCT	
XbaI _{L52#} DMP1_F	ACGG TCTAGA ATGC CGGAACCTCTTTGGTC			
XbaI _{L57#} DMP1_F	ACGG TCTAGA ATGA CGGAACCTCTTTGGTC			
XbaI _{L55#} DMP1_F	ACGG TCTAGA ATGTCT GAAACTCTTTGGTC			
XbaI _{L53#} DMP1_F	ACGG TCTAGA ATGTT CGAACTCTTTGGTC	PstI_DMP1ORF without STOP_	AA CTGCAG C GGC AGA GAC CGA GGC TTT C	pPGTkan3
XbaI _{L52#} DMP1_F	ACGG TCTAGA ATGCC C C C A C T C T T T G G T C			
KpnI-mRFP_F	GTGGTACCATGGGCTCTCGAGGACGTC	XbaI_mRFP without STOP_R	C GG TCTAGA GGGCCGGT GGA GTGGGGCC	5S:DMP1 (pPTkan3 containing DMP1
XbaI_Met_20-207_F	siehe oben	XhoI_DMP1 without STOP_R	TAGA CTCGAG GGCAGA GACCGAGGCTTCTT	pPRtkan3
DMP1-int1	TTAGGCAGAGACCGAGGCTTTC			
Oligo d(T)-anchor_F	GACCACCGGTATCGATGTGACATTTTTTTTTTTTTTTT	DMP1-int2	GCAAAGCCA TGA CAAGTGTCTC	
anchor_F	GACCACCGGTATCGATGTGAC	DMP1_int3	CGTCAAAGCGACA CGA GTGTACCA	

Chapter 4

***DMP1* is a senescence-associated WRKY-regulated gene presumably involved in cell death by protein-protein interaction with Bax Inhibitor-1 and Cytochrome b5**

Alexis Kasaras and Reinhard Kunze

Address:

Freie Universität Berlin, Institut für Biologie - Angewandte Genetik, Dahlem Centre of Plant Sciences (DCPS)

Keywords: DMP1, BI-1, CB5, senescence, early senescence phenotype, cell death, WRKY, W-box, unfolded protein response (UPR), jasmonates, OPDA, split-ubiquitin screen,

The work presented in this chapter will serve as basis for future publications

Abstract

DMP1 (DUF679 membrane protein 1) was identified in a screen for *Arabidopsis thaliana* senescence-associated genes encoding membrane proteins. *DMP1* is strongly upregulated during developmental and induced senescence. Both *DMP1* overexpressor and knockout mutant lines enter senescence earlier than wild-type plants when grown on low-fertilized soil. Using reporter gene constructs with GUS and eGFP, the promoter of *DMP1* was shown to be active in a patchy pattern in the senescing leaves reminiscent of lesion mimic mutants. Mutational analysis of the *DMP1* promoter identified two adjacent WRKY cognate binding site (W-boxes) in a palindromic configuration responsible for *DMP1* specific upregulation during senescence. Several WRKY TFs were able to bind to these W-boxes and to transactivate transcription as shown in transient assay suggesting that the senescence-specific regulation of *DMP1* is governed by WRKY transcription factors. Upregulation through cycloheximide treatment suggests additional presence of short-lived repressor protein(s) inhibiting *DMP1* expression during other developmental stages. Genome-wide transcriptome analysis performed on *DMP1-OE1* identified a downregulation of most jasmonate-related genes in unwounded plants. OPDA, an intermediate of the JA biosynthesis pathway, which is considered as intracellular senescence marker was shown to be twice as abundant in the mutant than in WT. This points towards a shift in the developmental state which could explain the early senescence phenotype observed in *DMP1-OE1*. A split-ubiquitin screen in yeast was carried out to isolate interaction partners of DMP1. DMP1 interacts with Bax Inhibitor-1 and the Cytochrome b5 (isoforms E and D), known to interact with each other. This finding suggests an involvement of DMP1 in cell death. Treatments with several ER stressors exclude an implication of DMP1 in the unfolded protein response (UPR) during ER stress. *DMP1* is predicted to be induced by several biotrophic and necrotrophic pathogens as well as bacterial elicitors suggesting a role in the plant innate response and corroborating its implication in cell death processes. Responses of the different *DMP1* mutants to various biotic stressors are currently under investigation and may help to elucidate its cellular function.

Introduction

DMP1 is a member of a protein family containing ten members in *Arabidopsis thaliana*. All AtDMP proteins are predicted to have four transmembrane spans, with cytosolic amino- and carboxy-termini. DMPs are expressed from intronless genes except *DMP7* which contains a short intron. Phylogenetic examination revealed an ubiquitous occurrence of DMPs in green plants (Kasaras and Kunze, 2010). DMPs are absent from other kingdoms which suggest an implication in plant-specific processes. *Chlamydomonas reinhardtii* and *Physcomitrella patens* genomes contain only one *DMP* gene whereas dicots possess five to 13 and monocots 11 to 16 *DMP* genes. *DMPs* expression pattern are highly tissue- and development-specific (Kasaras and Kunze, 2010). Their occurrence in tissues undergoing senescence (*DMP1*, -3, -4), dehiscence (*DMP1*) and abscission (*DMP1*, -2, -4, -7) suggest an involvement in different types of programmed cell death. Overexpression of DMP1-eGFP in *Nicotiana benthamiana* triggers complex remodeling of the ER and the tonoplast which culminate in fragmentation of these compartments ending in cell death (chapter 2). Expression of DMP1-eGFP by the native promoter highlighted the formation of “boluses” at the ER and vesiculation of the entire ER network preceding fragmentation of the central vacuole during the latest steps of natural senescence and dark-induced senescence in siliques, rosette and cauline leaves. This led to the assumption that DMP1 have membrane fission, fusion or remodeling properties required during breakdown of the ER and the vacuole in senescing cells undergoing cell death (chapter 2). All DMP proteins locate to the ER or the tonoplast or both when fused to eGFP (Kasaras and Kunze, 2010). However, closer investigation of DMP1 protein occurrence in tobacco and *Arabidopsis* revealed a much more complex distribution. Due to a leaky ribosome scanning at the first translation initiation site, two proteins isoforms (DMP1.1 and DMP1.2) are transcribed from single transcripts (chapter 3). DMP1.1 is targeted to the tonoplast whereas DMP1.2. locates to the plasma membrane. Mutations and truncations within the amino terminus of DMP1.1 lead to redirection of DMP1.1 to the plasma membrane which is thus believed to be the default pathway. However DMP1.2 subcellular localization is largely “eclipsed”. Upon protein-protein interaction with DMP1.1, DMP1.2 is redirected to the tonoplast (chapter 3). The molecular function of DMP1 and of all other DMP proteins remains to be elucidated.

In the present study, DMP1 function and involvement in senescence and cell death were investigated by using *dmp1* knock-out (*dmp1-ko*) and ectopic *DMP1* overexpressing lines (*DMP1-OE1*), by *DMP1* promoter analysis and by isolating putative protein interactors. Beside *DMP1* strong upregulation during developmental senescence, we show that *DMP1* is highly upregulated during dark-induced senescence in attached and detached leaves and in whole darkened plants. *dmp1-ko* and *DMP1-OE1* both enter senescence earlier than wildtype plants. The phenotype

Chapter 4

observed in *dmp1-ko* is proposed to be triggered by the presence of truncated transcripts that could potentially give rise to truncated and possibly dysfunctional proteins. In contrast, the phenotype observed in *DMP1-OEI* is likely due to deregulated jasmonates levels as quantification of JA-related transcripts and measurement of OPDA concentration suggest. The senescence-specificity of DMP1 was determined to be regulated by two w-boxes, responsible for WRKY binding. Mutations of these two motifs resulted in near-loss of *DMP1* expression during senescence. DMP1 function was further investigated by isolating putative protein interactors using the split-ubiquitin system in yeast. Bax Inhibitor-1 and two isoforms of cytochrome b5 were found to interact with DMP1 which reinforce an involvement of *DMP1* in cell death.

Results

Reverse genetic approaches to investigate *DMP1* function

To investigate *DMP1* function, several reverse genetic approaches were employed to manipulate *DMP1* expression. T-DNA insertion mutagenesis and artificial micro RNA technology were used to knock down/out *DMP1* expression and expression by the 35S promoter was used to study the effects of *DMP1* overexpression.

dmp1-ko displays an early senescence phenotype

Homozygous plants of the only available insertion line predicted to carry a T-DNA insertion inside the open reading frame of *DMP1* (GK-305G09-015571) were isolated by PCR (data not shown) and screened for phenotypical alterations. The mutant *dmp1-ko* displayed an early senescence phenotype compared to WT (Fig. 1A). This phenotype was observed under continuous light (data not shown) and long day (LD) conditions (Fig. 1A). It was found to be highly dependent on soil conditions and was visible on “low-fertilized” soil (Fig. 1A) but not on “high-fertilized” soil (Fig. 1B). We did attempt to regulate the level of soil fertilization in the hope of identifying the key factors leading to the phenotype. Unfortunately, these efforts were abandoned as we found that soil composition varied too much for any systematic regulation of the level of fertilization. Thus, further phenotypical characterizations such as quantification of chlorophyll were abandoned. No stable phenotype was observed *in vitro* on agar medium containing various nutrient compositions either (data not shown). Thus, the conditions leading to the early senescence phenotype on “low-fertilized” soil could not be determined neither on soil nor *in vitro*.

Truncated *DMP1* transcripts were detected in *dmp1-ko* plants by RNA gel blot analysis (Fig. 2B). The intensity of the signals detected in *dmp1-ko* was weaker than in WT, indicating that these transcripts were not as stable as the full length mRNA. Investigation of heterozygous *DMP1/dmp1*

Chapter 4

plants confirmed this result, the level of truncated transcripts being below the level of the full length transcripts and at lower detection limit. The insertion of the T-DNA was determined by sequencing at position 491 of the open reading frame of *DMP1* (Fig. 2A) and *dmp1-ko* was identified as single insertion mutant by DNA gel blot analysis (data not shown). A second probe (3' probe) was designed to bind to a sequence of *DMP1* located downstream of the T-DNA insertion site comprising the 3'-UTR. This probe was used to again investigate *DMP1* transcript occurrence in *dmp1-ko*, *DMP1/dmp1* and WT (Fig. 2A). No signals could be detected in *dmp1-ko* (Fig. 2B, lower panel, lane 3) confirming the absence of full length transcripts. The intensity of the transcripts detected in *DMP1/dmp1* confirmed that the WT allele was present in a single copy in this line. We are currently unable to conclude whether the phenotype observed in *dmp1-ko* is due to the presence of truncated transcripts (with its associated putative and dysfunctional proteins) or due to the absence of the full length ones.

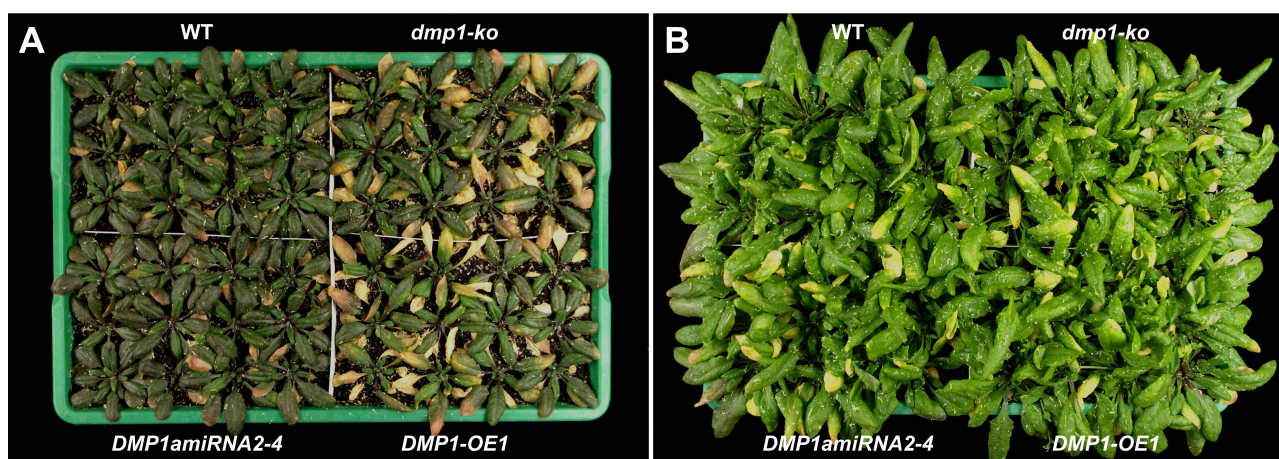


Figure 1. Phenotypal analysis of *dmp1-ko*, *DMP1-OE1* and *DMP1amiRNA2-4* compared to the wild type. *dmp1-ko* and *DMP1-OE1* exhibit early senescence phenotypes compared to WT on low fertilized soil (A). These phenotypes were not visible on standard high-fertilized soil (B). *DMP1amiRNA2-4* did not display any phenotypical alterations on low (A) or high fertilized soil (B) compared to WT.

DMP1amiRNA2-4 mutant lines do not display an early senescence phenotype

The implication of truncated transcripts in the phenotype observed in *dmp1-ko* was further investigated using the artificial micro RNA technology. Different transgenic lines were generated to knock down/out *DMP1* expression. Four different constructs were generated, two of them containing the native *DMP1* promoter (*DMP1p:DMP1amiRNA1* and 2), the two others containing the *CaMV 35S* promoter (*35S:DMP1amiRNA1* and 2) (Fig. 2C). *DMP1p:DMP1amiRNA1* and *35S:DMP1amiRNA1* were targeted against the same fragment of *DMP1* while *DMP1p:DMP1amiRNA2* and *35S:DMP1amiRNA2* against another *DMP1* fragment. The 35S promoter knocked down *DMP1* expression more efficiently than the native one in senescent rosette

leaves (Fig. 2C). *35S:DMP1amiRNA1* appeared to knock down *DMP1* gene expression slightly more efficiently than *35S:DMP1amiRNA2* and was therefore used in further studies. This line was screened in the third generation for homozygosity by kanamycin resistance and used for phenotypical analyses. It did not exhibit an early senescence phenotype similar to *dmp1-ko* (Fig. 1A). Thus, the phenotype observed in *dmp1-ko* could originate from truncated and possibly dysfunctional proteins due to the presence of truncated transcripts. However, despite the fact that almost no transcripts were detected on RNA gel blot analysis in *35S:DMP1amiRNA2-4* (Fig. 2C), a complete silencing of *DMP1* expression during senescence is unlikely using artificial micro RNA technology. Thus, residual *DMP1* transcripts may allow translation of DMP1 proteins to a sufficient level during senescence. Figure 2C shows transcripts from independent transformants in the first generation. Transcript occurrence may be verified by RNA gel blot analysis in the third generation to exclude putative loss of silencing over generations.

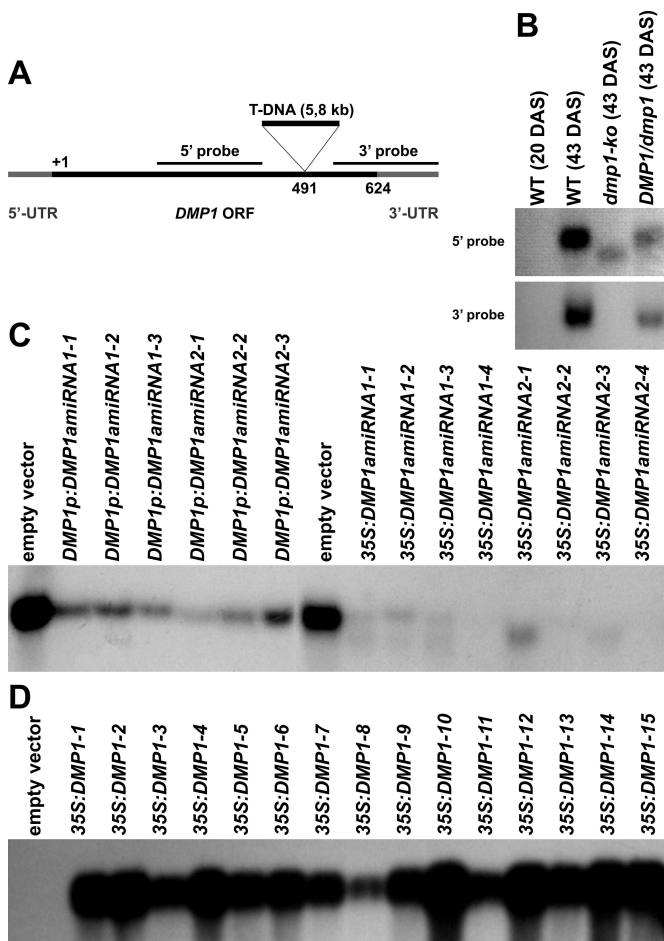


Figure 2. Investigation of *DMP1* expression level in different transgenic lines by RNA gel blot analysis. (A) Schematic representation of the intronless ORF of *DMP1* flanked by the 5'- and 3'-UTR on genomic DNA. T-DNA insertion is shown in position 491. Positions of the two different *DMP1* probes used in (B) are shown. (B) RNA gel blot analysis of homozygous *dmp1-ko* and heterozygous *DMP1/dmp1* plants compared to WT plants at 43 DAS using two different probes. Comparison of juvenile (20 DAS) and senescing rosette leaves (43 DAS) show *DMP1* senescence-associated expression. (C) Downregulation of *DMP1* transcripts in primary transformants mediated by the constructs *DMP1p:DMP1amiRNA1* and -2 and *35S:DMP1amiRNA1* and -2. Senescing rosette leaves 5-8 from 43 DAS old transgenic plants were pooled and used for total RNA extraction. Transgenic plants carrying the empty vector show native expression of *DMP1* at 43 DAS. (D) *DMP1* overexpression shown in 15 independent primary transformants by RNA gel blot analysis. Juvenile rosette leaves 5-8 from 20 DAS old transgenic plants were pooled and used for total RNA extraction. Empty vector was used as negative control showing native *DMP1* expression at 20 DAS. 10 μ g total RNA were loaded and equal loading was verified directly on RNA gel (not shown) for all experiments (B-D).

DMP1-OE1 displays an early senescence phenotype similar to *dmp1-ko*

The effect of *DMP1* overexpression *in planta* was investigated by generating transgenic lines containing *DMP1* under the control of the 35S promoter. On RNA gel blot, the transcript level of

Chapter 4

DMP1 in juvenile leaves was strongly increased in all different primary transformants tested (Fig. 2F). *DMP1-OE1* and *DMP1-OE2* were chosen for further analyses. Using *DMP1*-antibody, *DMP1* proteins were already shown to be overexpressed in these lines (chapter 3). Surprisingly, they exhibited a similar phenotype to *dmp1-ko*, entering senescence earlier than WT plants (Fig. 1). *DMP1-OE1* and *DMP1-OE2* senesced slightly earlier than *dmp1-ko*. No other macroscopic alterations were visible in both *dmp1-ko* and *DMP1-OE* lines.

Transcriptional profiling of *DMP1-OE1* by microarray analysis

A comparative genome-wide transcriptome analysis of *DMP1-OE1* and WT plants was performed to detect genes with altered expression levels in *DMP1-OE* plants. For this experiment Agilent type "Arabidopsis 4" microarrays carrying 43.603 features were used. To avoid analyzing tissues at different developmental stages, leaf 6 of *DMP1-OE1* and WT was harvested at 28 DAS when the plants did not display any phenotypical differences yet. The first senescence symptoms which appeared in the *DMP1-OE1* line were not visible before 36 DAS in leaf 6. We aimed to detect even subtle changes in gene expression in response to *DMP1* overexpression which may lead to the phenotype observed later during development. We did not observe a significant up- or down-regulation of large number of genes. Apart from the 2570-fold *DMP1*-upregulation in the mutant, the strongest upregulation observed was an 11-fold change in expression compared to WT. The strongest downregulation reached a 22,8-fold change. Database analyses were performed to find a connection between the senescence phenotype and the function of these upregulated genes, but no plausible explanation was found. Thus, the upregulated genes will not be presented here in more detail.

However, we observed that almost every gene involved in the biosynthesis and regulation of jasmonates (JA) as well as jasmonate-responsive genes was downregulated in the *DMP1-OE1* mutant (Table 1). Most JA biosynthesis genes underwent slight downregulation (see reviews for the JA biosynthesis pathway (Wasternack, 2007; Acosta and Farmer, 2010; Wasternack and Kombrink, 2010)). JAZ proteins have been recently identified as negative regulators of the transcription of jasmonate-responsive genes (Chini et al., 2007; Chico et al., 2008; Chini et al., 2009). A majority of JAZ proteins were downregulated in *DMP1-OE1* (Table 1). JAZ7 was the most strongly downregulated JAZ protein (Table 2). MYC2, the key transcriptional activator of jasmonate responses (Boter et al., 2004; Wasternack and Kombrink, 2010), and ORA47, another TF involved in JA signaling (Pauwels et al., 2008) were downregulated by a factor of 1,4 and 12,5 respectively. Several other known JA-responsive genes such as *MBP1* and 2 or *STZ* also showed significant lower expression level in resting *DMP1-OE1*. The gene showing the strongest downregulation was

Chapter 4

CYP94B3 (Table 1). This gene has been recently identified as JA-Ile-12-hydroxylase (Koo et al., 2011) mediating inactivation of JA-Ile to the largely inactive form 12OH-JA-Ile. Thus, an accumulation of the active form JA-Ile could occur in *DMP1-OE1* due to a decreased catabolism rate. In turn, the cell may try to compensate this accumulation by decreasing the expression level of JA-related genes which would fit with our findings.

	x fold change (qRT-PCR)	x fold change (micro-array)
Genes involved in JA biosynthesis		
<i>LOX2</i>	-1,8	-1,8
<i>AOS</i>	-1,5	-1,2
<i>AOC1</i>	-1,4	-1,4
<i>AOC2</i>	-1,6	-1,7
<i>AOC3</i>	-2,3	-1,6
<i>PXA1</i>	-1,0	-1,2
<i>OPR3</i>	-1,4	-1,2
<i>OPCL1</i>	-1,4	-1,4
<i>ACX1</i>	-1,6	-1,2
JA modifying enzymes		
<i>JMT</i>	<i>n.d.</i>	-1,2
<i>JAR1</i>	-1,1	-0,9
JA-Ile catabolism gene		
<i>CYP94B3</i>	-40,3	-22,8
components of jasmonate co-receptor complex		
<i>COI1</i>	1,0	1
<i>JAZ1</i>	-2,7	-2,1
<i>JAZ2</i>	-1,4	-1,3
<i>JAZ3</i>	-1,3	-1,3
<i>JAZ4</i>	-1,2	-1,3
<i>JAZ5</i>	-2,3	-2,4
<i>JAZ6</i>	-1,3	-1,2
<i>JAZ7</i>	-4,8	-6,7
<i>JAZ8</i>	-3,2	-3,3
<i>JAZ9</i>	-1,3	-1,4
<i>JAZ10</i>	-2,3	-1,9
<i>JAZ11</i>	-1,1	1
<i>JAZ12</i>	1,0	-1,1
TFs regulating JA-responsive genes		
<i>MYC2</i>	-1,7	-1,4
<i>ORA47</i>	-13,6	-12,5
JA-responsive genes		
<i>PEPR1</i>	-1,6	-1,4
<i>JR1</i>	-2,1	-2
<i>MBP2</i>	-5,3	-3,9
<i>MBP1</i>	-5,1	-4,7
<i>STZ/ZAT10</i>	-3,5	-7,3
<i>ZAT11</i>	-2,1	-4,7
<i>EXT4</i>	-2,0	-1,7
<i>CYP94C1</i>	-1,5	-1,4

Table 1. Most JA-related genes are down-regulated in *DMP1-OE1* plants compared to WT plants. Microarray analyses were performed using cDNA from 28 DAS old *DMP1-OE1* and WT plants (rosette leaf 6 respectively). Most JA-related genes showed moderate down-regulation in *DMP1-OE1* compared to WT with only a few of them showing strong downregulation. Gene regulation was verified by qRT-PCR. Genes are classified according to their function in the JA pathway and response.

Abbreviations

LOX, lipoxygenase
AOS, allene oxide synthase
AOC, allene oxide cyclase
PXA1, peroxisomal ABC transporter
OPR3, oxophytodienoic acid reductase 3
OPCL1, OPC-8:0 CoA ligase1
ACX1, acyl-CoA oxidase 1
JMT, S-adenosyl-L-methionine:jasmonic acid carboxyl methyltransferase
JAR1, jasmonate resistant1 (jasmonate-amido synthetase)
COI1, component of JA co-receptor complex
JAZ, jasmonate zim domain
MYC2, MYC-related transcriptional activator
ORA47, member of the DREB subfamily A-5 of ERF/AP2 transcription factor family.
CYP94B3, cytochrome P450, family 94, subfamily B, polypeptide 3, monooxygenase involved in jasmonoyl-L-isoleucine catabolism
PEPR1, PEP1 receptor 1
JR1, JA-responsive 1
MBP1, myrosinase-binding protein 1
STZ/ZAT10, salt tolerance zinc finger, subclass C1-2i C2H2-zinc-finger-type nucleic acid binding protein
ZAT11, subclass C1-2i C2H2-zinc-finger-type nucleic acid binding protein
EXT4, extensin 4
CYP94C1, cytochrome P450, family 94, subfamily C, polypeptide 1

Quantification of JA content in *DMP1-OE1*

Based on the above-mentioned assumption on the compensatory mechanisms of JA level regulation in *DMP1-OE1*, we quantified JA, JA-Ile and 12OH-JA-Ile by GC-MS. Unfortunately, the levels of all isoforms were mostly below detection limit. JA measurements are usually performed on treated plants, especially wounded plants which show dramatically increased JA-concentrations within minutes.

OPDA, a precursor of JA, considered as an intracellular marker of senescence was also quantified. It was found to be more than twice as high in *DMP1-OE1* as in WT (data not shown). We further grew *DMP1-OE1*, *dmp1-ko* and *DMP1amiRNA2-4* on 1 μ M, 25 μ M and 50 μ M (\pm)-jasmonic acid and (\pm)-jasmonic acid methyl ester. None of them exhibited any phenotypical difference compared to WT (data not shown). Thus, increased OPDA levels and lower transcript level of JA-related genes in *DMP1-OE1* did not modify JA perception and signaling.

DMP1* transcriptional regulation during development and in response to stressesDMP1* expression during natural and induced senescence

DMP1 was isolated in a genome-wide screen for senescence-associated genes as a highly upregulated gene during natural and induced senescence (Van der Graaff et al., 2006). *DMP1* expression was found to be upregulated at the onset of senescence and to strongly increase until death during natural senescence (NS), dark-induced senescence in individually darkened attached leaves (DIS) and detached leaves (DET) (Fig. 3A). In all cases, *DMP1* upregulation coincided or slightly followed upregulation of *SAG12* and occurred in rosette leaves where *RBCS-1B* expression was already strongly downregulated indicating that *DMP1* is belatedly induced during NS, DIS and DET. The senescence-specific expression of *DMP1* during natural senescence in silique walls, rosette and cauline leaves was confirmed by semi-quantitative RT-PCR (Fig. 3C) (Kasaras and Kunze, 2010), and RNA gel blot analysis (Fig. 3C). GUS staining of senescing siliques of transgenic plants carrying *DMP1*_{p_{2kb}}:*uidA* showed that *DMP1* expression started at the floral organ abscission zone and silique wall dehiscence zone (Kasaras and Kunze, 2010) and then progressed from base to tip (Fig. 3D). RNA gel blot analysis confirmed that *DMP1*_{p_{2kb}}:*uidA* undergoes a senescence-specific regulation comparable to the native expression of *DMP1* in WT (Fig. 3E). Interestingly, *DMP1* appeared to be expressed in a patchy pattern during NS (Fig. 3F) and in response to darkening (Fig. 3G) reminiscent of patterns seen in lesion mimic mutants (Lorrain et al., 2003). Concordant results were obtained by investigating *DMP1*_{p_{2kb}}:*uidA* plants as well as the translational fusion *DMP1-eGFP* expressed from *DMP1*_{p_{2kb}}. However, we could not investigate

Chapter 4

DMP1 expression pattern in late senescing tissues since these tissues could not be properly GUS-stained and showed a too high fluorescence background masking eGFP-specific signals at macroscopic level (data not shown). The only non-photosynthetic tissue to express *DMP1* were the roots (Fig. 3C) (Kasaras and Kunze, 2010) showing the highest expression level of *DMP1* in the phloem bundles and the root tips.

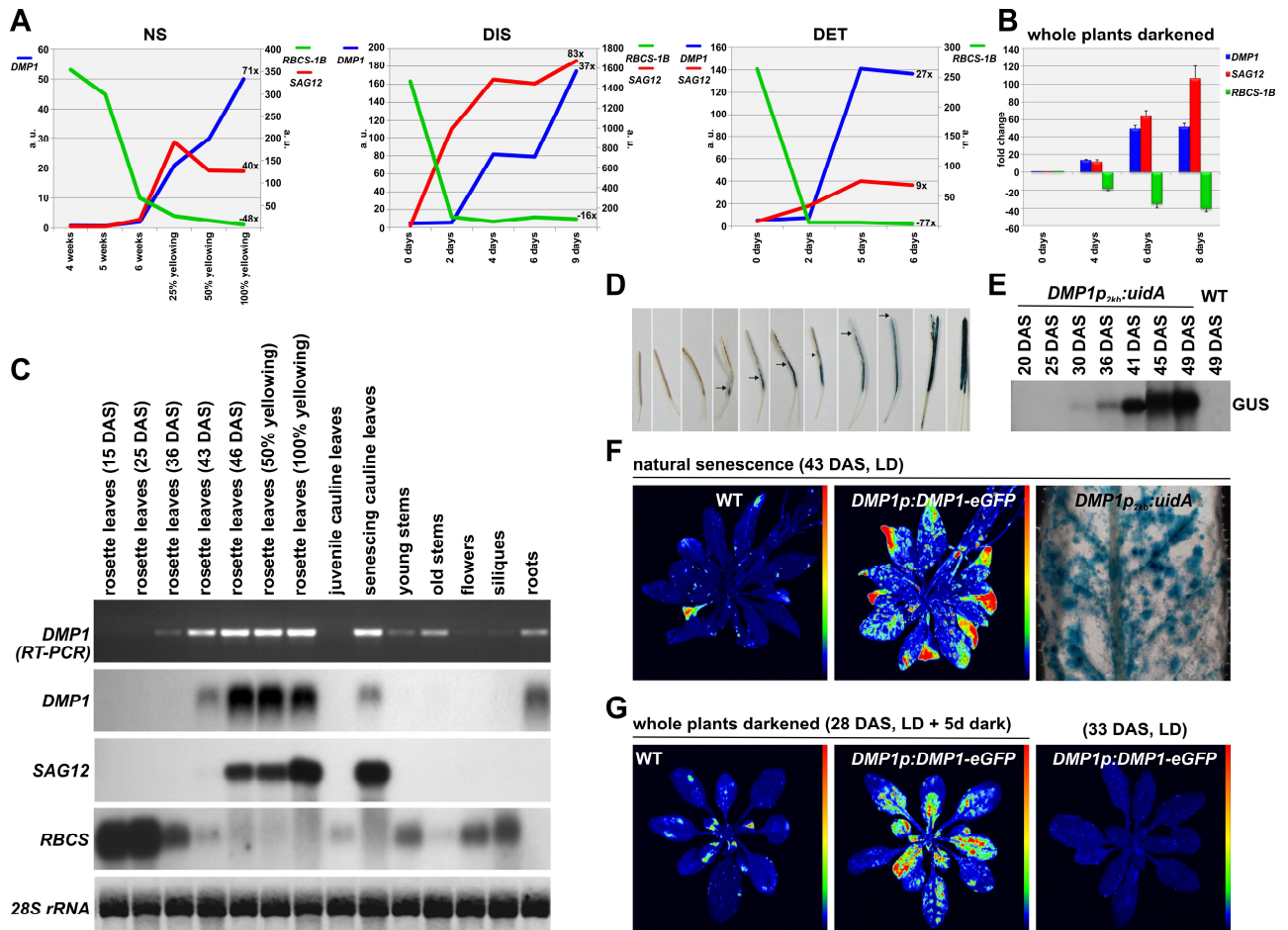


Figure 3. Investigation of *DMP1* expression patterns during natural and induced senescence. (A) Expression profiles of *DMP1*, *SAG12* and *RBCS-1B* during natural senescence (NS), dark-induced senescence in individual attached (DIS) and detached (DET) leaves extracted from the microarray experiment described in Van der Graaff et al., (2006). Fold changes in expression level are shown for each gene and treatment. (B) Expression profiles of *DMP1*, *SAG12* and *RBCS-1B* following darkening of whole plants for 2, 4, 6 and 8 days were determined by qRT-PCR. Values are expressed in fold change compared to non-darkened plants of the same age and normalized using *UBQ10*. (C) Semi-quantitative PCR and RNA gel blot analysis of *DMP1* in different tissues and developmental stages compared to expression levels of *SAG12* and *RBCS*. 10 µg total RNA were loaded and equal loading is shown by 28S rRNA on RNA gel. (D) GUS staining of juvenile to senescent siliques (from left to right) from *DMP1p::uidA* plants show progression of expression from base to tip during silique senescence. (E) RNA gel blot analysis of *DMP1p_{2kb}::uidA* whole rosettes at different developmental stages shows senescence-associated regulation of *DMP1p_{2kb}*. A probe raised against GUS was used for hybridization and 49 DAS old WT plants were taken as negative control. (F) *DMP1* promoter activity pattern during NS visualized by *DMP1*-eGFP or GUS, both expressed from the native promoter. Both transcriptional and translational reporter systems showed comparable patchy activity of *DMP1p*. (G) *DMP1p* activity pattern in dark-treated plants visualized by *DMP1*-eGFP expressed from the native promoter. 28 DAS old WT and transgenic plants were put into the dark for 5 days. 33 DAS old transgenic plant grown under LD conditions is shown as control.

DMP1 regulation through chemicals, hormones, biotic and abiotic stresses

DMP1 is largely senescence-specific. During the other developmental stages of these tissues, *DMP1* is not or only weakly expressed. To gain more insight into *DMP1* involvement in responses to diverse stresses and treatments which might give hint to its cellular function, we screened publicly available databases (<https://www.genevestigator.com>, <http://bar.utoronto.ca/efp/cgi-bin/efpWeb.cgi>). A reduced number of treatments were found to induce *DMP1* expression. Strikingly, several biotic stresses appeared to induce *DMP1* transcription. *DMP1* moderately to strongly responded to *Botrytis cinerea* (~ 8-fold increase), *Phytophthora infestans* (~ 25-fold increase), virulent and avirulent *Pseudomonas syringae* strains (~ 6- and 25-fold increases respectively) and several bacterial elicitors: Flg22, HrpZ and NPP1 (20-, 47- and 21-fold increases respectively). Thus, *DMP1* might be involved in the plant immune system. To test this hypothesis, monitoring the response of the different mutants *dmp1-ko*, *DMP1-OE1* and *DMP1amiRNA2-4* to the above-mentioned pathogens and elicitors as well as other biotroph and necrotroph pathogens is crucial. Enhanced resistance or susceptibility to particular pathogens and elicitors would identify *DMP1* as a factor required in plant immunity. In the end, it may help to shed more light on *DMP1* cellular function. These experiments are currently carried out.

No phytohormone was found to induce *DMP1* (<https://www.genevestigator.com>). Only the ethylene inhibitor AgNO₃ was predicted to induce *DMP1* which was confirmed experimentally (Table 2). A link between *DMP1* and ethylene signaling is speculative. Overexpression of *DMP1* did not lead to obvious transcriptional activation or repression of ethylene-related genes (data not shown). Moreover, aminoethoxyvinyl (AVG),

another ethylene inhibitor does not induce *DMP1* according to publicly available databases. Thus, *DMP1* expression and ethylene signaling are most probably not linked. Cycloheximide, the other chemical predicted to induce *DMP1* was shown to strongly upregulate *DMP1* expression using quantitative real time PCR (Table 2). By comparing the absolute values obtained by qRT-PCR, the values obtained following cycloheximide treatment were largely superior to those obtained during late NS and DIS (data not shown). Cycloheximide is a strong protein synthesis inhibitor and could inhibit the synthesis of putative new repressors. Their possible rapid turn-over would result in a strong derepression of *DMPp* leading to a strong accumulation of *DMP1* transcripts.

Table 2. *DMP1* expression is upregulated by AgNO₃, cycloheximide, mannitol, and NaCl. 18 DAS old WT plantlets grown on plates were transferred to liquid ½ MS media and allowed to acclimate for one day under gentle shaking. Treatments with AgNO₃, cycloheximide (CHX), mannitol and NaCl were performed for 6 hours. *DMP1* regulations following these treatments were quantified by qRT-PCR using untreated plants as control and *UBQ10* for normalization. *DMP1* upregulations are expressed in fold changes compared to untreated plants.

	AgNO ₃	CHX	Mannitol	NaCl
DMP1	39,2	657	11,2	4,5

Chapter 4

Two abiotic stresses were found to induce *DMP1* expression: mannitol (300 mM) and NaCl (150 mM) (<https://www.geneinvestigator.com>). These results were confirmed by qRT-PCR (Table 2). We investigated *dmp1-ko*, *DMP1-OE1* and *DMP1amiRNA2-4* on different mannitol and NaCl concentrations but none of them showed any phenotypical difference compared to WT (data not shown). Thus, we conclude that DMP1 is not essential in the response to salt and osmotic stresses.

DMP1 regulation through ER stressors

DMP1 was found to interact with Bax Inhibitor-1 (BI-1) in yeast (this chapter) and to locate to the ER (chapter 1 and 2). Tunicamycin (TM) and dithiothreitol (DTT) are common chemicals used as ER stress inducers and have been used in microarray experiments to identify genes involved in the unfolded protein response (UPR) (Martinez and Chrispeels, 2003; Kamauchi et al., 2005). *BI-1* was found to be induced by TM and DTT. The calcium pump inhibitor cyclopiazonic acid (CPA) and the proline analog L-azetidine-2-carboxylate (AZC) were also shown to induce the UPR leading ultimately to cell death in a comparable manner to TM (Watanabe and Lam, 2008). The drug thapsigargin (TG) which inhibits sarco/endoplasmic reticulum Ca^{2+} ATPase (SERCA) was also shown to induce ER stress by raising the cytosolic calcium concentration. To test if *DMP1* is involved in the UPR, we tested *DMP1* response to the chemicals TM, DTT, AZC, CPA and TG. As control, several known UPR marker genes (Martinez and Chrispeels, 2003; Kamauchi et al., 2005) were used. All treatments clearly induced ER stress (Table 3). DTT and to a lesser extend TM

Table 3. *DMP1* expression in response to different ER stressors. Expression of *DMP1*, *BI-1* and different genes involved in the UPR was investigated by qRT-PCR in *Arabidopsis* WT plantlets treated with 5 µg/ml TM, 2 mM DTT, 5 mM AZC, 50 µM CPA and 5 µM TG. Drugs applications were performed for 6 hours except for AZC (24 hours).

gene	treatment				
	TM	DTT	AZC	CPA	TG
DMP1	2	10,1	-37,5	-11	-1,3
BI-1	14,6	3,2	2	-1,2	-3
BIP1	13,6	17,3	14,9	14	12,6
BIP2	15,5	19,2	29,7	15,3	12,7
HRD1	8,7	3,6	1,8	2,9	1,4
CRT1B	14,3	4,7	3,3	7,1	12
CNX1	21,7	6,3	8,7	7,2	6,8
PDIL1-1	9,3	3	3,5	22,4	39,1
GPT	7,5	1	1,5	4,3	5,1

induced *DMP1* expression. However, *DMP1* is obviously not required *per se* in the UPR. Indeed, AZC strongly downregulated *DMP1* expression. This is surprising since plantlets were used for these treatments in which *DMP1* resting expression was already very low. However, CPA and TG which both inhibit ER calcium pumps leading to depletion of ER calcium stores and consequently

to ER stress, also downregulated *DMP1* expression. Thus, *DMP1* is not required to counterbalance depleted ER calcium stores and is not directly involved in the UPR during ER stress.

Mutational approach to study *DMP1* senescence-specific regulation

Identification of two W-boxes within *DMP1p* responsible for *DMP1* senescence-specific expression

We showed by GUS staining and RNA gel blot analysis that a 2 kb long *DMP1* promoter (*DMP1p*) fragment led to expression levels and patterns comparable to those promoted by the native *DMP1* gene during NS. We tried to identify the motifs or regions within *DMP1p* which are responsible for its senescence-specific regulation. We scanned the 2 kb long promoter fragment for motifs related to senescence using the publicly available database PLACE (Higo et al., 1998). W-boxes are well described as WRKY cognate binding site (Rushton et al., 1996; Ciolkowski et al., 2008). WRKY TFs constitute one of the largest TF families in plants. They regulate many processes unique to plants such as senescence (Rushton et al., 2010). Four W-boxes were found within the first kb upstream of the start codon (Fig. 4A). Two W-boxes located at position - 165 to - 151 bp, which we named W-box 1 and 2 form a perfect palindrome 77 bp in front of the TATA box (Fig. 4A). Due to their configuration and their spatial vicinity to the TATA box, we hypothesized that they might be responsible for the regulation of *DMP1* during senescence. To test this hypothesis, the two W-boxes were mutated in the 2 kb long *DMP1* promoter-GUS construct (Fig. 4B and C). In parallel, the minimal length of the *DMP1* promoter was identified by constructing a promoter deletion series. Promoter fragments from 2 kb to 0,5 kb in 0,5 kb-steps as well as a 165 bp fragment starting at W-box 2 and a 151 bp fragment starting just behind W-box 1 such that they lack all W-boxes were generated (Fig. 4C). All constructs were tested in stably transformed independent *Arabidopsis* lines in the first generation. Leaf 6 of individual plants was subjected to GUS staining at 28 DAS, 36 DAS and 42 DAS. Leaves had reached adult size at 28 DAS, they showed first senescence symptoms at 36 DAS and were clearly senescing at 42 DAS. For each point in time and transgenic line, 24 plants were analyzed (Fig. 4D). Promoter activity visualized by GUS staining was almost not detectable at 28 DAS, it was clearly visible at 36 DAS and strongest at 42 DAS in lines *DMP1p_{2kb}:uidA* (Fig. 4D), *DMP1p_{1,5kb}:uidA*, *DMP1p_{1kb}:uidA* and *DMP1p_{0,5kb}:uidA* (data not shown). All these lines exhibited similar staining intensities and patchy expression patterns over time (data not shown). In contrast, mutation of W-boxes 1 and 2 in line *DMP1p_{2kb/Wbox1-2mut}:uidA* almost abolished promoter activity (Fig. 4D). In other words, transactivation of *DMP1p_{2kb}* by putative WRKY TF(s) is lost in *DMP1p_{2kb/Wbox1-2mut}*. Almost none of the independent primary transformants showed any GUS staining. Additionally, we generated a construct where the two W-boxes were deleted. The same loss of promoter activity was observed (data not shown).

Chapter 4

DMP1p_{165bp}:uidA and *DMP1p_{151bp}:uidA* also showed comparable loss of promoter activity (data not shown). Promoter activity was then quantified by measuring MU fluorescence using MUG as substrate. Leaves 5, 6 and 7 of new primary transformants were analyzed at 36 DAS and 42 DAS for each transgenic line. Quantification of promoter activity corroborated the results obtained by GUS staining (Fig. 4E). The promoter fragments from 2 kb to 0,5 kb showed comparable expression level and increased from 36 DAS on to 42 DAS in leaves 5, 6 and 7. Thus, the minimal promoter length lies below 500 bp. We observed a slight gradient in the expression levels of the four different constructs between leaf 5, 6 and 7. These promoter fragments showed activities

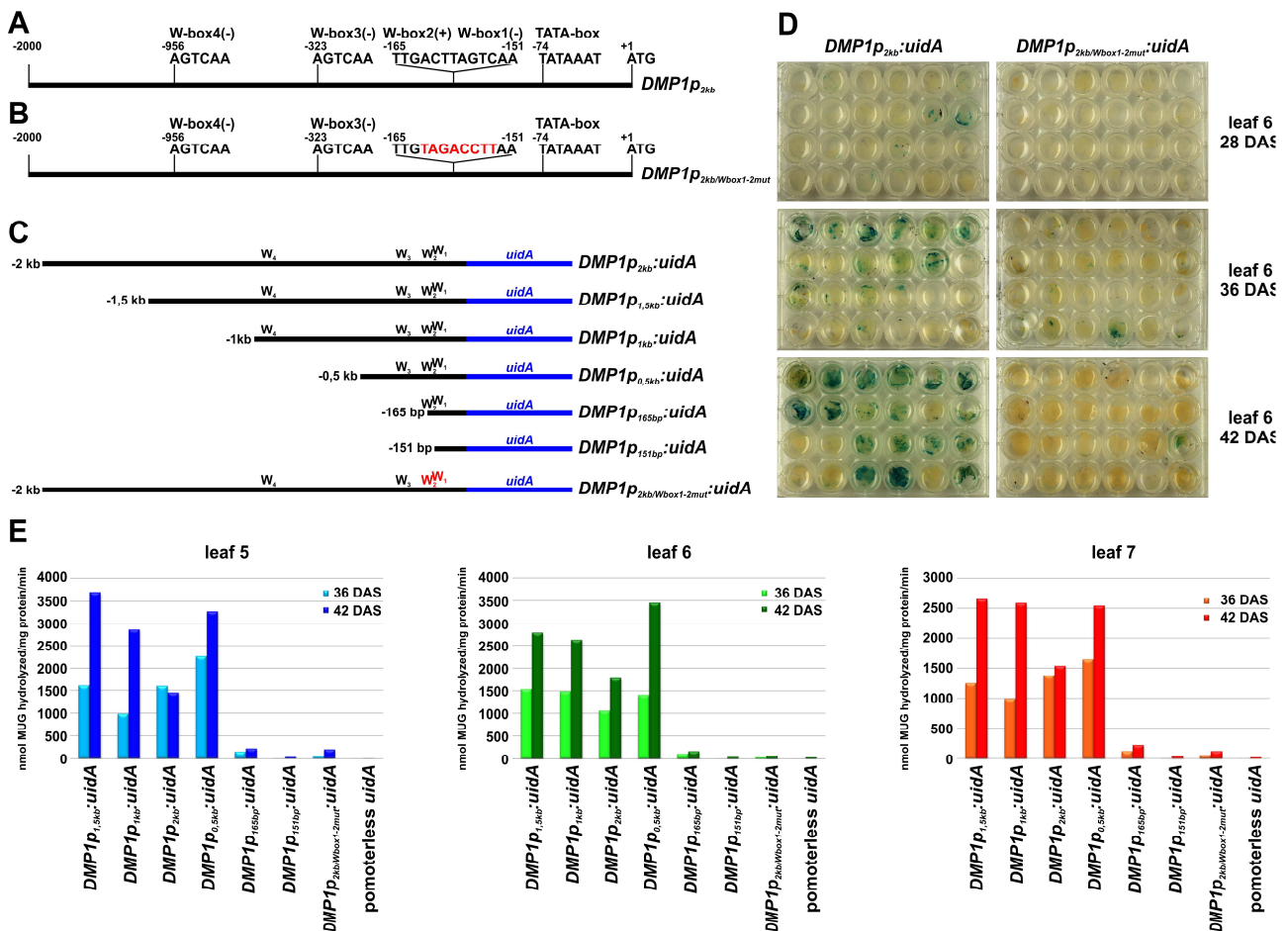


Figure 4. Near-loss of *DMP1p* activity due to mutation of two *W*-boxes and determination of the minimal *DMP1p* length by deletion series. (A) Schematic representation of the distribution of the four *W*-boxes found within *DMP1p_{2kb}*. Position of the *W*-boxes on upper/coding (+) or lower/non-coding strand (-) is shown. (B) Schematic representation of *DMP1p_{2kb/Wbox1-2mut}* corresponding to *DMP1p_{2kb}* (A) carrying mutations within *W*-boxes 1 and 2 shown in red. (C) Schematic representation of the promoter deletion series consisting of fragments of different length (2 kb; 1,5 kb; 1 kb; 0,5 kb; 165 bp and 151 bp) fused to *uidA* encoding GUS. *DMP1p_{2kb/Wbox1-2mut}* is additionally represented with the mutated *W*-boxes shown in red. (D) GUS staining of rosette leaf 6 of independent primary transformants carrying *DMP1p_{2kb}:uidA* or *DMP1p_{2kb/Wbox1-2mut}:uidA* at 28 DAS, 36 DAS and 42 DAS, respectively. 24 independent primary transformants were stained for each time point and transgenic line. (E) Quantification of promoter activity by measuring MU fluorescence mediated by the different promoter fragments shown in (C). Rosette leaves 5, 6 and 7 undergoing early (36 DAS) or late senescence (42 DAS) of 13 independent primary plants were used for each time point and transgenic line. Means of these independent plants are shown. Due to the different genetic background of the individual primary transformants of each line, no standard deviation could be calculated and therefore no error bars were indicated.

Chapter 4

slightly higher in leaf 5 than in leaf 6, themselves higher than those of leaf 7 probably reflecting the slightly shifted senescence states between them. Mutation of W-boxes 1 and 2 led to a near loss of promoter activity and showed a low expression level comparable to the 165 bp promoter fragment (Fig. 4E). The 151 bp promoter fragment appeared to have an expression level comparable to the empty vector control. This indicates that WRKY transcription factors were still able to bind, though very inefficiently, to the mutated W-boxes as well as to the W-boxes present in the 165 bp construct. In an independent experiment, we generated two other construct, one carrying a mutated W-box 1 and the other a mutated W-box 2. None of them showed significant variations in expression level compared to the unmutated promoter fragment *DMP1p_{2kb}* (data not shown). Thus, a single W-box at this position appears sufficient to promote *DMP1* expression during senescence.

DMP1 is regulated by several WRKY transcription factors

We showed that the mutation of eight nucleotides within the palindrome formed by W-box elements 1 and 2 led to a near-loss of *DMP1* promoter activity during senescence. We next tried to identify which WRKY members specifically bind to *DMP1p* conferring strong *DMP1* expression during senescence. We first screened the 75 WRKY TFs for senescence-associated candidates likely to be involved in *DMP1p* regulation using our own microarray analysis (Van der Graaff et al., 2006), publicly available data and publications (Hinderhofer and Zentgraf, 2001; Robatzek and Somssich, 2001; Guo and Gan, 2005). We cloned *WRKY6*, -8, 25, -26, -40, -45, -51, -53, -60 and -75 in binary vectors to generate constructs overexpressing the different WRKY in plant cells. To test the binding capacity of the different WRKY proteins to *DMP1p* W-boxes 1 and 2, we co-expressed them individually with either the native *DMP1p_{2kb}:uidA* reporter construct or the mutated version *DMP1p_{2kb/Wbox1-2mut}:uidA*. We performed experiments in stably transformed tobacco epidermis cells (data not shown) and in a transient expression system using *Arabidopsis thaliana* protoplasts (Berger et al., 2007). Transactivation of *DMP1p_{2kb}* and *DMP1p_{2kb/Wbox1-2mut}* by the different WRKYs in tobacco epidermis cells were quantified via a MUG assay (data not shown) and visualized by GUS staining in the protoplast assay (Fig. 5). We reproducibly found transactivation of *DMP1p_{2kb}* by WRKY45, -51, -53 and -75 (Fig. 5A and data not shown). *DMP1p_{2kb/Wbox1-2mut}* did not yield strong MU fluorescence compared to *DMP1p_{2kb}* and did not lead to GUS staining above the level of the negative controls lacking any WRKY (Fig. 5A). This shows that several WRKY TFs were able to bind to W-boxes 1 and 2 and to transactivate transcription. However, the fact that WRKY6, -8, -25, -26, -40 and -60 did apparently not bind to *DMP1p_{2kb}* suggest a certain specificity. However, expression level of the different WRKY TFs was not determined.

We further generated several stably transformed *Arabidopsis* WRKY overexpression lines and acquired a number of WRKY knockout lines in order to investigate *DMP1* expression by

Chapter 4

quantitative real time RT-PCR. Unfortunately, no significant up or downregulation of DMP1 was observed in any of the transgenic lines. Unfortunately, in none of the transgenic lines significant up- or downregulation of *DMP1* was observed. Thus, no WRKY TF was identified as the clear activator or repressor of *DMP1* (data not shown) suggesting that *DMP1* is cooperatively regulated by several WRKY TFs.

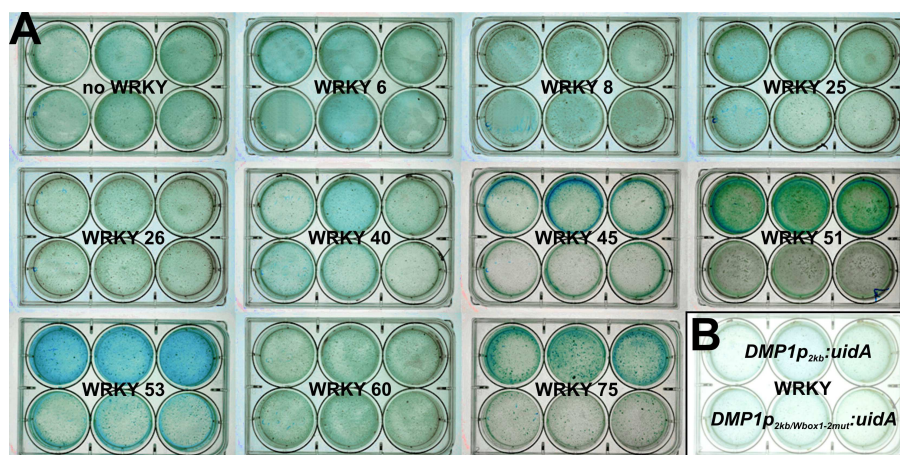


Figure 5. WRKY TFs-*DMP1p_{2kb}* interactions shown by protoplast transfection assay. (A) Co-transfection of *Arabidopsis* protoplasts with individual WRKY TFs and either *DMP1p_{2kb}:uidA* or *DMP1p_{2kb/Wbox1-2mut}:uidA*. (B) Design of the individuals experiments shown in (A), the three upper slots containing *DMP1p_{2kb}:uidA* and the three lower slots *DMP1p_{2kb/Wbox1-2mut}:uidA* respectively, all in combination with one given WRKY TF shown in the middle of each plate. Each slot represents one independent technical replicate (transformation). WRKY45, -51, -53 and -75 show transactivation of *DMP1p_{2kb}:uidA* but not of *DMP1p_{2kb/Wbox1-2mut}:uidA*.

DMP1 protein-protein interactions

DMP1 interacts with Bax Inhibitor-1, Cytochrome B5 (isoforms D and E) and Plasma membrane Intrinsic Protein 1B in yeast

In order to gain insight into DMP1 cellular function, identification of interaction partners of DMP1 was attempted. A split-ubiquitin screen was carried out in yeast for this purpose. Since *DMP1* is predominantly expressed in tissues undergoing senescence, a cDNA library was constructed from mRNA of senescing rosette leaves. An entry library was generated via Gateway® recombination cloning technology. The cDNA library titer was determined by plating assay and was above 3×10^6 cfu. 96 primary clones were tested by PCR to determine the quality of the cDNA library (Fig. 6A). The calculated average insert size was 1,4 kb and ranged from 0,2 kb to 4,5 kb with a percentage of recombinants of 96 %. The entry library was then transferred into a destination vector to generate a library expressing NubG-X fusion proteins in yeast. To avoid significant loss in complexity of the initial library, we produced an expression library comprising more than 3×10^7 cfu. By testing 96 “primary clones” of the expression library by PCR, we did not observe any alteration in the quality of the expression library compared to the entry library, the average insert size and the percentage of

Chapter 4

recombinants being conserved in both libraries (Fig. 6B). In first attempts, a bait was generated consisting of DMP1 fused C-terminally to Cub (DMP1-Cub) expressed from a methionine repressible promoter allowing fine-tuning of the expression level (data not shown). Unfortunately, the bait showed significant auto-activation even at high methionine concentrations preventing screening of the cDNA library. We next generated an N-terminal fusion (Cub-DMP1) expressed from the *CYCI* promoter. A vector allowing expression of N-terminal Cub fusion proteins (Cub-X) expressed from the same promoter as above was not available at this time. Cub-DMP1 also showed background activity but to a lesser extent compared to DMP1-Cub. Addition of 3-AT lowered background activity to an acceptable level. Optimal screening conditions showing only weak background activity were obtained by adding 10 mM 3-AT to the required medium (Fig. 6C).

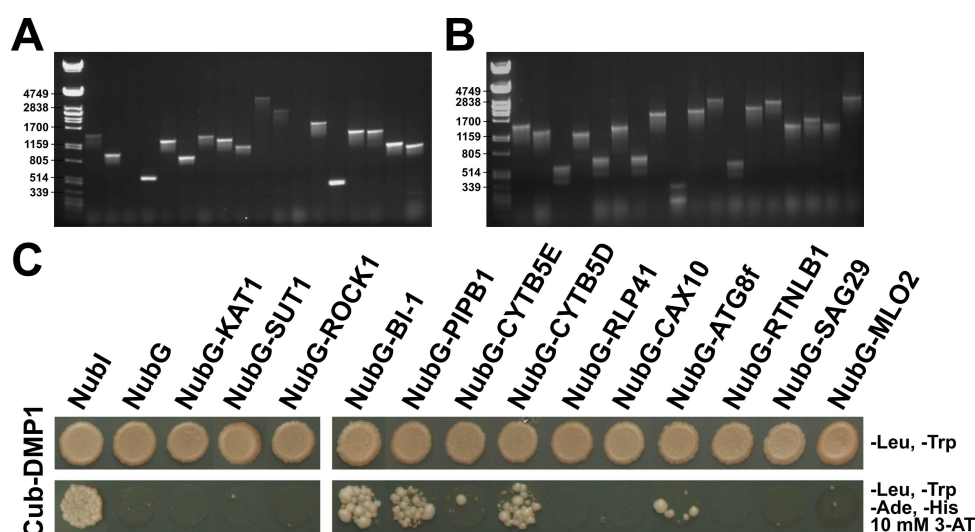


Figure 6. Quality control of the cDNA entry and expression libraries and confirmation of DMP1 interaction partners using the split-ubiquitin system. (A) Average insert size and percentage of recombinants within the entry library determined by colony PCR on 96 individual primary clones (18 are shown). (B) Quality control as in (A) of the expression library after shuttling of the entry library by LR reaction. (C) Confirmation of protein-protein interactions found in a preliminary split-ubiquitin screen. Cub-DMP1 was used as bait against NubI used as positive control. NubG and the unrelated fusion proteins NubG-KAT1, NubG-SUT1 and NubG-ROCK1 were used as negative control. 10 mM 3-AT was used to diminish background activity due to leakiness of the reporter genes. SD media lacked Trp and Leu for vector selection and additionally lacked Ade and His for selection of interactors. Pictures were taken after 5 days at 28 °C.

For the library screen, yeasts previously transformed with the vector containing *Cub-DMP1* were transformed with the expression library allowing simultaneous expression of Cub-DMP1 and NubG-X fusion proteins and detection of protein-protein interaction. The 384 colonies out of $2,7 \times 10^7$ primary transformants showing the strongest growth on minimal media (SD-Leu, -Trp, -Ade, -His, +10 mM 3-AT) were transferred to medium supplemented with increasing 3-AT concentrations (15 mM and 25 mM, data not shown). The colonies showing the strongest growth were then subjected to X-Gal assay in order to isolate the strongest interactions (data not shown). Vectors

Chapter 4

having passed the different stringency tests were isolated from yeasts and transformed into bacteria for further characterization. Presence of single or multiple vectors which would have led to unique or multiple prey proteins within given yeasts were investigated by colony PCR (data not shown). Finally 144 vectors originating from independent clones were sequenced. All genes occurring more than twice and other promising candidates are presented in decreasing order of occurrence in Table 4.

occurrence	accession	gene	gene description
15	At2g45960	PIP1B	(Plasma membrane Intrinsic Protein 1B), aquaporine
12	At3g21520	DMP1	(DUF679 Membran Protein 1)
6	At5g47120	BI-1	(Bax Inhibitor-1), suppresses Bax-mediated cell death
4	At3g25010	RLP41	(Receptor Like Protein 41)
2	At5g53560	CB5-E	(Cytochrome B5 isoform E)
2	At5g48810	CB5-D	(Cytochrome B5 Isoform D)
2	At3g61430	PIP1A	(Plasma membrane Intrinsic Protein 1A), aquaporine
1	At1g54115	CAX10	(putative calcium/proton cation antiporter)
1	At4g16520	ATG8F	(autophagy 8F)
1	At4g23630	RTNLB1	(reticulon)
1	At5g13170	SAG29	(Senescence-Associated Protein 29), putative nodulin-MtN3-type protein

The ORFs of the most promising candidates (PIP1B, DMP1, BI-1, RLP41, CB5-E and D, CAX10, ATG8F, RTNLB1, and SAG29) were cloned again to yield full length proteins fused N-terminally to NubG (NubG-X). Additionally, MLO2 was found in an independent preliminary screen as an interaction partner of DMP1 (<http://www.associomics.org>). MLO2 is a membrane protein implicated in the susceptibility to powdery mildew (Consonni et al., 2006). *MLO2* is upregulated during senescence and is predicted to enter the secretory pathway. Both eGFP-MLO2 and MLO2-eGFP were generated and were located to the ER membrane in transiently transformed *Nicotiana benthamiana* (data not shown). For these reasons, MLO2 appeared as a good candidate and a NubG-MLO2 fusion protein was generated. The different fusion proteins were retested in an independent experiment with Cub-DMP1 for protein-protein interactions (Fig. 6C and 7). Cub-DMP1 did clearly interact with the positive control NubI, the putative interactors NubG-BI-1, NubG-PIP1B, and NubG-CB5D but not with the negative controls NubG, NuG-KAT1, NubG-SUT1, NubG-ROCK1 and the putative interactors NubG-RLP41, NubG-CAX10, NubG-SAG29, and NubG-MLO2 (Fig. 6C). Generation of C-terminal fusions (X-NubG) failed due to problems during cloning. New attempts might be undertaken in the future to generate them and to test them with Cub-DMP1 for protein-protein interaction. Reciprocal experiments using the different interactors found in the screen as baits (*i.e.* fused either C- or N-terminally to Cub) and NubG-DMP1 as prey failed. Each construct was successfully cloned but the resulting bait proteins required specific optimization of the 3-AT and methionine concentrations. Most of them exhibited either

Chapter 4

strong autoactivation or absence of interaction with the positive control NubI suggesting extra-cytosolic location of Cub due to their own topology.

We then focused on the most promising interactors found: BI-1, CB5D, CB5E and PIPB1. BI-1 is an evolutionary conserved cell death suppressor across kingdoms (Xu and Reed, 1998; Watanabe and Lam, 2009; Ishikawa et al., 2011) and was shown to interact with the five cytochrome b5 isoforms present in *Arabidopsis* (Nagano et al., 2009). The fact that BI-1, CB5D and -E were found in six, two and two independent clones out of 144 clones, respectively (Fig. 6C) and the fact that BI-1 and CB5 are known to interact in yeast and *Arabidopsis* strongly suggest that they might represent true protein interactors of DMP1. A double overexpressor line *DMP1-OE* x *4xMyc-BI-1-OE* was generated in order to confirm protein-protein interaction *in planta*. Unfortunately 4xMyc-BI-1 was only weakly expressed despite expression from the 35S promoter and was almost not detectable on Western blot. Crosslinking experiments with DMS, DMP and DMA using microsomal fractions of *DMP1-OE* x *4xMyc-BI-1-OE* plants therefore failed. *In planta* assays based on bimolecular fluorescence complementation or Förster resonance energy transfer were not used due to predominant tonoplast-association and membrane remodeling observed by overexpressing DMP1-eGFP in tobacco as well as the PM localization of eGFP-DMP1 and DMP1.2-eGFP (chapter 2 and 3). DMP1 protein-protein interaction with BI-1, CB5E and Cb5D which all located to the ER membrane would not have been shown via these techniques. Thus interaction *in planta* could not be shown so far. Interaction with PIP1B was not investigated *in planta* yet. The fact that it represented more than 10 % of all clones found in the screen (Table 4) might either identify PIPB1 as a strong interactor of DMP1 or as a recurrent false positive.

DMP1 dimerizes and forms heterodimers with DMP4 in yeast

The finding that 12 out of 144 clones contained DMP1 as prey is a strong indication that DMP1 dimerizes in yeast (Fig. 6C). This dimerization was confirmed independently by generating *NubG-DMP1* consisting only of the ORF of *DMP1* fused N-terminally to *NubG* (Fig. 7). Evidence for the formation of dimers and higher oligomers *in planta* using direct or indirect methods are shown in chapter 3. We further tested the other DMP family members in order to see if DMP1 is able to form heterodimers. DMP4 was the only protein found to interact with DMP1 (Fig. 7). Thus DMP1 and DMP4 may form heterodimers and possibly higher oligomers similarly to DMP1-DMP1 complexes.

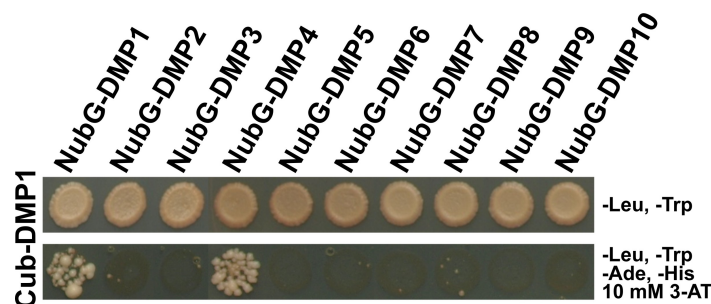


Figure 7. DMP1 homo- and heterodimerization shown using the split-ubiquitin system. Cub-DMP1 was used as bait against all 10 DMP members fused N-terminally to NubG as prey. DMP1 was found to interact with itself and to form heterodimers with DMP4 in yeast. The controls are shown in Figure 6.

Induction of cell death by overexpression of DMP members

N-terminal but not C-terminal fusions induce cell death in tobacco

We determined the subcellular localization of DMP3 and DMP5 in tobacco and *Arabidopsis* using the C-terminal fusions DMP3-eGFP and DMP5-eGFP (Kasaras and Kunze, 2010). We clearly showed that both fusion proteins located to ER membranes. By testing the N-terminal fusions eGFP-DMP3 and eGFP-DMP5, we observed rapid yellowing of the infiltrated areas at 3 dpi (Fig. 8C) which developed into necrotic-like lesions at 4 dpi (Fig. 8D). These lesions did not spread out but remained confined to the infiltrated areas. The lesions observed with eGFP-DMP3 and eGFP-DMP5 were comparable in terms of progression and intensity. This cell death was not observed following infiltration of the C-terminal fusions (Fig. 8A and B). Infiltration of unfused DMP3 expressed from the 35S promoter did not induce cell death (data not shown). Thus, the position of the fluorescent Tag appeared to be responsible for the cell death. This discrepancy between N- and C-terminal fusions was correlated by different subcellular localizations. DMP3-eGFP and DMP5-eGFP both located to the ER but were not associated with Golgi bodies (Fig. 1E-G). In contrast, the N-terminal fusions eGFP-DMP3 and -5 were first found in the ER and Golgi bodies at 2 dpi (Fig. 8H-J). Twenty-four hours later, as yellowing became visible (Fig. 8C) most of the signals were associated with Golgi bodies (Fig. 8K and M). The ER still exhibited a normal shape despite yellowing and showed only weak eGFP-DMP3 and -5 signals (Fig. 8L and M). At 4 dpi, the integrity of the cells was completely lost (Fig. 8N) correlating with the phenotypical observations (Fig. 8D).

In order to further characterize this cell death transgenic plants carrying estrogen-inducible unfused DMP3 or DMP5 were generated. Preliminary experiments did not result in the expected cell death phenotype. Exposure to estrogen did not induce cell death in these plants. However the transcript and proteins levels were not yet determined.

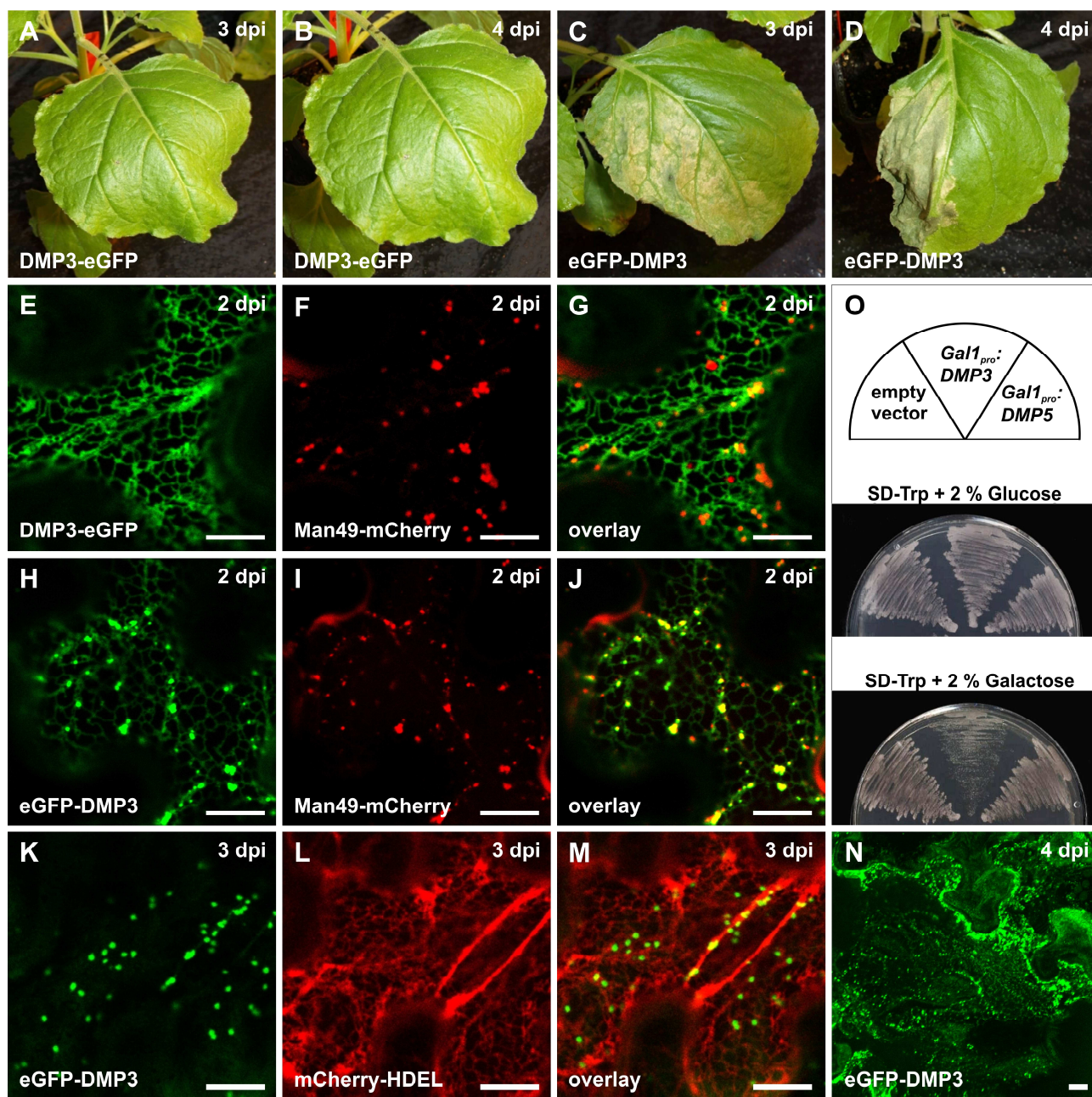


Figure 8. Cell death induced by DMP3 and DMP5 in tobacco and yeast. Transient overexpression of DMP3-eGFP at 3 dpi (A) and 4 dpi (B) and eGFP-DMP3 at 3 dpi (C) and 4 dpi (D) following *Agrobacterium*-mediated infiltration of tobacco lower epidermis. Similar phenotypical observations were done with DMP5 and comparable discrepancies between N- and C-terminal fusions were observed. DMP3-eGFP (E) does not colocalize with Man49-mCherry (F and overlay G) labeling Golgi vesicles. Colocalization of eGFP-DMP3 (H) and Man49-mCherry (I) show colocalization in Golgi (J) at 2 dpi, the ER network being labeled only by eGFP-DMP3 (H and J). At 3 dpi, the ER network showing standard architecture (L) did almost not contain eGFP-DMP3 which is confined to Golgi bodies (K and overlay M). Loss of cell integrity at 4 dpi is accompanied by increased background fluorescence, Golgi vesicles being still labeled by eGFP-DMP3 (N). Comparable observations were done with eGFP-DMP5. Overexpression of *DMP3* from the galactose-inducible promoter *Gal1* confers a lethal phenotype in yeast when grown on medium containing galactose as sole carbon source (O). Tryptophan depletion was used for plasmid selection.

Chapter 4

Unfused DMP3 but not DMP5 induces cell death in yeast

In contrast to the observations made in tobacco, overexpression of unfused DMP3 led to cell death in yeast (Fig. 10). Overexpression of DMP5 did not confer a lethal phenotype. Yeast cells overexpressing DMP1, -2, -4, -6, -7, -8, -9 and -10 remained viable and did not show any changes in growth compared to the empty vector (data not shown). Thus, DMP3 is the only DMP member able to induce cell death in yeast. Subcellular localization of the different plant-specific DMP proteins was not investigated in yeast and a correlation between subcellular localization and cell death could therefore not be established.

Discussion

DMP1-OE1 and *dmp1-ko* but not *DMP1amiRNA2-4* display early senescence phenotypes

To study *DMP1* function *in planta*, three different reverse genetic approaches were chosen. T-DNA insertion mutagenesis and the artificial micro RNA technology were used to study the effects of knocking out/down *DMP1* expression, while expression from the 35S promoter was used to investigate the effects of overexpressing *DMP1* *in planta*. The T-DNA insertion mutant *dmp1-ko* entered senescence earlier than WT plants whereas *DMP1amiRNA2-4* did not. RNA gel blot analysis showed that homozygous *dmp1-ko* plants expressed truncated *DMP1* transcripts with a reduced abundance compared to *DMP1* transcripts in WT plants. This transcript potentially could encode truncated DMP1 proteins. The T-DNA insertion site was determined on genomic DNA by sequencing at position 491 of the ORF which would correspond to a truncation of the last 44 amino acids of the native protein. The truncated protein would lack two thirds of the fourth and last transmembrane domain and the entire cytosolic carboxy-terminus. The presence of stable truncated proteins could not be verified since the DMP1-antibody was raised against amino acids 181 to 197 of the native protein (chapter 3). *dmp1-ko* was identified as a single T-DNA insertion mutant by DNA gel blot analysis indicating that the phenotype observed is due to loss of *DMP1* integrity and not to a second insertion inside the genome. Remarkably, the senescence phenotype of *DMP1amiRNA2-4* plants deviates from that of *dmp1-ko*. We therefore speculate that the *dmp1-ko* phenotype is caused by truncated and dysfunctional proteins rather than by a lack of wild-type DMP1 protein. However, we cannot exclude that a certain loss of silencing over generations may have occurred in the *DMP1amiRNA2-4* line. RNA gel blot analysis may be undertaken with plants of this line in the third generation to test this assumption.

We showed that truncation of the whole cytosolic C-terminal part of DMP1 (DMP1 $_{\Delta 183-207}$ -eGFP) led to improper targeting (chapter 3). This indicates that the C-terminal part is required for proper

Chapter 4

targeting and may be indirectly linked to proper folding or translocation. Thus, if truncated proteins occur in *dmp1-ko*, they may be misfolded or mislocated. We showed that DMP1 is able to dimerize in yeast (chapters 3 and 4). Several observations point to dimerization and higher oligomerization capacities of DMP1 *in planta* (chapter 3). We might speculate whether the dimerization domain is located in the C-terminal part of DMP1. Thus, loss of proper targeting and possibly protein functionality may be due to loss of dimerization capacity. Similar crosslinking experiments *in planta* as presented in chapter 3 using mutated N-terminal eGFP-DMP1 proteins would confirm or reject this assumption.

Interestingly, *DMP1-OE1* also enters senescence earlier compared to WT. This phenotype is comparable to that of *dmp1-ko*. The first senescence symptoms were even slightly more precocious in *DMP1-OE1* than in *dmp1-ko*. Investigation of the whole *DMP1-OE1* transcriptome showed that most JA-biosynthesis and -related genes were downregulated. JA-Ile ((+)-7-iso-jamonooyl-L-isoleucine) is the bioactive jasmonate *in planta* (Fonseca et al., 2009). *CYP94B3* was recently identified as a JA-Ile-12-hydroxylase mediating inactivation and catabolism of JA-Ile (Koo et al., 2011). This gene showed the strongest downregulation of all genes in the whole *DMP1-OE1* transcriptome. Jasmonates accumulate during natural and induced senescence (He et al., 2002; Seltmann et al., 2010a ; Seltmann et al., 2010b). Thus, a strong downregulation of *CYP94B3* in *DMP1-OE1* might result in an accumulation of JA-Ile leading to precocious senescence. Quantification of JA, JA-Ile and 12OH-JA-Ile were undertaken but the concentrations were too low in *DMP1-OE1* and WT plants to be reliable. Thus, a direct link between possible increased jasmonate concentration in *DMP1-OE1* and early senescence remains speculative.

OPDA level was also quantified and was found to be more than twice as high in *DMP1-OE1* as in WT. OPDA belongs itself to jasmonates. It derives from linolenic acid and is a precursor of jasmonic acid (Wasternack, 2007; Wasternack and Kombrink, 2010). OPDA concentration increases during senescence (Seltmann et al., 2010b). In *Arabidopsis*, OPDA occurs not only as a free molecule but can be esterified in galactolipids called arabidopsides (Stelmach et al., 2001). Arabidopside A has been shown to promote senescence in oat leaves more efficiently than JA and free OPDA (Hisamatsu et al., 2006). Thus, the increased levels of free OPDA in *DMP1-OE1*, which may be accompanied by increased arabidopsides concentrations, might promote senescence leading to the observed phenotype. However, the increased OPDA level in *DMP1-OE1* conflicts with the downregulation of the enzymes LOX2, AOC1-3 and AOS which lead to the synthesis of OPDA in chloroplasts. Indeed, these enzymes are upregulated during natural senescence (Van der Graaff et al., 2006). Downregulation of these enzymes in *DMP1-OE1* might reflect the response of the cell to counterbalance accumulation of OPDA and possibly JA-Ile directly linked to the downregulation of

Chapter 4

CYP94B3. Increased OPDA concentration could be explained by a shift in development and early senescence state in *DMP1-OE1* compared to WT, not detectable at a macroscopic level. Indeed, linolenic acid is assumed to be released by lipases during degradation of plastid membranes which may successively be converted in OPDA and JA (Seltmann et al., 2010b). These results have to be confirmed in further experiments and quantification of OPDA and other compounds such as arabidopside A should be done. The *in vitro* experiments in presence of different concentrations of (\pm)-jasmonic acid and (\pm)-jasmonic acid methyl ester suggested that increased OPDA levels and deregulated transcript levels of JA-related genes in *DMP1-OE1* did not modify JA perception and signaling.

***DMP1*, a senescence-associated gene involved in the innate immune response?**

DMP1 was found in a screen for senescence-associated membrane proteins using own micro-array data (Van der Graaff et al., 2006) and publicly available data. *DMP1* senescence-specific expression was verified by semi-quantitative RT-PCR (Kasaras and Kunze, 2010), by RNA gel blot analysis (this chapter) and was correlated on protein level (chapter 3). Rosette leaves were not the only tissue where *DMP1* underwent upregulation during natural senescence. Other photosynthetic tissues such as cauline leaves and siliques showed comparable *DMP1* regulation. Darkening of single attached or detached leaves as well as darkening of whole plants also resulted in induction of *DMP1* expression. *DMP1* was found to be most strongly expressed in late-senescing tissues and in tissues undergoing abscission or dehiscence, suggesting a role in different cell death programs. Interestingly, *DMP1p* exhibited a patchy activity pattern during natural and induced senescence. This uneven expression pattern may reflect the asynchronous progression of leaf senescence. Indeed cell death does not occur simultaneously but starts at local patches and then propagates into the whole-leaf area (Lim et al., 2007). Patchy expression patterns were also observed with *DMP3* and *DMP4* (Kasaras and Kunze, 2010). However, the pattern observed with *DMP3* was more evenly distributed over the leaf area and the expression levels of *DMP3* and *-4* were lower than that of *DMP1*. Expression of *DMP1*, *-3* and *-4* culminate in late senescence indicating a specific role of these *DMP* members in cell death.

Cell death plays a central role in the plant and animal innate immune responses (Coll et al., 2011). Several biotic stresses induce *DMP1* transcription. *Botrytis cinerea* (~ 8-fold increase), *Phytophthora infestans*, virulent and avirulent *Pseudomonas syringae* strains and the bacterial elicitors Flg22, HrpZ and NPP1 all induce *DMP1* expression according to publicly available databases. This stress response could hint towards an involvement in the plant immune system. The different mutants *dmp1-ko*, *DMP1-OE1* and *DMP1amiRNA2-4* are currently tested for enhanced resistance or

Chapter 4

susceptibility in reaction to the mentioned pathogens and elicitors. Enhanced resistance or susceptibility by overexpressing or knocking out *DMP1* would identify DMP1 as a factor required in plant immunity. It may help to shed more light on *DMP1* cellular function.

Considering the induction of *DMP1* by several biotic and abiotic stresses, its upregulation during senescence until death and the early senescence phenotypes observed in *dmp1-ko* and *DMP1-OE1*, DMP1 is probably involved in different types of programmed cell deaths.

***DMP1* expression is regulated by WRKY TFs in a senescence-specific manner**

We showed by generating a truncation series of *DMP1p* that the minimal promoter length lies under 500 bp. By mutating the two W-box elements forming a palindrome in position -165 bp to -151 bp, the senescence-specific activity of *DMP1p* was almost abolished. This strongly suggests that binding of WRKY TFs is responsible for the senescence-specific expression of *DMP1* during development. Closely adjacent W-box elements have been mentioned in several cases in the literature (Eulgem et al., 1999; Yang et al., 1999; Yu et al., 2001; Chen and Chen, 2002; Mare et al., 2004; Zhang et al., 2004). However, a comparable palindromic configuration is not described. The multiple W-box elements in the promoter of *PcWRKY1* appear to have a synergistic effect on transcription (Eulgem et al., 1999) and *HvWRKY38* requires two closely adjacent W-boxes for DNA binding (Mare et al., 2004). Some WRKY proteins contain leucine zippers enabling the formation of homo- or heterodimers (Cormack et al., 2002; Robatzek and Somssich, 2002; Xu et al., 2006; Shen et al., 2007) which presumably bind to W-box element pairs in sense and antisense orientation. However the majority of WRKY TFs likely bind as monomers (Ciolkowski et al., 2008). Our observations showed that only the simultaneous mutation of W-box 1 and 2 leads to the loss of *DMP1p_{2kb}* activity during senescence, but not the single mutation of W-box 1 or W-box 2. This indicates that dimerization of WRKY proteins is not required for binding to *DMP1p*.

By using a protoplast transfection assay and GUS as reporter, we tried to isolate WRKY TFs which bind to and activate *DMP1p*. Publicly available data and publications were screened to identify WRKY TF candidates. *WRKY6*, -8, 25, -26, -40, -45, -51, -53, -60 and -75 were chosen and their binding to *DMP1_{2kb}* and transactivating capacity was tested in *Arabidopsis* protoplasts. The mutated form *DMP1p_{2kb/Wbox1-2mut}* was used as negative control. Transactivation of *DMP1p_{2kb}* was observed by WRKY45, -51, -53 and -75. This may be interpreted as specific binding of four different WRKY TFs, or instead, as a lack of binding specificity due to overexpression. Using electromobility gel shift assays it has already been shown that the core sequence TTGACC/T is sufficient for binding but that adjacent sequences also contribute to binding site preference (Rushton et al., 1996; Eulgem et al., 2000; Ciolkowski et al., 2008; Rushton et al., 2010). Thus, the flanking regions of W-boxes 1

Chapter 4

and 2 might have conferred a certain specificity preventing WRKY6, -8, -25, -26, -40 and -60 to bind to *DMP1*_{2kb}.

Alternatively, one could envisage that WRKY6, -8, -25, -26, -40 and -60 act as putative repressors of *DMP1*_{p2kb}. WRKY TFs have been shown to act as activators or as repressors (Miao et al., 2004; Rushton et al., 2010). Thus, they may have bound to W-boxes 1 and 2 without promoting transcriptional activation. Such a negative regulation would not have been visible in our assay system since the steady state of *uidA* expression was very low. Cycloheximide rapidly induced *DMP1* expression to a level far beyond its strongest expression during late senescence. Two explanations for cycloheximide inducibility, characteristic of so-called “primary response genes”, have been proposed (Taiz and Zeiger, 2010). First, transcription of cycloheximide-inducible genes may be under the control of short-lived repressor protein(s). Second, mRNA transcripts of cycloheximide-inducible genes may be short-lived and therefore stabilized in the presence of cycloheximide. The first explanation is the most plausible in the case of *DMP1*. Thus, it might indicate that one or several WRKY TFs act permanently as *DMP1* repressors in developmental stages where *DMP1* is not, or only weakly expressed. This would suggest that *DMP1* expression is modulated by several repressors which might be replaced by activators during senescence or following *DMP1*-inducing treatments. Using the protoplast transfection assay presented, competition experiments between the WRKY TFs showing transcriptional activation of *DMP1*_{p2kb} and other WRKYs not showing transactivation may identify the latter as repressors and not as factors which do not bind to *DMP1*_{p2kb}.

Does DMP1 regulate cell death through interaction with BI-1?

DMP1, BI-1 and CB5 are interaction partners in yeast

Bax Inhibitor-1 (BI-1) was first identified in 1998 as a suppressor of BAX-induced cell death in yeast and mammals (Xu and Reed, 1998). Despite many publications about BI-1 since then, the exact molecular function of BI-1 remains unknown. So far, several studies have suggested that BI-1 interacts with several partners to alter intracellular Ca²⁺ fluxes and lipid dynamics (Chae et al., 2004; Ihara-Ohori et al., 2007; Xu et al., 2008; Watanabe and Lam, 2009; Ishikawa et al., 2011). In plants, it was found to interact with the five isoforms of cytochrome b5, themselves interacting with FAH1 and 2 which are involved in 2-hydroxylation of sphingolipids (Nagano et al., 2009). At least 168 different sphingolipids have been reported in *Arabidopsis* so far (Markham and Jaworski, 2007; Pata et al., 2010). Sphingolipids are not only structural elements of membranes but have been shown to act as second messengers involved in cell death regulation (Brodersen et al., 2002; Liang et al., 2003; Chen et al., 2008). For this reason, it has been suggested that BI-1 may regulate cell

Chapter 4

death through interaction with the CB5-FAH complex (Nagano et al., 2009). The fact that DMP1 was found to interact with BI-1 in yeast and that isoforms of cytochrome b5 are shared interaction partners strongly suggests that these proteins are true interactors. The investigation of 2-hydroxy fatty acids in *DMP1-OE1* and *dmp1-ko* lines, complemented by analysis of double knockout (*dmp1-ko x bi-1-ko*) and double overexpressor (*DMP1-OE x 4xMyc-BI-1-OE*) lines, would help to show if *DMP1* is involved in the same pathway. However, attempts to isolate double knockout plants failed so far. It will be interesting to clarify if the double mutants are lethal.

DMP1 is not involved in the UPR during ER stress

BI-1 is induced during ER stress. It has been shown to be upregulated in response to TM, DTT and AZC and was therefore classified as gene involved in the unfolded protein response (UPR) (Kamauchi et al., 2005). The UPR encompasses several signaling pathways which activate a cellular response that attempts to maintain or restore homeostasis and normal protein flux in the ER (Sitia and Braakman, 2003; Malhotra and Kaufman, 2007; Schroder, 2008). If the UPR is insufficient and the ER homeostasis cannot be restored, cell death is induced. Mutant analyses showed that *bi-1* knockout plants displayed hypersensitivity to TM and accelerated cell death progression whereas overexpression of *BI-1* reduced sensitivity to TM confirming *BI-1* involvement in the response to ER stress (Watanabe and Lam, 2008). However, altered *BI-1* gene expression did not have effects on expression of typical stress-inducible genes. *BI-1* was then proposed to act as pro-survival factor during ER stress but in parallel to the UPR (Watanabe and Lam, 2008).

Due to DMP1 interaction with BI-1 and DMP1 localization to ER membranes, the regulation of DMP1 during ER stress was investigated. Various drugs which have been described as inducing the UPR were used: TM, DTT, AZC, CPA and TG. TM inhibits Asn-linked glycosylation of newly synthesized proteins resulting in accumulation in the ER of unfolded proteins. DTT interferes with oxidative protein folding in the ER by preventing disulfide bond formation. The calcium pump inhibitors CPA and AZC, a proline analog, were shown to induce cell death in a comparable manner to TM (Watanabe and Lam, 2008). The drug thapsigargin (TG) which inhibits sarco/endoplasmic reticulum Ca^{2+} ATPase (SERCA) was shown to induce ER stress by raising the cytosolic calcium concentration.

All agents induced the UPR in our experiments as monitored by the induction of various UPR genes. We confirmed *BI-1* upregulation by TM, DTT and AZC, whereas *DMP1* was upregulated only by DTT and to a lower extent TM which indicates that *DMP1* does not respond like a typical UPR gene. AZC and CPA strongly downregulated *DMP1* and TG did not have any effect. *BI-1* was

Chapter 4

slightly downregulated by CPA and TG treatment, both depleting ER calcium stores. *BI-1* was mainly reported to be involved in regulation of ER Ca^{2+} stores in mammals (Chae et al., 2004). Similarly as in mammals, *bi-1* k-o plants showed increased sensitivity to CPA whereas BI-1 overexpressors showed decreased sensitivity to this agent (Watanabe and Lam, 2008) which led the authors to suggest an implication of BI-1 in ER calcium homeostasis. However, *BI-1* was never shown to be directly upregulated transcriptionally by CPA and TG in *Arabidopsis*. Thus, downregulation of *DMP1* by CPA and absence of response in presence of TG are not sufficient to fully exclude a role of *DMP1* in regulation of ER calcium homeostasis. The strong downregulation by AZC is quite puzzling. It should be mentioned that AZC treatment was performed for 24 hours according to Zuppini et al., (2004) whereas all other treatments were stopped after 6 hours. Therefore, the regulation between the treatments may not be comparable. However, the UPR markers showed more or less the same regulation following the different treatments. AZC is a four-membered ring analog of L-proline which causes misfolding of the proteins into which it is incorporated leading to ER stress and induction of the UPR. Why this type of protein misfolding downregulates *DMP1* whereas DTT, also acting on protein folding, induces *DMP1* cannot be explained on the basis of these data. Altogether, our data show that *DMP1* is not involved in the UPR during ER stress but responds differentially to different ER stressors.

Other potential DMP1 interaction partners

BI-1 and isoforms of cytochrome b5 were not the only proteins found to interact with DMP1 in yeast. PIP1B and -1A, ATG8F, RLP41, CAX10, RTNLB1 and SAG29 were also found in the screen. Cloning the entire ORF of the above mentioned proteins and retesting them against DMP1 did not lead to protein-protein interactions with the exception of PIP1B (PIP1A was not retested). However, this failure does not absolutely preclude *in vivo* interaction of the proteins with DMP1. Indeed, a limitation of the split-ubiquitin systems is that both Cub and NubG moieties have to be cytosolic to be able to reassemble upon interaction of the two proteins tested (Stagljar et al., 1998; Fetchko and Stagljar, 2004). Thus, due to the topology of the different tested protein, NubG might have faced an extra-cytosolic environment preventing reassembly of the two ubiquitin moieties despite interaction of DMP1.

PIP1B and -1A localize to the PM *in planta* (Marmagne et al., 2004) and might therefore specifically interact with DMP1.2 (chapter 3). The fact that two PIP proteins were found as putative interactors of DMP1 suggests that members of this protein family are either strong interactors of DMP1 or recurrent false positives. Elsewhere, DMP10 was included in the membrane interactome program (<http://www.associomics.org>) and was found to interact with 63 different proteins which

Chapter 4

per se suggest the presence of numerous false positives. However, PIP1D, another aquaporine, was found as interactor of DMP10 suggesting strong interaction propensity between the DMP and PIP protein families. The formation of DMP-PIP heterodimers should be verified in the future and might open up new perspectives concerning DMP1 function in plant.

DMP1 potentially forms heterodimers with DMP4 *in planta*

DMP1 homodimerizes in yeast. Evidence for the formation of dimers and higher oligomers *in planta* are given in chapter 3. Due to the similarity on protein level of DMP1 with the other DMP family members, heterodimerization with all DMPs family members was tested. DMP4 was the only protein found to interact with DMP1 in yeast. Thus DMP1 and DMP4 may form heterodimers and possibly higher oligomers as DMP1-DMP1 complexes *in planta*. Both were coregulated in senescing tissues including rosette and cauline leaves and senescing silique walls (Kasaras and Kunze, 2010). Moreover, both were found to be expressed in a patchy pattern in senescing leaves suggesting the presence of both proteins in the same tissue at the same developmental stage. Thus, interaction of DMP1 and -4 *in planta* is likely.

DMP3 did not form heterodimers with DMP1 in yeast. Nevertheless, it may be interesting to take it also into account for putative interactions *in planta* or as having a possible redundant function with DMP1 and DMP4. Indeed *DMP3* also showed upregulation during senescence as well as a patchy promoter activity pattern in rosette leaves (Kasaras and Kunze, 2010). Unfortunately, no T-DNA insertion lines with the T-DNA lying inside the ORF are available for *DMP3* and *DMP4*. However, lines with T-DNA in the respective promoter regions are available and may be investigated in the future. One could consider the generation of multiple mutants such as a *dmp1 x dmp3 x dmp4* triple k-o which may show more severe senescence symptoms. Unfortunately, the artificial micro-RNA technology cannot be used for this purpose as any microRNA directed specifically against these three DMP would affect transcript levels of other members.

Overexpression of DMP3 and -5 induces cell death

We found that the cell death in tobacco by overexpressing DMP3 and DMP5 was due to the position of the tag influencing subcellular localization of the fusion proteins. This is reminiscent of the effect described in chapter 3 where we showed that the presence of the tag at the N-terminus of DMP1 led the fusion protein to escape tonoplast targeting. Indeed, the full length N-terminal fusion protein was found at the plasma membrane, unlike the full length C-terminal fusion one which was targeted to the tonoplast. In the case of DMP3 and -5, the presence of the fluorescent tag at the N-terminus might impair proper retrograde Golgi to ER transport of the fusion proteins: DMP3 and -5

Chapter 4

which might first be targeted to Golgi for modifications before retrieval from the Golgi bodies to the ER might accumulate inside Golgi bodies leading to cell death. An alternative scenario is that the DMP3 and -5 proteins reside permanently inside the ER. Thus, addition of a tag to the N-terminus might have created a recognition site which targeted them to Golgi bodies where they accumulated and induced cell death. In both hypotheses, the molecular mechanism inducing death is unknown. Whether cell death simply results from DMP3 and -5 accumulations in Golgi bodies is speculative. This cell death might point to inherent properties of DMP3 and -5 related to cell death. The cell death observed in yeast by overexpressing unfused DMP3 argues in favor of that. DMP3 and DMP5 are close homologues (Kasaras and Kunze, 2010). Thus, the comparable subcellular localization of the respective N- and C-terminal fusions as well as the position effects observed might indicate similar functions at cell level. However, whereas *DMP3* was clearly detected, *DMP5* was the only DMP whose expression could not be detected in *Arabidopsis* (Kasaras and Kunze, 2010). It is tempting to speculate that they might originate from gene duplication and that *DMP5* became obsolete. However, *DMP5* might still be expressed below detection level or in restricted developmental stages. Interestingly, *DMP3* was also found to be senescence-associated and to have its highest expression during the latest developmental stage of rosette and cauline leaves as well as silique walls (Kasaras and Kunze, 2010), which would be consistent with a specific implication in cell death, the latest and irreversible step of senescence. The lethal phenotype conferred by DMP3 in yeast may be a powerful tool in the future to search for revertants. Proteins counteracting its action would help in the end to unravel the function of DMP3 and DMP proteins in general. A comparable screen in yeast using Bax as a proapoptotic protein led to the identification and isolation of the conserved cell death regulator BI-1 (Xu and Reed, 1998).

Conclusions and Outlook

DMP1 is a plant-specific gene highly induced during natural and induced senescence. Its senescence-specific expression is driven by WRKY TFs which bind specifically to two W-boxes in a palindromic configuration within *DMP1p*. Both knockout and overexpressing lines display early senescence phenotypes on low-fertilized soil. The molecular function of DMP1, however, remains unknown. Its putative interaction with the cell death regulator BI-1, its strong induction through various biotic pathogens and different elicitors and its strong senescence-specificity with the expression peak during late senescence suggest an involvement in cell death. Analysis of the double *k-o* (*dmp1-ko* x *bi-1-ko*) could be an efficient tool to gain insight in DMP1 molecular function. Surprisingly, preliminary results suggest that the combined knockout of both genes may be lethal. A double heterozygous line was screened for double homozygotes which should be observed in a 1:16 ratio. Far more than 100 plants were screened but the double *k-o* genotype was the only missing

Chapter 4

combination. We are currently investigating siliques of different segregating lines for embryo lethality. Although this finding would be unexpected since *DMP1* is not expressed in seeds, its strong expression in senescing silique walls may be needed for proper embryo development. Alternatively, the cell death occurring in the endosperm layer during seed maturation may be altered. Examination of embryo and seed development in mutants might help to elucidate this question.. The individual single knockout lines *dmp1-ko* and *bi-1-ko* did not show any phenotype related to embryo development or germination. Thus, such a dramatic phenotype concerning only the double knockout mutant would strongly indicate a synergistic function of both proteins in a common pathway and would ultimately help to elucidate the cellular function of *DMP1*.

Material and methods

Generation of constructs

35S:DMP1 and *DMP1p:DMP1-eGFP* were generated as described in chapter 3 and 2 respectively. *35S:DMP1amiRNA1*, *35S:DMP1amiRNA2*, *DMP1p:DMP1amiRNA1* and *DMP1p:DMP1amiRNA2* were generated following designer's instructions (<http://wmd2.weigelworld.org>). By successive overlapping PCR reactions using the vector RS300 as template and the different primers listed in Table T1, the fragments *microRNA1* and *microRNA2* were generated. By using the unique primer pair XbaI_miR319a/PstI_miR319a, the fragments *amiRNA1* and *amiRNA2* were generated (Table T1). These two fragments were then digested with *XbaI-PstI* and ligated to *XbaI-PstI* digested pPTkan3 to generate *35S:DMP1amiRNA1* and *35S:DMP1amiRNA2*. Similarly the same two fragments were ligated to the promoterless vector pTkan+. A 2,4 kb *DMP1* promoter fragment amplified by PCR using the primer listed in Table T1 were then inserted in front of *amiRNA1* and *amiRNA2* by *KpnI/XbaI* digestion to generate *DMP1p:DMP1amiRNA1* and *DMP1p:DMP1amiRNA2*.

To generate the promoter deletion series including the constructs *DMP1p_{0,5kb}:uidA*, *DMP1p_{1kb}:uidA*, *DMP1p_{1,5kb}:uidA*, *DMP1p_{2kb}:uidA*, *DMP1p_{165pb}:uidA* and *DMP1p_{151pb}:uidA*, the different *DMP1* promoter fragments were amplified from *Arabidopsis thaliana* genomic DNA by PCR. The primer pairs listed in Table T1 and KOD HiFi DNA polymerase (Novagen) were used. The resulting PCR products were digested with *XbaI-PstI* and ligated to *XbaI-PstI* digested pUTkan3 to generate the different constructs. To generate *DMP1p_{2kb/Wbox1-2mut}:uidA*, *DMP1p_{2kb}* was first subcloned into pJET1 using the CloneJet™ PCR cloning kit (Fermentas). W-boxes 1 and 2 were mutated by using the primer pair *DMP1p_{2kb/Wbox1-2mut}-F/DMP1p_{2kb/Wbox1-2mut}-R* (Table T1) and the QuikChange™ Site-Directed Mutagenesis Kit according to manufacturer's instructions. *pJET1-DMP1p_{2kb/Wbox1-2mut}*

Chapter 4

was then digested with *XbaI-PstI* and the resulting *DMP1*_{p2kb/Wbox1-2mut} fragment was ligated to *XbaI-PstI* digested pUTkan3 to generate *DMP1*_{p2kb/Wbox1-2mut:uidA}.

pBT3-N was purchased from Dualsystems Biotech and used for generation of *Cub-DMP1*. The open reading frame of *DMP1* was amplified via PCR with KOD HiFi DNA polymerase (Novagen) and the primer pair PstI-DMP1-F/NcoI-DMP1-R (see Table T1). This PCR product was digested with *PstI-NcoI* and ligated to *PstI-NcoI* digested pBT3-N to generate *Cub-DMP1*. To create all *NubG-X* constructs (*NubG-BI-1*, *NubG-PIP1*, *NubG-CB5E*, *NubG-CB5D*, *NubG-RLP41*, *NubG-CAX10*, *NubG-ATG8F*, *NubG-RTNLB1*, *NubG-SAG29*, *NubG-MLO2*, *NubG-DMP1*, *NubG-DMP2*, *NubG-DMP3*, *NubG-DMP4*, *NubG-DMP5*, *NubG-DMP6*, *NubG-DMP7*, *NubG-DMP8*, *NubG-DMP9*, *NubG-DMP10*) the ORF of the different genes were amplified on cDNA or gDNA in the case of intronless genes (*DMP1*, -2, -3, -4, -6, -7 and -9) and rare transcripts (*DMP5*, -8, and -10) using the primers listed in Table T1 and Phusion[®] High-Fidelity DNA Polymerase (Thermo scientific). The amplicates were recombined with pDONR[™]222 by BP reaction. The different ORFs were then shuttled into the modified pNXgate32-3HA (see section “Generation of the expression library”) by LR reaction to create all *NubG-X* constructs.

To generate *35S:WRKY6*, *35S:WRKY8*, *35S:WRKY25*, *35S:WRKY26*, *35S:WRKY40*, *35S:WRKY45*, *35S:WRKY51*, *35S:WRKY53*, *35S:WRKY60* and *35S:WRKY75*, the different ORF were PCR amplified from cDNA using the primers listed in Table T1 and Phusion[®] High-Fidelity DNA Polymerase (Thermo scientific). The primers contained the attachment sites B1 and B2 allowing recombination with pDONR[™]222 by BP reaction using BP Clonase[™] enzyme mix (Invitrogen). The ten different construct mentioned above were generated by LR reaction using pGWB2 as destination vector using LR Clonase[™] enzyme mix (Invitrogen). The construction of *35S:DMP3-eGFP* and *35S:DMP5-eGFP* is described in Kasaras and Kunze (2010). To generate *eGFP-DMP3* and *eGFP-DMP5*, *DMP3* and *DMP5* were amplified via PCR from genomic DNA using Phusion[®] High-Fidelity DNA Polymerase (Thermo) and the primer pairs 5'-ACGGTCTAGAATGTCTTCACCATCTTCCCTA-3'/5'-GAGACTCGAGCTAACGACGACCCCGTCTCC-3' and 5'-ACGGTCTAGAATGTCTGCCCTTCGGCTAAGA-3'/5'-GAGACTCGAGTCATCGGCGATCTACGCTACC-3' respectively. The amplicates were digested with *XbaI-XhoI* and ligated into *XbaI-XhoI* -digested pNGTkan3 to produce *35S:eGFP-DMP3* and *35S:eGFP-DMP5*.

Chapter 4

To generate *Gall_{pro}:DMP3* and *Gall_{pro}:DMP5*, the entry clones *pDONR222-DMP3* and *pDONR222-DMP5* were used in a LR reaction with the destination vector pAG424GAL-ccdB using LR Clonase™ enzyme mix (Invitrogen).

The sequences of all constructs were verified by sequencing (GATC Biotech, Germany).

Generation and isolation of *Arabidopsis thaliana* transgenic lines

Arabidopsis thaliana ecotype Columbia was grown on soil in the greenhouse at 22°C under long day conditions (16-h light/8-h dark cycle). Six weeks old *Arabidopsis* plants were used for *Agrobacterium tumefaciens*-mediated transformation by floral dipping (Clough and Bent, 1998). Transgenic plants were selected on 0,8 % agar plates containing ½ MS medium supplemented with 50 µg/ml kanamycin for 10 days. The transgenic line *DMP1-OE* was generated by transforming *Arabidopsis* plants with the construct *35S:DMP1*. Similarly *35S:DMP1amiRNA1* and *35S:DMP1amiRNA2* as well as *DMP1p:DMP1amiRNA1* and *DMP1p:DMP1amiRNA 2* were generated by transforming *Arabidopsis* plants with the corresponding constructs. For clarity, the artificial microRNA constructs and the corresponding lines share the same name. Gene expression was investigated in the first generation by RNA gel blot analysis.

dmp1-ko (GK-305G09-015571) was ordered from the Nottingham *Arabidopsis* Stock Centre (NASC). The genotype of plants was investigated in a PCR screen using gene-specific primers (5'-AGGAACATGCAAGTACGGGAC-3' and 5'-CTGTCCTCACTAACGACGGTG-3') and a T-DNA specific primer (5'-CCATTTGGACGTGAATGTAGACAC-3'). Isolated homozygotes were kept and their progeny analysed in the next generation.

Soil composition for phenotypical analyses

The analysis of soil composition which led to best visualization of *dmp1-ko* and *DMP1-OE1* phenotypes was performed by AGROLAB GmbH (Germany). Following parameters were determined: pH 5,3; salt content, 870 mg/l; nitrate, 42 mg/l; ammonium, 3 mg/l; phosphate, 17 mg/l; potassium, 28 mg/l; magnesium, 114 mg/l; conductivity, 264 µS/cm.

Treatments with TM, DTT, AZC, CPA, TG, CHX, AgNO₃ mannitol and NaCl

Treatments with tunicamycin (TM), dithiothreitol (DTT), L-azetidine-2-carboxylate (AZC), cyclopiazonic acid (CPA), thapsigargin (TG), cycloheximid (CHX), mannitol and NaCl were performed in liquid culture on *Arabidopsis thaliana* plantlets. *Arabidopsis* wild-type plants were grown *in vitro* on ½ MS media supplemented with 0,7 % agarose for 18 days. Ten plantlets per biological replicate were transferred and pooled in 250 ml flasks containing 20 ml sterile ½ MS

Chapter 4

solution and allowed to acclimate for 24 hours under gentle shaking. $\frac{1}{2}$ MS solution was then replaced by 20 ml of sterile $\frac{1}{2}$ MS solution supplemented with 5 μ g/ml TM (Sigma), 2 mM DTT (Roth), 5 mM AZC (Sigma), 50 μ M CPA (Sigma), 5 μ M TG (Sigma), 50 μ M CHX (Roth), 10 μ M AgNO₃ (Roth), 300 mM mannitol (Roth) or 150 mM NaCl (Roth). Treatments were performed during exactly 6 hours except for CPA treatment which was performed during 24 hours (Zuppini et al., 2004). Plant material was then frozen in liquid nitrogen. Total RNA extraction, reverse transcription and quantification of transcripts were performed as described in the “Quantitative real time PCR” section.

GUS staining

Plant tissues were fixed in 90% ice-cold acetone for 1 hour at -20 °C, washed twice with 50 mM NaPO₄ buffer pH 7.0, vacuum-infiltrated with X-Gluc solution (50 mM NaPO₄ buffer pH 7.0, 0.1% Triton[®] X-100, 10 mM potassium ferricyanide, 10 mM potassium ferrocyanide and 0,5 mg/ml 5-bromo-4-chloro-3-indolyl- β -D-glucuronide) and incubated overnight in this solution at 37°C.

Quantification of GUS activity by MUG fluorescent assay

Leaves were collected, frozen in liquid nitrogen and grinded individually in Eppendorf-tubes in a Mixer Mill MM 400 (Retsch). Extraction buffer (50 mM NaPO₄, pH 7,0; 10 mM DTT; 1 mM Na₂EDTA; 0,1 % sodium lauryl sarcosine; 0,1 % Triton[®] X-100) was added and homogenates were centrifuged for 5 min at 4°C and 15000 rpm. Supernatants were used to determine both protein concentration and GUS activity. Protein concentration was determined using Bio-Rad Protein Assay (Bio-Rad). For quantification of GUS activity, supernatants were incubated for 60 min at 37 °C with assay buffer consisting of extraction buffer supplemented with 1 mM MUG. Reactions were stopped by adding 0,2 M Na₂CO₃. MU concentrations were measured in a Synergy 2 Multi-Mode Microplate Reader (BioTek) (365 nm excitation/455 nm emission) using MU standards (10 μ M, 1 μ M, 100 nM, 50 nM, and 10 nM in 0,2 M in Na₂CO₃). GUS activity was expressed in nmol MUG hydrolyzed/mg protein/min.

Protoplast transfection assay

The protoplast transfection assay to investigate binding of WRKY TFs to *DMP1p* was performed as described (Berger et al., 2007).

Macroscopic non-invasive visualization of eGFP fluorescence

eGFP fluorescence was visualized at plant level in a non-invasive manner using a FluorCam 800MF (Photon Systems Instruments). Actinic light 2 was used as light source with an appropriate filter

Chapter 4

(high pass 495 nm, low pass 660 nm and band pass 505/560 nm). All pictures were taken with the same settings (50 % actinic light 2, electronic shutter 4 ms, sensitivity 24 %) and the same color scale.

cDNA library construction from senescing rosette leaves

Total RNA was extracted from senescing rosette leaves (43 DAS) as described (Downing et al., 1992). Polyadenylated mRNA was purified using Oligo(dT)-Cellulose Type 7 (Amersham Biosciences) according to manufacturer's instructions. The cDNA library was constructed as described in the CloneMiner™ Library Construction Kit (Invitrogen) manual. We opted for the radiolabeling method and the size fractionating of the cDNA by column chromatography. pDONR™222 was used for recombination with the *attB*-flanked cDNA to generate the entry library. The cDNA library titer was determined by plating assay and the average insert size and percentage of recombinants were determined by testing 96 primary clones by PCR using M13 forward and reverse primers. Plasmid DNA was isolated using QIAfilter Plasmid Mega Kit (Qiagen).

Generation of the expression library

To generate the destination library for expression of NubG-X fusion proteins in yeast, the entry cDNA library was shuttled into pNXgate32-3HA (Obrdlik et al., 2004) by LR reaction using LR Clonase™ enzyme mix (Invitrogen). pNXgate32-3HA does not contain the required *attR* sites but *attB* sites and was therefore modified prior to LR reaction. pNXgate32-3HA was used in a BP reaction using BP Clonase™ enzyme mix with pDONR™222 to exchange KanMX from pNXgate32-3HA with the cassette from pDONR™222 containing the chloramphenicol resistance gene and the *ccdB* gene. The modified, *attR*-sites containing pNXgate32-3HA, was then used with the entry library to produce the destination library by LR reaction. The cDNA library titer and the quality of the expression library were determined as described above. The primers (Nub-F/HA-R2) used to determine average insert size are listed in Table T1. Plasmid DNA was isolated using QIAfilter Plasmid Mega Kit (Qiagen).

Yeast transformation

THY.AP4 (MATa *ura3 leu2 lexA::lacZ::trp1 lexA::HIS3 lexA::ADE2*) was used as yeast strain. 50 ml YPAD were inoculated with several colonies taken from a fresh plate and grown overnight at 30 °C with shaking. Cultures were diluted to OD_{600nm}=0,2 and regrown to OD_{600nm}=0,6. Cultures were pelleted for 5 min at 2500 g, washed twice with water and resuspended in 2,5 ml water. 1,5 µg of each construct were mixed with PEG/LiOAc master mix (50 % PEG, 1M LiOAc, single-stranded

Chapter 4

carrier DNA) by vortexing. 100 µl resuspended yeast cells were added and vortexed thoroughly for 1 min. Samples were incubated in a 42 °C water bath for 45 minutes, pelleted for 5 min at 700 g, resuspended in 200 µl 0,9 % NaCl and plated.

Split-ubiquitin screen

The split-ubiquitin screen using Cub-DMP1 as bait and the NubG-X library as prey was performed as described in the DUALmembrane Kit 3 protocol (Dualsystems Biotech).

RNA gel blot analysis

10 µg total RNA per sample were size-separated by electrophoresis through agarose gel containing formaldehyde as described (Sambrook and Russell). 10 x SSC and neutral nylon membranes (Hybond-NX, Amersham Biosciences) were used for the transfers. The primers used on cDNA in PCR reactions to amplify the different probes (*DMP1_5'* probe and 3' probe, *SAG12*, *RBCS* and *GUS*) are listed in Table S1. All DNA probes mentioned were radiolabeled using DecaLabel™ DNA Labeling Kit (Fermentas) and radiolabeled dCTP according to manufacturer's instructions and were column-purified using Illustra Microspin™ S-200 HR columns (GE Healthcare).

Semi-quantitative RT-PCR

Total RNA was extracted using TRIzol® Reagent (Invitrogen) and column-purified using RNeasy® Mini Kit (Qiagen). Genomic DNA was removed by DNase I treatment and 2 µg total RNA was reverse transcribed using Superscript III reverse transcriptase (Invitrogen) following manufacturer's instructions. Semi-quantitative RT-PCRs were performed as described (Kasaras and Kunze, 2010).

Quantitative real time PCR

Total RNA extraction and reverse transcription were performed as described above. Quantitative real-time PCR was performed as described (Kosmehl, 2010). The primers used for all qRT-PCR investigations were designed using the publicly available software QuantPrime (<http://www.quantprime.de>). All primers are listed in Table S1.

Microarray analysis of *DMP1-OE1*

Leaves number 6 of eight individual plants were pooled for each biological replicate. Three biological replicates of *DMP1-OE1* and WT respectively were harvested at 28 DAS, approximately one week before the first senescence symptoms were visible in the *DMP1-OE1* line. Total RNA was extracted using TRIzol® Reagent (Invitrogen) and column-purified using RNeasy® Mini Kit (Qiagen). Two biological replicates of *DMP1-OE1* and WT respectively were used for dye

Chapter 4

incorporation and hybridization to *Arabidopsis* Agilent microarray. These steps as well as data analysis were performed by Imagenes, Source BioScience.

Tobacco transformation

Nicotiana benthamiana plants were grown and transformed as described (Kasaras and Kunze, 2010).

Acknowledgments

pUTkan3 and pTkan+ were kindly provided by Guillaume Pilot (Virginia Tech, Blacksburg). NubG-SUT1 and NubG-ROCK1 were kindly provided by Undine Krügel (Institute of Plant Biology, University of Zürich) and Michael Niemann (Free University, Berlin) respectively. The soil composition analysis was conducted by Christine Rausch (Free University, Berlin). The protoplast transfection assays were performed in Cologne under the guidance of Tamara Gigolashvili (University of Cologne, Germany). The quantification of jasmonates was performed by Stefan Meldau (Max-Planck-Institute for Chemical Ecology, Jena).

References

- Acosta, I.F., and Farmer, E.E. (2010). Jasmonates. *The Arabidopsis Book* **8**.
- Berger, B., Stracke, R., Yatusevich, R., Weisshaar, B., Flugge, U.I., and Gigolashvili, T. (2007). A simplified method for the analysis of transcription factor-promoter interactions that allows high-throughput data generation. *Plant J* **50**, 911-916.
- Boter, M., Ruiz-Rivero, O., Abdeen, A., and Prat, S. (2004). Conserved MYC transcription factors play a key role in jasmonate signaling both in tomato and *Arabidopsis*. *Genes Dev* **18**, 1577-1591.
- Brodersen, P., Petersen, M., Pike, H.M., Olszak, B., Skov, S., Odum, N., Jorgensen, L.B., Brown, R.E., and Mundy, J. (2002). Knockout of *Arabidopsis* accelerated-cell-death11 encoding a sphingosine transfer protein causes activation of programmed cell death and defense. *Genes Dev* **16**, 490-502.
- Chae, H.J., Kim, H.R., Xu, C., Bailly-Maitre, B., Krajewska, M., Krajewski, S., Banares, S., Cui, J., Digicaylioglu, M., Ke, N., Kitada, S., Monosov, E., Thomas, M., Kress, C.L., Babendure, J.R., Tsien, R.Y., Lipton, S.A., and Reed, J.C. (2004). BI-1 regulates an apoptosis pathway linked to endoplasmic reticulum stress. *Mol Cell* **15**, 355-366.
- Chen, M., Markham, J.E., Dietrich, C.R., Jaworski, J.G., and Cahoon, E.B. (2008). Sphingolipid long-chain base hydroxylation is important for growth and regulation of sphingolipid content and composition in *Arabidopsis*. *Plant Cell* **20**, 1862-1878.
- Chen, Z.X., and Chen, C.H. (2002). Potentiation of developmentally regulated plant defense response by AtWRKY18, a pathogen-induced *Arabidopsis* transcription factor. *Plant Physiology* **129**, 706-716.
- Chico, J.M., Chini, A., Fonseca, S., and Solano, R. (2008). JAZ repressors set the rhythm in jasmonate signaling. *Curr Opin Plant Biol* **11**, 486-494.
- Chini, A., Fonseca, S., Chico, J.M., Fernandez-Calvo, P., and Solano, R. (2009). The ZIM domain mediates homo- and heteromeric interactions between *Arabidopsis* JAZ proteins. *Plant J* **59**, 77-87.
- Chini, A., Fonseca, S., Fernandez, G., Adie, B., Chico, J.M., Lorenzo, O., Garcia-Casado, G., Lopez-Vidriero, I., Lozano, F.M., Ponce, M.R., Micol, J.L., and Solano, R. (2007). The JAZ family of repressors is the missing link in jasmonate signalling. *Nature* **448**, 666-671.
- Ciolkowski, I., Wanke, D., Birkenbihl, R.P., and Somssich, I.E. (2008). Studies on DNA-binding selectivity of WRKY transcription factors lend structural clues into WRKY-domain function. *Plant Molecular Biology* **68**, 81-92.

Chapter 4

- Clough, S.J., and Bent, A.F.** (1998). Floral dip: a simplified method for *Agrobacterium*-mediated transformation of *Arabidopsis thaliana*. *Plant J* **16**, 735-743.
- Coll, N.S., Eppele, P., and Dangl, J.L.** (2011). Programmed cell death in the plant immune system. *Cell Death and Differentiation* **18**, 1247-1256.
- Consonni, C., Humphry, M.E., Hartmann, H.A., Livaja, M., Durner, J., Westphal, L., Vogel, J., Lipka, V., Kemmerling, B., Schulze-Lefert, P., Somerville, S.C., and Panstruga, R.** (2006). Conserved requirement for a plant host cell protein in powdery mildew pathogenesis. *Nature Genetics* **38**, 716-720.
- Cormack, R.S., Eulgem, T., Rushton, P.J., Kochner, P., Hahlbrock, K., and Somssich, I.E.** (2002). Leucine zipper-containing WRKY proteins widen the spectrum of immediate early elicitor-induced WRKY transcription factors in parsley. *Biochimica Et Biophysica Acta-Gene Structure and Expression* **1576**, 92-100.
- Downing, W.L., Mauxion, F., Fauvarque, M.O., Reviron, M.P., de Vienne, D., Vartanian, N., and Giraudat, J.** (1992). A *Brassica napus* transcript encoding a protein related to the Kunitz protease inhibitor family accumulates upon water stress in leaves, not in seeds. *Plant J* **2**, 685-693.
- Eulgem, T., Rushton, P.J., Robatzek, S., and Somssich, I.E.** (2000). The WRKY superfamily of plant transcription factors. *Trends Plant Sci* **5**, 199-206.
- Eulgem, T., Rushton, P.J., Schmelzer, E., Hahlbrock, K., and Somssich, I.E.** (1999). Early nuclear events in plant defence signalling: rapid gene activation by WRKY transcription factors. *EMBO J* **18**, 4689-4699.
- Fetchko, M., and Stagljar, I.** (2004). Application of the split-ubiquitin membrane yeast two-hybrid system to investigate membrane protein interactions. *Methods* **32**, 349-362.
- Fonseca, S., Chini, A., Hamberg, M., Adie, B., Porzel, A., Kramell, R., Miersch, O., Wasternack, C., and Solano, R.** (2009). (+)-7-iso-Jasmonoyl-L-isoleucine is the endogenous bioactive jasmonate. *Nat Chem Biol* **5**, 344-350.
- Guo, Y., and Gan, S.** (2005). Leaf senescence: signals, execution, and regulation. *Curr Top Dev Biol* **71**, 83-112.
- He, Y., Fukushige, H., Hildebrand, D.F., and Gan, S.** (2002). Evidence supporting a role of jasmonic acid in *Arabidopsis* leaf senescence. *Plant Physiol* **128**, 876-884.
- Higo, K., Ugawa, Y., Iwamoto, M., and Higo, H.** (1998). PLACE: a database of plant cis-acting regulatory DNA elements. *Nucleic Acids Res* **26**, 358-359.
- Hinderhofer, K., and Zentgraf, U.** (2001). Identification of a transcription factor specifically expressed at the onset of leaf senescence. *Planta* **213**, 469-473.
- Hisamatsu, Y., Goto, N., Hasegawa, K., and Shigemori, H.** (2006). Senescence-promoting effect of arabidopside A. *Z Naturforsch C* **61**, 363-366.
- Ihara-Ohori, Y., Nagano, M., Muto, S., Uchimiya, H., and Kawai-Yamada, M.** (2007). Cell death suppressor *Arabidopsis* bax inhibitor-1 is associated with calmodulin binding and ion homeostasis. *Plant Physiol* **143**, 650-660.
- Ishikawa, T., Watanabe, N., Nagano, M., Kawai-Yamada, M., and Lam, E.** (2011). Bax inhibitor-1: a highly conserved endoplasmic reticulum-resident cell death suppressor. *Cell Death Differ* **18**, 1271-1278.
- Kamauchi, S., Nakatani, H., Nakano, C., and Urade, R.** (2005). Gene expression in response to endoplasmic reticulum stress in *Arabidopsis thaliana*. *FEBS J* **272**, 3461-3476.
- Kasaras, A., and Kunze, R.** (2010). Expression, localisation and phylogeny of a novel family of plant-specific membrane proteins. *Plant Biol (Stuttg)* **12 Suppl 1**, 140-152.
- Koo, A.J.K., Cooke, T.F., and Howe, G.A.** (2011). Cytochrome P450 CYP94B3 mediates catabolism and inactivation of the plant hormone jasmonoyl-L-isoleucine. *Proceedings of the National Academy of Sciences of the United States of America* **108**, 9298-9303.
- Kosmehl, T.** (2010). Senescence-associated P₄-type ATPases in the model plant *Arabidopsis thaliana*. Ph. D. dissertation, Free University of Berlin
- Liang, H., Yao, N., Song, J.T., Luo, S., Lu, H., and Greenberg, J.T.** (2003). Ceramides modulate programmed cell death in plants. *Genes Dev* **17**, 2636-2641.
- Lim, P.O., Kim, H.J., and Nam, H.G.** (2007). Leaf senescence. *Annual Review of Plant Biology* **58**, 115-136.
- Lorrain, S., Vaillau, F., Balague, C., and Roby, D.** (2003). Lesion mimic mutants: keys for deciphering cell death and defense pathways in plants? *Trends Plant Sci* **8**, 263-271.

Chapter 4

- Malhotra, J.D., and Kaufman, R.J.** (2007). The endoplasmic reticulum and the unfolded protein response. *Semin Cell Dev Biol* **18**, 716-731.
- Mare, C., Mazzucotelli, E., Crosatti, C., Francia, E., Stanca, A.M., and Cattivelli, L.** (2004). Hv-WRKY38: a new transcription factor involved in cold- and drought-response in barley. *Plant Molecular Biology* **55**, 399-416.
- Markham, J.E., and Jaworski, J.G.** (2007). Rapid measurement of sphingolipids from *Arabidopsis thaliana* by reversed-phase high-performance liquid chromatography coupled to electrospray ionization tandem mass spectrometry. *Rapid Commun Mass Spectrom* **21**, 1304-1314.
- Marmagne, A., Rouet, M.A., Ferro, M., Rolland, N., Alcon, C., Joyard, J., Garin, J., Barbier-Brygoo, H., and Ephritikhine, G.** (2004). Identification of new intrinsic proteins in *Arabidopsis* plasma membrane proteome. *Mol Cell Proteomics* **3**, 675-691.
- Martinez, I.M., and Chrispeels, M.J.** (2003). Genomic analysis of the unfolded protein response in *Arabidopsis* shows its connection to important cellular processes. *Plant Cell* **15**, 561-576.
- Miao, Y., Laun, T., Zimmermann, P., and Zentgraf, U.** (2004). Targets of the WRKY53 transcription factor and its role during leaf senescence in *Arabidopsis*. *Plant Molecular Biology* **55**, 853-867.
- Nagano, M., Ihara-Ohori, Y., Imai, H., Inada, N., Fujimoto, M., Tsutsumi, N., Uchimiya, H., and Kawai-Yamada, M.** (2009). Functional association of cell death suppressor, *Arabidopsis* Bax inhibitor-1, with fatty acid 2-hydroxylation through cytochrome b. *Plant J*.
- Obrdlik, P., El-Bakkoury, M., Hamacher, T., Cappellaro, C., Vilarino, C., Fleischer, C., Ellerbrok, H., Kamuzinzi, R., Ledent, V., Blaudez, D., Sanders, D., Revuelta, J.L., Boles, E., Andre, B., and Frommer, W.B.** (2004). K⁺ channel interactions detected by a genetic system optimized for systematic studies of membrane protein interactions. *Proc Natl Acad Sci U S A* **101**, 12242-12247.
- Pata, M.O., Hannun, Y.A., and Ng, C.K.** (2010). Plant sphingolipids: decoding the enigma of the Sphinx. *New Phytol* **185**, 611-630.
- Pauwels, L., Morreel, K., De Witte, E., Lammertyn, F., Van Montagu, M., Boerjan, W., Inze, D., and Goossens, A.** (2008). Mapping methyl jasmonate-mediated transcriptional reprogramming of metabolism and cell cycle progression in cultured *Arabidopsis* cells. *Proceedings of the National Academy of Sciences of the United States of America* **105**, 1380-1385.
- Robatzek, S., and Somssich, I.E.** (2001). A new member of the *Arabidopsis* WRKY transcription factor family, AtWRKY6, is associated with both senescence- and defence-related processes. *Plant J* **28**, 123-133.
- Robatzek, S., and Somssich, I.E.** (2002). Targets of AtWRKY6 regulation during plant senescence and pathogen defense. *Genes Dev* **16**, 1139-1149.
- Rushton, P.J., Somssich, I.E., Ringler, P., and Shen, Q.J.** (2010). WRKY transcription factors. *Trends Plant Sci* **15**, 247-258.
- Rushton, P.J., Torres, J.T., Parniske, M., Wernert, P., Hahlbrock, K., and Somssich, I.E.** (1996). Interaction of elicitor-induced DNA-binding proteins with elicitor response elements in the promoters of parsley PR1 genes. *Embo Journal* **15**, 5690-5700.
- Sambrook, J., and Russell, D.W.** *Molecular cloning: a laboratory manual*. Cold Spring Harbor, N.Y. : Cold Spring Harbor Laboratory Press **12 Suppl 1**.
- Schroder, M.** (2008). Endoplasmic reticulum stress responses. *Cellular and Molecular Life Sciences* **65**, 862-894.
- Seltmann, M.A., Hussels, W., and Berger, S.** (2010a). Jasmonates during senescence: signals or products of metabolism? *Plant Signal Behav* **5**, 1493-1496.
- Seltmann, M.A., Stingl, N.E., Lautenschlaeger, J.K., Kruschke, M., Mueller, M.J., and Berger, S.** (2010b). Differential Impact of Lipoxigenase 2 and Jasmonates on Natural and Stress-Induced Senescence in *Arabidopsis*. *Plant Physiology* **152**, 1940-1950.
- Shen, Q.H., Saijo, Y., Mauch, S., Biskup, C., Bieri, S., Keller, B., Seki, H., Ulker, B., Somssich, I.E., and Schulze-Lefert, P.** (2007). Nuclear activity of MLA immune receptors links isolate-specific and basal disease-resistance responses. *Science* **315**, 1098-1103.
- Sitia, R., and Braakman, I.** (2003). Quality control in the endoplasmic reticulum protein factory. *Nature* **426**, 891-894.
- Stagljar, I., Korostensky, C., Johnsson, N., and te Heesen, S.** (1998). A genetic system based on split-ubiquitin for the analysis of interactions between membrane proteins in vivo. *Proc Natl Acad Sci U S A* **95**, 5187-5192.

Chapter 4

- Stelmach, B.A., Muller, A., Hennig, P., Gebhardt, S., Schubert-Zsilavec, M., and Weiler, E.W.** (2001). A novel class of oxylipins, sn1-O-(12-oxophytodienoyl)-sn2-O-(hexadecatrienoyl)-monogalactosyl Diglyceride, from *Arabidopsis thaliana*. *J Biol Chem* **276**, 12832-12838.
- Taiz, L., and Zeiger, E.** (2010). *Plant Physiology*, Fifth Edition, 782 pages.
- Van der Graaff, E., Schwacke, R., Schneider, A., Desimone, M., Flugge, U.I., and Kunze, R.** (2006). Transcription analysis of *Arabidopsis* membrane transporters and hormone pathways during developmental and induced leaf senescence. *Plant Physiology* **141**, 776-792.
- Wasternack, C.** (2007). Jasmonates: An update on biosynthesis, signal transduction and action in plant stress response, growth and development. *Ann Bot-London* **100**, 681-697.
- Wasternack, C., and Kombrink, E.** (2010). Jasmonates: Structural Requirements for Lipid-Derived Signals Active in Plant Stress Responses and Development. *ACS Chemical Biology* **5**, 63-77.
- Watanabe, N., and Lam, E.** (2008). BAX inhibitor-1 modulates endoplasmic reticulum stress-mediated programmed cell death in *Arabidopsis*. *Journal of Biological Chemistry* **283**, 3200-3210.
- Watanabe, N., and Lam, E.** (2009). Bax Inhibitor-1, a Conserved Cell Death Suppressor, Is a Key Molecular Switch Downstream from a Variety of Biotic and Abiotic Stress Signals in Plants. *International Journal of Molecular Sciences* **10**, 3149-3167.
- Xu, C.Y., Xu, W.J., Palmer, A.E., and Reed, J.C.** (2008). BI-1 regulates endoplasmic reticulum Ca²⁺ Homeostasis downstream of bcl-2 family proteins. *Journal of Biological Chemistry* **283**, 11477-11484.
- Xu, Q.L., and Reed, J.C.** (1998). Bax inhibitor-1, a mammalian apoptosis suppressor identified by functional screening in yeast. *Molecular Cell* **1**, 337-346.
- Xu, X.P., Chen, C.H., Fan, B.F., and Chen, Z.X.** (2006). Physical and functional interactions between pathogen-induced *Arabidopsis* WRKY18, WRKY40, and WRKY60 transcription factors. *Plant Cell* **18**, 1310-1326.
- Yang, P.Z., Chen, C.H., Wang, Z.P., Fan, B.F., and Chen, Z.X.** (1999). A pathogen- and salicylic acid-induced WRKY DNA-binding activity recognizes the elicitor response element of the tobacco class I chitinase gene promoter. *Plant Journal* **18**, 141-149.
- Yu, D.Q., Chen, C.H., and Chen, Z.X.** (2001). Evidence for an important role of WRKY DNA binding proteins in the regulation of NPR1 gene expression. *Plant Cell* **13**, 1527-1539.
- Zhang, Z.L., Xie, Z., Zou, X.L., Casaretto, J., Ho, T.H.D., and Shen, Q.X.J.** (2004). A rice WRKY gene encodes a transcriptional repressor of the gibberellin signaling pathway in aleurone cells. *Plant Physiology* **134**, 1500-1513.
- Zuppini, A., Navazio, L., and Mariani, P.** (2004). Endoplasmic reticulum stress-induced programmed cell death in soybean cells. *Journal of Cell Science* **117**, 2591-2598.

List of abbreviations, gene names and units

A	adenine	E	acid glutamic
A	alanine	EDTA	ethylenediaminetetraacetic acid
<i>A. thaliana</i>	<i>Arabidopsis thaliana</i>	eGFP	enhanced green fluorescent protein
aa	amino acid	ER	endoplasmic reticulum
ACX1	acyl-CoA oxidase 1	EST	expressed sequence tag
AgNO₃	silver nitrate	<i>et al.</i>	<i>et alii</i> ; and others
amiRNA	artificial micro RNA	EXT4	extensin 4
AOC	allene oxide cyclase	F	phenylalanine
AOS	allene oxide synthase	G	guanine
ARA7	arabidopsis RAB GTPase homolog	G	glycine
ATG8F	autophagy gene 8F	Gal	galactose
att	attachement	GC-MS	gas chromatography–mass spectrometry
AVG	aminoethoxyvinyl	gDNA	genomic DNA
AZC	L-azetidine-2-carboxylate	GLNI	glutamine synthetase 1
BI-1	bax inhibitor-1	GOGAT	glutamate synthase
BIP1	binding protein 1	GPT	N-acetylglucosamine-1-phosphate transferase
C	cytosine	GS	glutamine synthetase
CaMV	cauliflower mosaic virus	GUS	β-glucuronidase
CAX10	proton/calcium exchanger 10	h	hour
CB5-D	cytochrome b5 isoform D	HA	hematoglutinin
CB5-E	cytochrome b5 isoform E	HEPES	4-(2-hydroxyethyl)-1-piperazineethanesulfonic acid
cDNA	copy DNA	HXK	hexokinase
CHX	cycloheximide	I	isoleucine
ClpP	chloroplast protease	JA	jasmonic acid
CND41	DNA-binding protein 41	JARI	jasmonate resistant1 (jasmonate-amido synthetase)
CNX1	calnexin 1	JAZ	jasmonate zim domain
COII	component of jasmonate co-receptor complex	JMT	S-adenosyl-L-methionine:jasmonic acid carboxyl methyltransferase
CPA	cyclopiazonic acid	JRI	JA-responsive 1
CRT1B	calreticulin 1B	K	lysine
Cub	C-terminal ubiquitin moiety	k	kilo
CYCI	cytochrome-C oxidase 1	KATI	potassium channel protein 1
CYP94B3	cytochrome P450, family 94, subfamily B, polypeptide 3, monooxygenase involved in jasmonoyl-L-isoleucine catabolism	kb	kilobase
CYP94C1	cytochrome P450, family 94, subfamily C, polypeptide 1	kDa	kilodalton
Δ	deletion	ko	knock-out
DAS	days after sowing	L	leucine
DET	detached leaves	l	liter
DIS	dark-induced senescence	LD	long day
DMA	Dimethyl adipimidate	LOX	lipoxigenase
DMP	DUF679 membrane protein	M	methionine
DMP_p/DMP_{pro}	DMP promoter	M	molar
DMS	Dimethyl Suberimidate	m	milli
DNA	deoxyribonucleic acid	μ	micro
DNase	deoxyribonuclease	<i>Man49</i>	α-1,2-mannosidase I (49 aa)
dNTP	deoxynucleotide triphosphate	MBP1	myrosinase-binding protein 1
dpi	days post infiltration	min	minute
DTT	dithiothreitol	MLO2	mildew resistance resistance o2
DUF679	domain of unknown function 679	mRFP	monomer red fluorescent protein
		mRNA	messenger RNA

MRP2	multidrug resistance-associated protein 2	PLACE	plant cis-acting regulatory DNA elements
MS	Murashige-Skoog	PM	plasma membrane
MU	4-methylumbelliferone	PXA1	peroxisomal ABC transporter 1
MUB2	membrane-anchored ubiquitin-fold protein 2	qRT-PCR	quantitative real time PCR
MUG	4-methylumbelliferyl-beta-D-glucuronide	5'-RACE-PCR	rapid amplification of cDNA ends with polymerase chain reaction
Myc	c-myc, similar to myelocytomatosis viral oncogene (v-Myc)	RCB	Rubisco-containing bodies
MYC2	MYC-related transcriptional activator	RCC	chlorophyll catabolite
N	asparagine	RCCR	RCC reductase
n	nano	RLP41	receptor like kinase 41
N.D.	not detected/determined	RNA	ribonucleic acid
Na₂CO₃	sodium carbonate	ROS	reactive oxygen species
Na₂EDTA	disodium ethylenediamine tetraacetic acid	rpm	rotation per minute
NAC	no apical meristem domain containing	RT	reverse transcription
NaCl	sodium chloride	RTNLB1	reticulum like protein B1
NaPO₄	sodium phosphate	Rubisco	ribulose-1,5-bisphosphate carboxylase oxygenase
NCBI	National Center for Biotechnology Information	S	serine
NCC	non-fluorescent chlorophyll catabolites	SAG12	senescence-associated gene 12
NdhF	Chloroplast encoded NADH dehydrogenase unit	SAG29	senescence associated gene 29
NO	nitric oxide	SAVs	senescence-associated vacuoles
NRT2	nitrate transporter 2	SFP1	ERD subfamily monosaccharide transporter
Nub	N-terminal ubiquitin moiety	SIRK	senescence-inducible receptor-like protein kinase
OD	optical density	STZ/ZAT10	salt tolerance zinc finger, subclass C1-2i C2H2-zinc-finger-type nucleic acid binding protein
OE	overexpressor	SUT1	sucrose transporter 1
OPCL1	OPC-8:0 CoA ligase1	SYP41	syntaxin of plants 41
OPR3	oxophytodienoic acid reductase 3	T	thymine
ORA47	member of the DREB subfamily A-5 of ERF/AP2 transcription factor family.	T	threonine
ORF	open reading frame	Taq	<i>Thermus aquaticus</i>
P	proline	TG	thapsigargin
PaO	Pheide <i>a</i> oxygenase	TM	tunicamycin
PCD	programmed cell death	TM	transmembrane
PCR	polymerase chain reaction	TMD	transmembrane domain
PDIL1-1	protein disulfide isomerase-like (PDIL) protein 1-1	TPK1	two pore K ⁺ channel 1
pDNA	plasmid DNA	TVS	transvacuolar strand
PEPR1	PEP1 receptor 1	UPR	unfolded protein response
PI1A	PM intrinsic protein 1A	VT111	vesicle transport v-snare 11
PI1B	PM intrinsic protein 1B	WT	wildtype
		X-Gluc	5-bromo-4-chloro-3-indolyl glucuronide
		ZAT11	subclass C1-2i C2H2-zinc-finger-type nucleic acid binding protein

Acknowledgements

I thank Prof. Dr. Reinhard Kunze for the interesting research topic and the opportunity to work in his group for so many years.

I would like to thank Prof. Dr. Wolfgang Schuster for being the second referee of my thesis.

I would like to acknowledge all my colleagues from the “Altbau” and “Neubau” of the Institute of Biology/Applied Genetics especially my colleagues from the AG Kunze for creating a pleasurable atmosphere during my Ph.D.

I thank Christine R., Elisabeth O., Nathalie F. and Sean T. for critical reading of parts of my thesis.

Most of all I would like to thank my friends and family for their support of any kind.

Eidesstattliche Erklärung

Hiermit versichere ich, die vorliegende Arbeit selbständig angefertigt und keine anderen als die angegebenen Quellen und Hilfsmittel verwendet zu haben. Weiterhin erkläre ich, dass diese Arbeit an keiner anderen Hochschule als der Freien Universität

Berlin eingereicht wurde.

Berlin, den 19. Januar 2012

Alexis Kasaras